HIG-77-15

GEOELECTRIC STUDIES ON THE EAST RIFT, KILAUEA VOLCANO, HAWAII ISLAND

By

G. V. KELLER, C. K. SKOKAN,
J. J. SKOKAN, and J. DANIELS
Colorado School of Mines
Golden, Colorado

J. P. KAUAHIKAUA and D. P. KLEIN
Hawaii Institute of Geophysics
Honolulu, Hawaii

C. J. ZABLOCKI
U.S. Geological Survey
Denver, Colorado

Geothermal Resources Exploration in Hawaii:
Number 3

DECEMBER 1977

Prepared for
NATIONAL SCIENCE FOUNDATION, Grant GI-38319
and
ENERGY RESEARCH AND DEVELOPMENT AGENCY, Grant E(04-3)-1093

HAWAII INSTITUTE OF GEOPHYSICS
UNIVERSITY OF HAWAII

HIG-77-15

GEOELECTRIC STUDIES ON THE EAST RIFT, KILAUEA VOLCANO, HAWAII ISLAND

By

G. V. Keller, C. K. Skokan,
J. J. Skokan, and J. Daniels

Colorado School of Mines
Golden, Colorado

J. P. Kauahikaua and D. P. Klein

Hawaii Institute of Geophysics
Honolulu, Hawaii

C. J. Zablocki

U. S. Geological Survey
Denver, Colorado

Geothermal Resources Exploration in Hawaii:

Number 3

December 1977

Prepared for

NATIONAL SCIENCE FOUNDATION, Grant GI-38319
and
ENERGY RESEARCH AND DEVELOPMENT AGENCY, Grant E(04-3)-1093

Charles E. Helsley
Director,
Hawaii Institute of Geophysics

ABSTRACT

Three geophysical research organizations, working together under the auspices of the Hawaii Geothermal Project, have used several electrical and electromagnetic exploration techniques on Kilauea volcano, Hawaii to assess its geothermal resources. This volume contains four papers detailing their methods and conclusions. Keller et al. of the Colorado School of Mines used the dipole mapping and time-domain EM sounding techniques to define low resistivity areas around the summit and flanks of Kilauea. Kauahikaua and Klein of the Hawaii Institute of Geophysics then detailed the East Rift with independent, two-loop induction and time-domain EM soundings. Finally, Zablocki of the U. S. Geological Survey delineated four anomalous areas on the East Rift with an extensive self-potential survey; one of these areas was chosen as the site of a test hole.

TABLE OF CONTENTS

Figures

Tables

ELECTRICAL RESISTIVITY AND TIME-DOMAIN ELECTROMAGNETIC SURVEYS OF THE PUNA AND KAU DISTRICTS, HAWAII COUNTY, HAWAII

G. V. Keller
C. K. Skokan
J. J. Skokan
J. Daniels

Colorado School of Mines
Golden, Colorado 47401

ABSTRACT

An electrical resistivity survey over the Kilauea shield area in Puna and the Kau district of the Island of Hawaii from May through July, 1973, sought areas favorable for the presence of geothermal reservoirs. The dipole mapping technique was used. A time-domain electromagnetic survey was conducted over the east rift zone to give a more complete picture of the geologic structure and hydrology of the rift. It was found that the flanks of Mauna Loa are underlain by rocks of high resistivity, and that such rocks probably extend into the Puna area along the projection of an ancient rift zone. The high resistivities probably represent the presence of dense, cool, dike complexes, so that this portion of the area is unlikely to have much prospect for geothermal development. On the other hand, resistivities as low as two ohm-m were mapped along the lower part of the east rift of Kilauea. Assuming reasonable values of porosity and water salinity, such resistivity values are compatible with the presence of thermal waters with temperatures above 180°C, probably extending to a depth of 2 km below sea level. Measurements taken around the summit area of Kilauea confirm the existence of a brackish-water geothermal system along the south side of Kilauea caldera, in the vicinity of the Kilauea Geothermal Test Well.

BACKGROUND

Geothermal energy has been of interest in the last few years because of the need for more sources of energy. Hawaii Island's volcanic origin points to the possibility of finding an economical source of geothermal power there (Macdonald, 1973).

The island of Hawaii is composed of five volcanoes. The youngest, Kilauea, is an asymmetrical shield-shaped dome cut by two zones of dikes, that are characterized by fissures and cones. The eastern zone, the east rift zone (Stearns and Macdonald, 1946, p. 129), is also called the Puna rift zone.

Regarding the possibility of geothermal resources, Macdonald (1973, p. 217) stated that "the most favorable area from the geologic point of view appears to be the east rift zone and summit of Kilauea volcano, but at depths considerably below sea level." To evaluate the geothermal potential of those areas, a dipole mapping survey and a time-domain electromagnetic sounding survey were conducted.

Geologic Structure

The east rift (Fig. 1) extends from Kilauea southeastward for 7.3 km, then turns N65°E and continues beyond Cape Kumukahi into the ocean for 70 km, then disappears. The submarine portion is a prominent ridge that contains a composite plug or dike complex (Malahoff and McCoy, 1967). Normal faults occur on the flanks of the ridge.

On land, the east rift zone is marked by many fissures, cones and pit craters. Macdonald and Eaton (1964, p. 6) stated that there are more than 70 lava vents on the surface and surely many hundred more that have been buried. Basaltic lava from these vents has built a broad arch with its crest along the rift. This lava comes from Kilauea through a continuous series of lava tubes. Finch (1946) reasoned that many pit craters are formed by engulfment into lava tubes. "The upper grouping of the craters is due to the intersection of the Puna Rift by a series of fissures trending NE-SW ... Any such intersection...would be a favorable location for the development of pit craters" (p. 2).

The northwest side of the rift, marked by vents, is the zone of faulting and cracking. The southeast side, marked by cinder cones, is the area of most eruptive activity. Moore and Richter (1962) interpret this zonation saying that "the rift

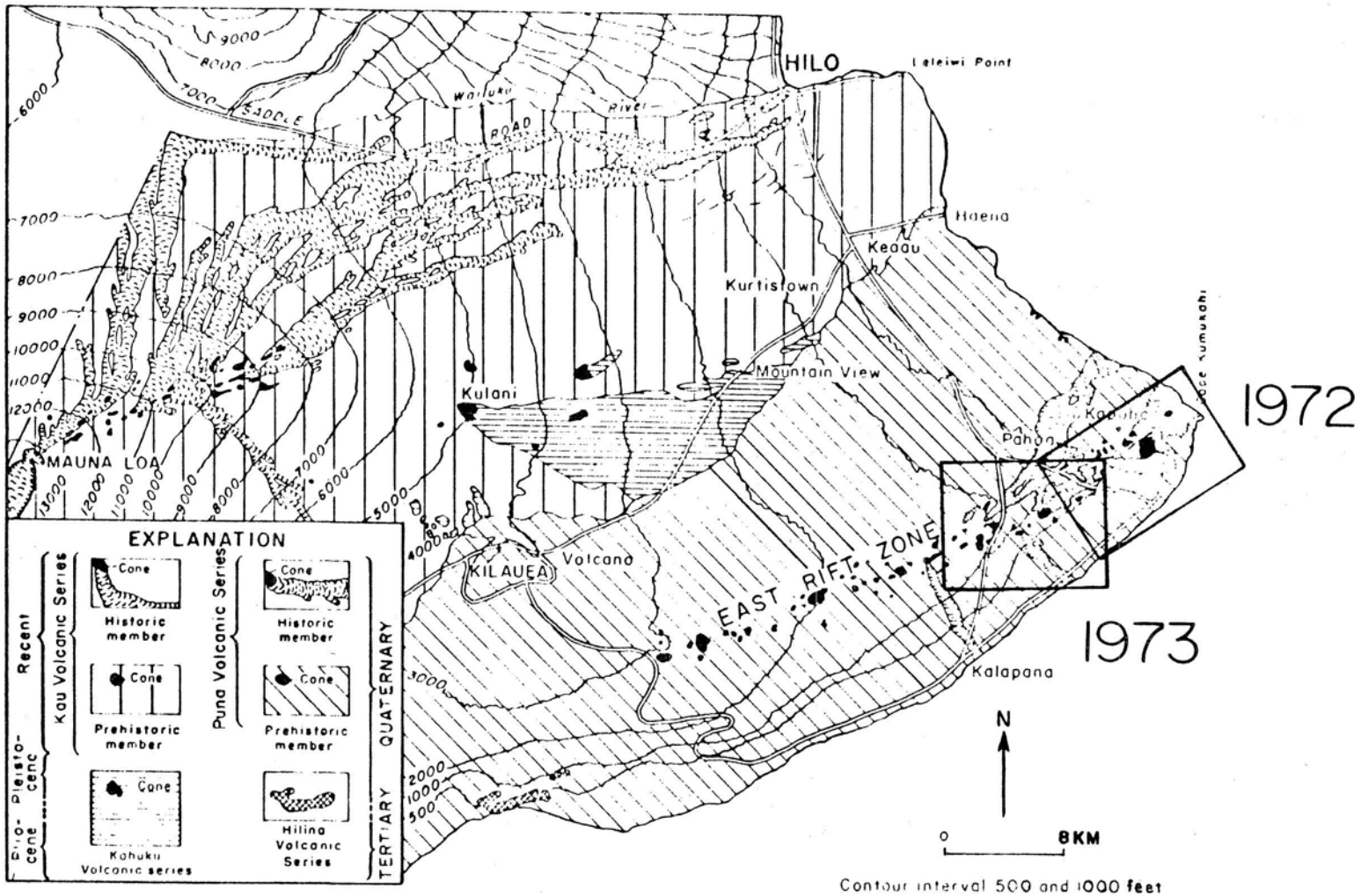

Figure 1. Generalized geologic map of the east rift and surrounding areas (after Davis and Yamanaga, 1968, p. 5). Showing location of the 1972 and 1973 time-domain electromagnetic surveys.

zone dips southeastward, with the zone of faulting marking its actual surface intersection and the zone of cones formed by piercing its hanging wall." The southside of the rift zone is steep from faulting. Many en echelon fissures follow the rift. Figure 2 shows the possible relationship of fissures, cinder cones, and grabens on the eastern part of the rift.

The rift zone is bounded by grabens. The graben area has been filled repeatedly, so that the total movement, while not measureable, must be considerable. For example, in 1924, vertical movement of 3.0 to 3.7 m was measured during an eruption (Finch, 1925). The rift is covered by alternating layers of ash and flows of unknown thickness.

There are two concepts to explain the existence of the east rift. Macdonald (1949, p. 63) believes that Kilauea results from the intersection of gravity faults in the flank of Mauna Loa with an easterly zone of fissuring. J.G. Moore (as reported by Macdonald, 1965, p. 327) feels that the rift is the result of large-scale landsliding. Moore believes that the southern slope of Kilauea is sliding seaward; the fractures on which the movement is taking place steepen to near vertical to form the east rift zone, with graben collapse along the upper edge of the sliding block. Magma then rises through the fractures. Macdonald disagrees and cites the gravity anomaly found along the rift zone. This gravity high shows dense material, such as dikes, at depth. Macdonald interprets this material as a continuation of the rift at depth. He feels the "most probable cause of the Hawaiian rift zone still appears to be inflation of the volcano by intrusion of magma within it" (Macdonald, 1965, p. 328). He claims that his theory is further supported by clay experiments in which cracking patterns extend from a center of inflation. Stearns (1966, p. 144) thinks that "subsidence appears to be due to the spreading of the dome under the influence of gravity and dike injection, possibly aided by melting and absorption of rocks in the grabens by the magma."

Hydrology

The eastern section if the island of Hawaii is generally underlain by fresh basal groundwater, with the exception of the east rift zone of Kilauea where groundwater is impounded at higher levels by dikes. Figure 3 is a generalized cross-section showing the groundwater levels within the east rift zone.

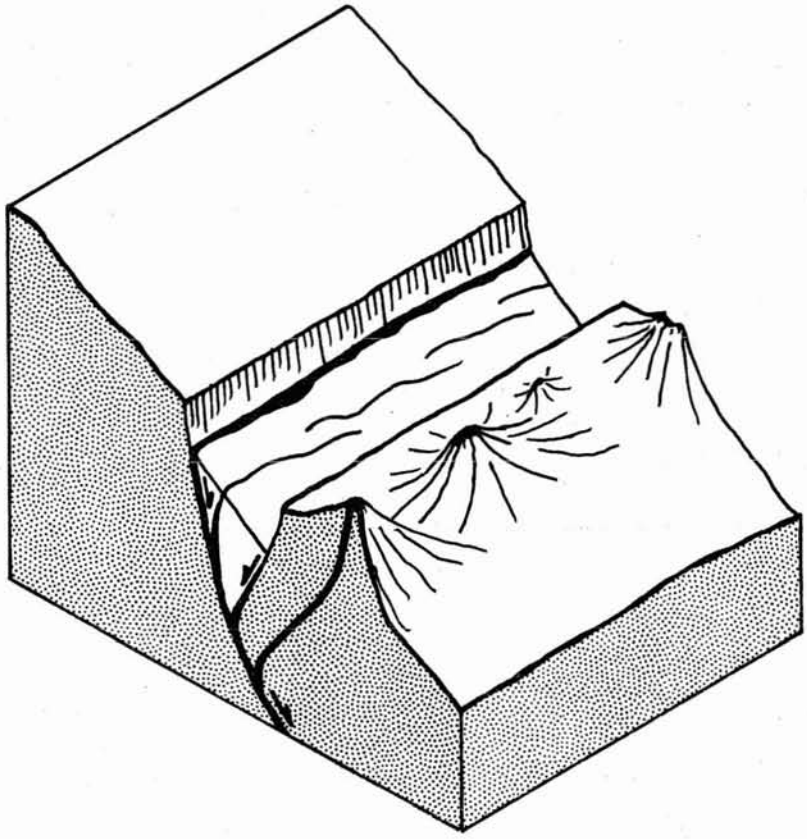

Figure 2. Block diagram showing the relationship between faulting, eruptive fissures, and cones in the eastern part of the Puna rift (after Moore and Krivoy, 1964, p. 2042).

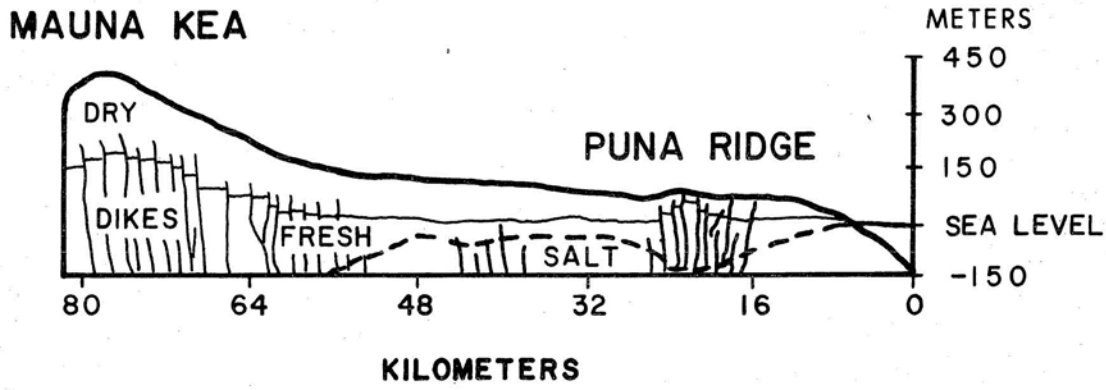

Figure 3. Generalized cross-section from Mauna Kea to the Puna Ridge showing fresh and salt-water distribution (after Stearns and Macdonald, 1946, p. 225).

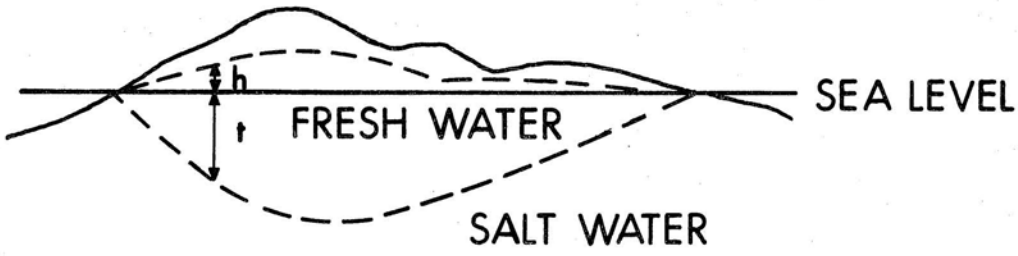

Figure 4. The Ghyben-Herzberg Principle showing the lens of fresh water depressed below sea level (after Stearns, 1966, p. 234).

Throughout many parts of the Hawaiian Islands chain, a Ghyben-Herzberg system is present. Figure 4 illustrates the Ghyben-Herzberg Principle: $t = 40\ h$. t is the thickness of fresh water depressed below sea level; h is the height of fresh water above sea level.

A permeable lava rock aquifer and impermeable coastal plain rock are necessary for developmnet of such a system. When the rock structure is not fairly homogeneous or when permeability of the rock is of too low permeability, the lens is either poorly developed or non-existent. Although Ghyben-Herzberg systems are well developed in some areas, especially Pearl Harbor, there appears to be none in the east rift zone of Hawaii. In this area, the structure is infavorable; the rocks are cut by numerous faults and dikes. These dikes also form a barrier to southward movement of groundwater from the north where the annual rainfall is great (Wentworth, 1947).

The annual rainfall near Hilo averages 200 inches/yr (508 cm/yr). This level drops to 100 to 125 inches/yr (254 to 317 cm/yr) in the east rift. The normal gradient of the groundwater level in areas of heavy rainfall, such as the east rift is 0.75 m/km from shore (Duncan, 1942).

Numerous wells drilled in the survey area reinforce this concept. Figure 5 shows the location of wells and shaft in the eastern section of the Puna Rift, and Table 1 summarizes the data. With a few exceptions, most of the well water temperatures are cool or warm, but not hot. Davis and Yamanaga (1968, p. 30), when discussing water resources in Puna, noted "sparse thermal anomalies to be seen on infrared images of near-shore water along the south shore suggest that much of the issuing groundwater is warmer than the surrounding sea water." Wells drilled by the Hawaii Thermal Power Company in 1961 confirm the presence of temperatures as high as 93°C to 102°C in one part of the east rift, but these temperatures are not high enough for a commercial geothermal system. Macdonald (1973) thinks the east rift might yield a geothermal system but at depths considerably below sea level, and present wells have not penetrated this deep. A resistivity survey can penetrate much deeper and may show evidence of greater temperatures at depth.

Table 1. Tabulation of wells in the eastern part of the Puna district, east rift zone

WELL NUMBER	ALTITUDE(m)	DEPTH (m)	WATER LEVEL ABOVE MSL(m)	Cl CONT. (PPM)	BOTTOM T (C°)	COMMENTS	REFERENCE
Thermal 1	308	54			54	Lost tool in hole	1
Thermal 2	315	169			132	Lost tool in hole	1
Thermal 3	172	210			167	Steady temperature	1
Thermal 4	76	88			43	Strong circulation of sea water	1
9-5	215	230	5	6	22	Taps water in pyroclastic material	2
9-6	87	103	1	350	33-34		2
9-7	229	244	1	90	*23	Fresh water	2
9-9	84	96	0.3	7,000	53-54	Very saline, unused	2
9-10	70	76	4	295	26	Unused	2
9-11	123	136	3	16	*23		2
	12	12		2.6		Domestic use, shaft	2

**The dug wells generally are about 9 meters deep. They have been used for either stock or industry. Most are brackish, and some water levels vary with the tide.

1 Stearns, 1966, p. 248

2 Davis and Yamanaga, 1968, p. 30

* Dept. of Land and Natural Resources of Hawaii, 1970, p. 145-146

** Ibid., p. 155-157

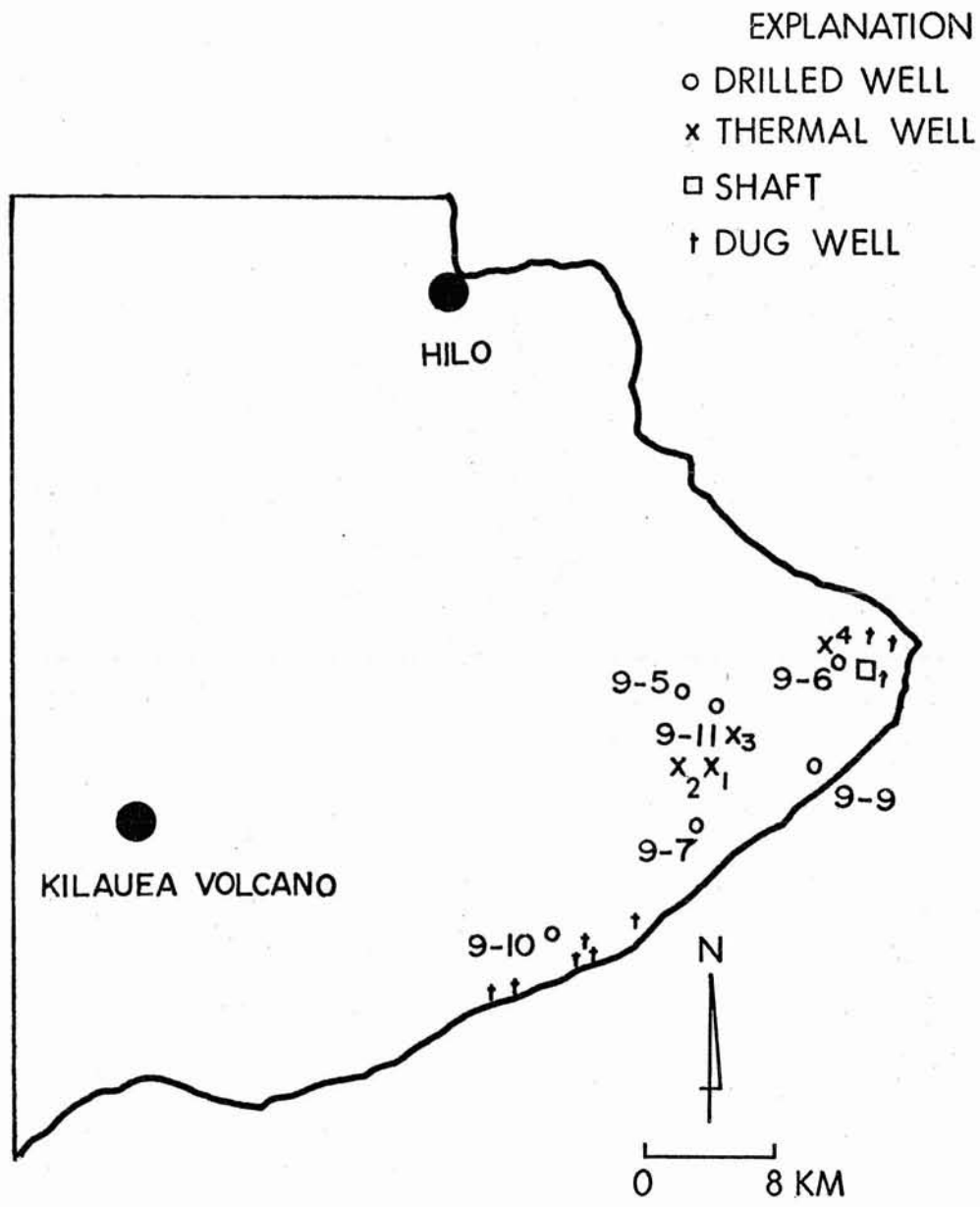

Figure 5. Map of the Puna district showing the location of wells and shafts.

AN ELECTRICAL RESISTIVITY SURVEY OF THE PUNA AND KAU DISTRICTS, HAWAII COUNTY, HAWAII

Introduction

From May 20, 1973 to July 31, 1973, an electrical resistivity survey was carried out over the Kilauea shield area of the island of Hawaii to find locations favorable for the occurrence of geothermal fluids. The areas surveyed lay mainly in the districts of Puna and Kau, county of Hawaii. In addition, a limited series of measurements was made in South Kohala district between Kamuela and Kawaihae.

The electrical surveys described in this section were for reconnaissance, rather than for detailed exploration. The dipole mapping technique was used (Keller et al., 1975). An electric field is set up by passing large amounts of low-frequency current into the earth between a pair of electrode contacts. The electric field developed by this current is mapped in detail with measurements of the voltage drop between closely spaced electrode pairs at many locations in the area around the source bipole. Local increases in the electrical conductivity of the rock, such as are usually associated with the occurrence of geothermal fluids (Keller, 1970; Keller and Rapolla, 1974), distort the pattern of current flow and the electric field patterns in ways that can usually be recognized.

The survey areas are indicated on Figure 6. The Kilauea shield area was selected for reconnaissance because a number of factors favor the occurrence of geothermal heat there. A major consideration is Kilauea's high level of volcanic activity during recorded history. In addition, a number of drilled wells along the northeast rift zone of Kilauea have encountered shallow thermal waters with temperatures ranging from 30° to 100°. Finally, the relatively low altitude of Kilauea's volcanic activity is favorable for bringing geothermal fluids to the surface.

Description of the Dipole Mapping Method

In a dipole mapping survey, a large amount of current is caused to flow in the earth between electrode contacts sited in the general vicinity to be investigated. The current flow pattern will be governed by variations in the resistivity of the ground to a depth comparable to the offset distance at which measurements are being made, or to the depth to basement rock with high resistivity, whichever is less. Because the

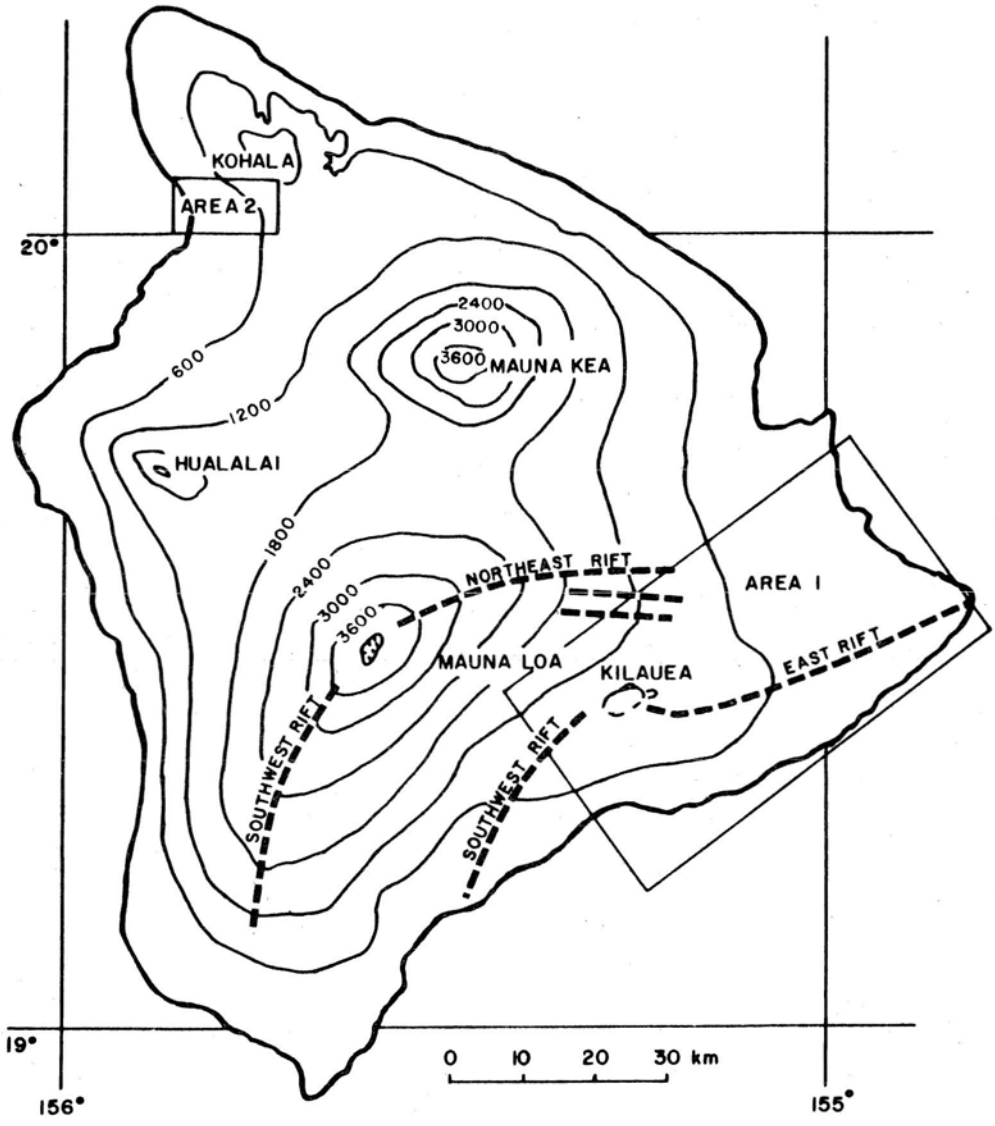

Figure 6. Map of the island of Hawaii showing the areas where electrical surveys were carried out. Area 1 covers the Kilauea shield in the Ka'u and Puna districts, while area 2 is in the South Kohala district. Elevation contours are in meters.

bipole source is fixed while many measurements of electric field are made around it, any electrical non-uniformities near the source will affect all the measurements to about the same extent, and variations in the behavior of the electric field from observation point to observation point will be indicative of the electrical structure of the ground.

The general scheme of a dipole mapping survey is shown in Figure 7. Most of the source bipole lengths were approximately 3 km, but in one case in which a pre-existing bipole was used (source 4), the length was 8 km. Power was provided from a 15-KVA, single-phase, motor generator set. The 115-volt, 60-Hz output was stepped up to 880 v with a transformer, switched mechanically and rectified to form direct-current steps. An 18-sec period of reversal was used to ensure enough time for the current to penetrate to the maximum depth possible during each current step. The current switches were operated at unequal intervals so that the current pulses were non-symmetrical, with current flow in one direction about 30% longer in duration than that in the opposite direction. This non-symmetry permitted determination of the polarity of the electric field at the receiver site.

Some problems were encountered in obtaining ground contacts that would permit the use of the high currents normally required in dipole mapping surveys. Recent surficial lavas covering almost the entire Puna and Kau districts have an extraordinarily high resistivity, so that even large-area electrodes planted at the surface have a high resistance. In cases where existing metal structures such as well casings or road culverts were available, such structures were used for grounds and good grounding was obtained. In the few areas where no such structures were available, lengths of metal pipe were buried in shallow trenches to serve as electrodes. With 12 m of pipe in a trench, wet down with salt water, a grounding resistance of 100 ohms could be obtained. Current step amplitudes ranged from 1 to 2 amps where ground contact was poor, and 10 to 20 amps where existing metal structures were used for grounds. The current step amplitudes were monitored visually with a meter and recorded.

The current field from a source bipole was mapped by recording the voltage drop between electrode pairs at many points around the source bipole. Because the direction of current flow at a measurement site is unpredictable, the total voltage drop must be determined by making a pair of measurements with electrode pairs oriented at right angles to one another and adding these voltages vectorially. Measurements

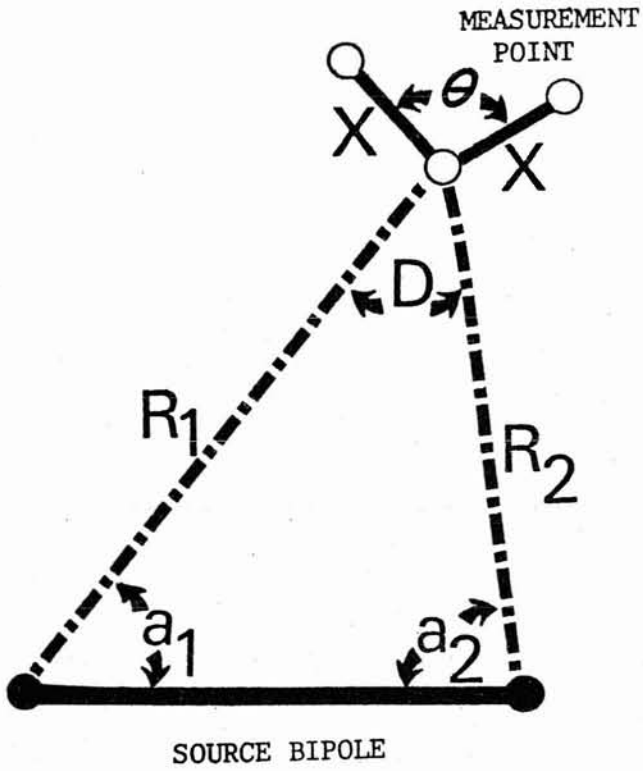

Figure 7. Layout of electrodes for a dipole mapping survey. The offset distance (source-receiver separation) is defined in this report as R2, the distance from the nearest source electrode to the measurement point.

were made with electrode separations of 30 to 300 m, the larger separations being used in areas where the signal level was low. The receiving system consisted of a sensitive DC electrometer-voltmeter and recorder, on which the deflection of the trace was measured as the direction of current flow in the earth reversed. At the maximum sensitivity of the recorder, deflections as small as 5 μv could be recognized. A record obtained with the recording system is shown in Figure 8.

The primary data obtained may be converted to values of apparent resistivity using several different formulas. The conventional manner of defining apparent resistivity is to consider what resistivity a uniform earth would have to have to provide the voltages actually observed in the real earth. In a uniform earth, current spreads out from a single electrode with spherical symmetry. The electric field along the surface of the earth at a distance R_1 from a single electrode through which a current I is flowing is given by:

$$E_1 = \frac{\rho I}{2\pi R_1^2} \qquad (1)$$

where ρ is the resistivity of the assumed uniform earth. When two source electrodes are used instead of one, there is a second contribution to the electric field from current flowing from the second electrode:

$$E_2 = \frac{-\rho I}{2\pi R_2^2} \qquad (2)$$

where R_2 is the distance from the observation point to the second current electrode.

The electric fields E_1 and E_2 are vector quantities, and so must be added vectorially to give:

$$E_T = \frac{\rho I}{2\pi R_1^2}\left[1 + \left(\frac{R_1}{R_2}\right)^4 - 2\left(\frac{R_1}{R_2}\right)\cos D\right]^{1/2} \qquad (3)$$

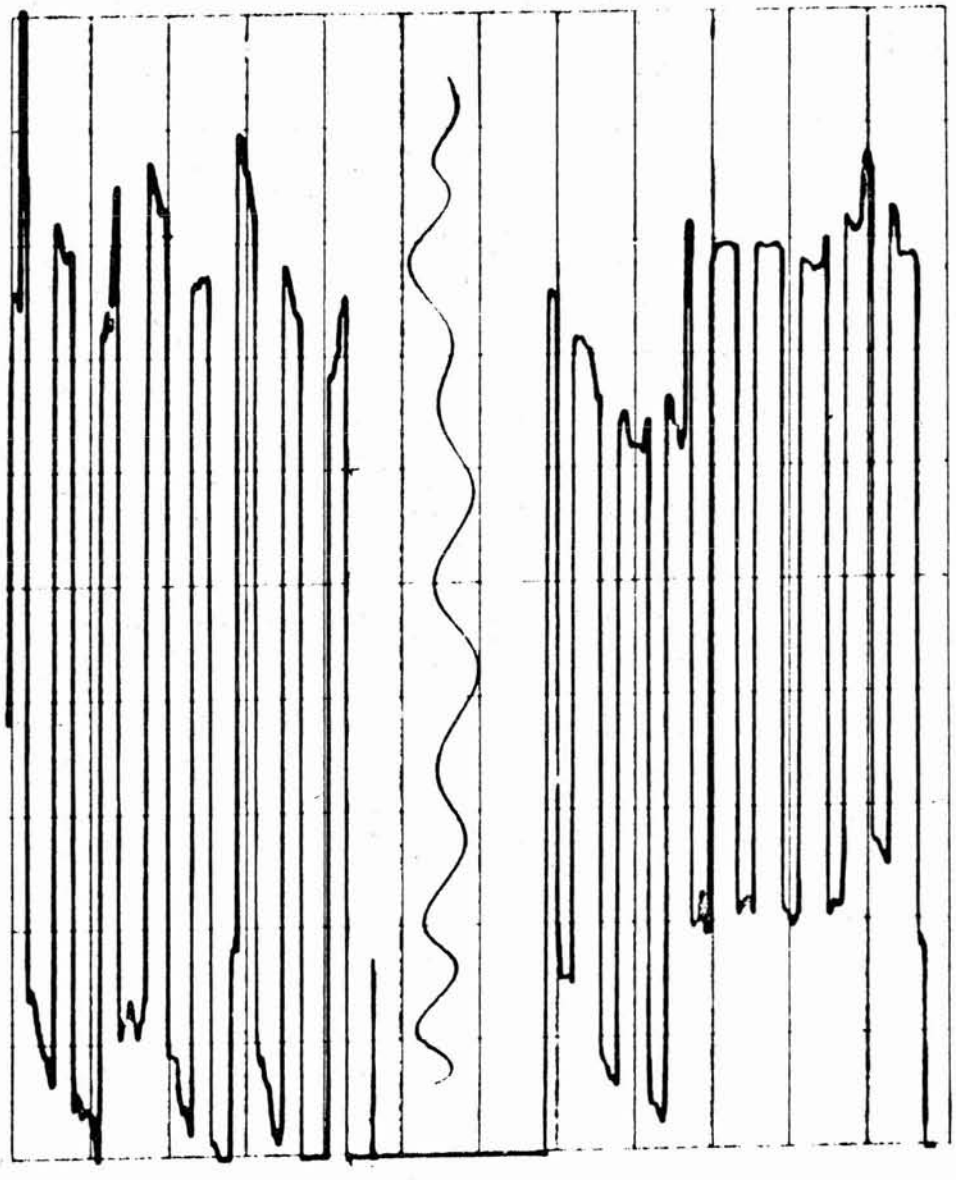

Figure 8. Example of a record of electric field components recorded at station 1434. Both components were recorded with a sensitivity of 10 μV per division. The component on the left was recorded along an azimuth of 52°; the component on the right was measured along an azimuth of 312°. Electrode separation for both components was 30 m.

Inversion of this equation to obtain an expression for ρ provides the definition of apparent resistivity used in dipole mapping:

$$\rho_a = K_{g1} K_{g2} \frac{E}{I} \qquad (4)$$

where $K_{g1} = 2\pi R_1^2$

and $$K_{g2} = \left(1 + \left(\frac{R_1}{R_2}\right)^4 - 2\left(\frac{R_1}{R_2}\right)^2 \cos D \right)^{-1/2} .$$

This formula is useful for computations in the field where a computer is not available. The first geometric factor, K_{g1}, is exactly the Schlumberger array geometric factor if the distance R_1 is considered to be equivalent to half the current electrode separation in the Schlumberger array (Keller, 1966). The second geometric factor, K_{g2}, can be considered to be a correction to the Schlumberger formula, and can be read from tables once the parameters R_1/R_2 and D have been scaled from the survey based map. A chart for determining the value for K_{g2} is shown in Figure 9.

In a real earth, the assumption of uniform resistivity is not normally warranted. In geothermal exploration, a more realistic model in many cases is that of a conductive section of rock resting on a high resistivity basement. In this case, the computation of apparent resistivity on the basis of assuming spherical spreading of current may not be appropriate. A more meaningful way to reduce the field data is to use a formula based on the assumption of cylindrical spreading in a plate, the electric field depends on the ratio of plate thickness to resistivity, h/ρ, a quantity known also as the conductance of the plate, S. The electric field at the surface of the plate for a current I spreading from a single electrode is:

$$E_1 = \frac{1}{2\pi S R_1} \qquad (5)$$

where R_1 is again the distance from the first current electrode to the observation point. With the addition of a second

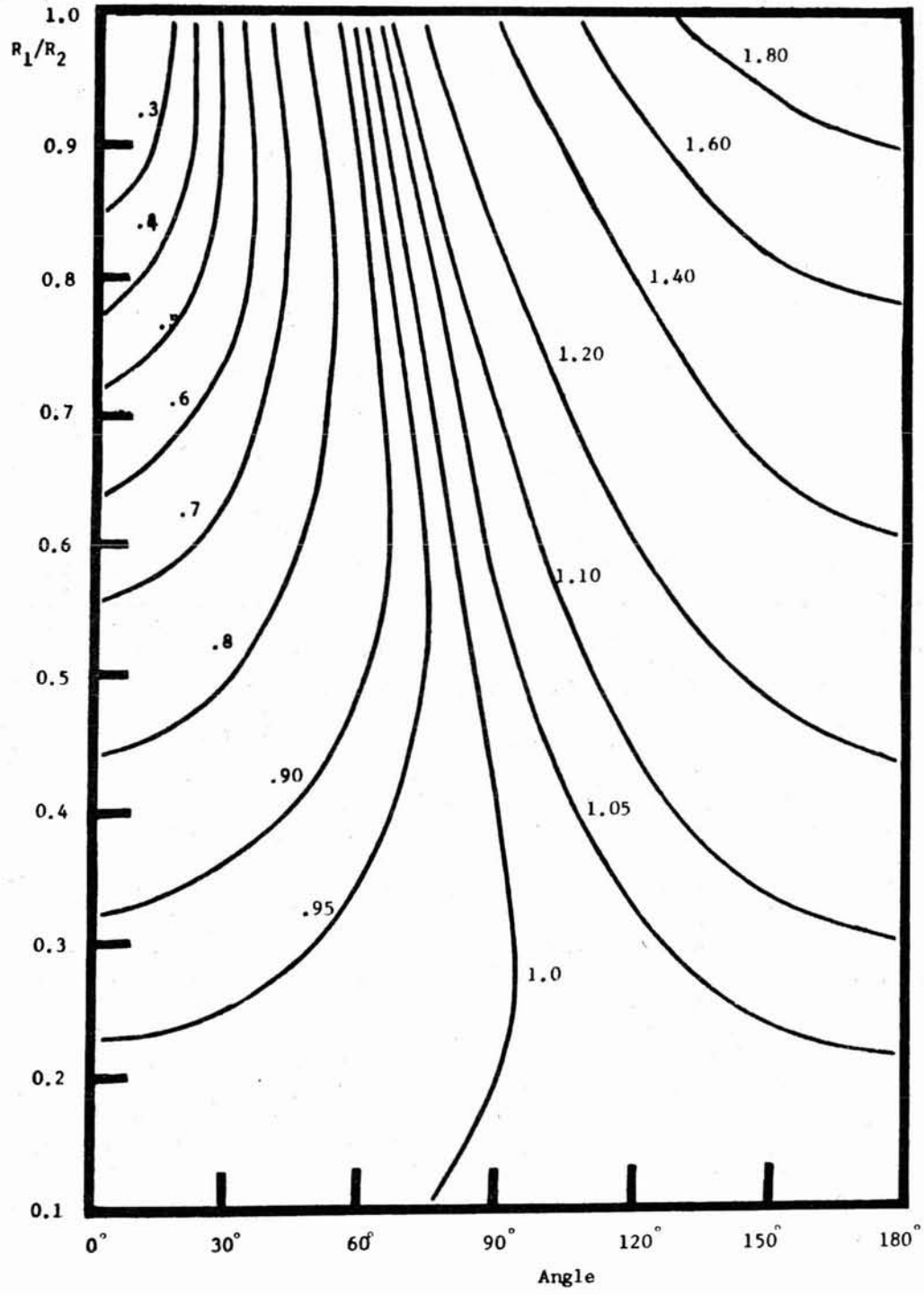

Figure 9. Chart of values for the geometric factor K_{g2}.

electrode to complete the bipole current source, the contribution of a second electric field at the observation point must be considered:

$$E_2 = \frac{-I}{2\pi\ SR_2} \qquad (6)$$

The vector sum of these two electric fields is:

$$E_T = \frac{I}{2\pi SR_1}\left[\ 1 + \frac{R_1}{R_2}^2 - 2\ \frac{R}{R_2}\qquad \cos\ D\ \right]^{1/2} . \qquad (7)$$

Solution of this equation for S provides the definition of "apparent conductance", S_a, under the assumption of cylindrical symmetry in the spreading of current through a uniform conducting plate.

Values were computed for both apparent resistivity and apparent conductance for all measurements made during this survey. These are merely different forms for presentation of the same original data. The choice of which form to use is a matter of convenience, and depends on the character of the data acquired.

Maps of apparent resistivity and apparent conductance obtained in a dipole mapping survey are useful primarily in looking for the boundaries of a conductive area such as may be associated with hot-water-filled geothermal reservoir. One of the primary evaluation methods is to compare the data obtained in the field survey with contour maps of data obtained in computer studies of hypothetical models (Lee, 1973; Furgerson and Keller, 1974; Keller et al., 1975). Figure 10 is a simple example of such a model study, a contour map of apparent resistivity for a single conductive layer on an insulating basement structure. The elliptical pattern on the apparent resistivity contours represents the increasing effect of the resistant basement on the measurements at greater distances from the source. If a geothermal reservoir were present and were characterized by a local area of low resistivity, these elliptical contours would be distorted. However, the effect of basement provides an interference that makes it difficult to recognize the presence of local anomalies in resistivity, unless they are profound.

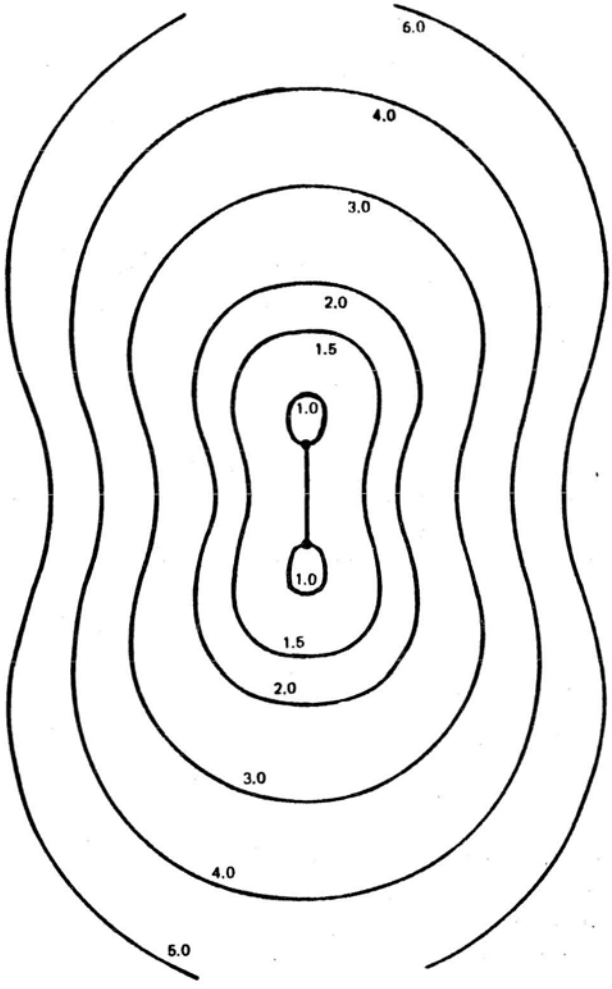

Figure 10. Apparent resistivity contours computed for the case of a conductive layer resting on an insulating substratum. The depth to the insulating layer is equal to half the source bipole length. Surface layer resistivity is unity.

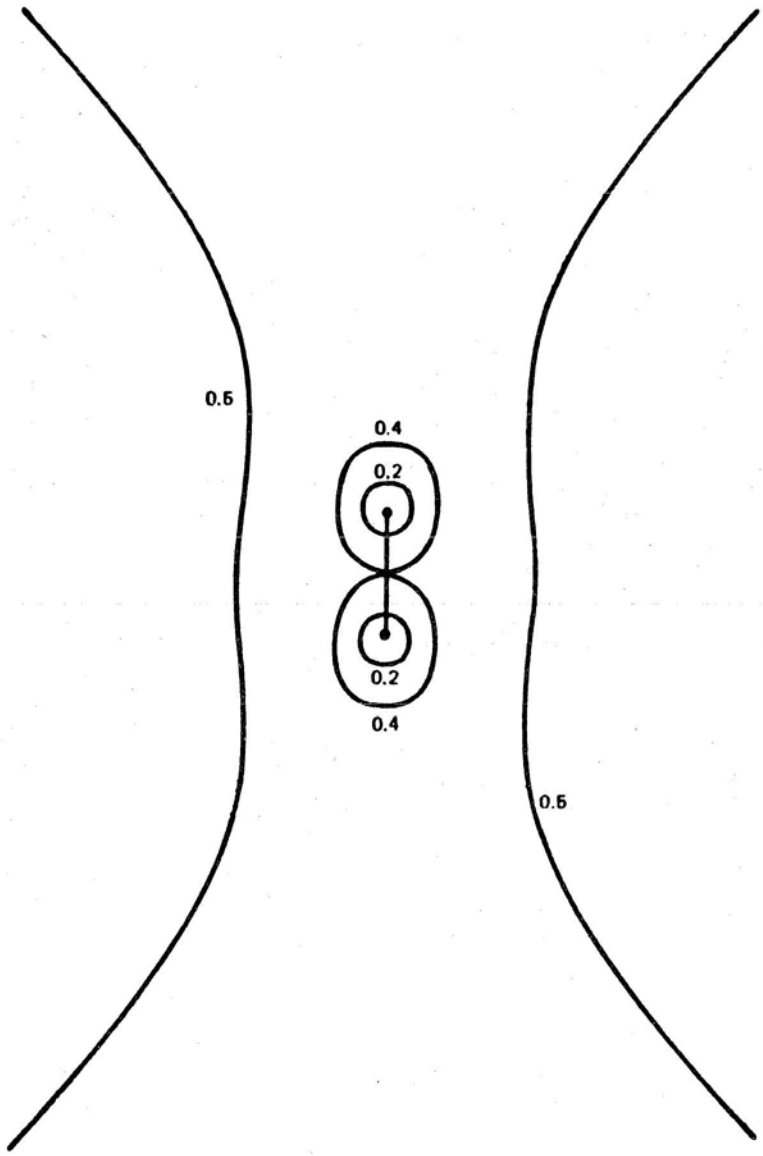

Figure 11. Apparent conductance contours computed for the case shown in Figure 12. Surface layer conductance is unity. If the depth to basement is made greater, both the contours shown here and the ones on Figure 12 will migrate outward.

A contour map of apparent conductance values for the same case (Figure 11) illustrates the advantage of using apparent conductance values when the effect of a resistant basement structure is obvious in the data. Use of apparent conductance removes the strong tendency for contours to form elliptical patterns and makes recognizing local anomalies somewhat easier.

If the lower layer were more conductive than the surface layer, the apparent resistivities would again form an elliptical pattern about the bipole source, with the value of apparent resistivity decreasing rapidly at distances greater from the source. It is possible to compute apparent conductance in this case, but the use of such values is not advantageous because the conductance will increase even more rapidly with distance from the source than the rate at which inverse resistivity would increase. Consequently, apparent conductance contours would provide an even more complicated elliptical pattern than would the apparent resistivity values; in this case, it is necessary to use the apparent resistivities.

Normally, the information needed to choose between the two forms of data presentation is not known at the time the survey is carried out. The best mode of presentation is usually determined by the overall behavior of the field data. A simple way of examining the data is to plot the apparent resistivity determinations for each dipole source as a function of the distance to the source (for standardization, the distance to the nearer end of the source was used here (R_2 in Fig. 7). Such a plot will show considerable scatter when there are lateral variations in the electrical properties of the ground, but it will also show the general trend of resistivities with distance, which reflects the variation of resistivity with depth in the earth. A summary of these trends for many of the bipole sources used in the Puna and Kau districts is shown in Figure 12. In many cases, the presence of resistant rock at a depth of about 2 to 2-1/2 km causes the data to exhibit behavior that would warrant the use of apparent conductance values, at least for measurements at distances greater than a few kilometers from the sources. However, many of the trend lines show a very large decrease in apparent resistivity with distance. These measurements were made at higher elevations where the effect of resistant basement beneath the conductive zone is not evident even at the largest distances. Because it would be inappropriate to use apparent conductance maps for these cases, apparent resistivity maps are presented for all bipole sources to provide consistency.

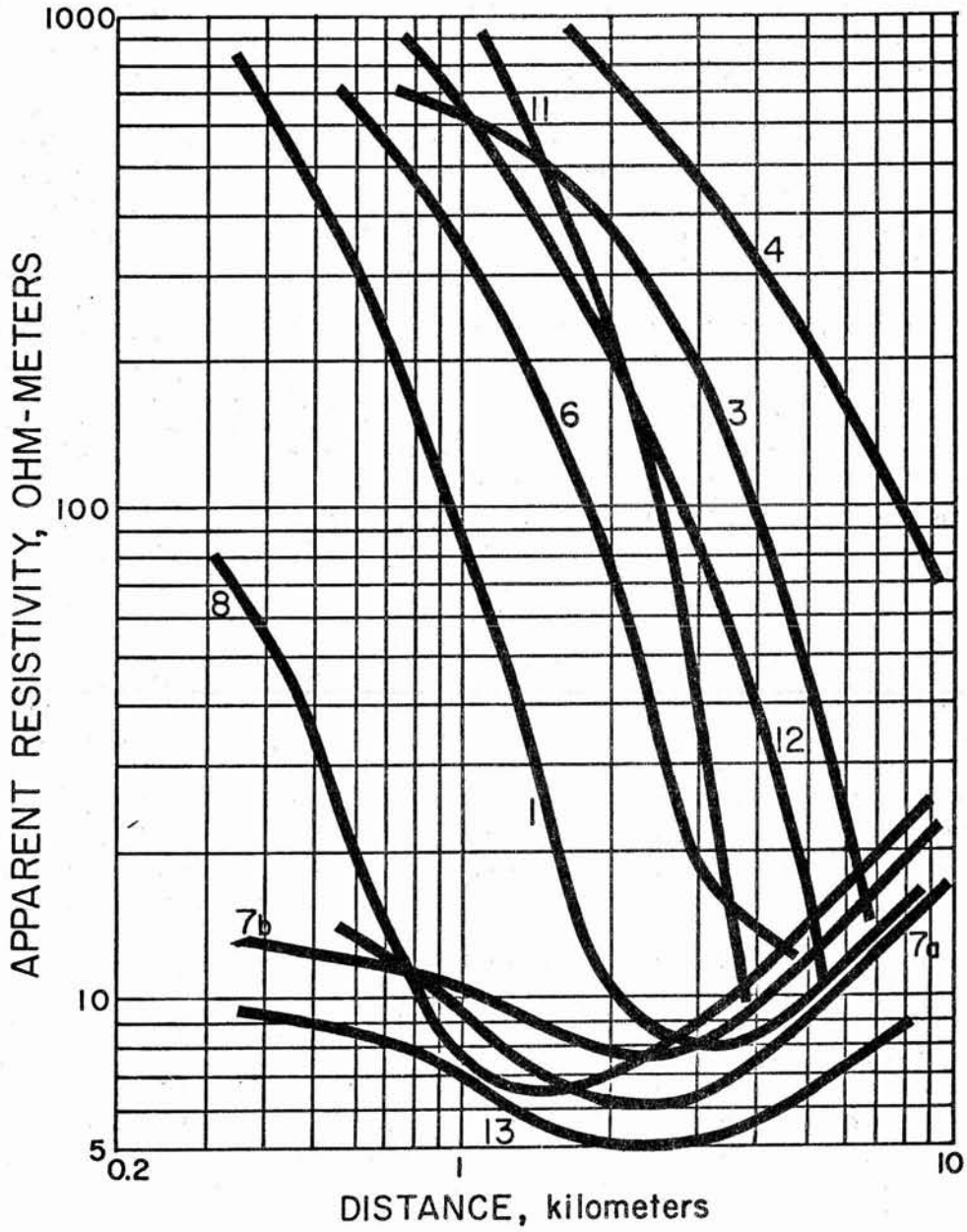

Figure 12. Trends of apparent resistivity values as a function of distance from the source. Numbers indicate sources. 7a and 7b indicate directions east and west, respectively, of source 7.

One would wish to have the contours of apparent resistivity follow closely the boundaries of regions having different electrical characteristics, so that a non-ambiguous interpretation might be made by examining contour maps of apparent resistivity value. Unfortunately, this is rarely the case. It is approximately true only when the dimensions of an anomalous area are small compared to the distance from the source, and then only if there are no other anomalous area within range of the same source. In the case of linear boundaries between regions with different resistivities, the apparent resistivity contour patterns may vary radically, depending on the position of the source bipole with respect to the boundary. Because of this, when a boundary is located from one bipole source, it is advisable to examine the same boundary as illuminated with current from other bipole sources situated with a different aspect to the boundary. The reason may be seen by examining computer model studies for the simple case of a single, vertical fault-like boundary.

Apparent resistivity contour maps are shown for the case of a single boundary separating two regions in which the resistivity varies by a factor of 10. The contour map in Figure 13 is for the case in which the bipole source lies on the conductive side of the boundary; Figure 14 is for the case in which the source lies on the resistive side of the boundary. From Figure 13, we see some of the patterns that make direct interpretation of dipole resistivity maps uncertain:

1. There is an area of anomalously low apparent resistivity on the side of the boundary facing the source bipole. This is lower than any real resistivity in the model by a factor of 2.

2. The apparent resistivity on the far side of the fault boundary is only slightly higher than that on the near side, even though the true resistivities vary by a factor of 10.

Because of these combined factors, it is possible for a resistive boundary such as a fault to be misinterpreted as being a local conductive feature if the area of low apparent resistivity is illuminated from only this one bipole source. If the anomalous area disappears or moves as the source is relocated, the reality of the anomaly must be suspect.

The behavior of the apparent resistivity contours is less misleading if the source is located on the high resistivity

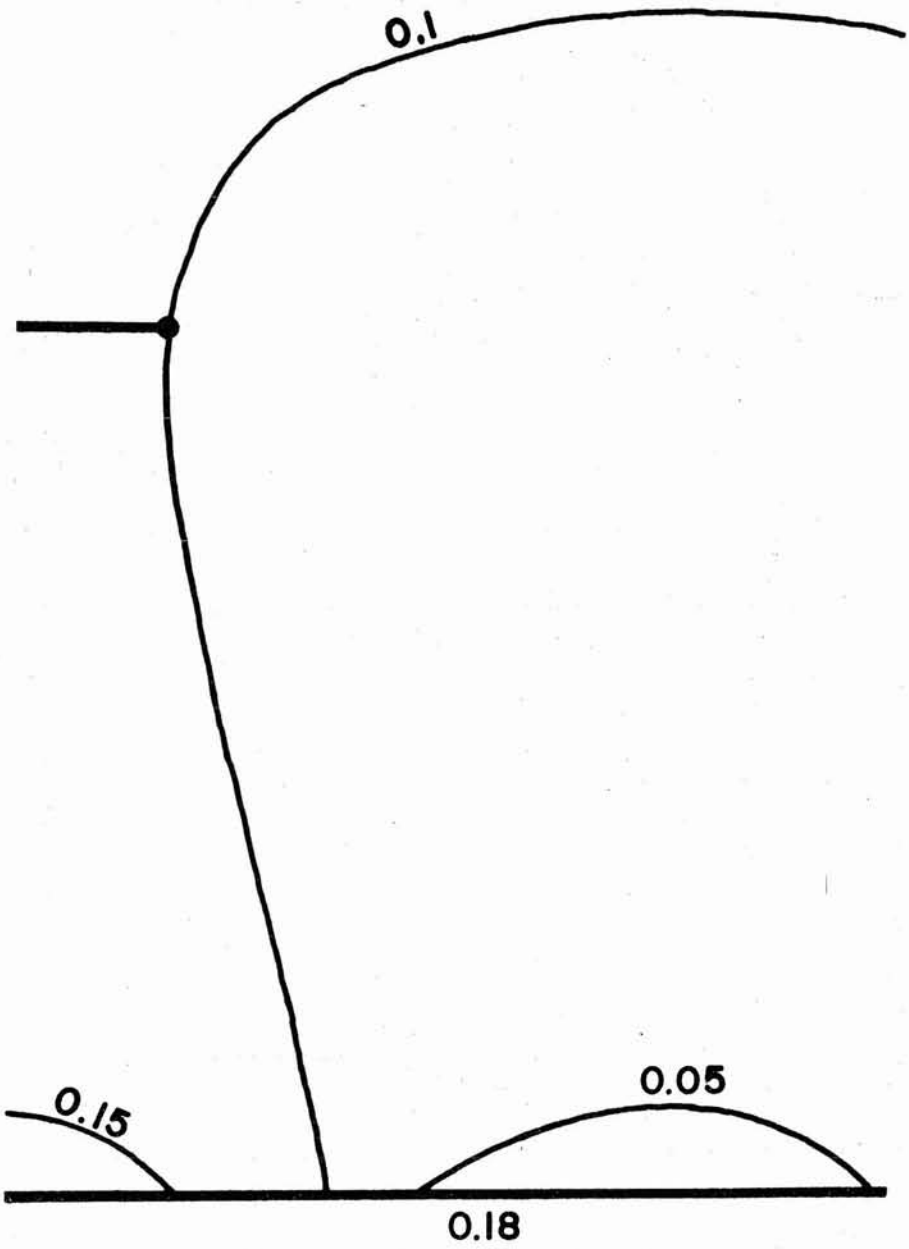

Figure 13. Bipole resistivity map for a boundary separating regions with a tenfold contrast in resistivity.

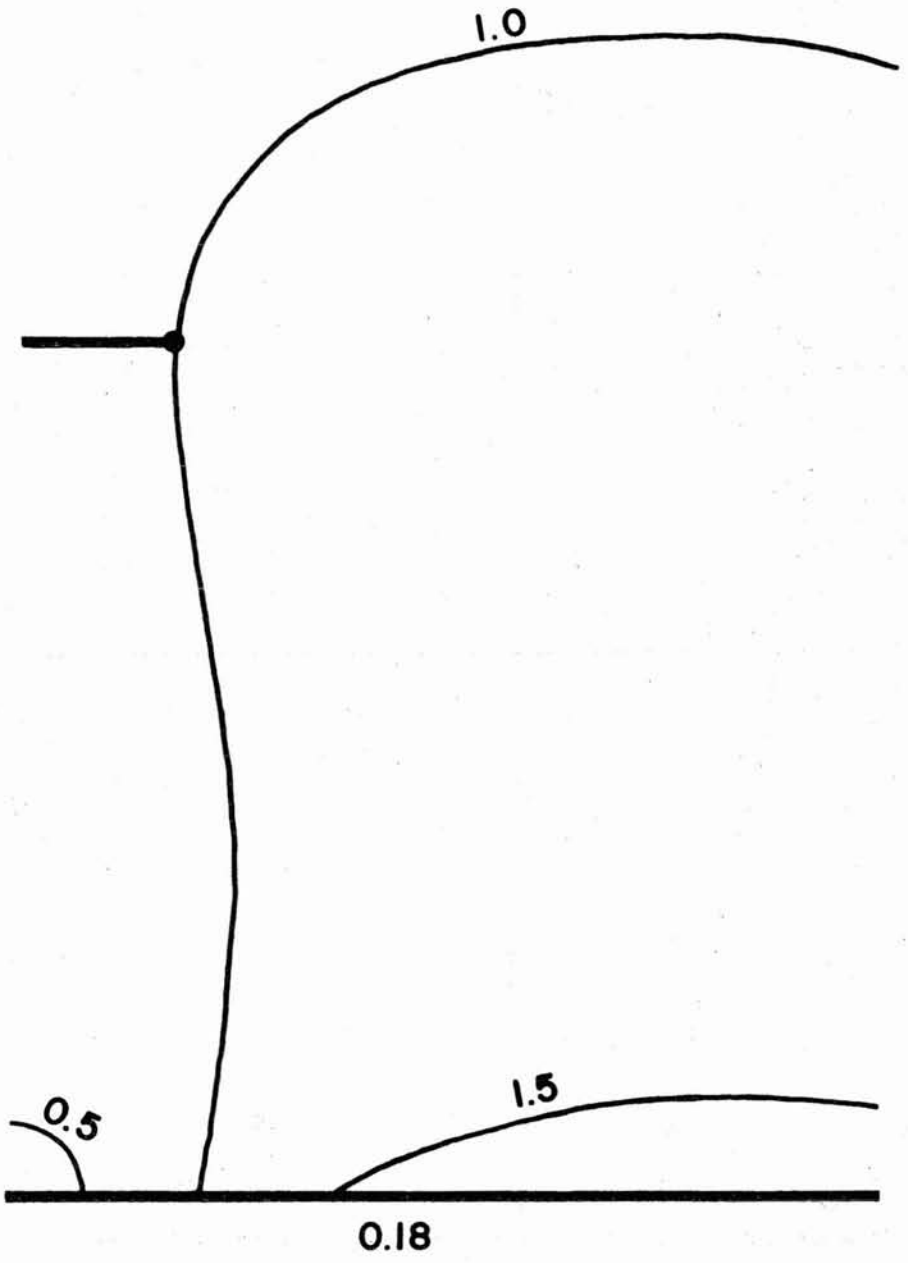

Figure 14. Dipole resistivity map for a boundary separating regions with a tenfold contrast in resistivity.

side of the boundary as in Figure 14. Here, there are minor increases and decreases in apparent resistivity on the side of the boundary facing the source, but the major change in apparent resistivity is the decrease observed in crossing the fault. It is clear that in dipole mapping results are more definitive when a conductive region is illuminated using a source located outside the conductive area than in the inverse case. This is further illustrated by profiles of apparent resistivity observed along traverses crossing the boundary (Figures 15 and 16). In Figure 15 such profiles are shown for two orientations of the source bipole, one perpendicular to the boundary (the upper curve), and one parallel to the boundary (the lower curve) for the case in which the source is located in the conductive region. The jump in apparent resistivity is only by a factor of 1.8 at the boundary, rather than by the actual factor of 10. Moreover, if the source is parallel to the boundary, a small area of very low resistivity appears on the side of the boundary facing the source. On the other hand, if the source is located on the resistive side of the boundary, as for the curves in Figure 16, the effect of the boundary on the measurements is profound and unmistakable. However, even in this case, the contrast in apparent resistivity on crossing the boundary is less than the contrast in actual resistivities.

Many more complicated models may be used for computer studies related to interpretation of dipole mapping surveys. However, these few examples are adequate to explain the strategies used in the survey of the Puna and Kau districts. Although 14 sources were used, each covering an area of 130 to 200 sq km, considerable overlapping coverage was provided in two areas where anomalously low resistivity features were recovnized. Because of this overlapping coverage, a total area of approximately 1560 sq km was covered by the surveys described in this report.

Results from Dipole Mapping Surveys

Thirteen bipole sources were used in mapping resistivity over the Kilauea shield area in Puna and Kau, and one additional source was used for measurements between Kamuela and Kawaihae, in South Kohala. The results are presented as apparent resistivity contour maps and plots of values of apparent resistivity as a function of distance from the near electrode of the source. Because values of apparent resistivity determined at a single receiver station using several different bipole sources may be radically different, it is not feasible to present overlapping coverage of an area on a single basemap. Therefore, the results will be presented for each bipole source individually. The source locations of these small maps are indicated on a larger map covering the entire survey area in the Puna and Kau districts (Figure 17).

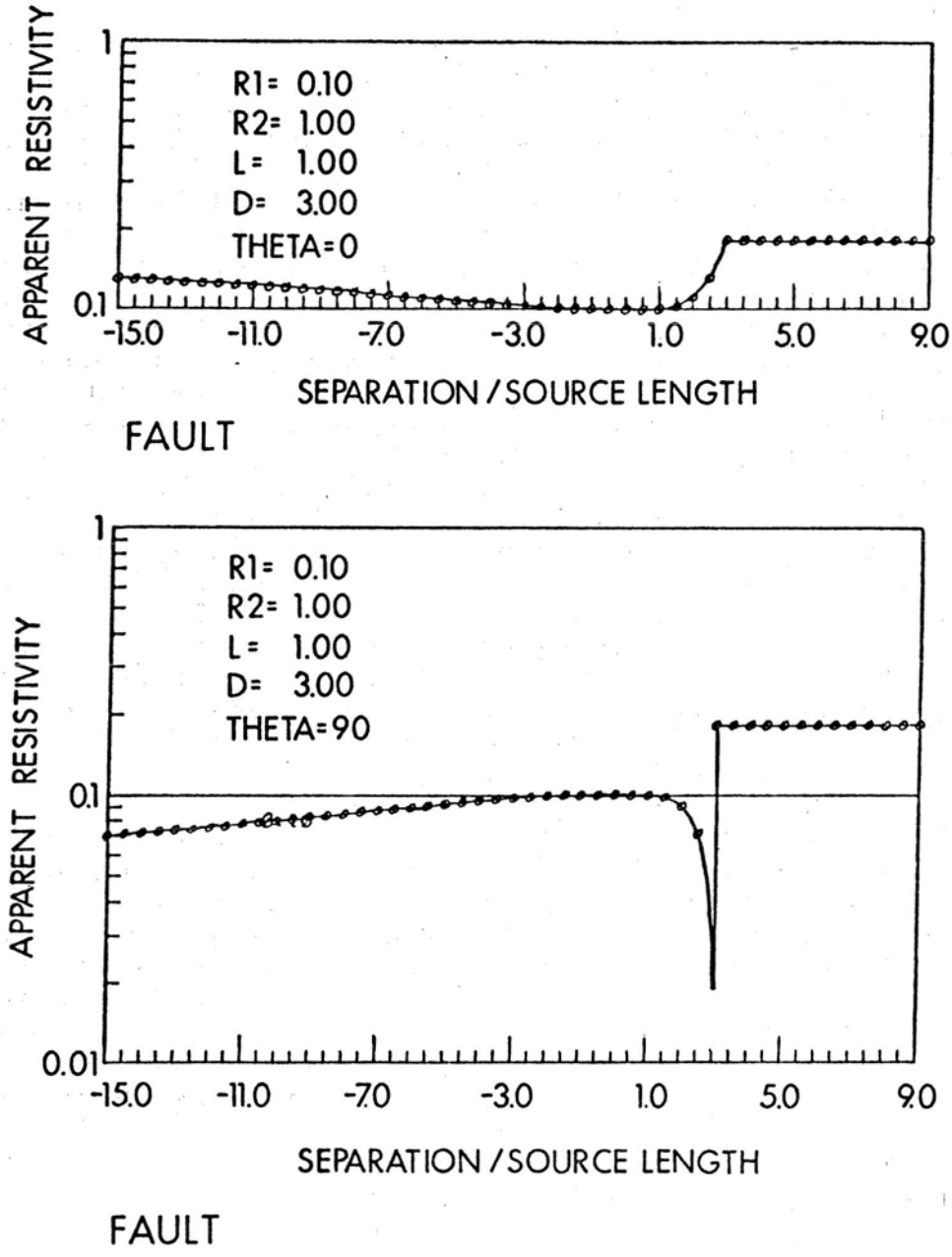

Figure 15. Apparent resistivity profiles for traverses crossing a boundary that separates two regions with tenfold different resistivities. The source is located on the conductive side of the boundary. The upper profile applies for the case in which the source is perpendicular to the boundary, while the lower profile applies in the case in which the source is parallel.

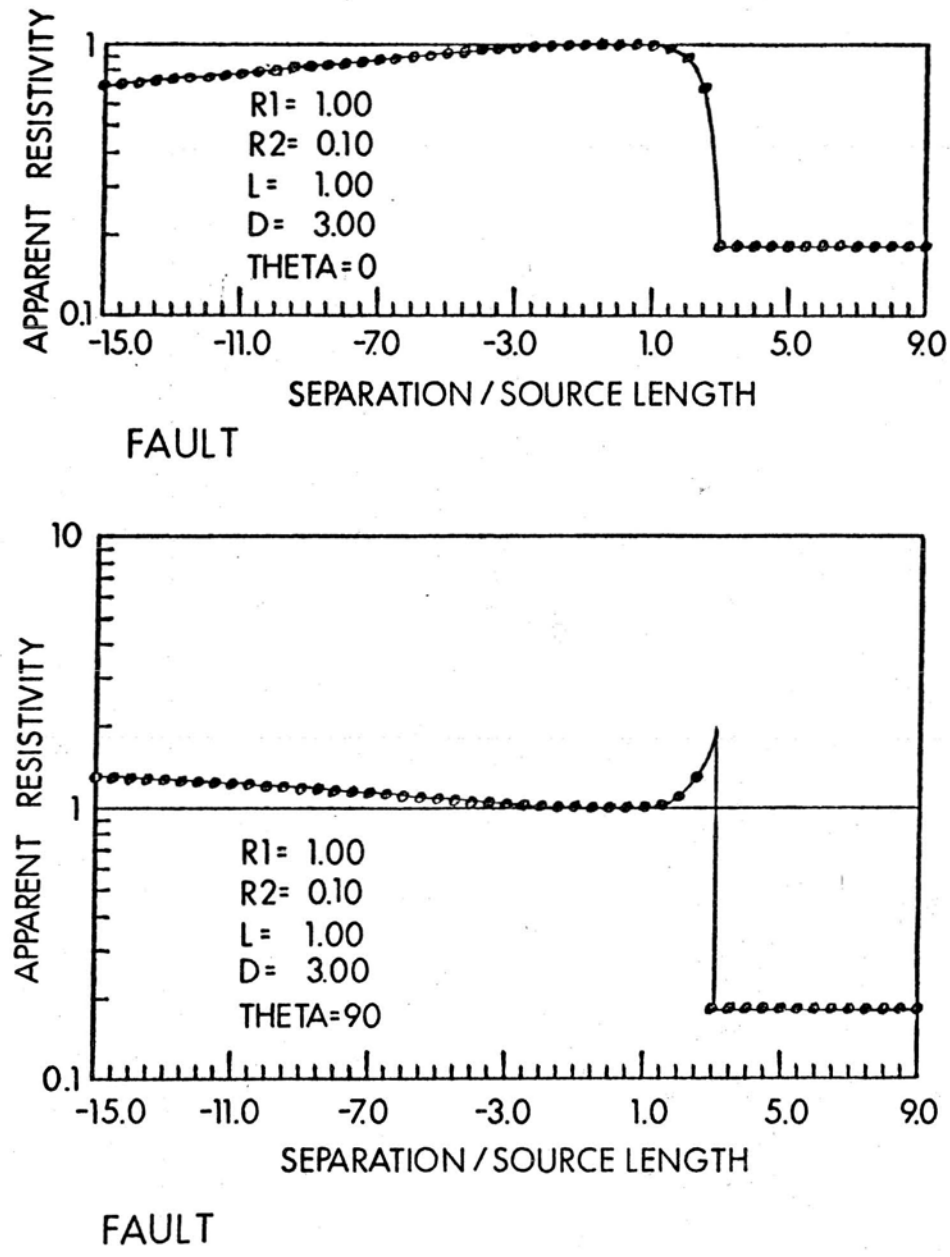

Figure 16. Apparent resistivity profiles for traverses crossing a fault that separates two regions with tenfold different resistivities. The source is located on the resistive side of the fault. The upper profile applies for the case in which the source is perpendicular to the fault, while the lower profile applies in the case in which the source is parallel.

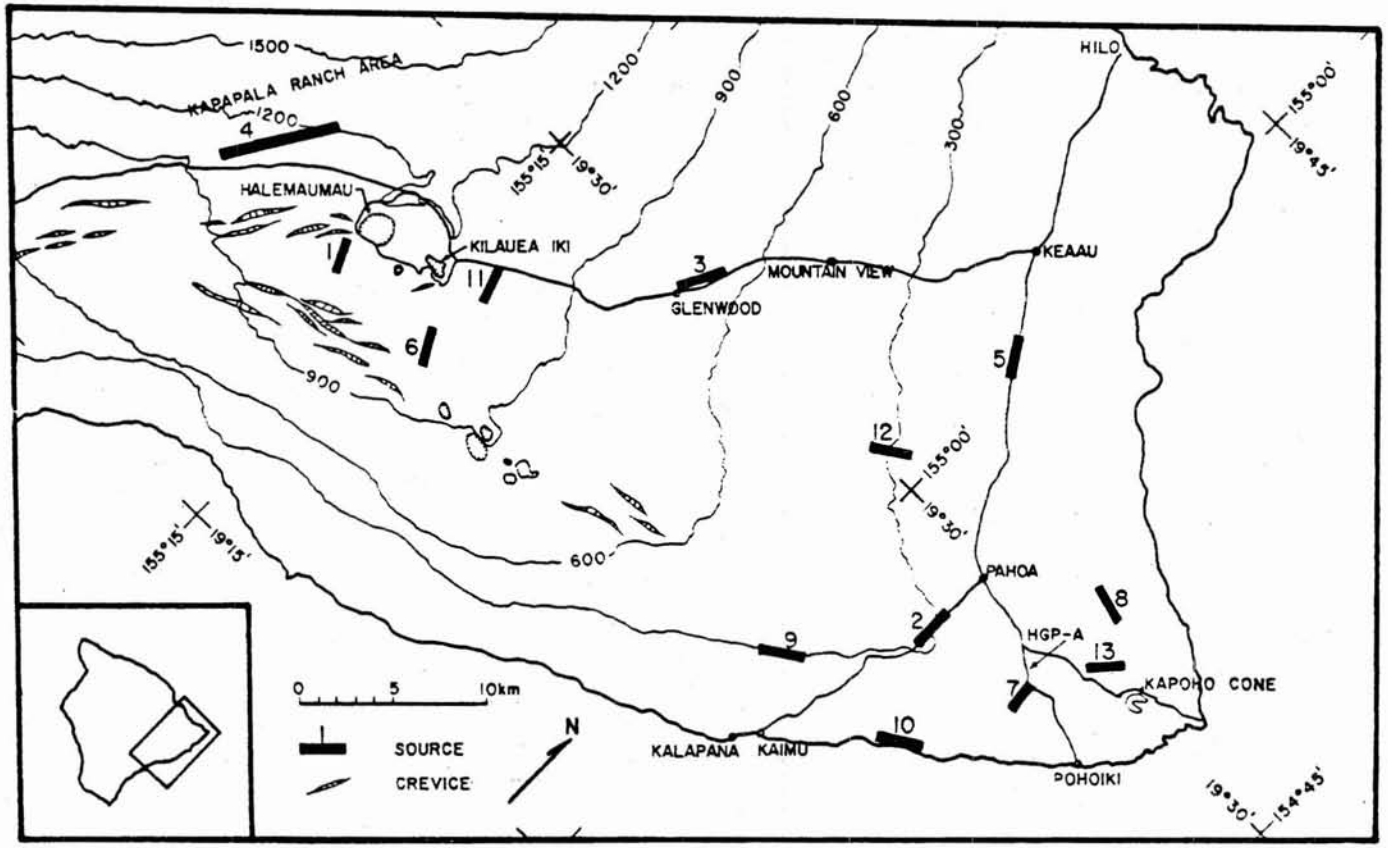

Figure 17. Source locations in the Puna and Ka'u districts.

Kilauea summit
R D
2K-5K 600m
6 200033

For the resistivity contour maps, a geometric progression of contoured intervals is used, that is, the contour levels are 2.5, 5, 10, 20, 40, 80, 150, 320 ohm-m. Considerable difficulties were caused by the presence of power lines along some of the major roads in the survey area. These power lines contained a neutral conductor grounded at intervals of 800 m or so. This gounded neutral conductor served to redistribute the normal current, causing a high resistivity anomaly along the power lines and for up to 400 m on either side of the lines. In the contour maps, these features are misleading, and should not be considered significant in terms of earth electrical structures.

Source 1 (Figs 18 and 19). Located at the summit of Kilauea volcano, a short distance south of Halemaumau Crater. Much of the area covered from this source lies within the Hawaiian Volcanoes National Park, and so cannot be considered a legitimate area for prospecting for commercial geothermal potential. However, this area includes the site of the Kilauea geothermal test well, drilled as part of a National Science Foundation-funded project, and at the time of this survey was the only location where detailed information was available on the electrical properties of rock at depth in Hawaii. Furthermore, it was necessary to determine whether or not the geothermal system associated with the summit acitvity of Kilauea might extend beyond the Park boundaries, where it might be exploited.

The source bipole was grounded at one end through the casing of the Kilauea test hole (the casing extended to 317-m depth, and had virtually no grounding resistance) and at the other end by lengths of pipe buried 30 to 60 cm deep in an ash deposit. Apparent resistivities measured from this source (Fig. 18) shows a strong elliptical pattern at distances less than a few kilometers about the source, with resistivity decreasing with distance. The lowest apparent resistivities are mapped at the easterly end of the southwest rift zone of Kilauea, with values of 3.5 to 4.0 ohm-m characterizing this anomalous area. Apparent resistivity values measured along the upper part of the East Rift, where there has been much recent volcanic activity, are only moderately low and are not obviously anomalous.

Apparent resistivity values as a function of distance from the source (Fig. 19) (the very low values observed along the southwest rift are deleted): These data may be interpreted as representing a surface layer of very high resistivity, between 2000 and 5000 ohm-m, extending to a depth of about 600 m. This is underlain in turn by rock with a resistivity of about 6 ohm-m extending to a depth of approximately 2000 m. The rock at greater depth appears to be much more resistant, but it is possible that the increase in apparent resistivity at the larger distances is caused by lateral changes in the resistivity of shallower rocks.

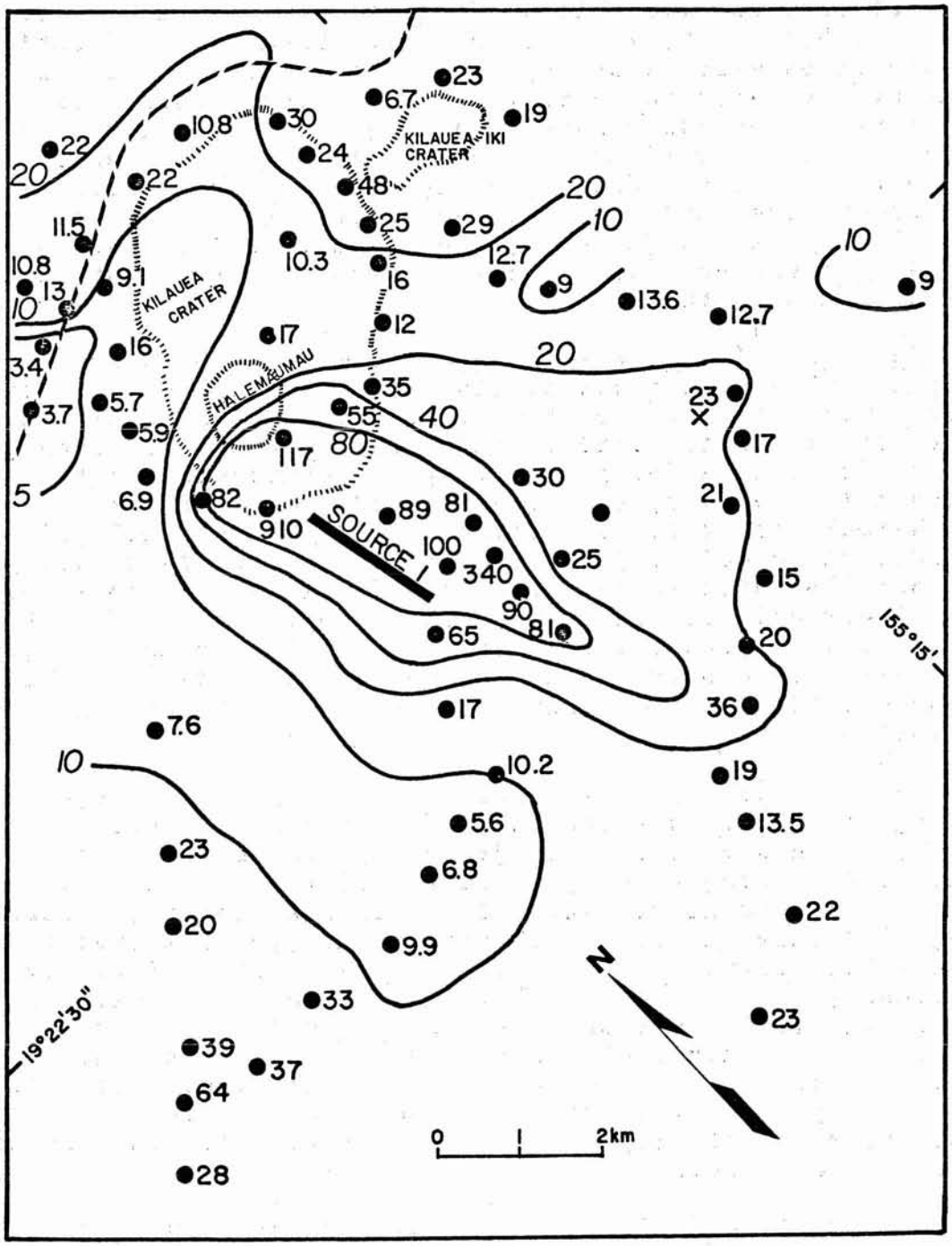

Figure 18. Apparent resistivity map about bipole source 1.

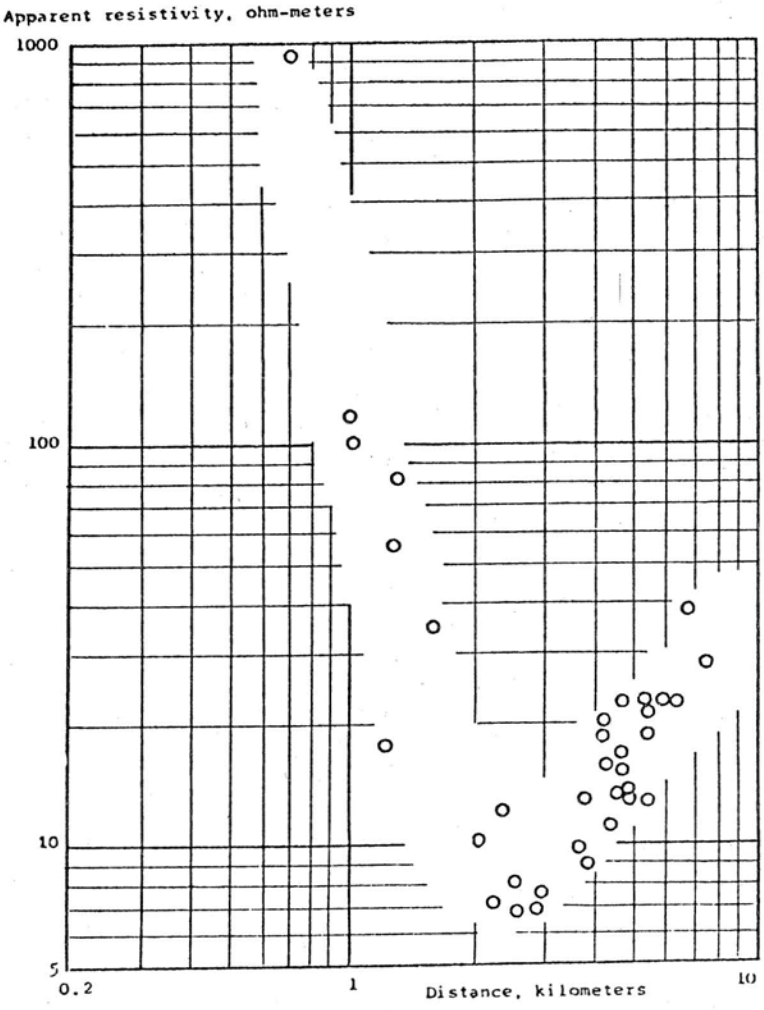

Figure 19. Apparent resistivity values measured from bipole source 1 plotted as a function of the distance to the nearer end of the source.

glenwood
DR D
700 3.2 km
36, 15(?)

Source 2 (Fig. 20). Located south of Pahoa on the road to Kaimu. This source was grounded at the south end through the casing of a geothermal well drilled in the early 1960's and at the north end through stakes driven into the ground. The apparent resistivity contours (Fig. 20) were not extended to include many of the measurements around Pahoa; the very high values of apparent resistivity observed in that area are erroneous, caused by a grounded neutral on the power line passing through Pahoa. An elliptical pattern characteristic of a surface layer with high resistivity may be seen for the measurements made within a kilometer's distance from this source, but the pattern is strongly distorted by other effects. Of greatest interest is the region of low resistivity just downhill from the rift zone, an area where the resistivities are less than 10 ohm-m.

No plot of apparent resistivity as a function of distance is included for the measurements made from source 2. The strong lateral changes in resistivity mask the effect of horizontal layering to such an extent that such a plot is not meaningful.

Source 3 (Figs. 21, 22, and 23). Located along the Volcano highway, in the vicinity of Glenwood. The source was grounded at both ends through highway culverts. Because of the relatively high current obtained, and because of the high apparent resistivities measured, a considerable area was covered by this source. The most impressive feature of the data from this source is the generally high apparent resistivity (Fig. 21). However, there appear to be boundaries separating this area of high resistivity from areas of lower resistivity in both directions, toward Kilauea caldera and toward Hilo.

Apparent resistivity as a function if distance (Figs. 22 and 23): The first was based on measurements in the uphill (southwest) direction. These data form a pattern that can be interpreted as indicating the presence of a surface layer with a resistivity of about 700 ohm-m extending to a depth of about 3.2 km. This layer is probably underlain by material with a resistivity of about 15 ohm-m, although even the measurements made at a distance of 10 km from the source are not far enough from the source to provide a definitive value for the second-layer resistivity.

Measurements in the downhill direction (northeast, Fig. 23) from this source show similar behavior, except that the depth to conductive rocks appear to be greater, in the range from 3.5 to 4 km. It is possible that no conductive rocks underlie this area and that the decrease in apparent resistivity with distance represents a lateral change in resistivity.

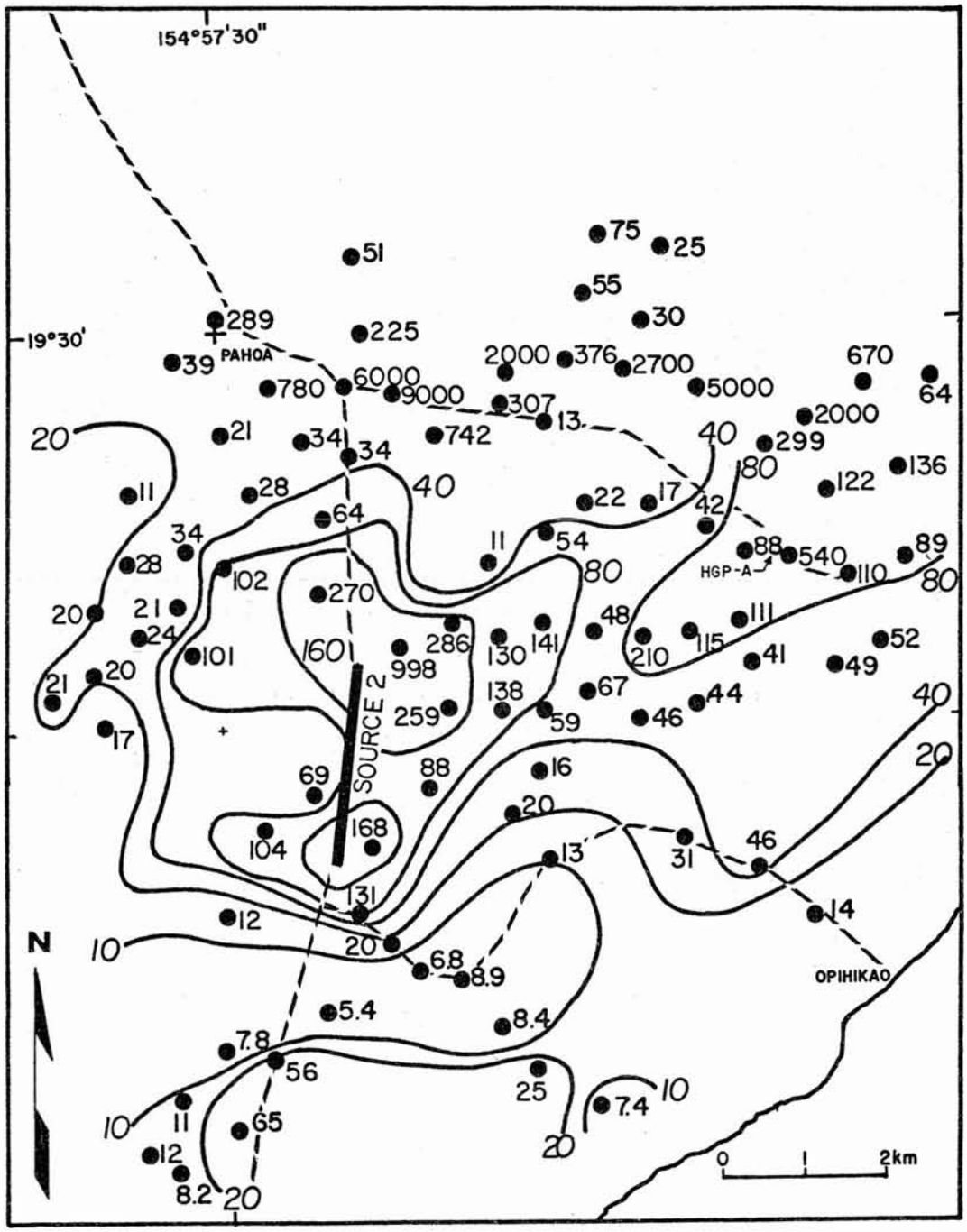

Figure 20. Apparent resistivity map about bipole source 2.

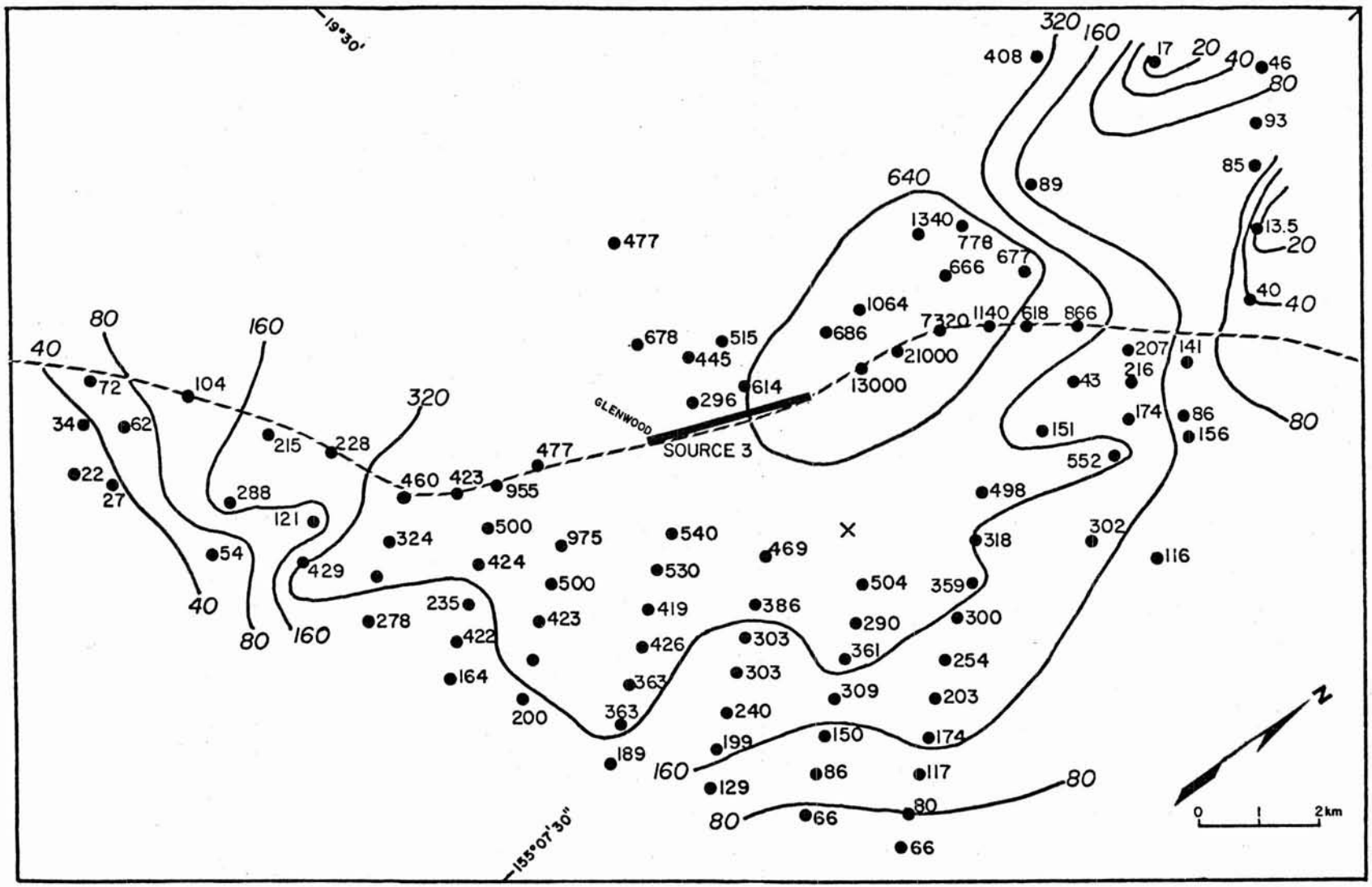

Figure 21. Apparent resistivity map for measurements made from source 3.

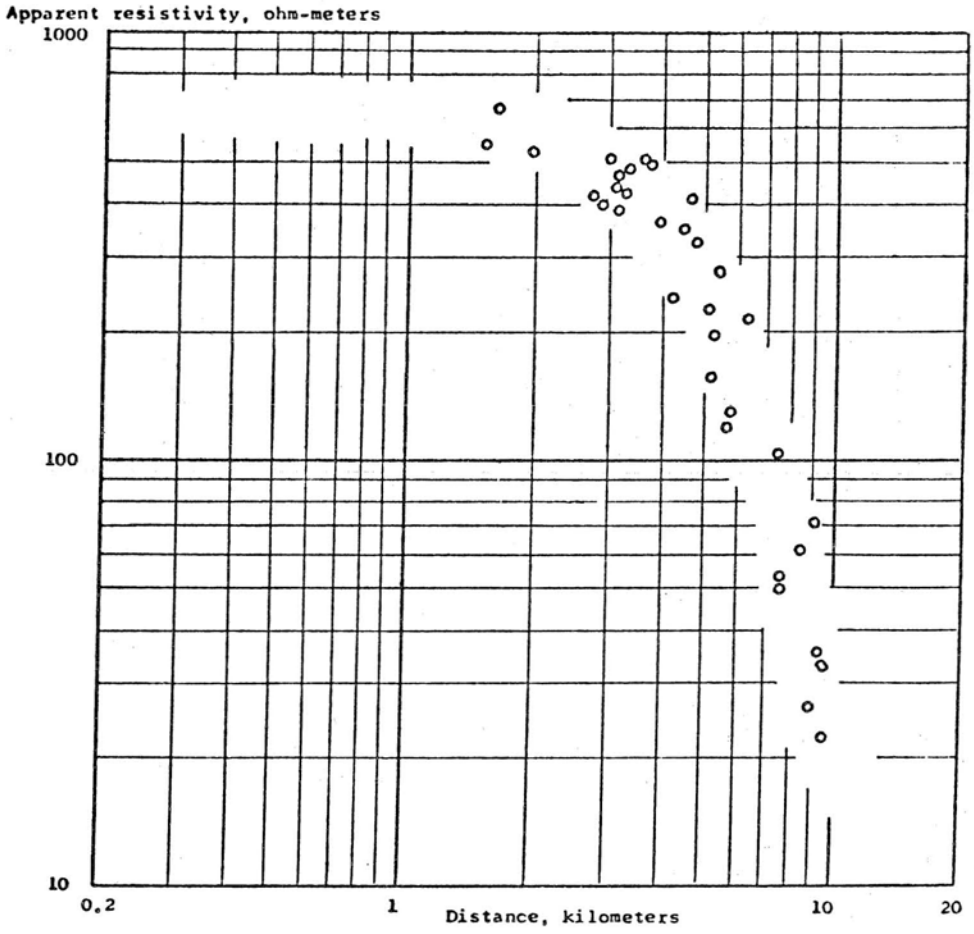

Figure 22. Apparent resistivity values plotted as a function of distance measured in the direction toward Kilauea Volcano from source 3.

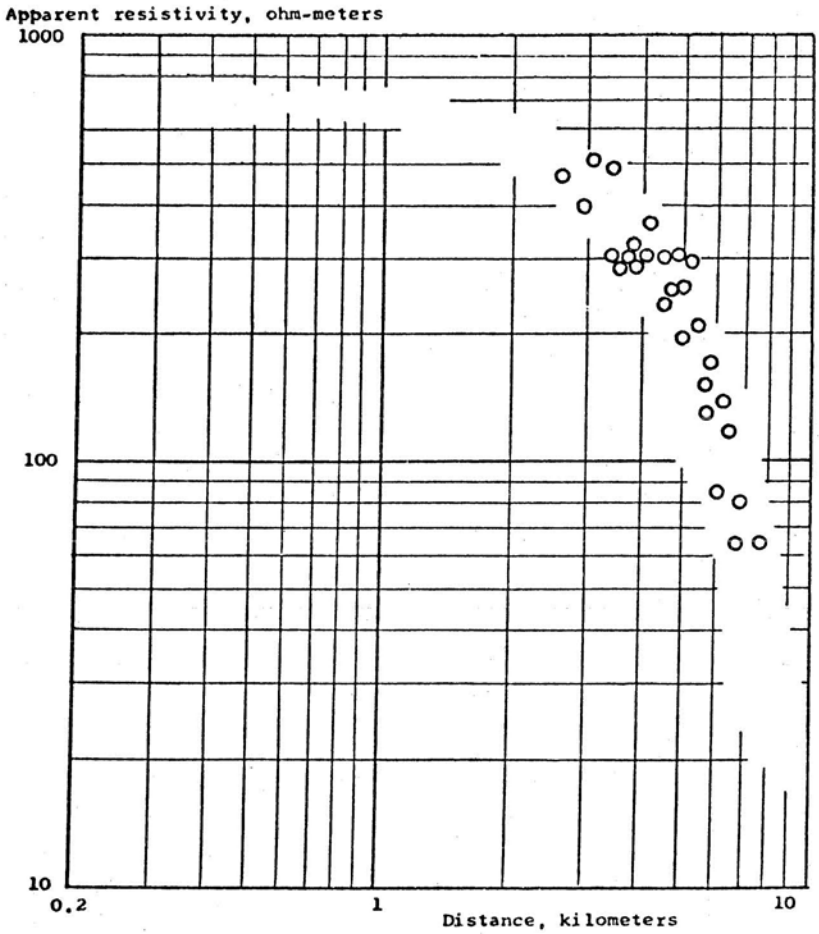

Figure 23. Apparent resistivity as a function of distance in the direction toward Hilo and Puna from source 3.

Source 4 (Figs. 24, 25, and 26). Located on the Kapapala Ranch, just outside the boundaries of Hawaii Volcanoes National Park. This dipole was about eight km long. It had been installed in 1969 as part of an electromagnetic sounding survey over the summit of Kilauea volcano (Jackson and Keller, 1972); fortunately, the heavy cable connecting the electrodes was still in place. The high current obtained and the high values of apparent resistivity measured allowed a large area to be covered from this source. No pronounced ellipticity is apparent in the data (Fig. 24), indicating that the behavior of the apparent resistivity values is not dominated by the effects of horizontal layering. The principal feature of the map is a rapid gradient in resistivity toward the southwest rift of Kilauea. This gradient is probably caused by a fault-like change in resistivity, with the line of delineation following the northern edge of Kilauea caldera and connecting with the boundary of a similar zone seen from source 3 at Glenwood. There is an area of moderately low resistivity extending southward from Halemaumau that is probably associated with the geothermal system beneath Kilauea summit. The values of apparent resistivity in the vicinity of Kilauea caldera seen from source 4 are somewhat higher than those seen from source 1. The difference is probably caused by the greater distance at which measurements were made using source 4, so that the influence of resistive basement rocks is greater for source 4 measurements.

Apparent resistivity as a function of distance (Fig. 25 and 26): Figure 25 includes only the values of apparent resistivity measured along the slopes of Mauna Loa, extending southwest. Also values in excess of 1000 ohm-m are not included; many of these values were caused by leakage of current along water pipe lines on the Kapapala Ranch. The behavior of the values used indicates that resistivity decreases gradually from values of aobut 2000 ohm-m in the near surface to values of about 30 to 50 ohm-m at depths beyond 3 km.

Measurements over Kilauea Volcano southeast from the source, (Fig. 26) show a rapid decrease in apparent resistivity at distances up to 4 km. The rate of change is too rapid to be a fault-like contact at 3.3-km distance from source 4. Measurements at distances beyond 3.3 km show a proportional increase of apparent resistivity with distance. This behavior probably represents the effect of resistive basement rock. If the resistivity of rocks above this level is 10 ohm-m, the depth to basement beneath Kilauea Summit would be approximately 2.5 km.

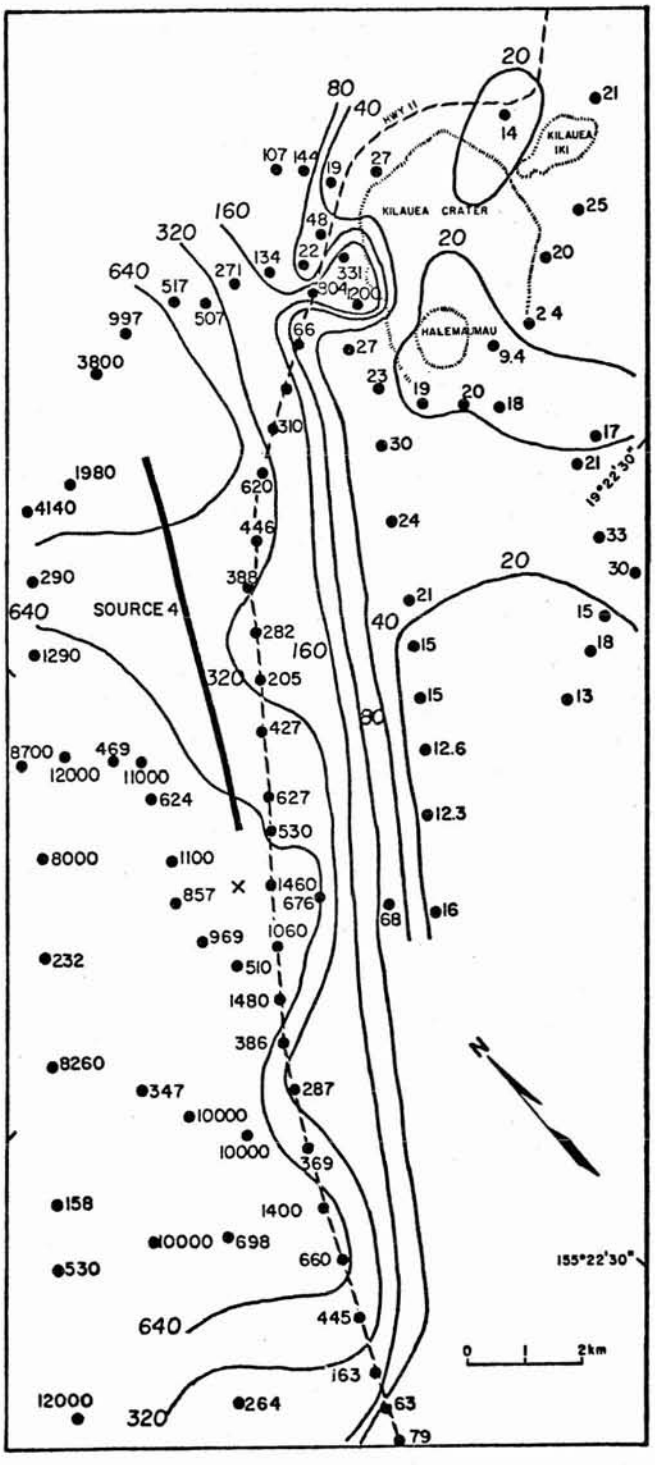

Figure 24. Apparent resistivity map for measurements made from source 4.

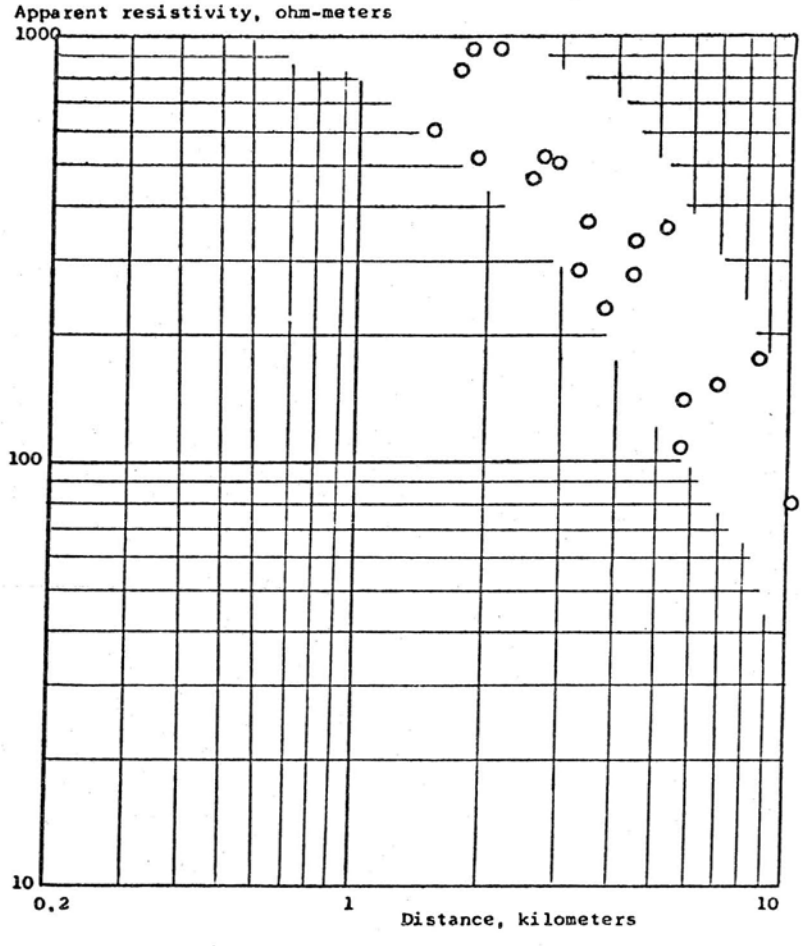

Figure 25. Apparent resistivity as a function of distance toward Pahala from source 4.

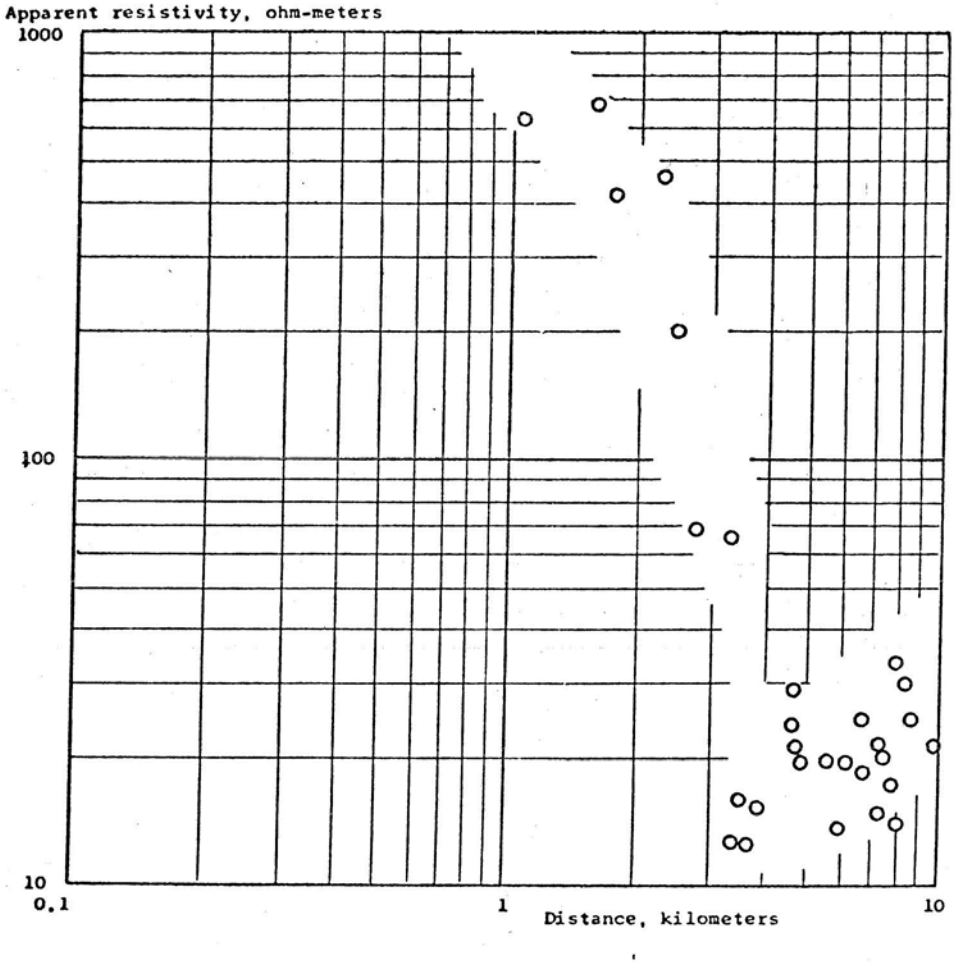

Figure 26. Apparent resistivity as a function of distance from source 4.

Keaau - Pahoa
500Ω to 400-500m
7Ω - 2 Km
7 - 2 Km 45
7000Ω

Source 5 (Figs. 27, 28, and 29). Located along the road from Keaau to Pahoa. Metal posts along the road were used for grounds. The apparent resistivities measured from this source are shown on Figure 27. The resistivities measured from this source were generally low, about 10 ohm-m, except for those values measured in the direction of Mountain View toward the west. Here, resistivities above 40 ohm-m were measured at distances even greater than 6 km from the source. These high values probably represent the presence of the same high resistivity mass seen from source 3. A few low values were observed in the direction of Pahoa, but these values may not be reliable. Some of the other sources indicate a resistant region near the locations where these low values were observed, and it is likely that the low seen here is an example of an erroneously low resistivity measured on the side of a high resistivity boundary facing the source. The very high values of resistivity measured along the Keaau-Pahoa road and the Volcano highway are caused by a grounded neutral line on the power distribution system.

Apparent resistivity as a function of distance (Figs. 28 and 29): The data in Figure 28 were measured at stations to the north and seaward from the source. These data indicate a surface layer with a resistivity of several hundred ohm-m extending to a depth of 400 to 500 m. This is underlain by rock with a resistivity of 7 to 8 ohm-m extending to a depth of approximately 2000 m. Rock at greater depth appears to have a high resistivity.

In Figure 29, data from stations to the south of the source and uphill show behavior is similar to that exhibited by the data in Figure 28 but the conductive layer appears to lie at a shallower depth of approximately 1.7 km.

Source 6 (Figs. 30 and 31). Located along the Escape Road, which parallels the upper east rift of Kilauea within the Hawaii Volcanoes National Park. It was located to examine the possible extension of the low resistivity area under Kilauea crater to the east near Kilauea Iki or along the east rift. Ground contacts were made through lengths of buried pipe, but grounding resistance was very high. Only limited measurements could be made from this source (Fig. 30). A strong elliptical pattern for the resistivity contours is apparent. No particularly low resistivity values were measured in the target areas for this dipole.

A plot of apparent resistivity as a function of distance is shown in Figure 31. These data indicate a high surface

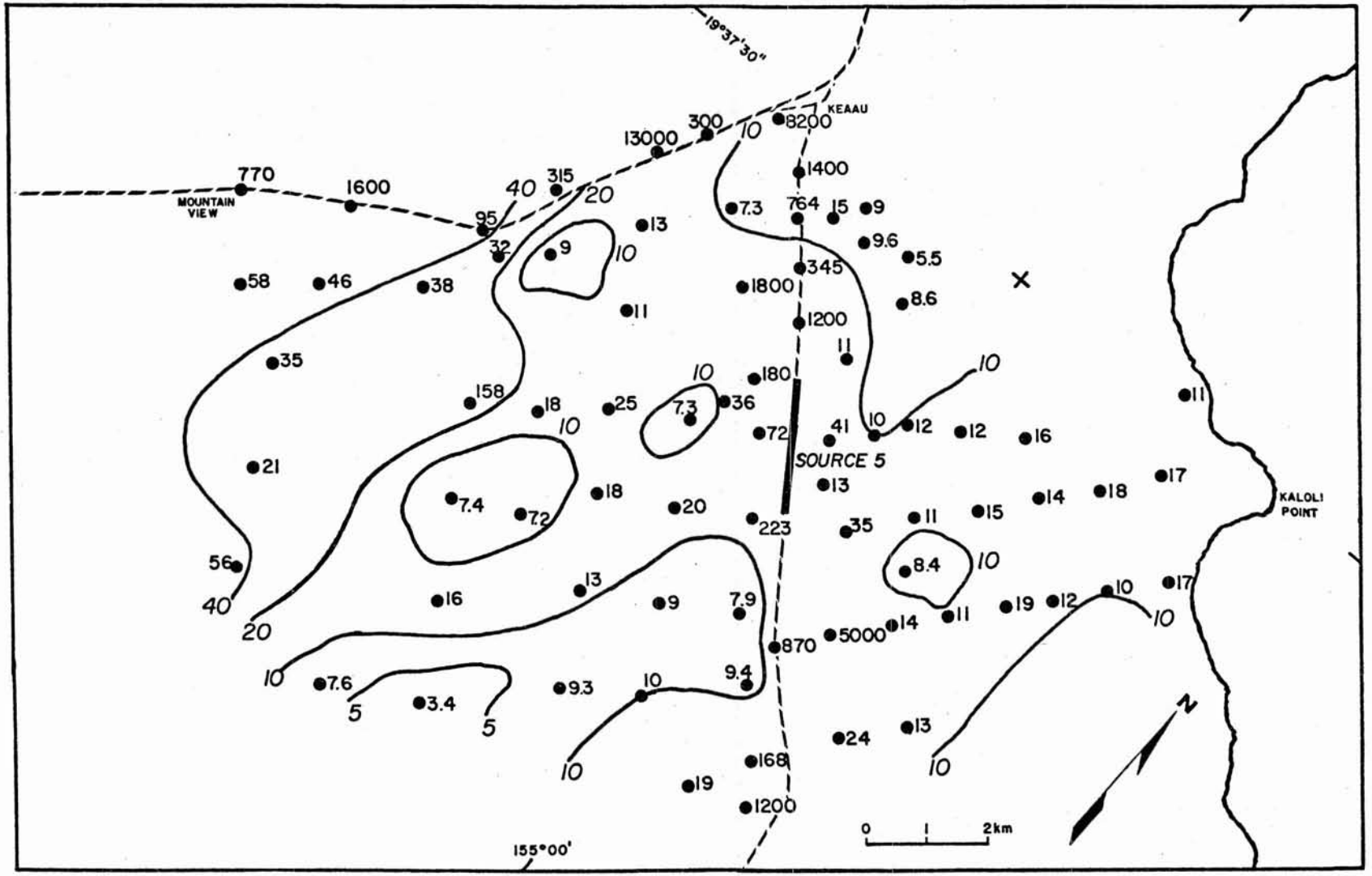

Figure 27. Apparent resistivity values measured from source 5, located on the road from Keaau to Pahoa.

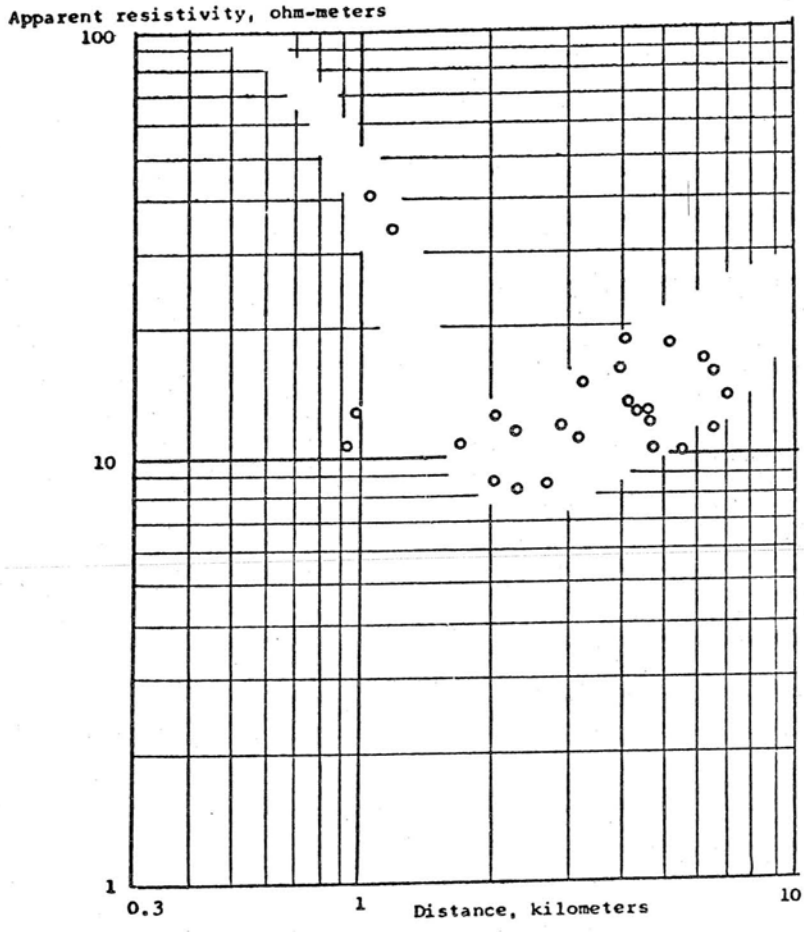

Figure 28. Apparent resistivity as a function of distance seaward from source 5.

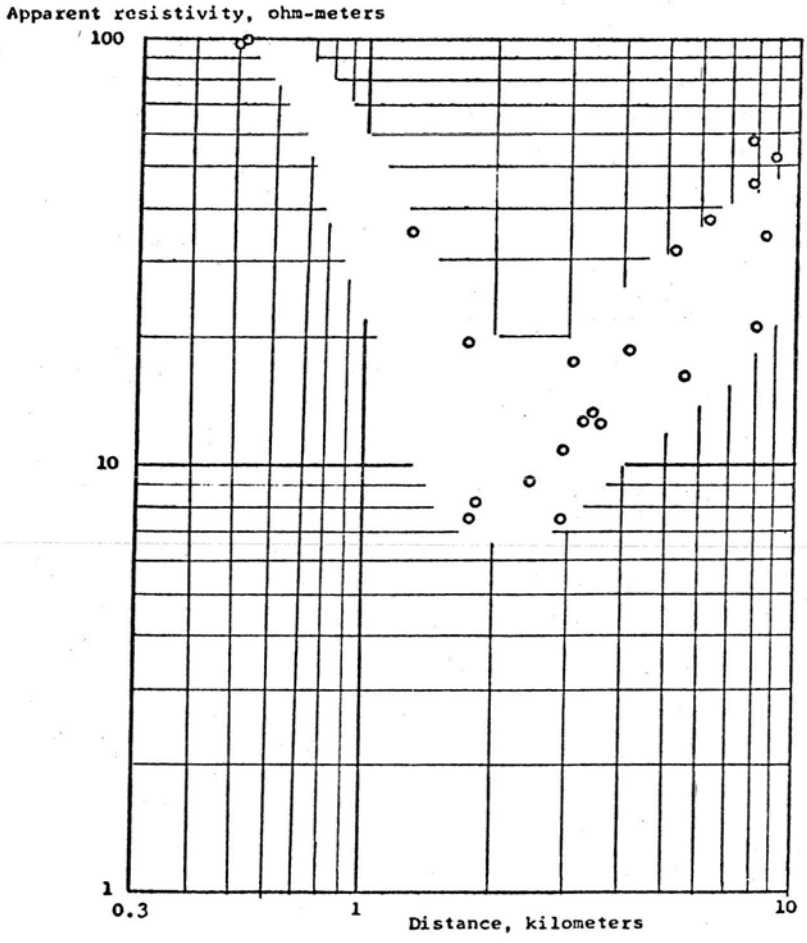

Figure 29. Apparent resistivity values as a function of distance uphill from source 5.

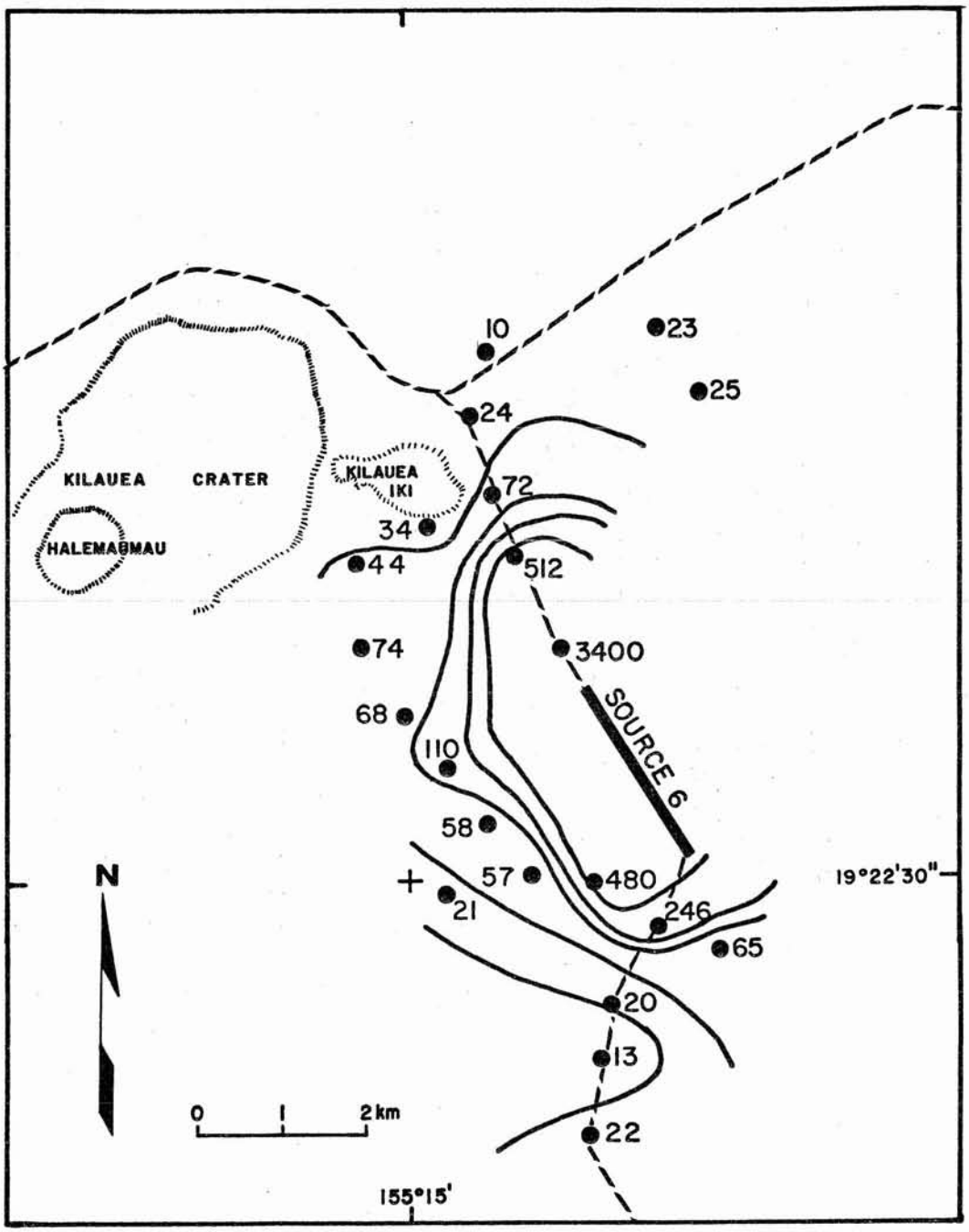

Figure 30. Apparent resistivity map measured from source 6.

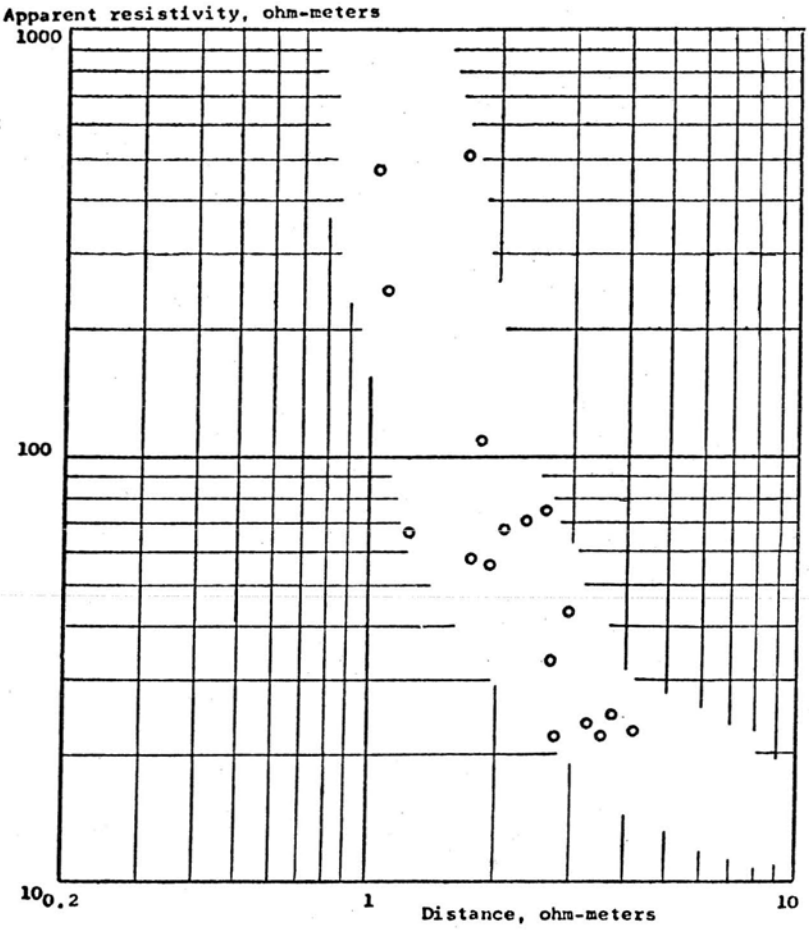

Figure 31. Apparent resistivities plotted as a function of distance from source 6.

resistivity, greater than several thousand ohm-m, probably extending to a depth of 1.0 to 1.3 km. The resistivity at greater depths is probably between 10 and 20 ohm-m, but measurements could not be made at a great enough distance to provide a definitive value.

Source 7 (Figs. 32, 33 and 34). Location on the seaward side of the east rift zone of Kilauea, just off the road connecting Pahoa and Pohoiki (Fig. 32). One ground contact was the casing of a water well on the University of Hawaii Agricultural Experiment Station; the other was lengths of pipe buried in the ground. Low resistivities were measured along the seaward side of the rift, while higher resistivities were measured about Kapoho cone and on the uphill side of the rift, particularly uprift from an offset of the surface expression of the rift that is apparent in the vicinity of the recently drilled geothermal hole, HGP-A.

Apparent resistivity values are plotted as a function of distance on Figure 33, which shows data obtained along the lower (northeast) part of the east rift around Kapoho crater, and Figure 34, which shows data obtained in the uprift (southwest) direction. The plots are similar but differ from most of the preceeding cases in that no high resistivity surface layer is recognized. This is probably a consequence of the low elevation of these measurements. The downrift data (Fig. 33) indicate a surface layer with a resistivity of approximately 20 ohm-m extending to a depth of about 600 m. This zone is underlain by rock with a resistivity of about 8 ohm-m extending to a depth of 2.1 to 2.3 km. Rock at greater depth is more resistant. The uprift data (Fig. 34) indicate the same surface layer, but the rock at depth appears to have a resistivity of about 5.5 ohm-m. It extends to about 2.1 to 2.3 km depth before more resistant rock is seen.

Source 8 (Figs. 35 and 36). Located north of Pahoa. Both ends of the source bipole were grounded through lengths of buried pipe. Only a small amount of current could be obtained; this, combined with the low resistivity measured in this area, made the coverage obtainable from this source quite small. The apparent resistivities are shown on Figure 35. A noteable feature is the low resistivity measured on the Hilo-side edge of the east rift near Kapoho crater. The rest of the resistivity values are only moderately low, and coincide with the measurements in the same general area from source 5.

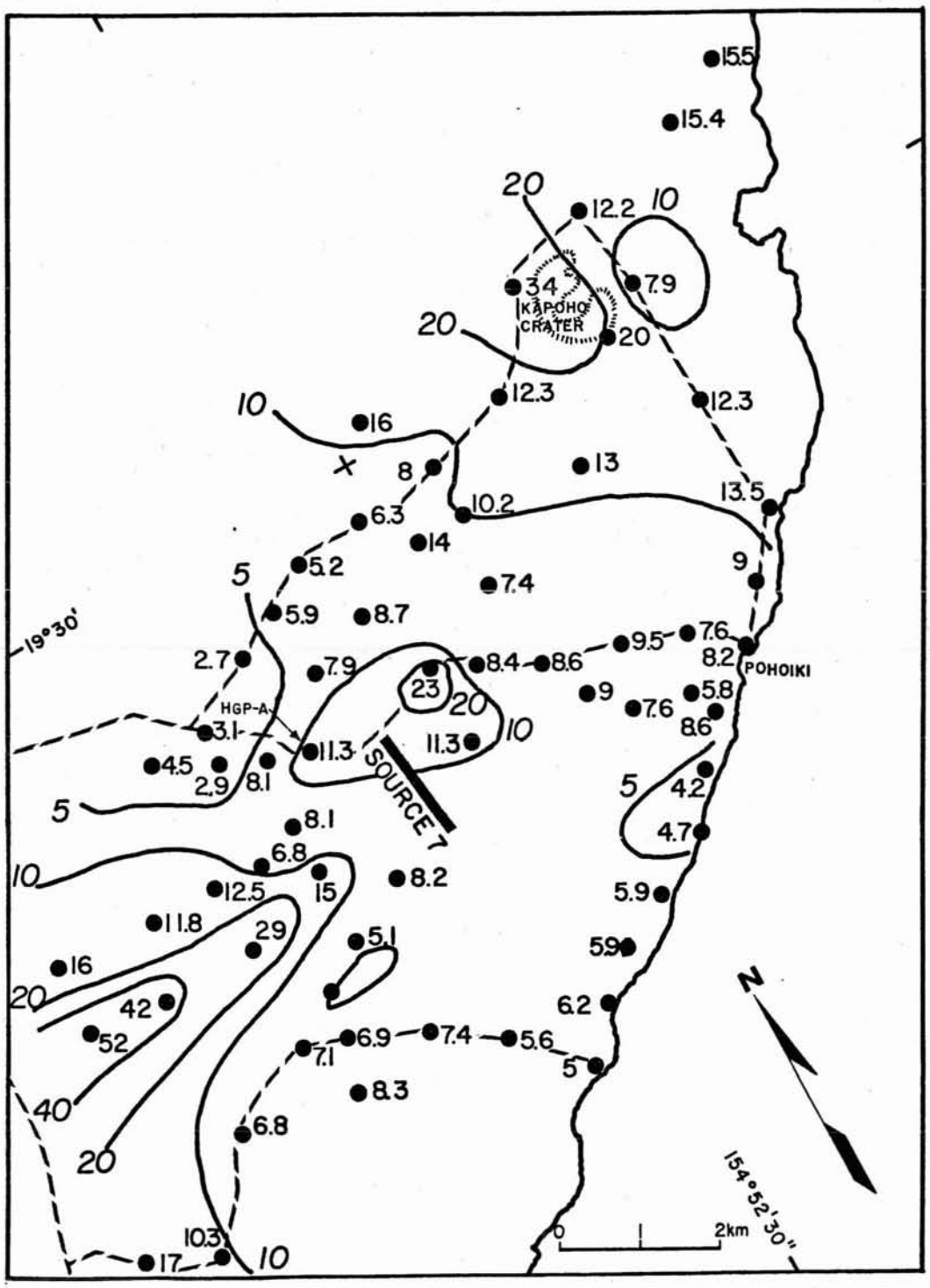

Figure 32. Apparent resistivities measured about source 7.

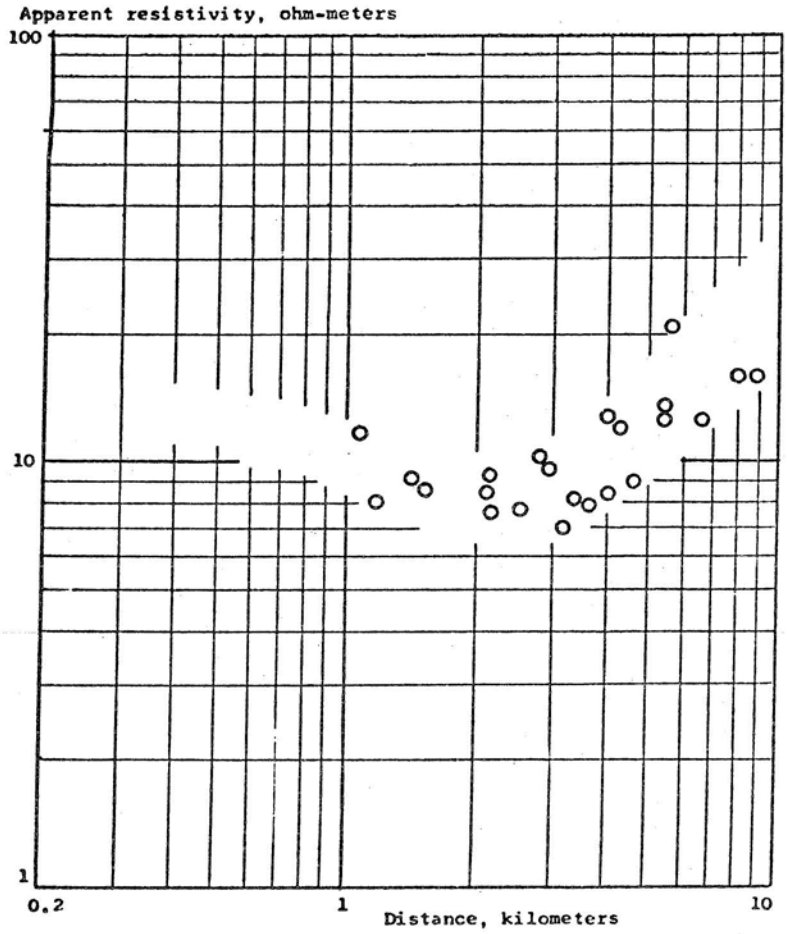

Figure 33. Apparent resistivity plotted as a function of distance downrift from source 7.

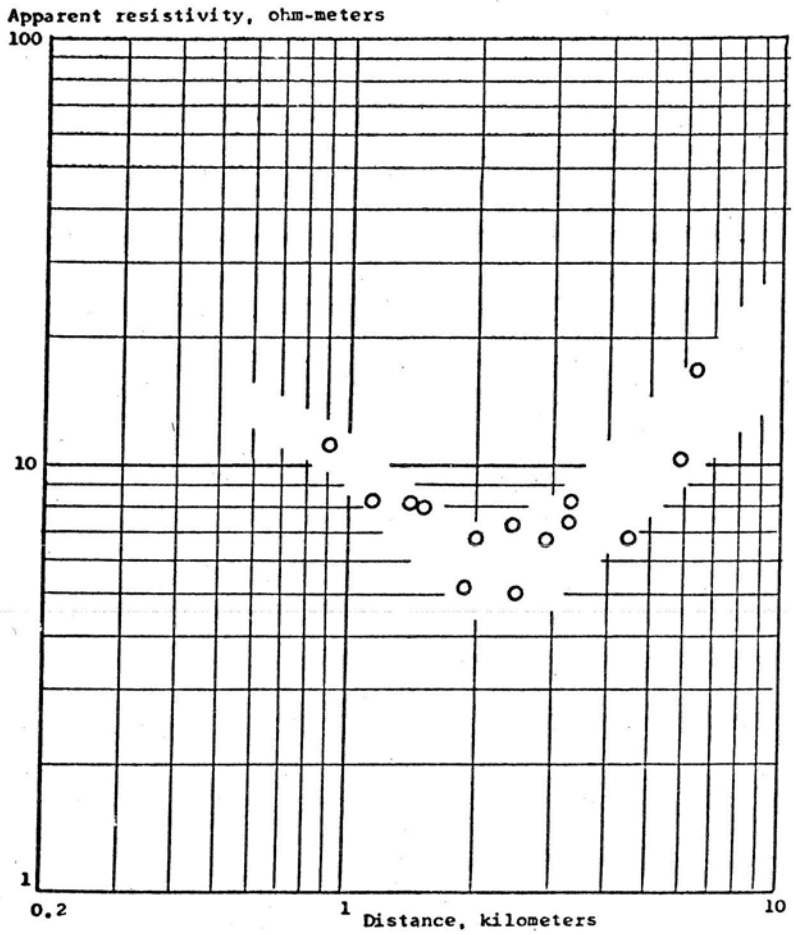

Figure 34. Apparent resistivity as a function of distance uprift from source 7.

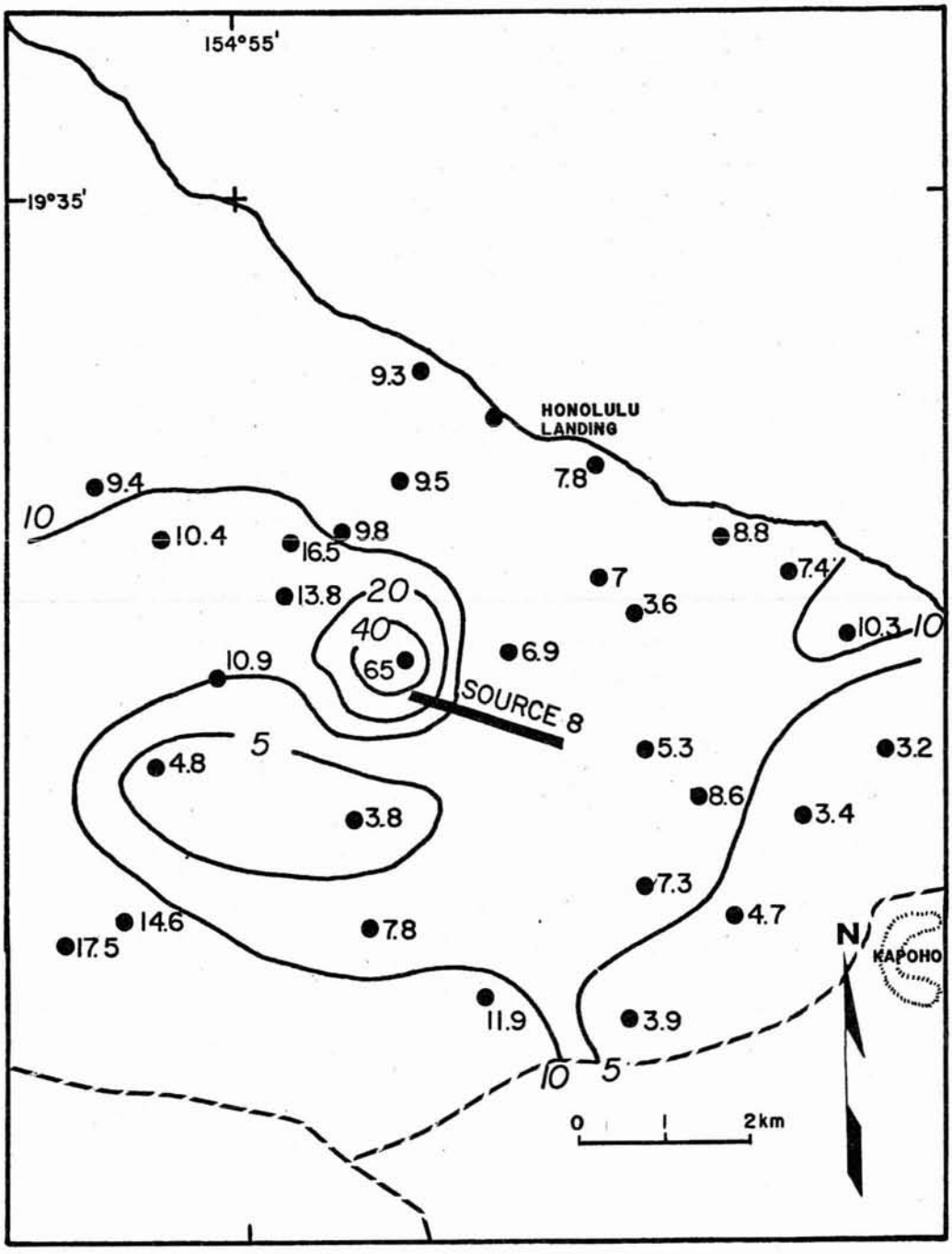

Figure 35. Apparent resistivities measured about source 8.

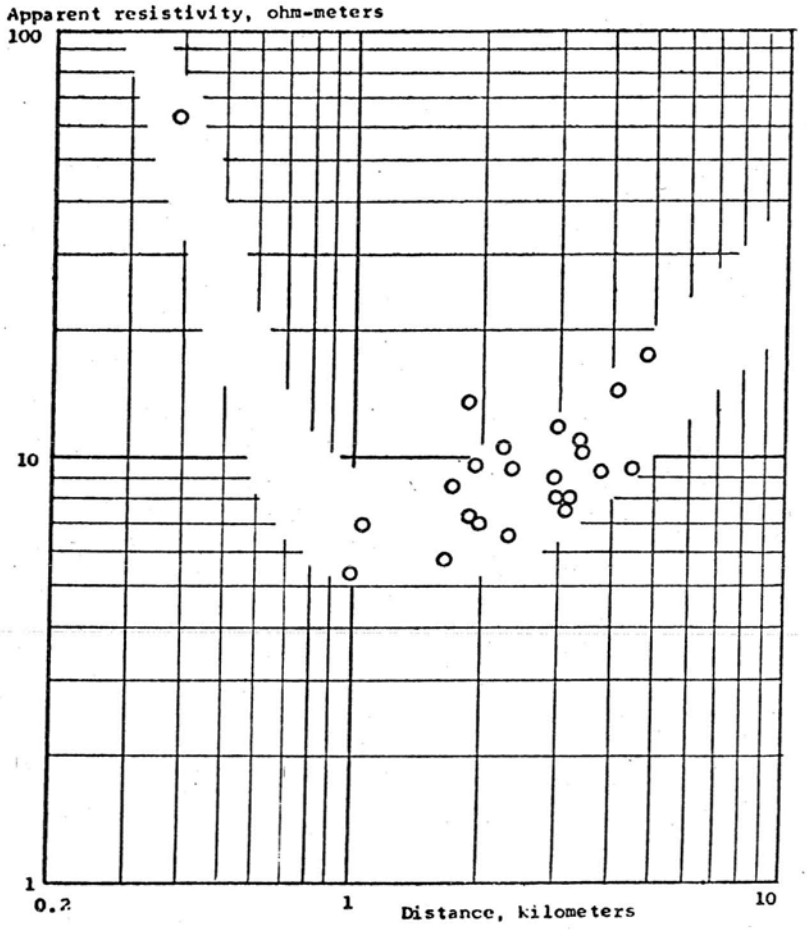

Figure 36. Apparent resistivity as a function of distance from source 8.

Apparent resistivity values measured from source 8 are plotted as a function of distance on Figure 36. A thin high-resistivity layer is indicated at the surface, with a resistivity of several hundred ohm-m, extending to a depth of about 300 m. The resistivity beneath this layer appears to be approximately 6 ohm-m, and it extends to a depth of about 1.6 to 1.8 km. Material at greater depths has a higher resistivity.

Source 9 (Fig. 37). Located along a back road paralleling the east rift of Kilauea several kilometers inland from Kalapana. Buried pipe was used for ground contacts at both ends of the source, and only limited current could be obtained. This source was located to investigate the low resistivity zone south of source 2 from outside the low resistivity zone (Fig. 37). High resistivities were measured from the southwest end of this source; the boundary to the low resistivity area that was the target for this source appears to lie along the Kaimu-Pahoa road. No plot of the apparent resistivity as a function of distance is included because of the strong lateral changes in resistivity apparent from these data.

Source 10 (Fig. 38). Located along the Kaimu-Pohoiki coastal road, with electrodes placed in tidal ponds along the shore. The sea has a profound effect on the measurements as seen by the low values of apparent resistivity. The intent of this source was to locate the seaward boundary of the low resistivity zone recognized in this area from sources 2 and 9, however, the low values must be viewed with suspicion because of the effect of the sea. Nevertheless, the presence of a low resistivity zone inland from the coast seems to be verified.

Because of the distortion of the current field caused by the presence of the ocean, no plot of apparent resistivity values as a function of distance is included.

Source 11 (Figs. 39 and 40). Located just outside the north entrance of Hawaii Volcanoes National Park in a possible area of low resistivity in the vicinity of Kilauea Iki and the upper east rift of Kilauea volcano. Contacts were made through buried lengths of pipe. Only a small amount of current was obtained, which limited the areal coverage. High resistivities were observed near the source. There is a rapid gradient in resistivity in going into the Kilauea caldera area, as had been noted in measurements from sources 3 and 4. No particularly low values were noted around Kilauea Iki or along the upper east rift.

Apparent resistivities as a function of distance from the source (Fig. 40): The behavior is similar to that seen

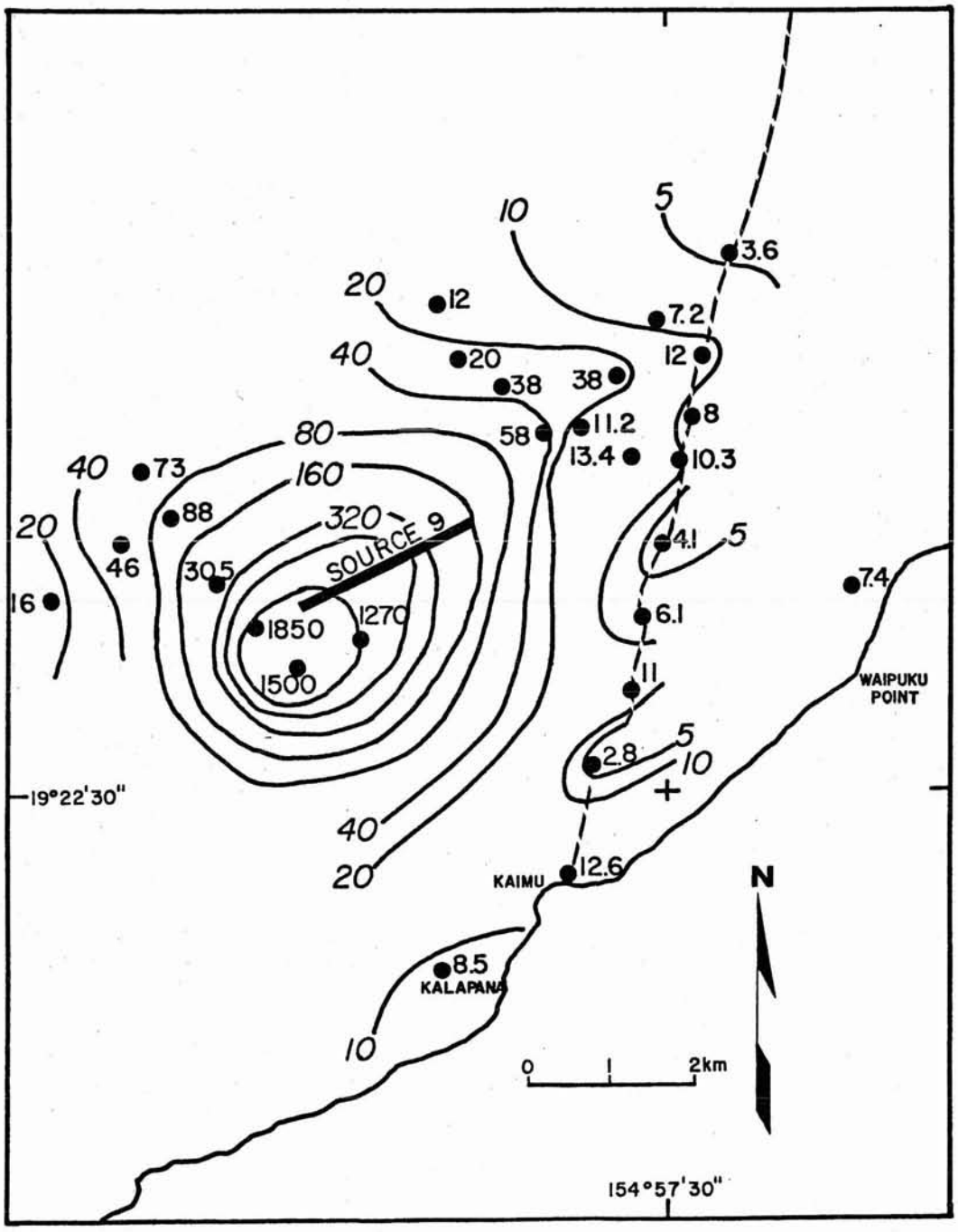

Figure 37. Apparent resistivities measured from bipole source 9.

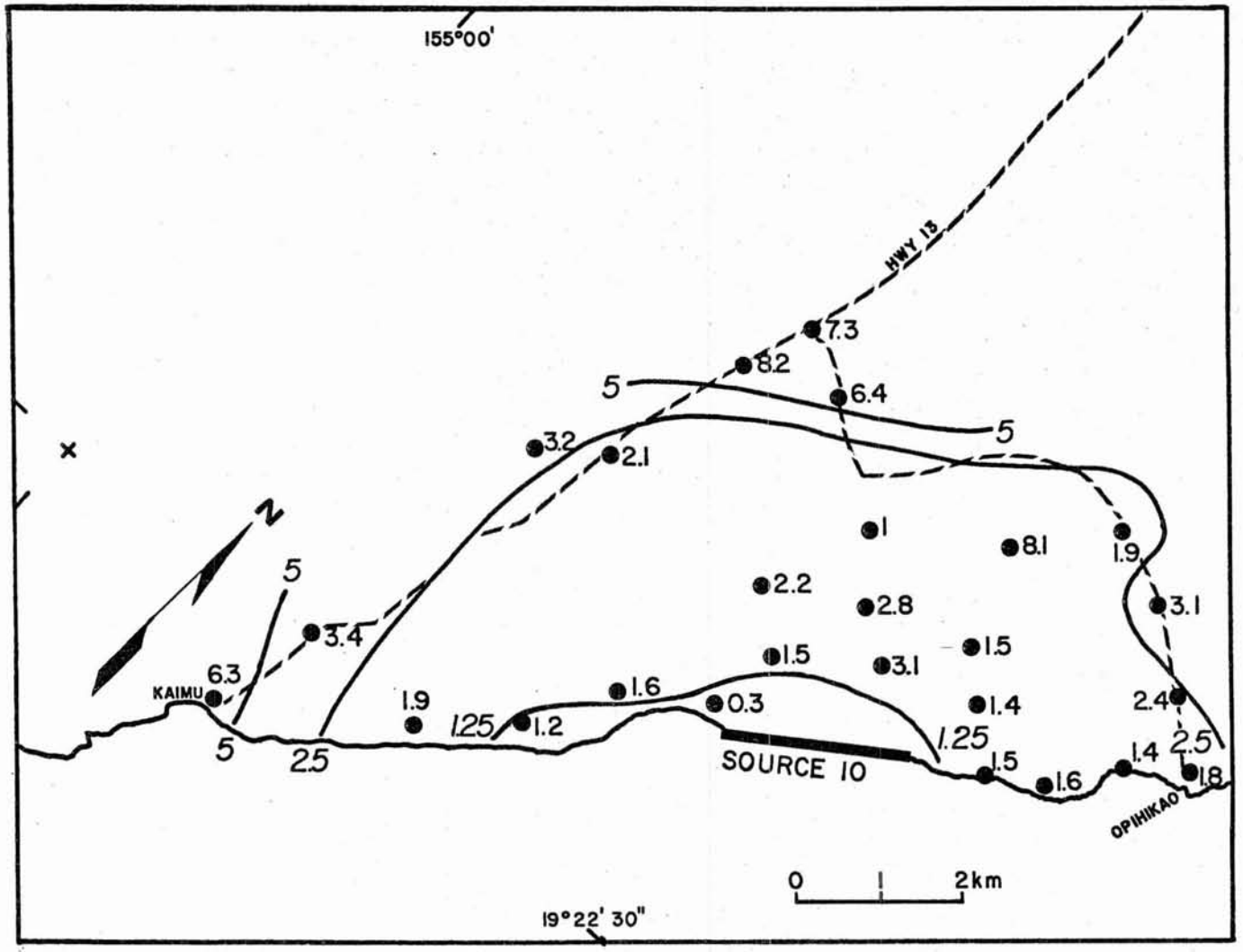

Figure 38. Apparent resistivity values measured from source 10.

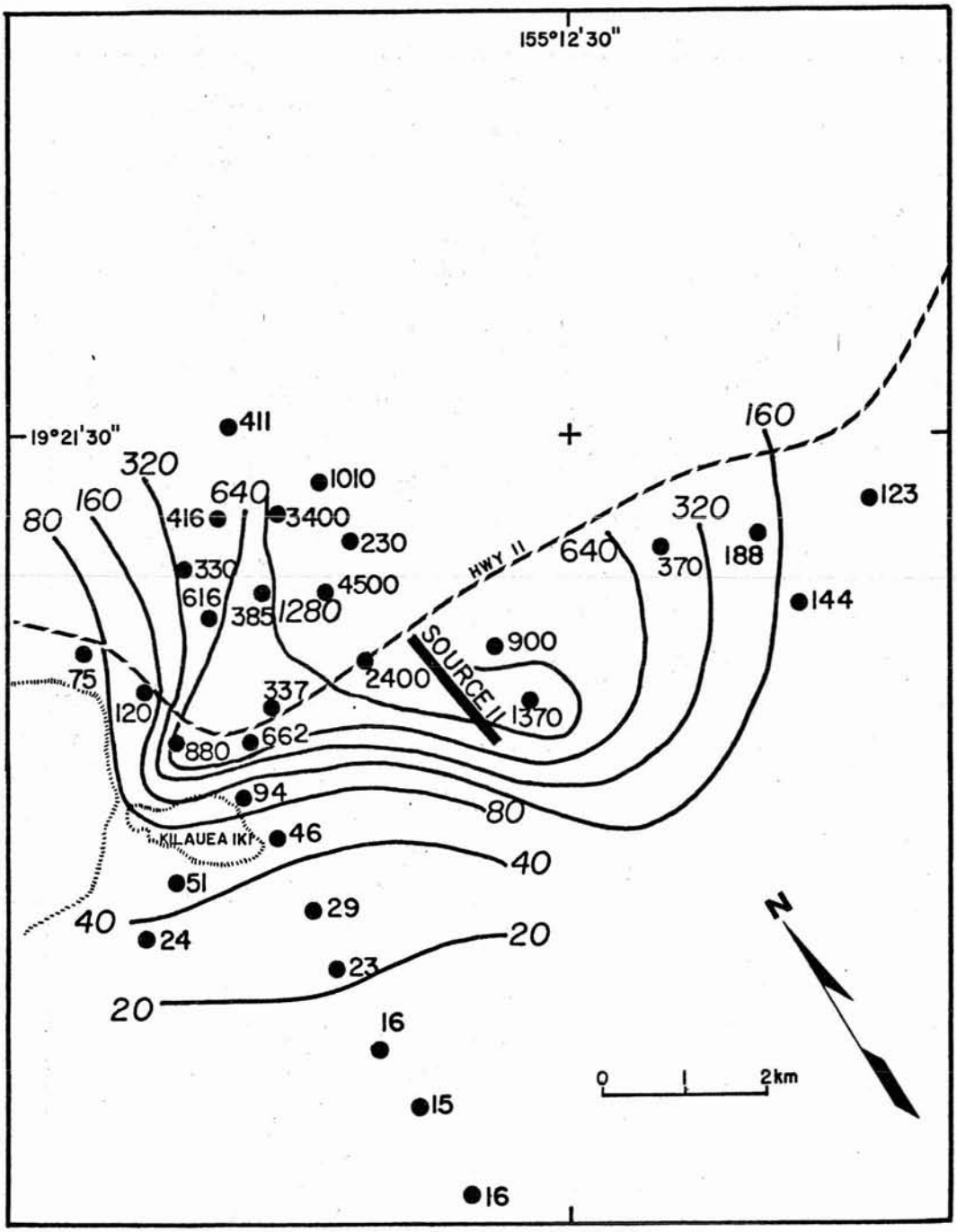

Figure 39. Apparent resistivities measured from source 11.

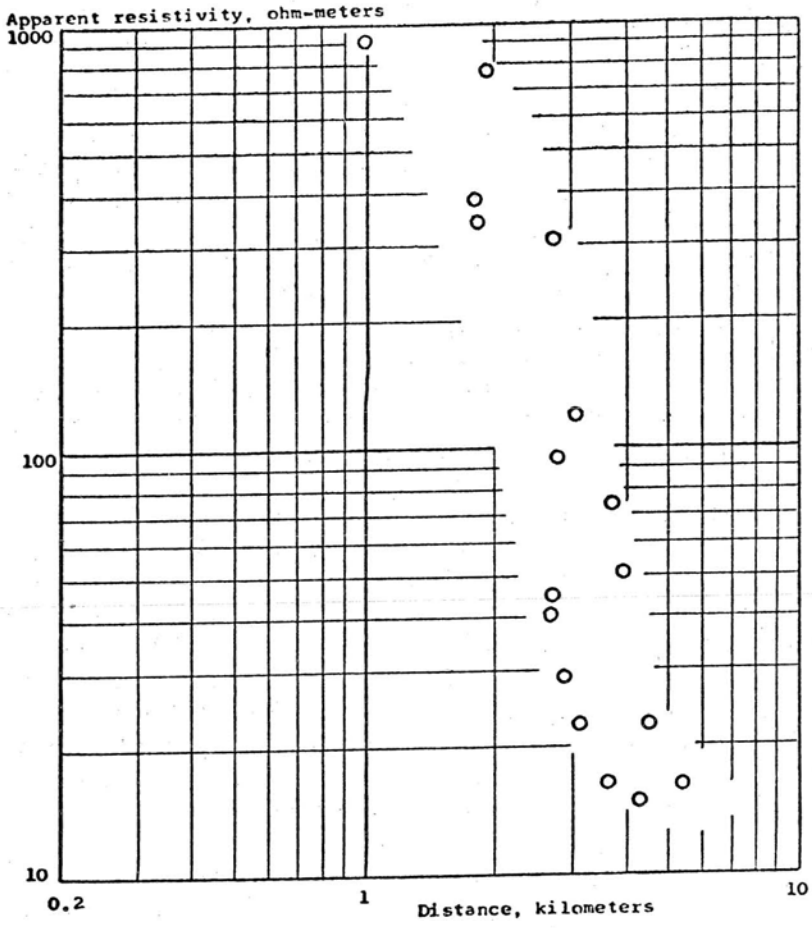

Figure 40. Apparent resistivities as a function of distance from source 11.

from source 6. Surface rocks have a high resistivity, greater than 1000 ohm-m, to a depth of about 1.5 km. These are underlain by rocks with a resistivity of about 10 to 20 ohm-m, but measurements could not be made at great enough distances to provide a definitive value for the resistivity at depth.

Source 12 (Figs. 41 and 42). Located several kilometers inland from the Keaau-Pahoa road. Buried pipes were used for electrodes, and only limited current could be obtained.

Apparent resistivities measured from the source (Fig. 41): The apparent resistivity values are generally high, confirming that the high-resistivity region first mapped in the vicinity of Glenwood continues downhill toward the east rift. Resistivity values drop rapidly toward the north, and agree with values measured from other sources for the area north of the Keaau-Pahoa road.

The apparent resistivity as a function of the distance from the source (Fig. 42): These data may indicate the presence of a high resistivity surface layer covering conductive rock at depth. In such a case, the surface layer is seen to have a resistivity of about 2000 ohm-m, and to extend to a depth of approximately 600 m. The rock at depth probably has a resistivity of 6 to 8 ohm-m. Alternately, the rapid decrease of resistivity with distance may indicate that the change is caused by a lateral decrease in resistivity, rather than by layering.

Source 13 (Figs. 43 and 44). Located just north of the east rift of Kilauea (Fig. 43), in an area where anomalously low resistivity values had been obtained from other sources. Such a placement of the source leads to problems in determining the resistivity outside the area of low resistivity, but it does allow a more accurate determination of resistivity within the area.

Apparent resistivity as a function of the distance from the source (Fig. 43): The data indicates resistivities generally below 5 ohm-m, and there is a small area with resistivities of approximately 2 ohm-m.

Apparent resistivity as a function of the distance from the source (Fig. 44): Some of the anomalously low values are not included on this plot. The data indicate the presence of a surface layer with a resistivity of appoximately 10 ohm-m, to a depth of about 700 m. This layer is underlain by rock with a resistivity of 3.5 to 4 ohm-m, extending to a depth of 2.0 to 2.5 km. Material at greater depths is more resistant.

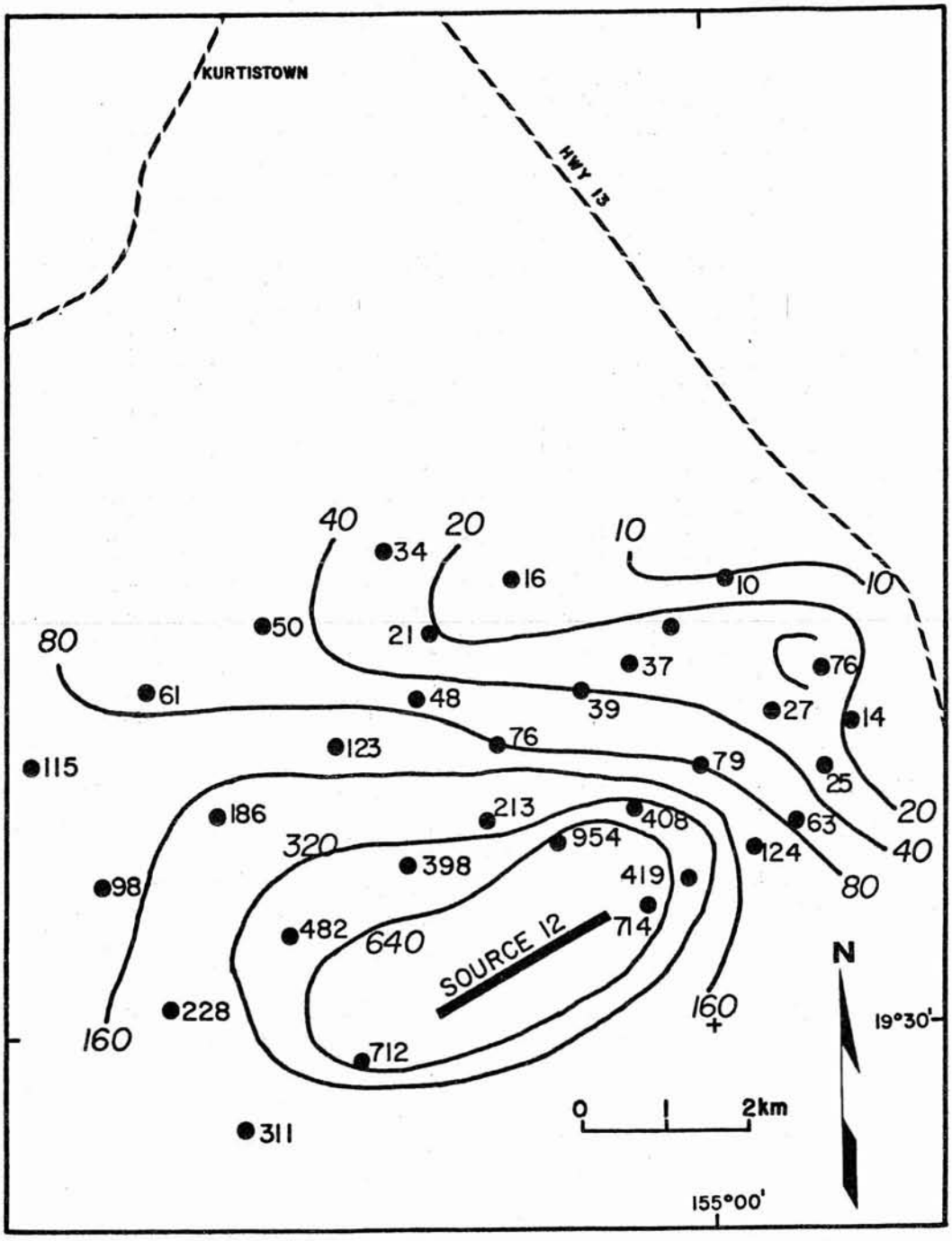

Figure 41. Apparent resistivities measured from source 12.

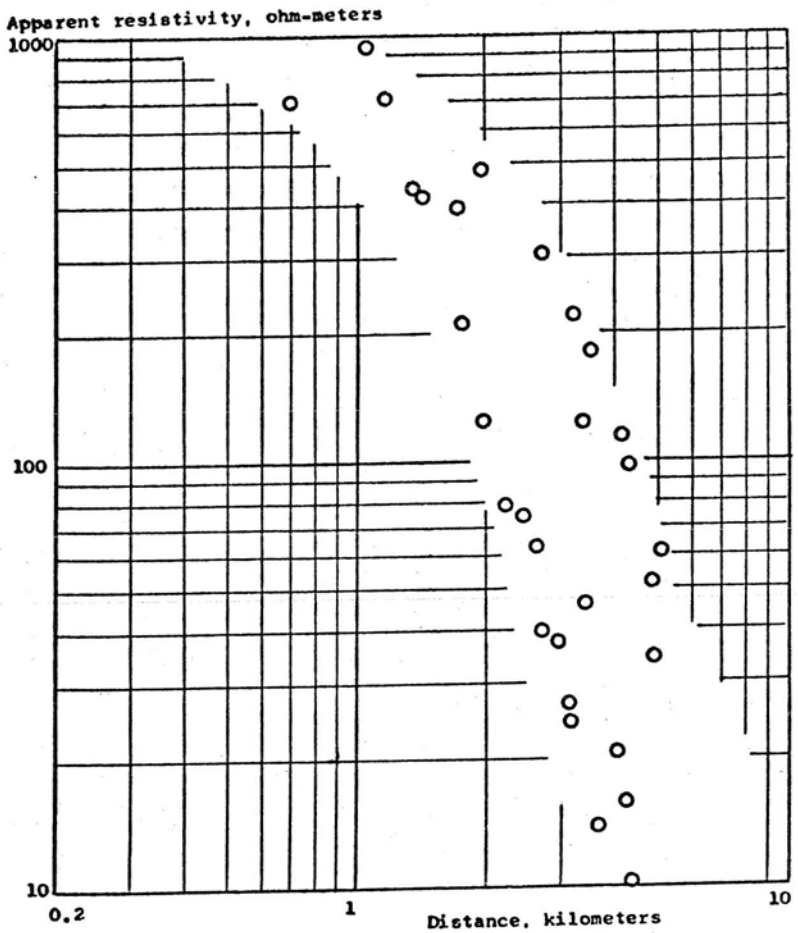

Figure 42. Apparent resistivities as a function of the distance from source 12.

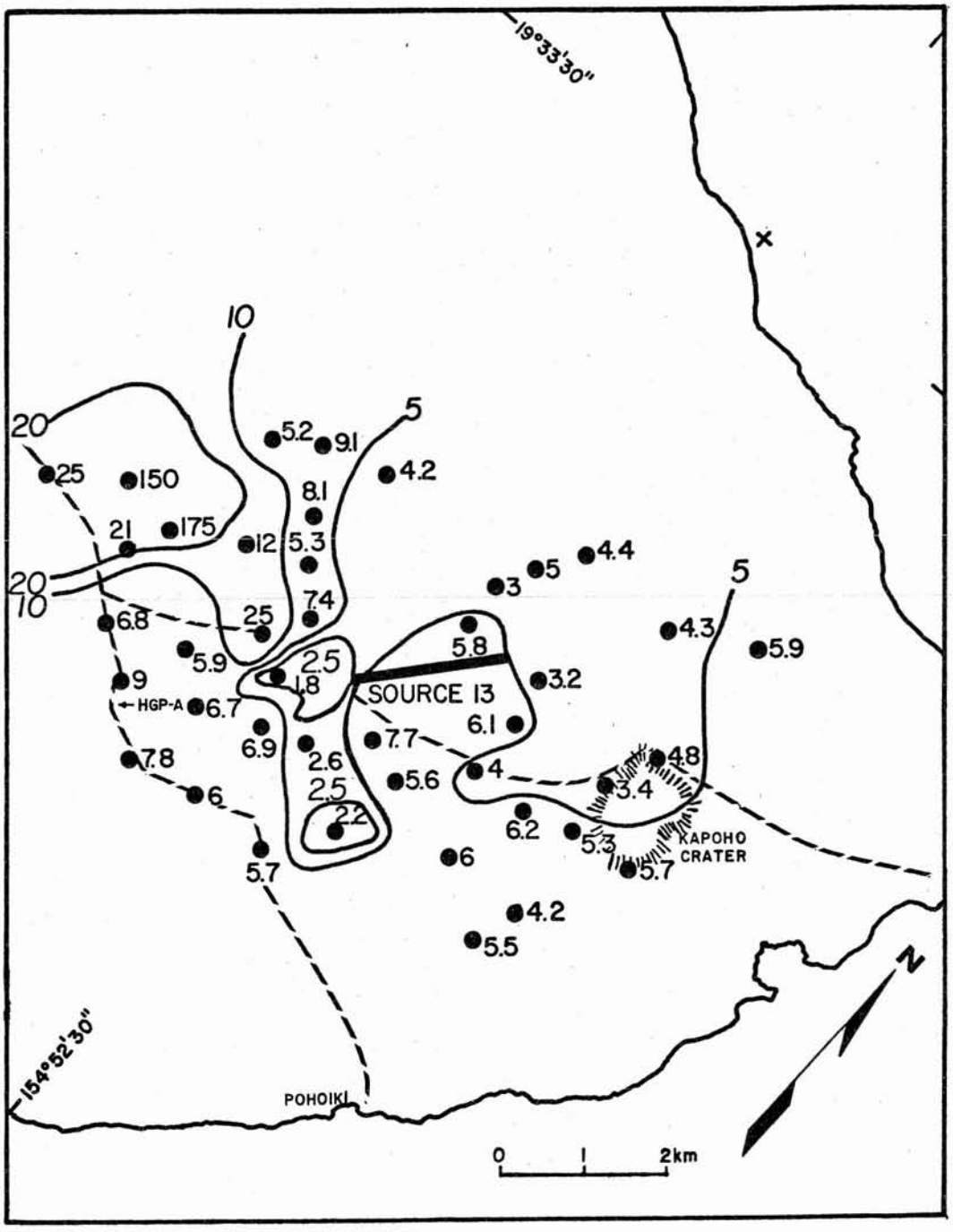

Figure 43. Apparent resistivities measured about source 13.

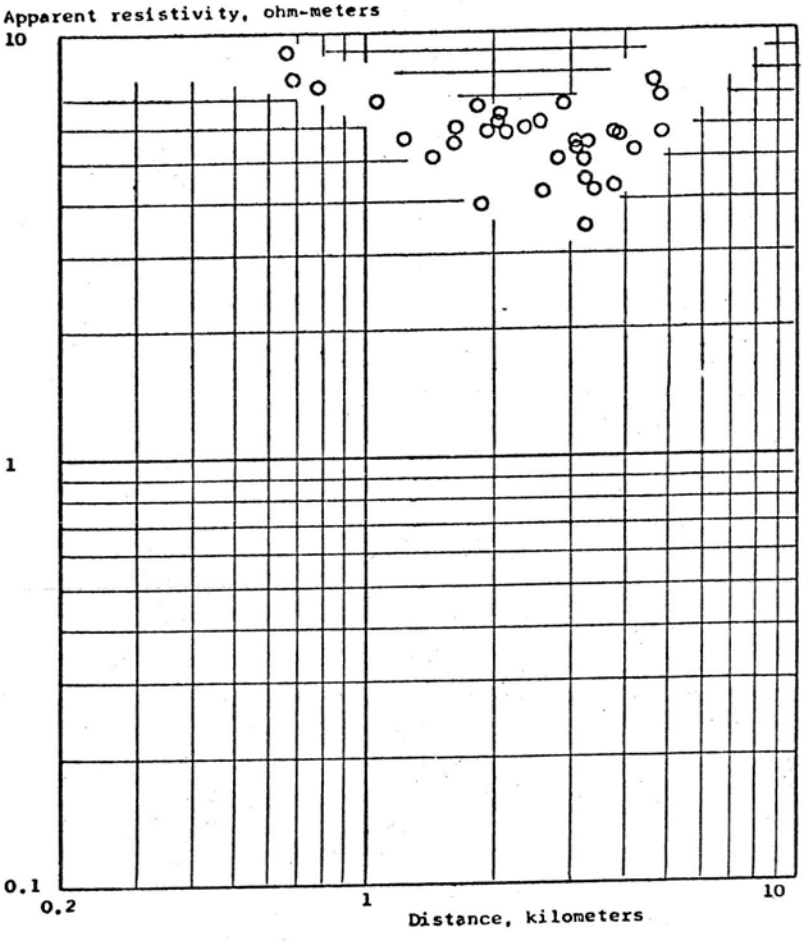

Figure 44. Apparent resistivities as a function of distance from source 13.

Source 14 (Fig. 45). Located on the north side of Hawaii Island along the Kamuela-Kawaihae road, in the South Kohala district. This source was set up to evaluate the practicality of making dipole resistivity measurements on the dry side of the island, and to examine the possible existence of a geothermal reservoir supplying warm water (about 27°C, Dept. Land and Natural Resources, 1970) found in an abandoned water well. One end of the source was grounded to the casing of that water well, which is located along the edge of the Kawaihae-Kamuela road at an elevation of 305 m. The other end of the source was grounded to a metal road culvert. Excellent ground contact was obtained, and from this experience, it is concluded that it is probably easier to make dipole surveys on the Kona and Kohala sides of Hawaii than on the Kilauea side. The older, weathered volcanic rocks on the Kona side provide far better ground contacts than the fresh young volcanic rocks on the Kilauea side.

Apparent resistivity measured from the source (Fig. 45): The values are relatively low compared with many of the values measured over the Kilauea shield. The very low resistivities measured along the coast near Kawaihae, probably reflect intrusion of salt water into the volcanic rocks near the surface. Measurements made inland from source 14 show moderately low resistivities. Measurements were insufficient to determine if areas of anomalously low resistivity might be present.

RESULTS FROM RESISTIVITY SECTIONING SURVEYS

The resistivity sectioning technique used here was the pole-dipole method; other methods that might have been used equally well are the dipole-dipole and Schlumberger sectioning methods. The pole-dipole technique was chosen because it required no change in instrumentaiton and virtually no change in field procedures. A bipole source 2 km long was used. The electric field component in line with the bipole source was measured at intervals of 100 m along a traverse extending from either end of the bipole source, from a closest distance of 150 m to a farthest distance of 1250 m. Values of apparent resistivity were computed exactly the same as for the dipole mapping results.

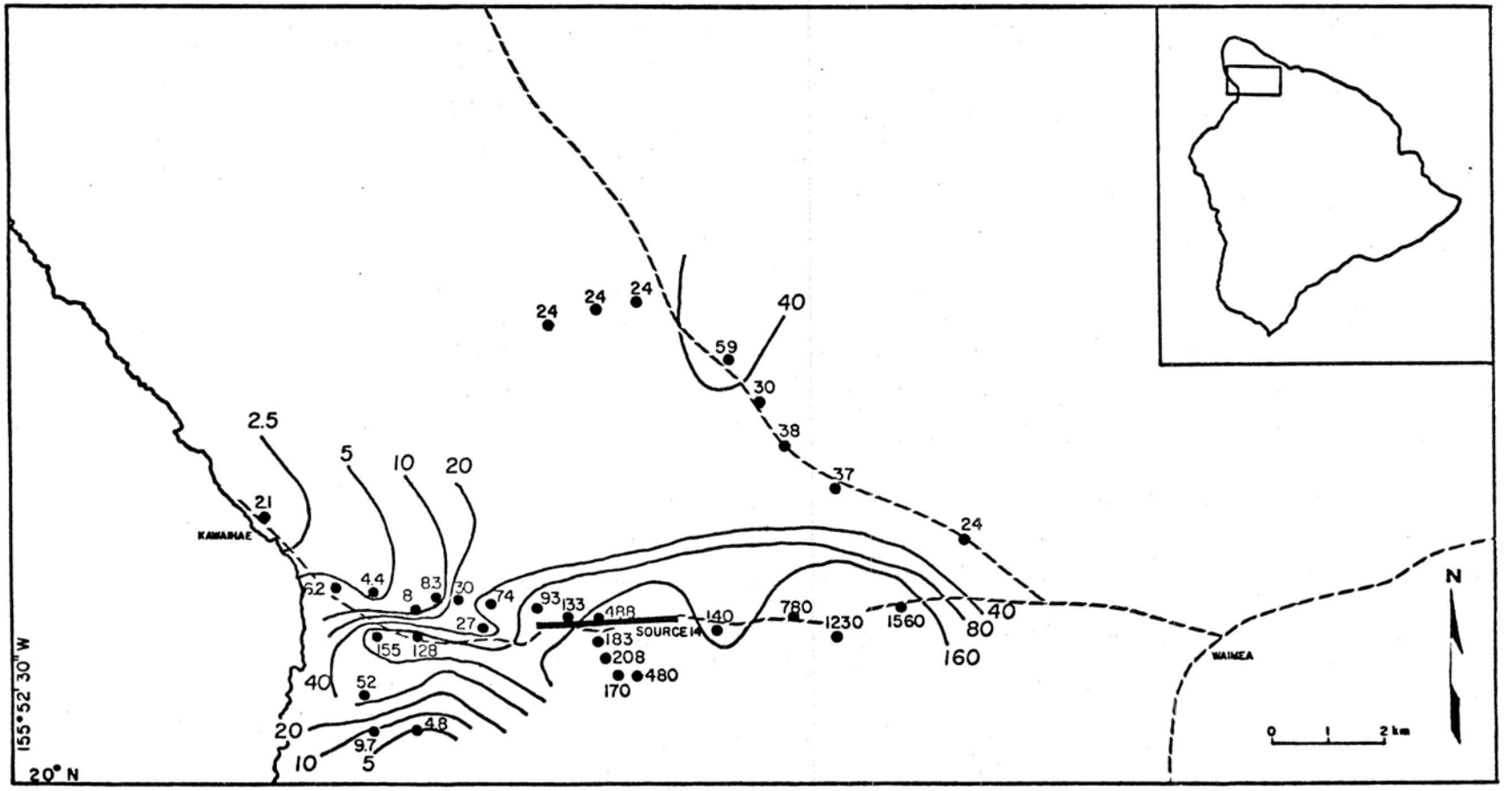

Figure 45. Apparent resistivities measured about source 14.

The term "resistivity sectioning" arises because of the manner in which the results from such surveys are presented. A section is prepared using the horizontal location of a measurement as the horizontal position at which a value is plotted, and using the distance from the end, or "pole", of the source as a vertical coordinate. The purpose is to suggest that the distance that a measurement is made from a pole is equivalent to the depth at which the resistivity is determined. This is not precisely true, but the resulting presentation resembles a resistivity-versus-depth section in many respects.

Resistivity sectioning was done along the road from Pahoa to Kaimu, and along the north side of the east rift near Kapoho crater. The locations are shown on Figure 46. The resistivity sections are shown on Figure 47.

The resistivity sectioning along the Pahoa-Kaimu road shows the presence of a narrow zone of low resistivity in the vicinity of the geothermal well drilled in the early 1960's (near 1S or 2N; Figs. 46 and 47). This is where the surface trace of the east rift crosses the Pahoa-Kaimu road. The lowest values of resistivity are somewhat less than 25 ohm-m, not as low as the lowest values seen with the dipole mapping survey in this area. However, the resistivity sectioning survey provides considerably less penetration than does the dipole mapping survey. With a maximum spacing of 1250 m, the apparent resistivities measured here are related primarily to rocks within the first 600 m of the surface.

A single setup was used to obtain sectioning data at locations offset seaward from the low resistivity zone seen on the Pahoa-Kaimu section (see point 5, on Fig. 47). Lower resistivities, near 5 ohm-m, were observed at the larger offset distances. It appears that depth to conductive rock at this location is only about 600 m.

Even lower apparent resistivities were measured along the section by Kapoho crater (locations 4 and 6, Fig. 47). The lowest resistivities were recorded from the north end of setup 6, with apparent resistivities of 5 ohm-m or less recorded for all spacings beyond 450 m. This indicates that the surface layer of high resistivity is only a few tens of meters thick at most, and that at depths beyond 1000 m, the resistivity is probably less than 2 ohm-m.

Discussion

The main features of the individual dipole resistivity maps are summarized on Figure 48. The most prominent feature

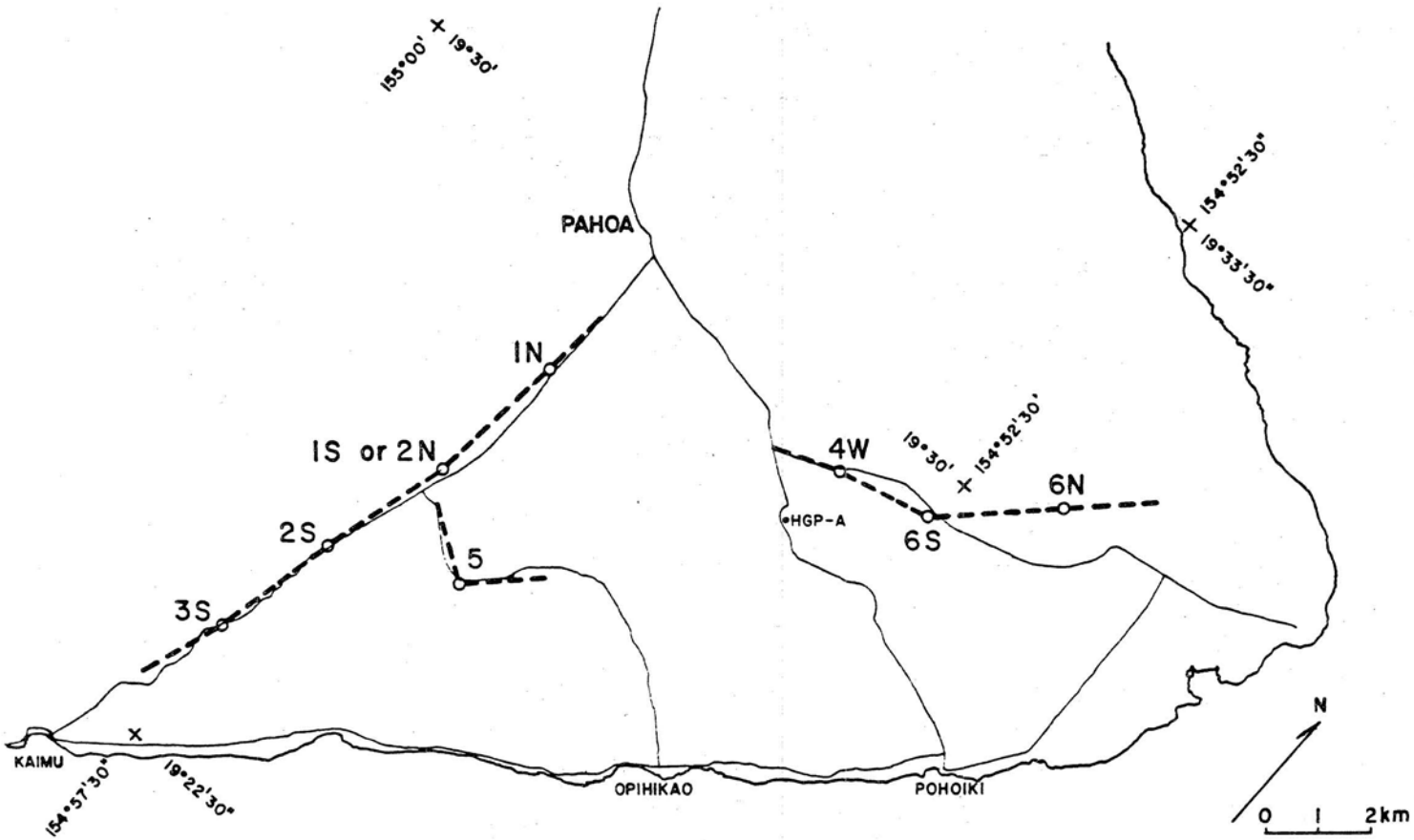

Figure 46. Location of pole-dipole resistivity sections.

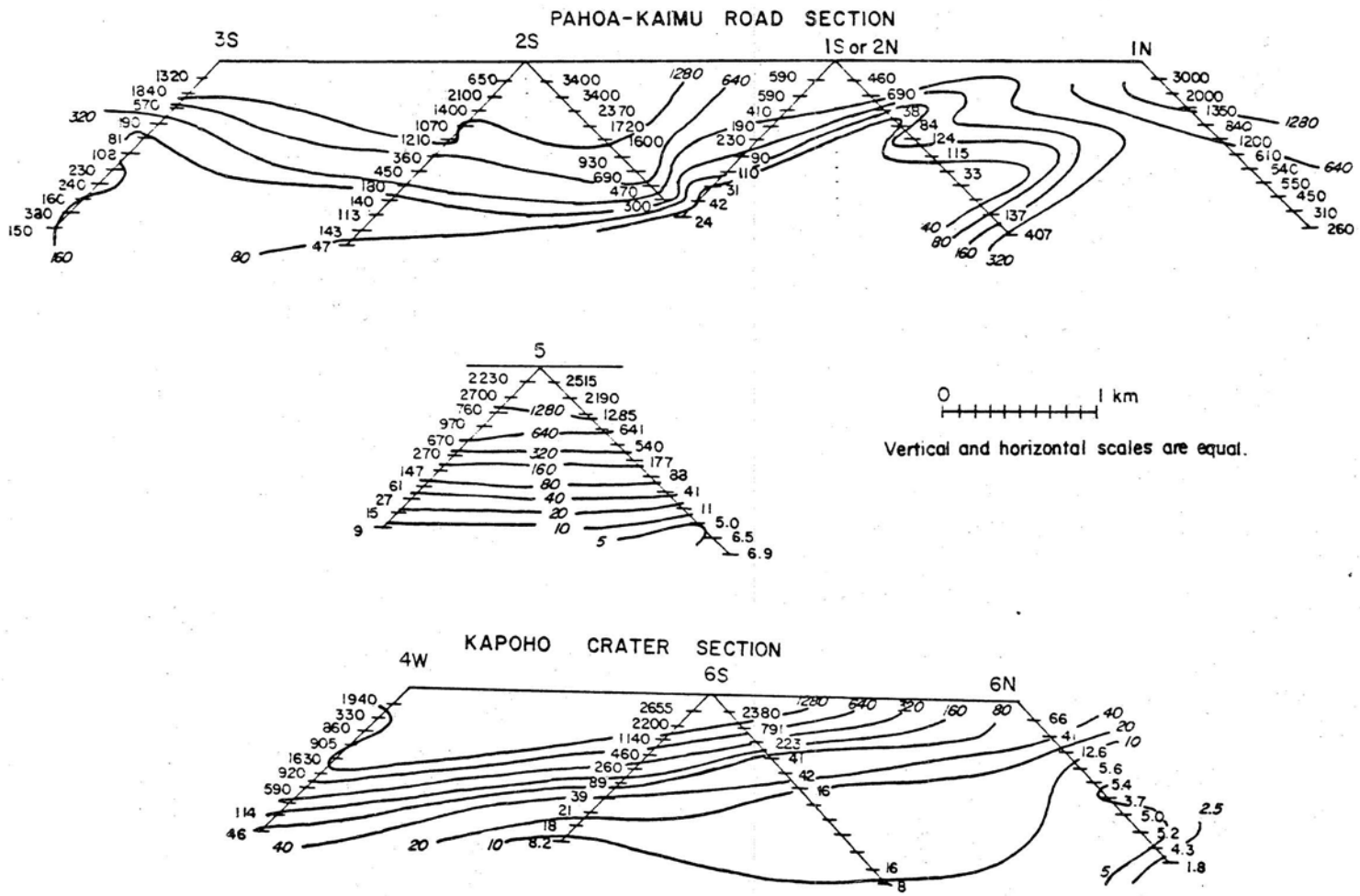

Figure 47. Pole-dipole resistivity sections.

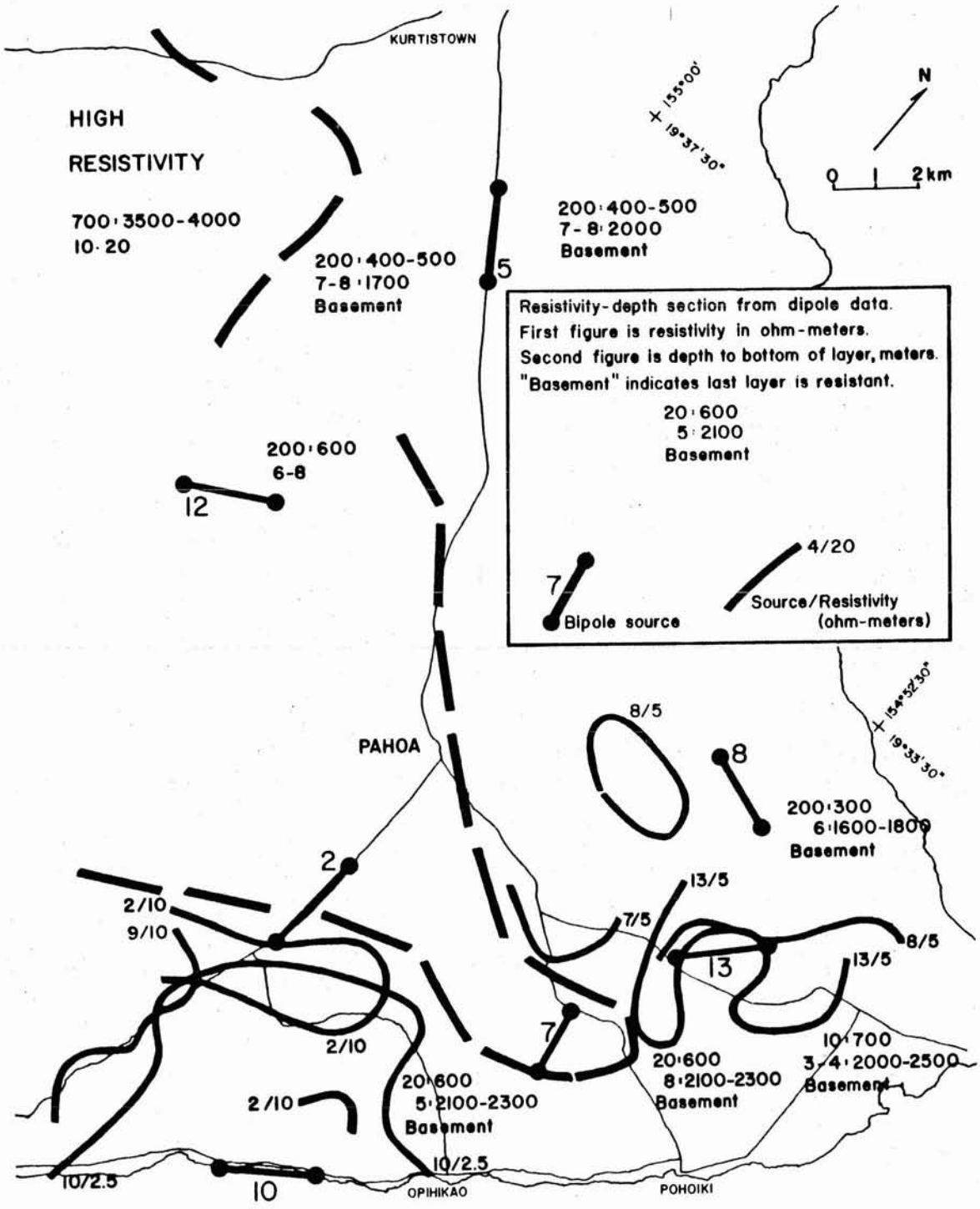

Figure 48a. Summary map of main results from the resistivity survey, lower east rift.

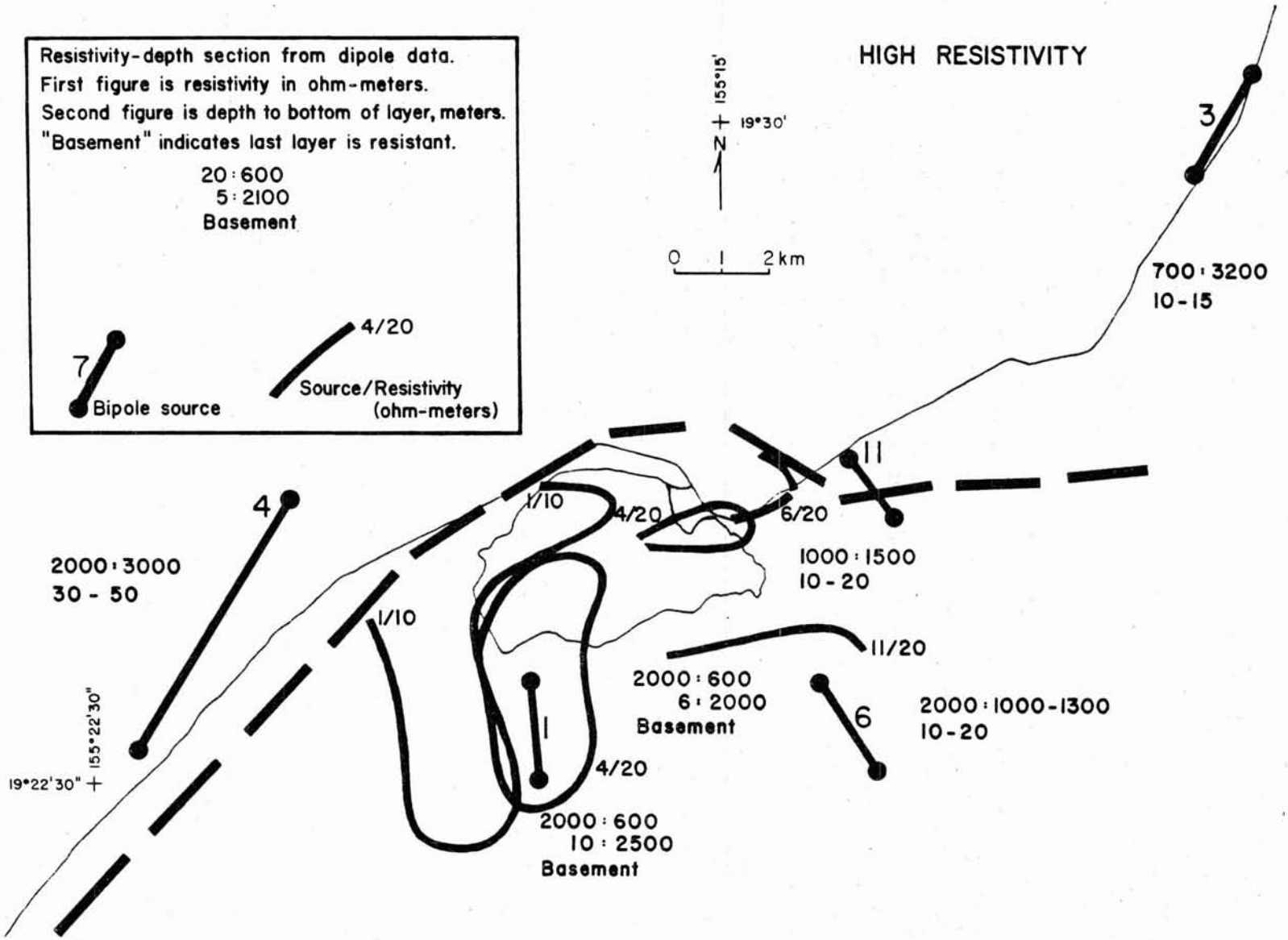

Figure 48b. Summary map of main results from the resistivity survey, summit of Kilauea Volcano.

is the contrast between the areas underlain by high resistivity material to the north of Kilauea caldera and extending into the Puna area east of Mountain View and reaching into the vicinity of Pahoa, and the surrounding areas of lower resistivity. This high resistivity zone coincides geographically with the eastward extension of the northeast rift zone of Mauna Loa under the recent Kilauea lavas; it is reasonable to assume that these high resistivities are associated with a Mauna Loa dike complex.

This high resistivity area is not of interest of exploration for a geothermal reservoir. A geothermal reservoir utilizeable for electric power generation would be characterized by a relatively high porosity and a temperature in excess of 180°C. Both factors will cause lower resistivity in rocks than might otherwise be the case. Thus, in prospecting for a geothermal reservoir, we search for a region with diagnostically low values of electrical resistivity.

The electrical resistivity of a water-bearing rock is determined by the amount of the water contained in the pore spaces of the rock, the resistivity of the water, and to some extent, the way in which the water is distributed through the rock. The relationships between these parameters has been determined experimentally for many types of rocks (Keller and Frischknecht, 1966; Keller, 1970; Keller and Rapolla, 1974). The results are shown graphically in Figure 49. For a specific rock type, and over a limited range in porosity, relationships such as those shown in Figure 49 can be described by the expression:

$$F = \rho/\rho_w = a\,\phi^{-m} \qquad (8)$$

where F is defined as the resistivity formation factor of a rock, ρ is the bulk resistivity of a rock completely saturated with water having a resistivity ρ_w, ϕ is the volume fraction of the pore water (the porosity if the rock is fully saturated), and a and m are experimentally determined parameters. These parameters, a and m, are determined by making measurements of resistivity, water resistivity, and water content on many small rock samples, and then fitting such an algebraic relationship to the data. Such a procedure has been employed for a number of samples of Kilauea flows on the surface (Fig. 50). The large scatter is typical of porosity and resistivity determinations made on small samples, with volumes of 10 to 20 cc. It is generally assumed that if measurements could be made on large enough samples, then the statistical variations in pore geometry would average out and the scatter

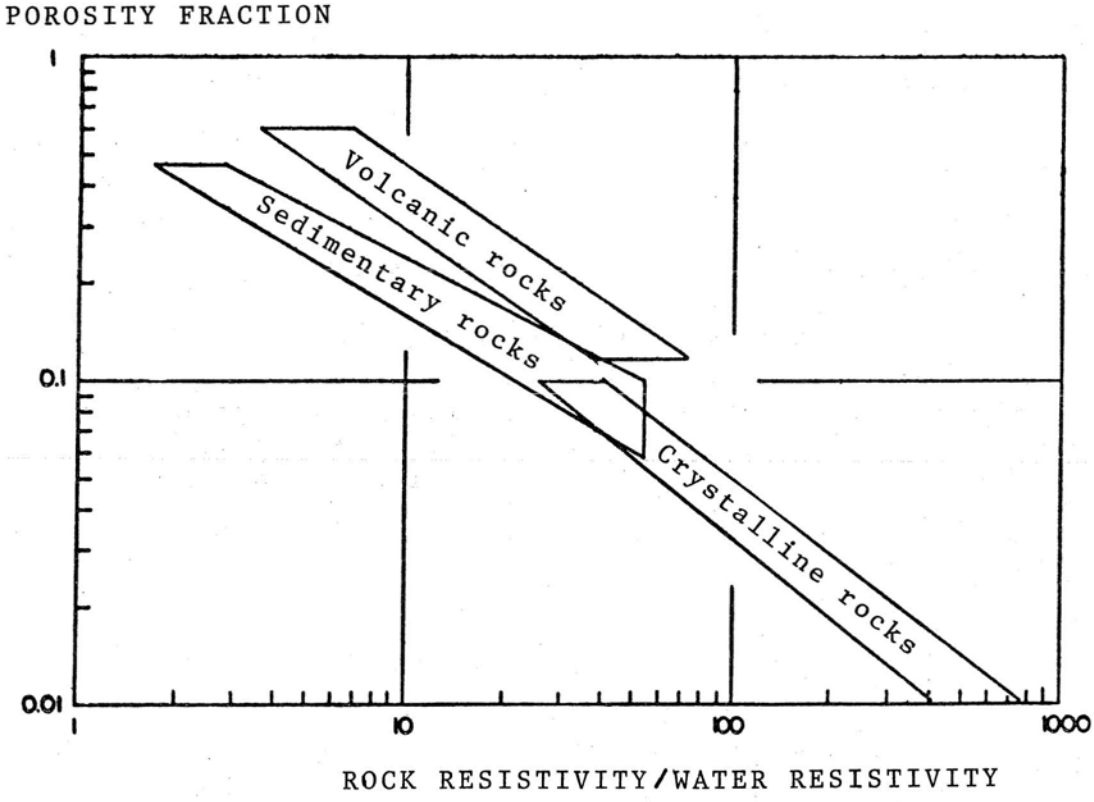

Figure 49. Summary of experimentally determined relationships between the electrical resistivity of a rock and its water content. Here, it is assumed that the pore spaces in the rock are completely filled with water.

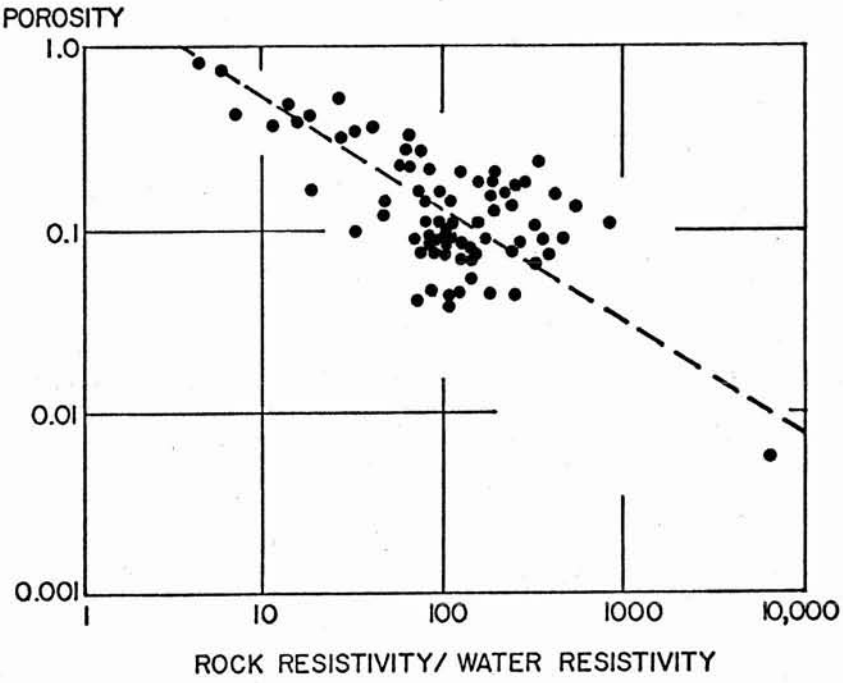

Figure 50. Relation between formation factor and amount of water-filled porosity for basalt samples from Hawaii.

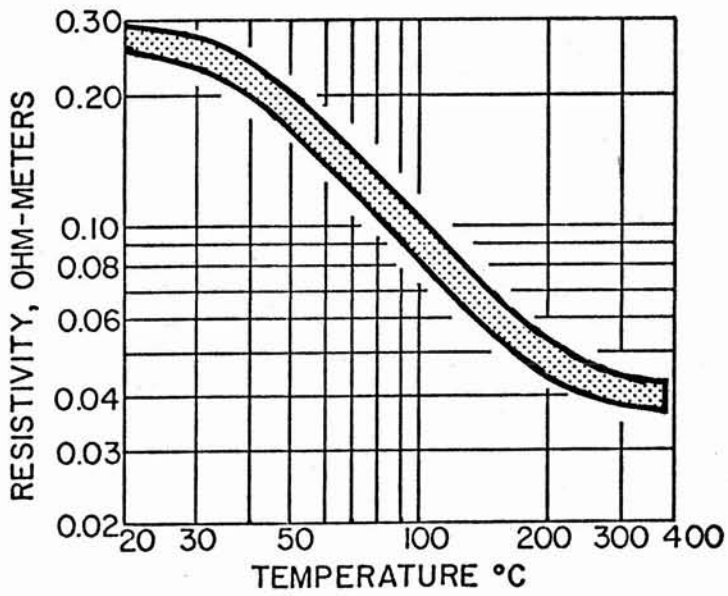

Figure 51. Relationship between the electrical resistivity of sea water and temperature.

would be reduced. Here, it is assumed that an average behavior such as is indicated by the dashed line on Figure 50 will provide a reliable means for converting values of formation factor determined from electrical surveys to porosity. This dashed line is described by the equation:

$$F = 3.5\ \phi^{-1.8} \qquad (9)$$

The samples used in compiling Figure 50 may not be representative of rocks at depth beneath Kilauea volcano. Alteration of older volcanic rocks may modify the pore structures so that such rocks may more closely resemble sandstones in their electrical behavior. However, samples of rock from depths as great as 1200 m have been obtained in the Kilauea Geothermal Test Hole (Zablocki et al., 1974), and the experimental data from these roughly agrees with parameters in eq. 9 (Keller, 1974, p. 38).

This relationship between rock resistivity and water content is of value in geothermal prospecting only insofar as the water resistivity can be determined and the temperature inferred from this information. The resistivity of an aqueous electrolyte depends on the amount of salt in solution, the types of salt ions present, and the temperature. Inasmuch as the resistivity surveys show the porous section of volcanics to extend approximately 2 km beneath sea level in the areas where they have low resistivities, it is probable that these rocks are saturated with sea water containing primarily sodium chloride in solution. Sea water normally has a resistivity of 0.25 to 0.30 ohm-m at a temperature of 20°C. At higher temperatures, the resistivity decreases, as shown by the curves in Figure 51, providing that there is sufficient pressure so that the water does not change to steam. At temperatures above 180°C., the resistivity of sea water is 0.025 to 0.040 ohm-m.

To estimate the rock resistivity that would correspond to this water resistivity, it is necessary to know the average porosity at a depth of 1 to 2km. As may be seen from Figure 50, porosity determinations made on small samples show a wide range, from less than 10% to over 50%. However, the high values of porosity seen with surface samples may not be present at depth because overburden pressures will tend to close the pores. A better estimate of average porosity is available from neutron irradiation well logs from the Kilauea Geothermal Test Hole. These show the porosity at a depth of a kilometer or so to be reasonably uniform, and to lie between 20 and 25%. The formation factors corresponding to

porosities of 20 and 25 percent are 42 and 30, respectively (Fig. 50). In order to have temperatures in excess of 180°, we must have rock resistivities below 1.7 ohm-m for a porosity of 20%, and below 1.2 ohm-m for a porosity of 25%.

The lowest resistivities observed were approximately 2 ohm-m, in several anomalous areas along the lower part of the east rift of Kilauea. Considering that the resistivity measured with a dipole survey is likely to be somewhat higher than the actual resistivity in a conductive anomaly, this result suggests that temperatures at depth in the anomalous areas may be as high as 180°C.

The validity of this conclusion depends on the reliability of our estimate of porosity at depth. Some check is available in the form of resistivity data from areas adjacent to the anomalous areas. In these regions, resistivities of 7 to 8 ohm-m appear to extend to a depth of about 2 km below sea level. Again assuming that the porosity at depth is 20 to 25%, the formation factor will be unchanged, being 42 and 30 respectively. The corresponding water resistivity is 0.16 to 0.25 ohm-m. These water resistivities correspond to temperatures in the range from 30° to 60°C. This is a reasonable temperature range for a depth up to 2 km in an area with a thermal gradient of 20°C. Thus, both the absolute value of resistivity observed in the areas of anomalously low resistivity, and the contrast between the low values of resistivity and more normal values of resistivity in adjacent areas, are compatible with the existence of geothermal reservoir to depths of about 2 km, with temperature of 180° or more.

No resistivity determinations below approximately 10 ohm-m were obtained over the summit area of Kilauea volcano, where it is believed a geothermal system is present at depths of 1 to 2 km below the surface. The pore waters in the geothermal system beneath the summit are primarily fresh waters, with only enough salinity to correspond to 10 to 20% sea water mixed in. The lower content of sea water in rocks penetrated by the Kilauea Geothermal Test Hole is probably a result of its great distance from the ocean, and the relatively large supply of surface waters from the flanks of Mauna Loa. The dipole resistivity data indicate that resistivities at depth under the flanks of Mauna Loa and in the Mountain View-Glenwood area are 20 to 50 ohm-m. The contrast between these values and the 10 ohm-m seen under the summit of Kilauea is fully compatible with a temperature at depth of 30 to 50°C in the areas outside the summit anomaly, and the 150° or higher temperature known to exist below sealevel at the Kilauea Geothermal Test Hole.

A TIME-DOMAIN ELECTROMAGNETIC SURVEY OF THE EAST RIFT ZONE, KILAUEA VOLCANO, HAWAII

A time-domain electromagnetic survey was conducted over the east rift zone of Kilauea volcano, to give a more complete picture of the geologic structure and hydrology of the rift, with special emphasis on its geothermal potential. This report summarizes that survey (Skokan 1974).

For the time-domain electromagnetic (TDEM) survey, a line source and a loop receiver were used. A square wave with a 15-sec period introduced between 5 and 15 amps of current into the ground. Measurements of the transient magnetic field resulting from the current step were made with a 305-m loop of 26-conductor cable laid out in a square. The observed transient (see Fig. 52 for example) was processed for interpretation by removing the step-response of the receiver equipment, stacking the data tenfold to enhance the signal, and filtering to remove high-frequency noise. The resultant voltage was converted to apparent resistivity using the equation:

$$\rho_a = \frac{2\pi R^4 \quad V(t)}{3 \; M \; A \cos \theta}$$

where ρ_a is apparent resistivity, R is the distance from the source to the receiver, V(t) is the processed signal voltage, M is the source moment (current x length), A is the area of the receiver loop, and θ is an offset angle to the receiver measured from a perpendicular to the source.

The processed ρ_a versus time curves were then plotted on bilogarithmic paper and a layered-earth interpretation was made using a curve-matching technique (Fig. 53). A layered-earth interpretation was not possible for all curves. For stations too close to the source, only a first-layer resistivity could be calculated from the maximum-received voltage. For the stations far from the source where extreme filtering was used, the transients were too distorted for a curve-matching interpretation.

Figures 54 and 55 are maps of the maximum apparent resistivity from the two TDEM sources, with the values indicating resistivities in an upper layer. The contoured maximum resistivity map reflects the geology. The Kilauea dike system is expressed by a high resistivity zone that is particularly noticeable on the 1972 resistivity map, and

displacement on the rift is characterized by a resistivity high on the 1973 map. As discussed in the hydrology section, it is thought that the east rift dike system forms a barrier to groundwater movement from the heavy rainfall area to the north. The higher resistivities to the north could result from saturation with fresh water instead of more saline sea water that produces lower resistivities toward the ocean.

Two cross sections are presented to summarize the electromagnetic sounding interpretation results. The cross sections were selected in two very different regions of the survey. Cross section A-A' (Fig. 56) illustrates a dike complex in the rift area. This type of structure is characterized by higher resistivities. Cross section B-B' (Fig. 57) shows a low-resistivity zone that begins at the surface and becomes more conductive at a depth of about 700 m. It is presumed that this resistivity low is a result of both salt in solution in groundwater and heat. Surrounding resistivity zones are also influenced by salt water underground.

The apparent resistivities from the bipole-dipole resistivity data were compared with the maximum-voltage resistivities from the TDEM data. In order to combine the dipole-bipole data, the survey area was broken into cells which were 2 km on each side and apparent resistivities from all sources were averaged for each cell. Apparent resistivity values less than 2 km from the source were rejected in the average so that source effects would be minimized. Resistivities from the two methods are very much alike (see Fig. 58). With the TDEM method, however, ρ versus depth information is gained at each station, while with the DC method, only a ρ_a value is obtained at each station.

This study was funded by Grant GI-38319, National Science Foundation.

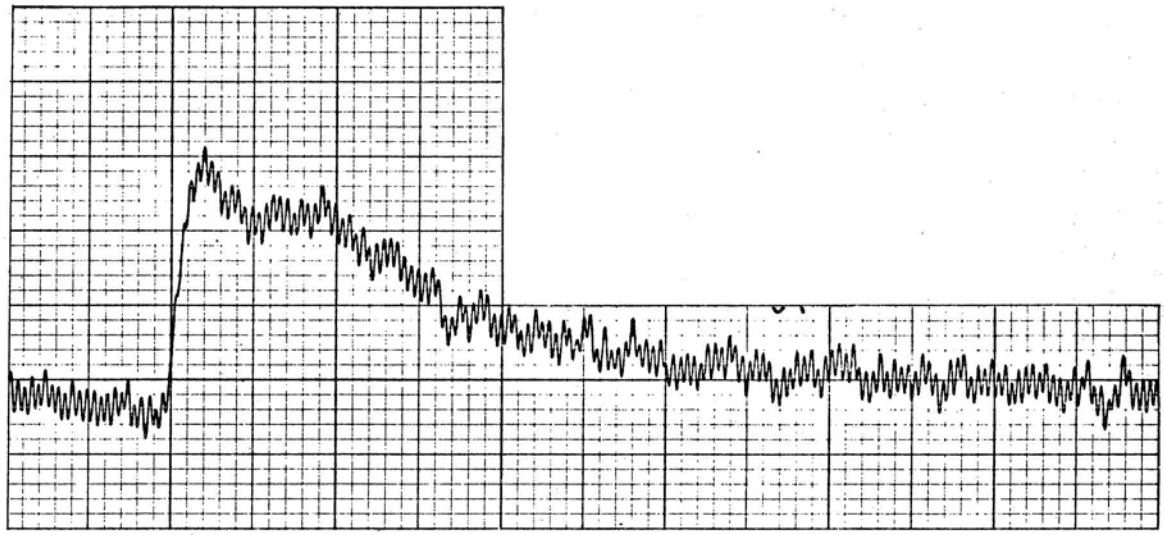

EM3-8
2μv/div.
0.02 sec/div
April 6,1973

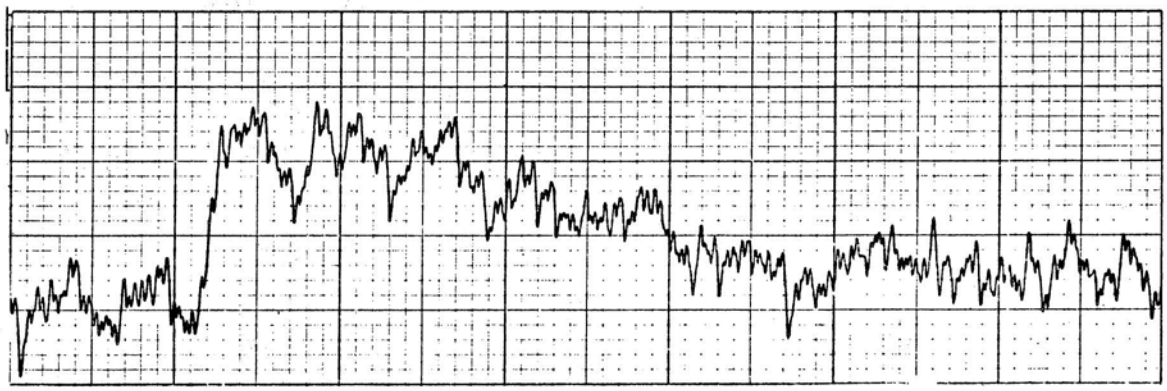

EM3-29
1μv/div
0.02 sec/div
April 26,1973

Figure 52. Sample recordings of field transients.

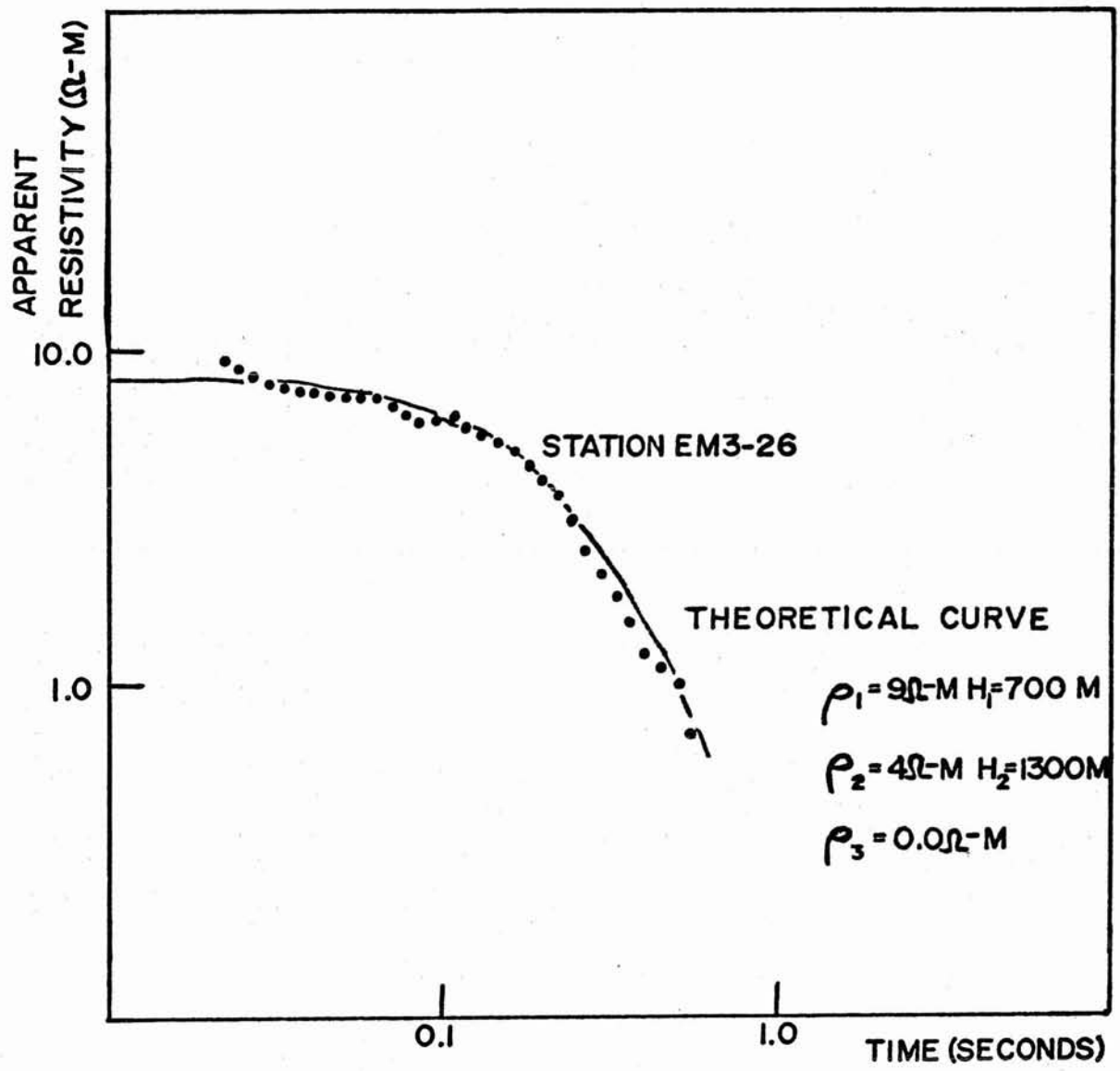

Figure 53. Sample time-domain curve match for Station EM3-26. The point set is the transformed field curve, see Skokan (1974) the solid line is the theoretically calculated curve.

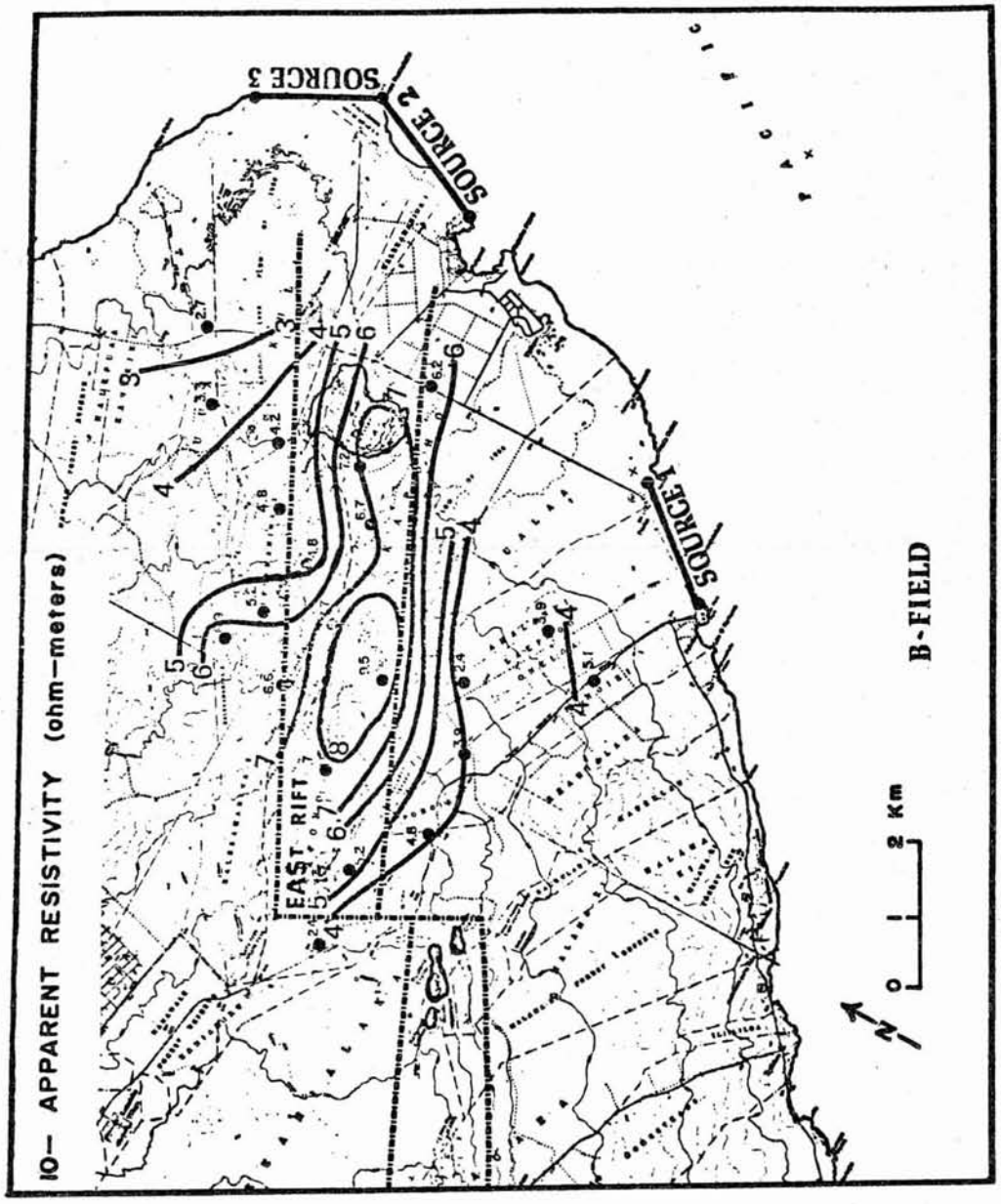

Figure 54. Maximum-voltage resistivity map from the 1972 survey.

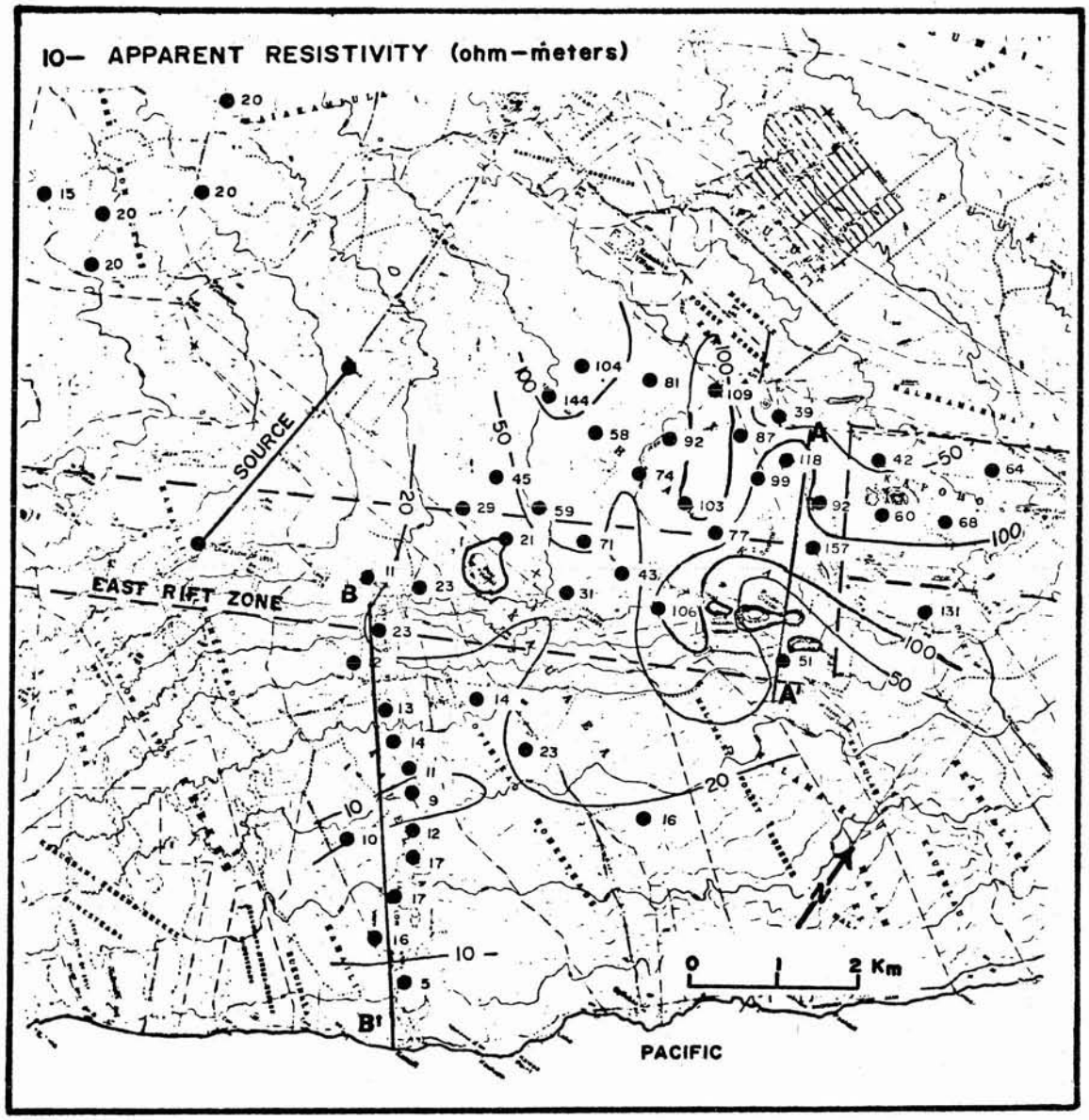

Figure 55. Maximum-voltage resistivity map from the 1973 survey.

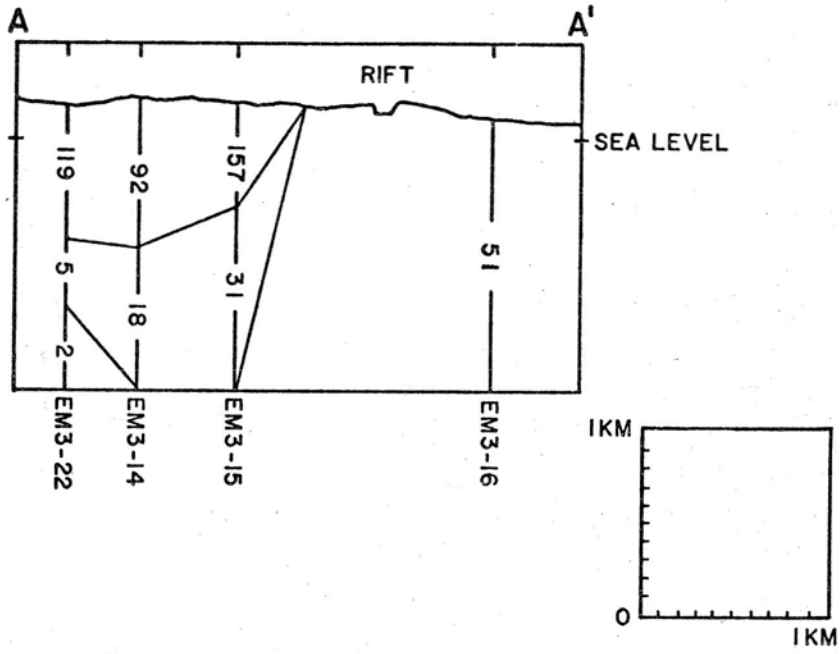

Figure 56. Cross section A-A' through the northern part of the survey. See Figure 55 for cross section location.

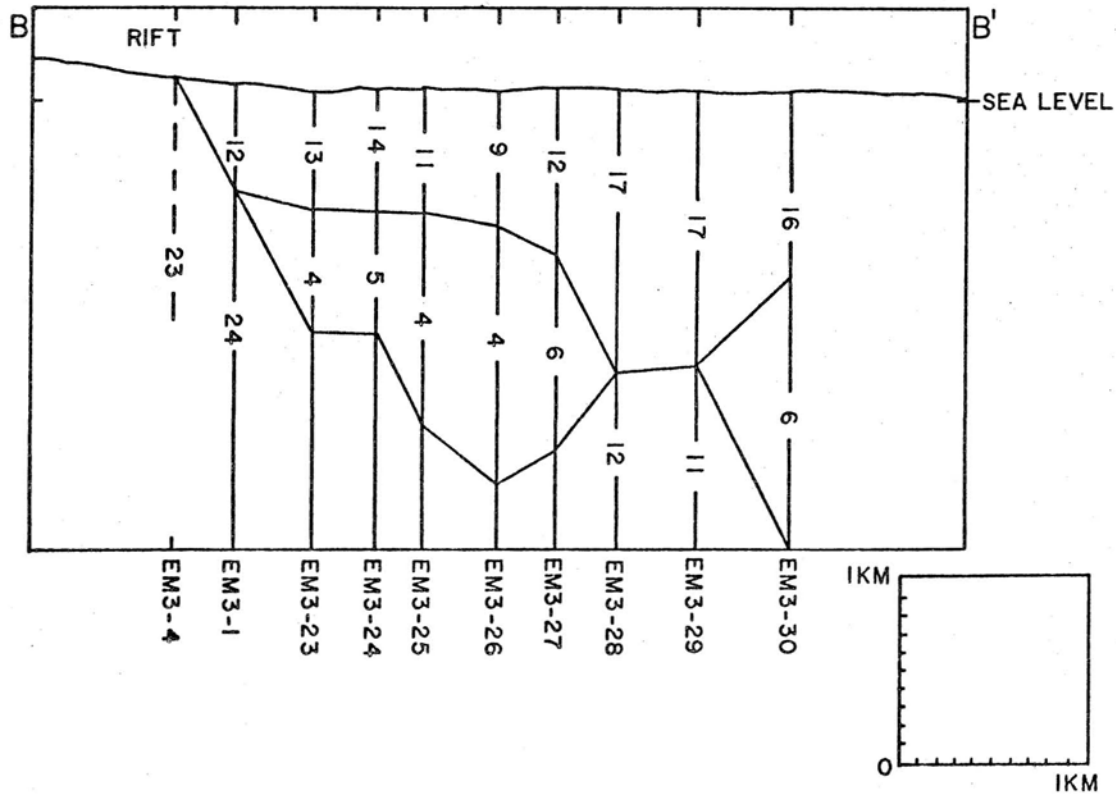

Figure 57. Cross section B-B' through the southern part of the survey. See Figure 55 for cross section location.

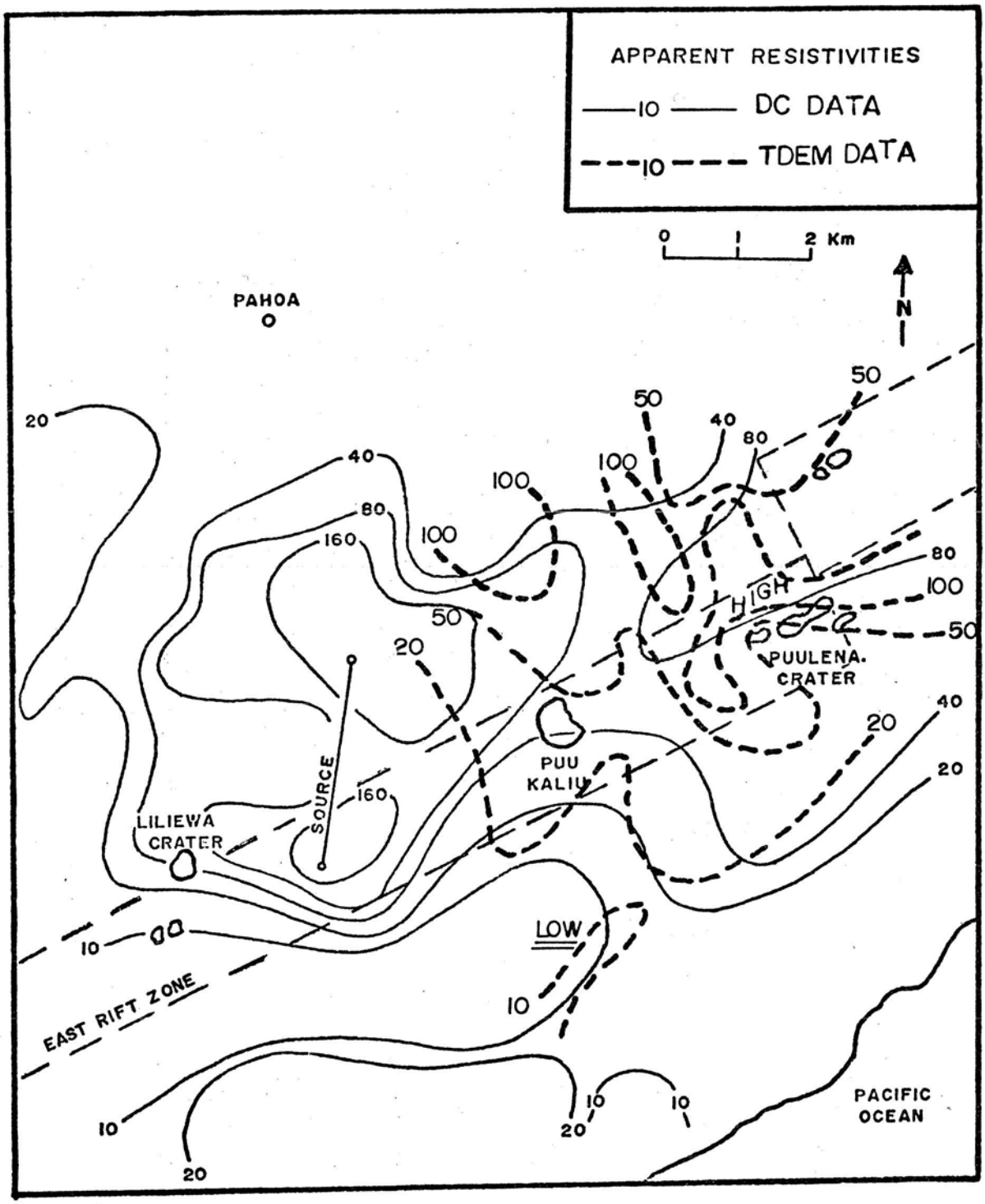

Figure 58. Summary map of DC and TDEM data.

REFERENCES

Davis, D. and Yamanaga, G., 1968. Preliminary report on the water resources of the Hilo-Puna area, Hawaii. U.S. Geol. Surv. in cooperation with Hawaii Div. of Water and Land Dev., Dept of Land and Nat. Res., Circ. C45, 38 pp., Honolulu, Hawaii.

Department of Land and Natural Resources, 1970. An Inventory of basic water resources data: Island of Hawaii. Hawaii Div. of Water and Land Dev. Rept. R34, 188 pp, Honolulu Hawaii.

Duncan, George, 1942. The dug well at Olaa Mill. Volcano Lett., no. 477, p. 1-2.

Finch, R.H., 1925. The earthquakes at Kapoho, island of Hawaii April 1924. Bull. Seismol. Soc. Am., v. 15, no. 2, p. 122-127.

Finch, R.H., 1946. The Puna rift of Kilauea. Volcano Lett., v. 493, p. 1-3.

Furgerson, R.B., and G.V. Keller, 1974. Computed Dipole resistivity effects for an earthmodel with vertical and lateral contrasts in resistivity. Unpub. Off. Nav. Res. Tech. Rep., 12 Mar., ONR Project NR-081-275, Colo. Sch. Mines.

Jackson, D.B. and G.V. Keller, 1972. An Electromagnetic sounding survey of the summit of Kilauea volcano, Hawaii. J. Geophys. Res., v. 77, p. 4957-4965.

Keller, G.V., 1966. Dipole method for deep resistivity studies. Geophysics, v. 31, p. 1088-1104.

Keller, G.V., 1970. Inductive methods in prospecting for hot water. Geothermics, Spec. Iss. 2, p. 318-332.

Keller, G.V., 1974. Drilling at the summit of Kilauea volcano. Unpub. report prepared for the Nat. Sci. Found., Mar. 15, Colo. Sch. Mines, 45 pp.

Keller, G.V., and F.C. Frischknecht, 1966. Electrical Methods in Geophysical Prospecting, Pergamon Press, 519 pp., N.Y.

Keller, G.V., and A. Rapolla, 1974, Electrical prospecting methods in volcanic and geothermal environments. In: (L. Civetta, P. Gasparini, G. Luongo, and A. Rapolla, eds.) Physical Volcanology, Elsevier Sci. Pub. Co. p. 133-166.

Keller, G.V., R. Furgerson, C.Y. Lee, N. Harthill, and J.J. Jacobson, 1975. The dipole mapping method, Geophysics, v. 40, p. 451-472.

Lee, C.Y., 1973. The dipping layer problem in resistivity, Thesis T1610, Colo. Sch. Mines, Colden, Colo. 114 p.

Macdonald, G.A., 1949. Petrography of the island of Hawaii, U.S. Geol. Surv. Prof. Pap. 214-D, pp. 51-93.

Macdonald, G.A., 1965. Hawaiian calderas. Pac. Sci. v. 19, no. 3, p. 320-334.

Macdonald, G.A., 1973. Geological prospects for the development of geothermal energy in Hawaii. Pac. Sci., v. 27, p. 209-219.

Macdonald, G.A., and J.P. Eaton, 1964. Hawaii volcanoes during 1955, U.S. Geol. Surv. Bull. 1171, 170 pp.

Malahoff, A., and F. McCoy, 1967. The geologic structure of the Puna submarine ridge, Hawaii. J. Geophys. Res., v. 72, p. 541-548.

Moore, J.G., and Krivoy, H.L., 1964. The 1962 flank eruption of Kilauea volcano and structure of the east rift zone. J. Geophys. Res., v. 69, no. 10, p. 2033-2045.

Moore, J.G., and Richter, D.H., 1962. The 1961 flank eruption of Kilauea volcano, Hawaii. Am. Geophys. Un. Trans., v. 43, no. 4, p. 446.

Skokan, C.K., 1974. A time-domain electromagnetic survey of the east rift zone, Kilauea volcano, Hawaii. Ph.D. Thesis, Colo. Sch. Mines, Golden, Colo., 152 pp.

Stearns, H.T., 1966. Geology of the State of Hawaii, Pacific Books, Palo Alto, California.

Stearns, H.T., and G.A. Macdonald, 1946. Geology and groundwater resources of the island of Hawaii. Hawaii Div. Hydrog. Bull. 9, 363 pp.

Wentworth, C.K., 1947. Factors in the behavior of ground-water in Ghyben-Herzberg system. Pac. Sci., v. 1, no. 3, pp. 172-184.

Zablocki, C.J., F.J. Tilling, D.W. Peterson, R.L. Christianson, G.V. Keller and J.C. Murray, 1974. A deep research hole at the summit of an active volcano, Kilauea, Hawaii. Geophys. Res. Lett., v. 1, p. 323-326.

ELECTROMAGNETIC INDUCTION SOUNDING MEASUREMENTS IN THE PUNA DISTRICT, HAWAII

James P. Kauahikaua*
Douglas P. Klein

Hawaii Institute of Geophysics
University of Hawaii
Honolulu, Hawaii 96822

*now with the U. S. Geological Survey.

ABSTRACT

Variable frequency inductive sounding measurements taken with the horizontal, coplanar two-loop configuration, as well as Schlumberger direct current sounding measurements, were made on the lower east rift of Kilauea volcano, Hawaii. Normalized amplitudes of receiver voltage over source current from the inductive soundings and Schlumberger apparent resistivities were interpreted with standard curve matching techniques. The geoelectric section obtained from these data consists of a highly resistive overburden (about 6000 ohm-m) extending downward to the water table surface. The saturated substratum shows resistivities of 100 to 600 ohm-m where fresh water is present and resistivities less than 6 ohm-m where water is more saline. The fresh water saturated zone, which in Hawaii usually occurs as a lens floating on top of the more dense sea-water, is not present everywhere in the survey area. Where this zone is absent the resistivities at the surface of the water table are anomalously low for saturated rocks at normal temperatures. Elevated temperatures (about 40° C) in the strata are partially responsible for this abnormality. An analysis of the direct current and the inductive data in conjunction with control available from wells in the area leads us to postulate significant electrical anisotropy in the strata. We suspect that weathering and higher porosities between lava flows as distinguished from the properties of the main flow masses are responsible for this effect, which increases the effective longitudinal conductivity of the section. In evaluating the direct current method against the inductive method, we found that the inductive soundings provided reliable information on both the structure and pore water properties of the saturated zone. On the other hand, using the direct current method with comparable spreads we were able to define the more resistive structure and thickness of the overburden but did not achieve accurate estimates of the saline water resistivity.

INTRODUCTION

Our primary objective was to determine the relationship between the electrical conductivities measured by inductive soundings and the hydrological conditions of the lower east rift zone on the northeastern flank of Kilauea volcano (Fig. 1). As part of a geothermal exploration program on Hawaii Island, we obtained variable-frequency inductive sounding data using the coplanar two-loop configuration, as well as Schlumberger direct current sounding data.

The effective depth of penetration for the inductive soundings reported here is less than 200 m. Although any exploitable geothermal resource would probably be much deeper, we supposed that the shallow hydrological conditions in the survey area would be related to deeper thermal sources. The results also provide an example of a hydrogeophysical survey in a volcanic area.

The induction survey method, as compared with the more commonly used direct current method, has the theoretical advantage of higher sensitivity to the low resistivities associated with geothermal anomalies (Keller, 1971; Keller and Rapolla, 1974). Induction surveys can also have a logistical advantage in areas where highly resistive surface cover causes difficulty in establishing galvanic ground contacts. Hawaii Island's large tracts of fresh, porous lava flows of high resistivity which often necessitate the use of induction methods for electrical surveys. Much of our survey was over such terrain. Fortunately, a thin layer (several inches) of weathered material on some of the older lava flows allowed the use of direct current sounding. Thus we have a unique opportunity to evaluate the advantages of the induction method against the direct current method in geothermal and hydrological exploration.

BACKGROUND GEOLOGY

Kilauea is an active basaltic shield volcano situated on the southeastern portion of Hawaii Island. Two rift systems extend from Kilauea's summit toward the southwest and east. Our studies were made in the Puna District on the lower east rift zone. The hydrological data and structural features of Puna are summarized in Table 1 and Figure 1.

The most prominent feature in this area is the east rift zone. Although it extends some distance from the volcanic summit, it has been the locus of considerable volcanic activity, the most recent eruptions (1955 and 1960) there are shown in Figure 1.

The rift zone is marked by surficial features such as steam seeps, recent volcanic extrusions, cinder cones, fissures, and

Table 1. Drill hole data: Puna district, Hawaii

No.	Well Source	Temperature °C	Elevations from Sea Level: Well Head m	Well Bottom m	Water Level m	Chlorides (ppt)
1	(1)	22.0	11.6	-0.9	0.9	.180
9-5	(1)	22.2	215	-15.2	5.5	.002
9-6	(1)	33.8	87.5	-15.2	0.9	.338
9-7	(1)	23.4	229	-15.2	0.9	.082
9-9	(1)	54.9	83.6	-12.8	0.3	6.2
9-11	(1)	21.6	25	-13.4	3.9	.016
Allison	(3)	39.0	39.3	- 3.4	0.6	2.6
I	(2)	54.5	308	253	---	---
II	(2)	102	315	146	---	---
III	(2)	93.3	172	-38.7	---	---
IV	(2)	43.4	76.1	-12.4	---	---

(1) DOWALD (1970).

(2) Stearns (1966).

(3) Hideo Gushiken, USGS (Water Resources), Hilo.

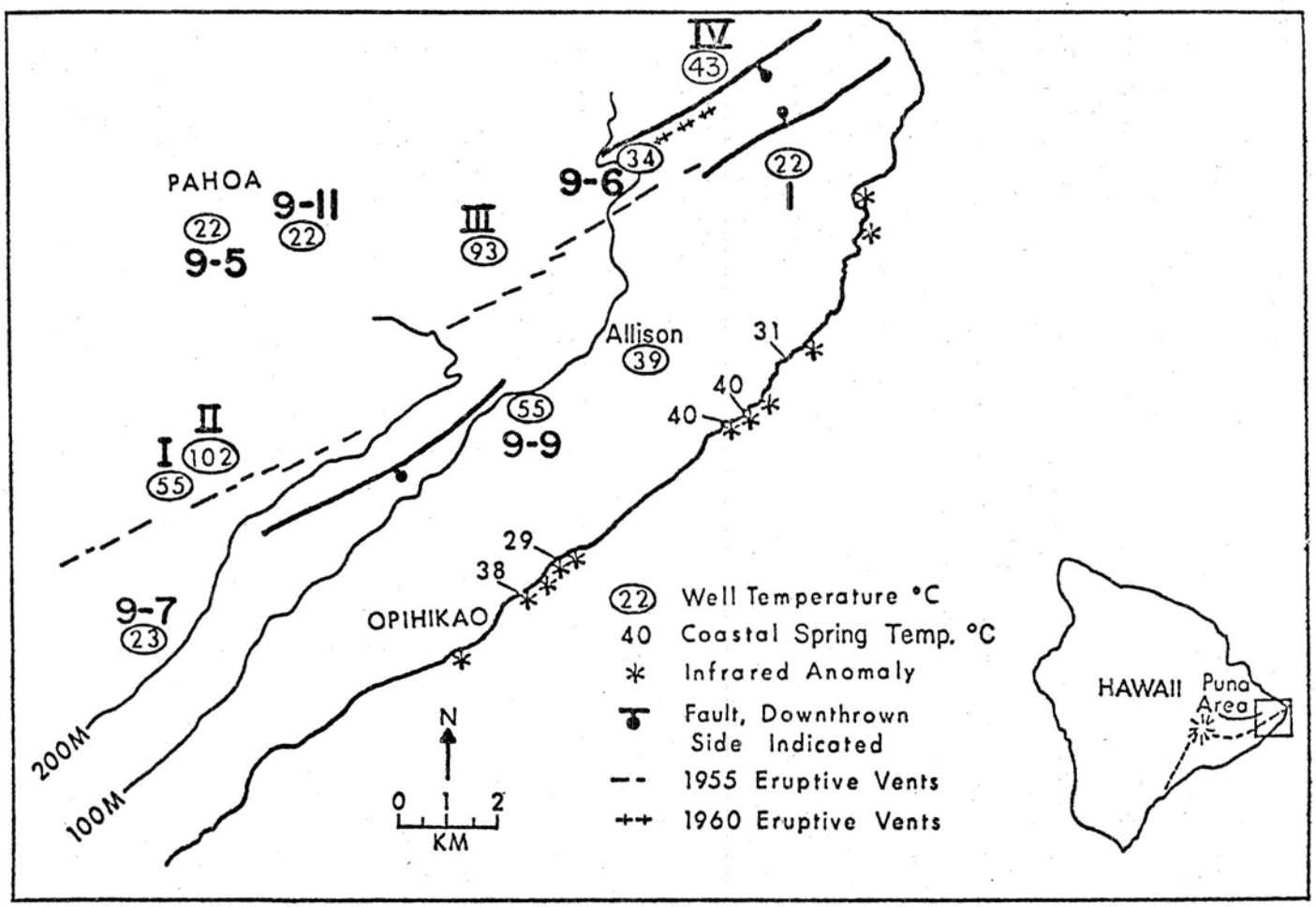

Figure 1. Primary geological features and reported water temperatures from the Puna area. More detailed hydrological data are listed in Table 1 that is keyed to the well numbers as shown on Figure 2.

pit craters, which cover a linear zone about a kilometer or two wide. The deeper rift structure is probably a dense complex of thin dike intrusives that have individual widths of two meters or less (Macdonald, 1956).

Studies of recent eruptions indicate that the rift is fed laterally by the summit reservoir of Kilauea volcano rather than vertically by independent magma sources. The dike complexes extend to depths probably not exceeding the depth of the summit reservoir, 2 to 4 km (Moore and Krivoy, 1964; Fiske and Kinoshita, 1969). Dieterich and Decker (1975) suggested that the recent surface deformation in the Puna area is best explained by the inflation of a southward dipping dike reservoir whose top is roughly one kilometer deep beneath the line of the most recent volcanic rextrusions. Petrological studies by Wright and Fiske (1971) also indicated that pockets of magma may exist within the rift which mix with magma from the summit reservoir prior to rift eruptions.

Because of the uniformity of Hawaiian lavas and the improbability of encountering magma at the shallow depths of our soundings, the electrical properties of the upper strata will be affected primarily by the local hydrological conditions (Schwartz, 1937; Zohdy and Jackson, 1969). The main parameters of concern are the porosity and permeability of the strata, and the ionic concentrations and temperature of the pore water (Keller and Frischknecht, 1966; Keller, 1970; Meidav, 1970; Keller and Rapolla, 1974).

Groundwater in Hawaii normally occurs in a Ghyben-Herzberg lens configuration with fresh water floating on the more dense salt water within the permeable mass of the island (Macdonald and Abbott, 1970). The ratio of hydraulic head (above sea level) to the depth to the salt water surface (below sea level) is commonly about 1:40. The stability of this fresh-salt water zonation deteriorates with increasing chloridity of the fresh water, increasing temperature and decreasing rate of fresh water recharge.

The well data in Table I indicate that well-defined Ghyben-Herzberg zonation does not occur in many places southwest of the rift and that groundwater is often brackish, grading into sea water. The hydraulic gradient is also very low southeast of the rift. Similar areas occurring on the west coast of Hawaii are attributed to low rates of fresh water recharge (Macdonald and Abbott, 1970). In Puna, fresh water from the area of high rainfall north of the rift apparently is not able to flow freely through the rift structure. The low volume of outflow from coastal springs inferred from the analysis of infrared imagery confirms the low volume of fresh water southeast of the rift (Fischer et al., 1966).

Table 2. Basic facts and interpretation of direct current soundings (resistivities, ρ_i (ohm-m) and elevation of the upper surface, d_i (m), of layer i).

Station	ρ_1/d_1	ρ_2/d_2	ρ_3/d_3	ρ_4/d_4	ρ_5/d_5
G1	20,000/244	6660/236	<100/20		
G3	3,150/275	6000/269	2500/193	600/71	
G4	34,000/131	3500/128	6100/126	600/4	50/-256
G5	6,000/105	70/7			
G6	4,300/165	7750/125	10/41		

Table 3. Basic facts and interpretations of induction soundings

A. Layered interpretations.

	r(m)	elev. H(m)	d/r	σ_2(mho/m)	H-d (m)
4-1	488	98	0.25	0.18	-24
6-1	341	47	0.25	0.17	-36
7-1	524	34	0.188	0.042-0.15	-62
10-1	356	46	0.125	0.64	+2
10-2	634	49	0.06	0.2	+9
10-3	521	56	0.1	0.38	+4
11-1	335	75	0.125-0.25	0.15	+33 to -9
15-2	462	113	0.29	0.16	-31
17-1	677	95	0.15	0.18	-5
27	366	38	0.125	0.45-0.55	-7
28	366	35	0.098	0.67-0.84	0
29	366	28	0.075	0.3-0.37	-0.5
30	366	18	0.05	0.37-0.45	0

B. Free Space

	r(m)	Elev. (m)
3-1	305	182
5-1	424	103
18-1	671	262
31	366	181
32A	366	201
32B	366	201
33	400	177
34	500	140

C. Non-layered Responses

	r(m)	Elev.(m)
13-2	491	101
14-1	450	110
15-1	533	82
19-1	594	197
20-1	671	244

Temperature measurements made in drill holes and coastal springs (Hawaii Board of Water Supply, unpub.; see Table 1 and Fig. 1) and temperature anomalies from the infrared imagery (Fig. 1) indicate that the ground water in some areas is still warm as it flows into the ocean. Drill hole temperatures within the rift have been measured at close to 100°C at near sea-level depths, and coastal springs have been measured at temperatures as high as 40°C.

DATA ANALYSIS

The principal data consist of the mutual impedance amplitudes (induced voltage in the receiver loop divided by the current in the source loop) measured at discrete frequencies in the range of 20 Hz to 10 KHz for each of 29 inductive soundings. The signals were generated and sensed in square coils of wire laid horizontally on the ground, with electronics similar to that described by Keller (1970, p. 136). Source and receiver loops were 76 m on a side having 1 to 3 and 42 turns respectively, and were separated by distances of 219 to 634 m. Supplementary data are provided by five Schlumberger direct current (d.c.) soundings having a maximum half-spacing (AB/2) of about 1000 m.

Prior to interpretation the inductive data were normalized as

$$|Z(f)|/|Z_o(f)|$$

where $|Z(f)|$ are the measured impedance amplitudes at frequency f and $|Z_o(f)|$ are the corresponding impedance amplitudes that theoretically would be measured in the absence of any conductors (free space). The $|Z_o(f)|$ values were determined empirically from data obtained in calibration soundings on the Humuula Saddle near the center of Hawaii Island, an area with a resistivity of at least 5000 ohm-m to a depth of a few hundred meters (Zohdy and Jackson, 1969.

The inductive and d.c. data both were interpreted using standard curve matching techniques (Keller and Frischknecht, 1966). For the inductive data, the normalized impedances were plotted bilogarithmically against a scaled frequency parameter $r\sqrt{f}$ (r= separation between loops) and were then compared against layered model curve sets. Frischknecht's (1967) catalogue of two-layer models was adequate in most cases; however, additional model curves were generated when necessary by using the "linear digital filter" computational procedure (Koefoed et al., 1972; Verma and Koefoed, 1973. The d.c. data were plotted bilogarithmically as Schlumberger apparent resistivities against AB/2 (the separation between outermost electrodes) and interpreted with an interactive computer program similar to that of Johansen (1975). The basic facts of these interpretations are presented in Tables 2 and 3 (d.c. and inductive data respectively). Station locations are shown in Figure 2.

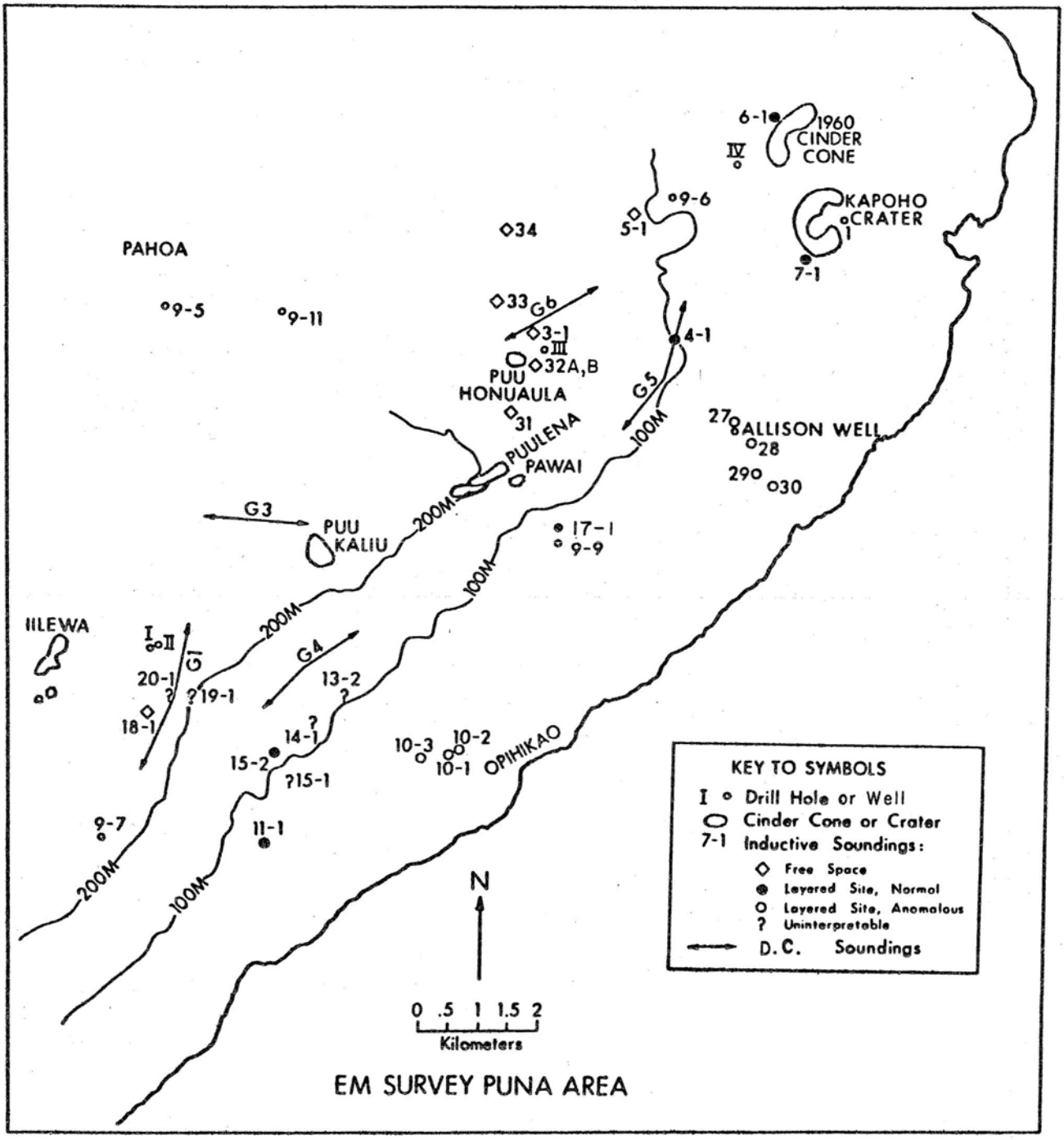

Figure 2. Electromagnetic induction and direct current sounding locations in the Puna area. The classification of inductive soundings is based on the interpretations discussed in the text; in general the anomalous sites show higher conductivities than do the others. Well locations are also shown.

The inductive data interpretations fall into three categories: (A) 13 soundings indicate a conductive substratum beneath a highly resistive overburden; (B) 11 stations show a response similar to the response of free space; and (C) 5 soundings cannot be fit to layered earth conductivity models. The data in category C may be interpretable in terms of more complex models than considered above; however, we believe that the data are too sparse to warrant a more detailed discussion here.

The data that are not distinguishable from the response of free space (category B) were obtained at elevations generally greater than 100 m, while those that sensed a conductive substratum were obtained at lower elevations. Since the top of the conductive second layer is interpreted to be near the plane of sea level or below for the soundings in category (A) (Table 3), the maximum depth at which our system could resolve a contrasting conductivity is apparently about 100 m.

The maximum demonstratable depth of resolution (144 m, station 15-1, see Table 3) is less than one third of the separation between source and receiver. This seems to be the limiting depth of resolution for a conductivity contrast as inferred from model two-layer responses for the coplanar two-loop system. Figure 3, for example, shows a plot of the data from sounding 32B (category B) superimposed on a set of model curves for a conducting half-space located at a depth "d" beneath a non-conducting overburden. The conductivity contrast has been made infinite in this set of models so this example indicates the maximum depth at which a set of measurements can resolve an underlying interface. Amplitude data with greater than about 5% accuracy are required for resolution of a conductor at depths exceeding one-third of the source receiver separation, "r". It is also evident that optimum resolution of the underlying interface occurs for a d/r value of less than about 1/8.

In all soundings of category A the conductivity of the overburden was too small to be determined (less than .002 mho/m) and was assumed to be zero for the purposes of interpretation (e.g. using model sets similar to that plotted on Figure 3). The conductivities interpreted for the second layer are generally greater than .1 (resistivities less than 10-ohm-m) (Table 3). When using the direct current interpretations (Table 2) as indicators of the true overburden conductivity, we are dealing with a conductivity contrast of about 1000.

The range of conductivity contrasts resolvable by the inductive method used here is theoretically limited only by the range of frequencies available for use. In the application of the curve-matching interpretational technique, however, the

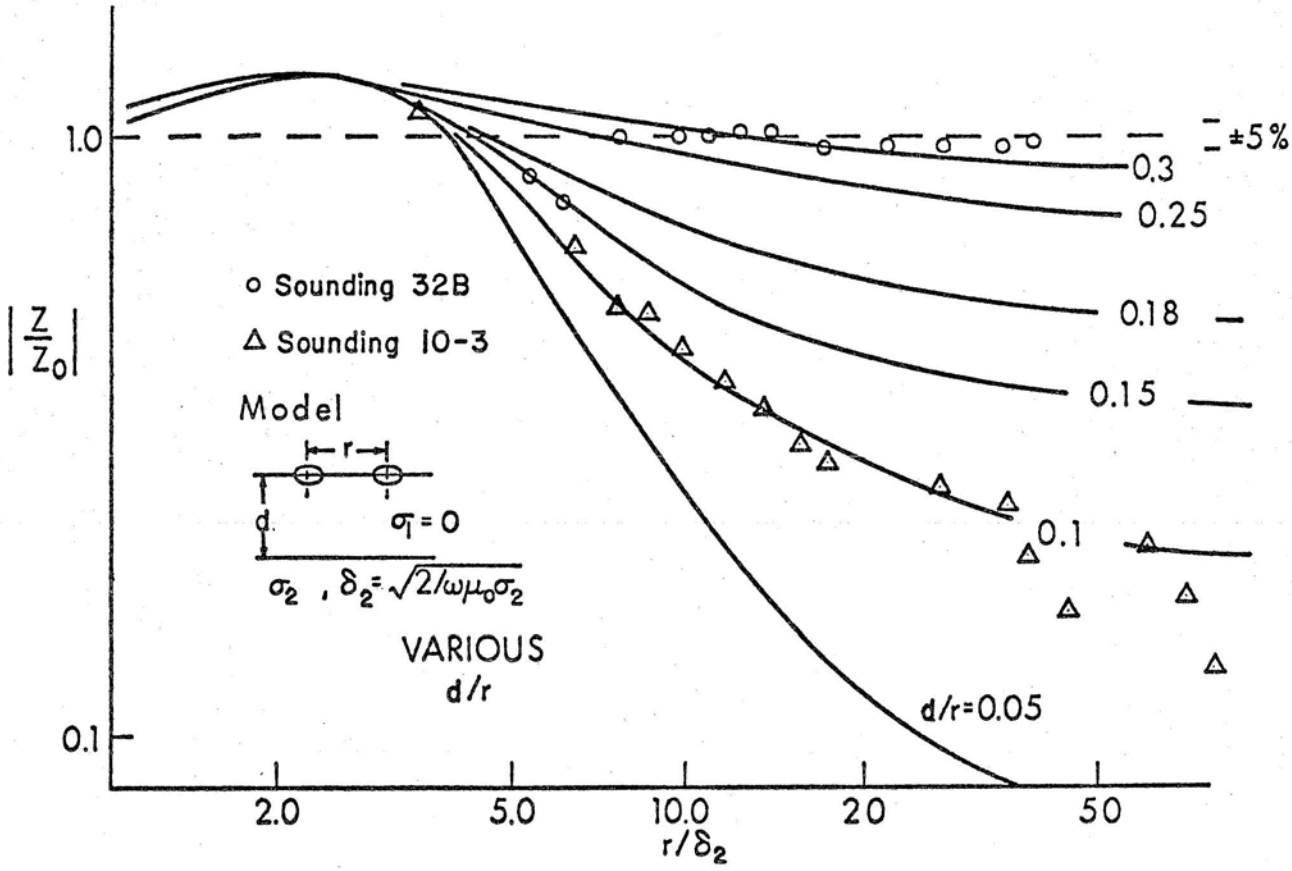

Figure 3. Two-layer models for a coplanar two-loop configuration for the conductivity model shown. This figure provides a relative indication of the depth of resolution of a conductivity contrast. $|Z|/|Z_o|$ is the normalized impedance amplitude (receiver voltage over source current for the data, Z, normalized to the corresponding Z_o for free space.) The skin depth ($_2$) is given in mks units where $_o = 4\pi\ 10^{-7}$ is the magnetic permeability of free space. Examples of sounding data are shown.

distinguishing parameter for the various models is the change in slope of the logarithmic response, log ($|Z|/|Z_o|$), with respect to the logarithmic frequency, 1/2 log f. This must be kept in mind when studying a set of models such as are presented in Fig. 4 (compiled from Frischknecht, 1967). This figure is a bilogarithmic plot of the frequency response for several two-layer models having different conductivity contrasts (k) and a constant depth separation ration(d/r = 1/8). The abscissa of these plots is the separation divided by the skin depth of the second layer instead of the first layers as usual. This normalization has the advantage of indicating the relative penetration into layer two necessary to resolve both conductivities. Observe that the shapes of curves for conductivity contrasts (k) less than 1 are practically indistinguishable, implying that curve matching cannot resolve conductivity contrasts in this range for this particular model set. For k between 1 and 100 the variations between the slopes of different models provide fairly good resolution of k(2 or 3 significant figures in thelower part of this range of k, and 1 or 2 significant figures in the higher range, depending on the accuracy of the data). For k greater than 100 the slopes rapidly approach that of an infinite conductivity contrast, implying that only limiting bounds on k can be established. In all three ranges of k, at least one conductivity can be estimated. For instance, when frequencies are available such that r/δ_2 (proportional to $r\sqrt{f}$) is less than about 5 (e.g. the skin depth of layer two is more than r/5), the response is like that of a half space having the conductivity of layer two. On the other hand, when r/δ_2 is greater than about 50 or 100 (e.g. the skin depth of layer two is less than r/50), the response is like that of a layer of conductivity σ, over a perfect conductor. A range of r/δ_2 between 5 and 100 is necessary to adequately define the shape of the curve, and both conductivities if k is between 1 and 100. For a k greater than 100, the conductivity of layer two can still be defined, but k and hence σ, may only be expressed as a limit. This last case is typical of most of our data (an example is shown on both Figs. 3 and 4) where we could only estimate an upper bound on conductivity σ, of .002 mho/m.

The inductive interpretations (category A) are divided into normal soundings (σ_2 from about 0.15 to .2 mho/m and interface elevations of the second layer from -5 to -62 m below sea level), and anomalous soundings (σ_2 from about .2 to .8 mho/m and interface elevations at sea level or above; see Table 3). The reason for this distinction will become apparent in the following discussion.

We note that although the d.c. soundings in the present survey provided estimates of the conductivity structure of the overburden, and depth estimates to a more conductive zone (Table 2), they did not provide good estimates of the conductivity of the substratum, even though the d.c. spreads were equivalent to those of the inductive soundings. The

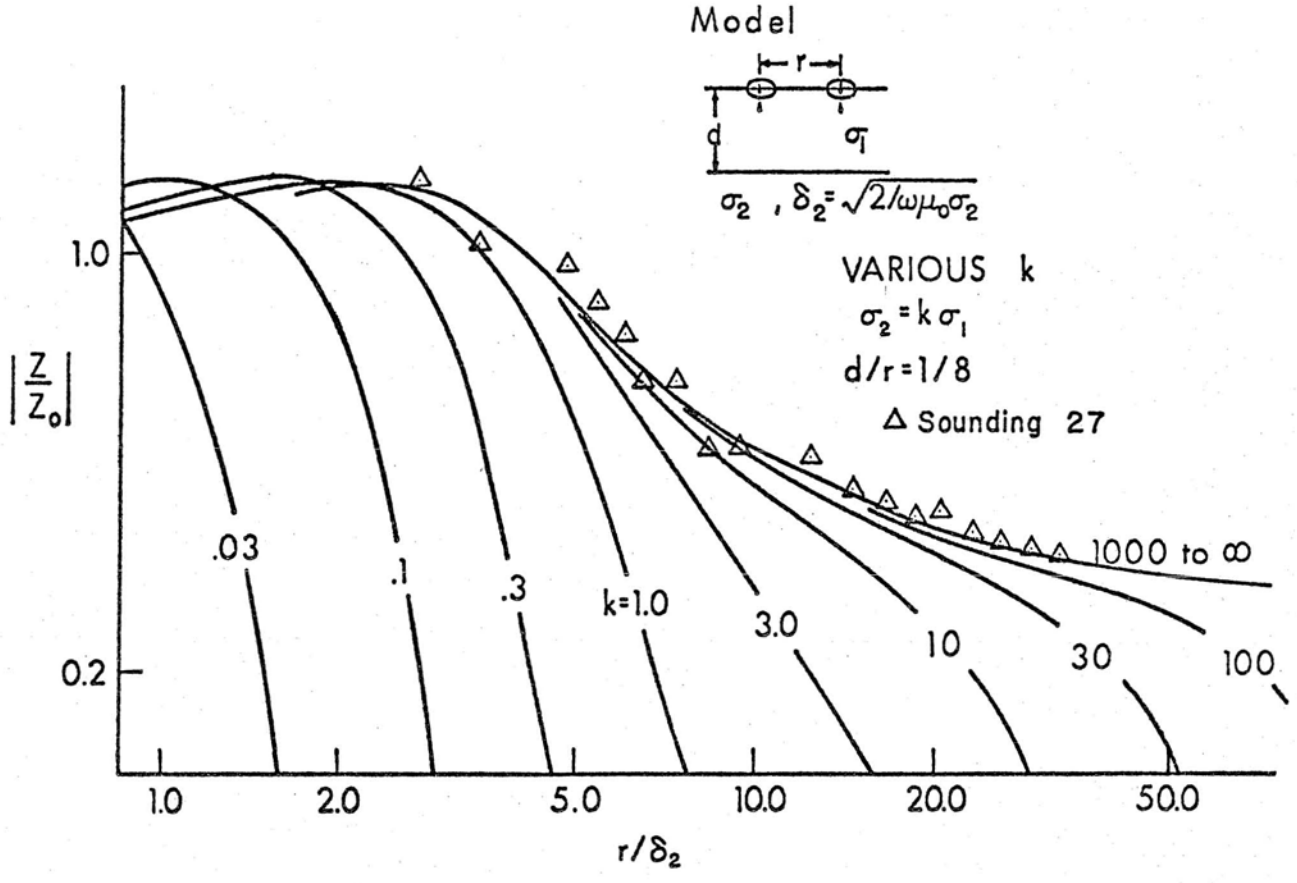

Figure 4. A set of two-layer models for a coplanar two-loop configuration and for the conductivity model shown. This figure indicates the resolution of a conductivity contrast for the case of d/r = 1/8. The normalized impedance amplitude $|Z|/|Z_o|$, and skin depth parameters are as defined in Figure 3. Examples of sounding data are shown.

explanation is evident in Figure 5, which shows two examples from the d.c. soundings. The conductivity contrast (10^2 to 10^4) is so great that spreads of (AB/2) of about 2 km would be necessary to define the asymptote of the sounding curve that would resolve the deep resistivity.

DISCUSSION

Our data show a very highly resistive overburden underlain by a more conductive zone. The lower, less resistive layer detected by the d.c. sounding occurred within 20 m of sea level for the three soundings on the southeast edge of the rift zone and about 71 m and 41 m above sea level for two soundings (G6 and G3, respectively) located to the northwest. The inductive soundings southeast of the rift zone generally detected a zone of low resistivity that began at greater depths (with respect to sea level) than the zone detected by the d.c. method.

In an area where the hydrology is described by a Ghyben-Herzberg relationship between fresh and salt water saturated strata, the top of the water table is at sea level or above, whereas the fresh-salt water interface is below sea level. The d.c. soundings detected a zone of moderate conductivity with different geometry and higher resistivity than the conductive zone detected in inductive soundings, which suggests that the d.c. methods sensed the water table surface whereas the inductive methods sensed the surface of the salt-water saturated rock. Hydrological data from well holes in Puna, as well as empirical relationships between pore water properties and bulk rock conductivity, generally support this view, as will be shown below. The anomalously high water table at sites G3 and G6 inferred from the present data cannot be directly confirmed. It is encouraging to note, however, that a seismic refraction experiment in the area near G3 detected a high velocity layer at the same elevation as the lowered resistivity layer that was interpreted as being water-saturated rock (W. Suyenaga, ms. in prep.).

On the southwest edge of the study area (Fig. 2), soundings 15-2 and 11-1 detected salt water at 31 and 9 m below sea level, respectively. By using the Ghyben-Herzberg ratio of 1:40, we should expect respective hydraulic heads of +0.8 and +0.2 m. Well 9-7, quite close to both 15-2 and 11-1 but about twice as far inland, has a static well head of +0.9 m and draws potable water, in good agreement with the inductive interpretation.

Kapoho well (number 1, Fig. 2) has a static water head of +0.9 m. The water is fresh and is thought to be perched on the relatively impermeable pyroclastics of Kapoho Crater (Stearns and Macdonald, 1946 state that a lake that formerly existed in the floor of Kapoho Crater, 2.5 m above sea level, was perched water.) Sounding 7-1 indicates a head of +1.5 m and sounding 6-1 indicates a head of +0.9 m. Sounding 4-1,

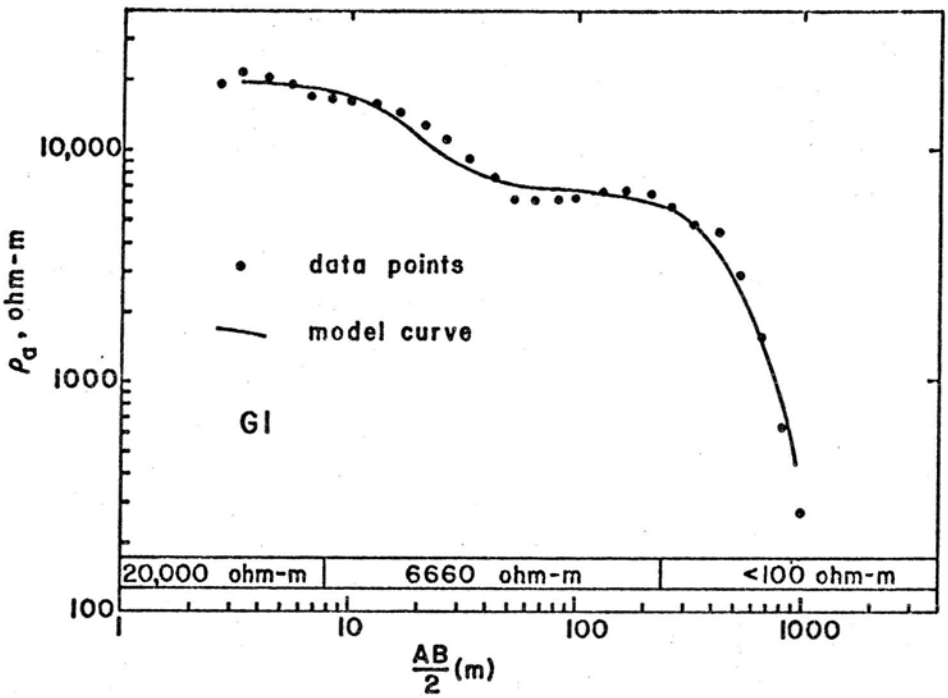

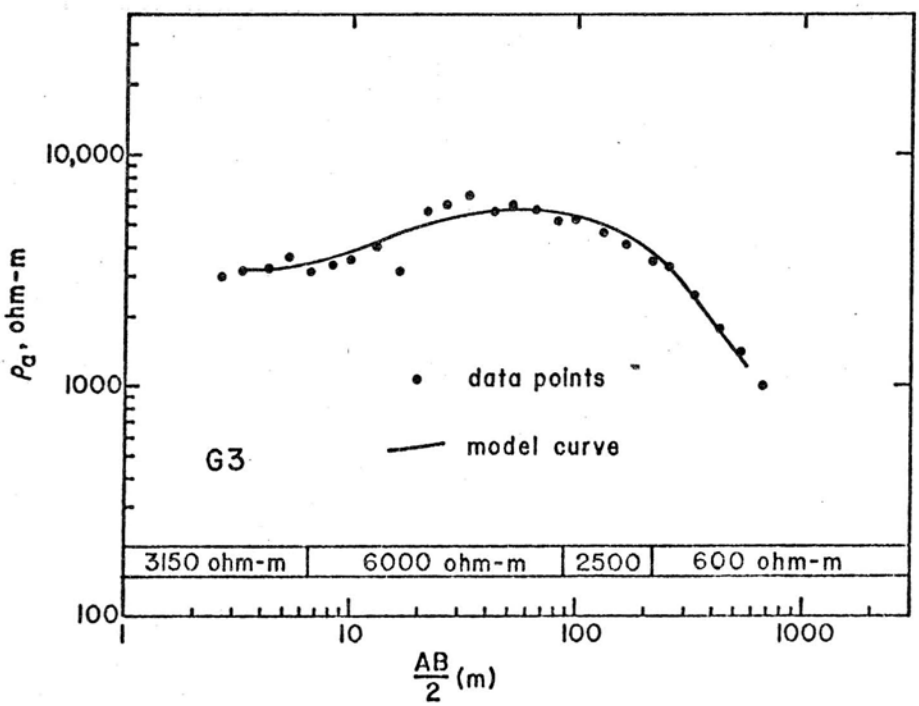

Figure 5. Examples of Schlumberger direct-current sounding data and their interpretations. Table 2 lists the interpreted models for these and other direct current soundings.

although it is twice as far inland and therefore is expected to show about twice the hydraulic head, indicates a head of only +0.6 m. The abnormally high hydraulic gradient in the immediate Kapoho area suggests the possibility of dike-impounded water rather than perched groundwater, a condition similar, for instance, to the hydrologic conditions found locally in the north rift zone of the Koolau mountains on Oahu (Takasaki and Valenciano, 1969).

The bulk resistivity of a rock with porosity fraction ϕ, saturated with water of resistivity ρ_ω, is given approximately by the empirical relationship

$$\rho = A\rho_\omega \varphi^m \qquad (1)$$

(Brace et al., 1965; Brace and Orange, 1968; Meidav, 1970). For the case of porous Hawaiian basalts, Keller (1970) and Manghnani et al. (1976) estimate (A, m) to be (3.5, -1.8), respectively. Using eq. (1) and assuming a porosity fraction of 0.2 to 0.3 (Zablocki et al., 1974) and a normal sea-water resistivity of .17 to .2 ohm-m (Schlichter and Telkes, 1942; Meidav, 1970), the bulk resistivities expected for rocks saturated with sea water range from 5.2 to 12.7 ohm-m. The interpreted inductive resistivities, which range from 5.6 to 6.7 ohm-m for the normal stations (Fig. 2, Table 3), are within this predicted range, although on the low side.

In contrast, the zone of lowest resistivity interpreted from d.c. soundings generally starts with a layer having a resistivity of about 100 to 600 ohm-m (Table 2). Station G6, the only d.c. sounding indicating an absence of this layer, is also the only direct current sounding that indicated a resistivity approaching those determined inductively. These higher resistivities must mean that if the rock is saturated, then the pore waters are much more resistive hence much less saline than sea water. These resistivities agree roughly with the Zohdy and Jackson (1969) estimate of 300 to 700 ohm-m for fresh-water saturated basalts and strengthens the hypothesis that the direct current sounding data detects the water table surface.

The anomalous inductive soundings near Opihikao and Allison well (Table 3 and Figure 2) detected bulk resistivities that are low even for sea-water saturated rock at normal temperatures. The profile of soundings 27, 28, 29 and 30, for instance, sensed resistivities of 1.2 to 4.9 ohm-m at elevations near sea level. Allison well, located next to sounding 27, has a static water level of +0.6 m, moderately high chloride content (2.6 ppt), and temperature (39°C) and specific water resistivity of 1.8 to 4.4 ohm-m. The bulk resistivities interpreted here are not significantly different from the resistivity of the sampled well water alone, implying that the pore waters within the saturated rock have an effective chloride content closer to that of sea water (35 ppt) or that the well temperature is lower than the mean temperature in the region sampled by the soundings.

The resistivity of an electrolytic pore liquid at temperature T is related to its resistivity at 18°C by

$$P_{\omega}(T) = \frac{P_{\omega}(18°C)}{(1. + 0.0025\ [T-18°C])} \qquad (2)$$

(Dakhnov, 1962; this equation is roughly valid for temperatures less than 200°C, as can be verified by comparison with the data in Quist and Marshall, 1968). Using Meidav's (1970) nomogram to combine equations (1) and (2) we find that the range of our interpreted resistivities for the well water's chloride content requires a temperature range of 110° to 300°C for a porosity fraction of 0.2, 40 to 140°C for a porosity of 0.3, or 20 to 90° for a porosity of 0.4. It is apparent that the lower range of our inductively determined resistivities implies pore water properties in conflict with those of the sampled well water if we accept a 0.2 to 0.3 porosity fraction as being representative for the area. Both inductive data and hydrological data, however, agree that Ghyben-Herzberg zonation is not present here. An analysis of the three anomalous soundings near Opihikao (10-1, 10-2, and 10-3) gives similar conclusions; no hydrological data exist for the area.

A review of previous inductive and galvanic surveys on Hawaii Island reveals that inductive resistivity determinations are commonly lower than galvanic resistivity measurements in corresponding areas. Between Puna and the summit of Kilauea volcano a series of two-loop induction soundings resolved a surface layer of 300 to 500 ohm-m over a layer of 1 to 30 ohm-m (Keller, 1971). Jackson and Keller, (1972) confirmed the detection of the lower layer near Kilauea's summit with an inductive transient survey. In contrast, direct current surveys in Puna have resolved a surface layer of 700 to 7000 ohm-m over a layer a 6 to 8 ohm-m, with occasional values as low as 2 ohm-m (Keller, 1973).

In the Humuula Saddle area, inductive data have indicated resistivities between 3000 and 5000 ohm-m (Keller, 1971); Schlumberger and dipole-dipole d.c. soundings indicate resistivities between 5500 and 6200 ohm-m (Zohdy and Jackson, 1969).

Note, however, that inductive soundings do not necessarily respond to the same resistivity parameter as do d.c. soundings. In particular, the coplanar two-loop system that generates and senses a vertical magnetic field at the earth's surface (plane of observation) is only sensitive to the longitudinal resistivity, ρ_{ℓ}, (parallel to the plane of observation). Direct current systems on the other hand are sensitive to the root-mean-square resistivity, $\rho_m = \sqrt{\rho_{\ell}\rho_n}$ where ρ_n is the resistivity in the direction normal to the plane of observation. The two methods of electrical sounding will determine the same resistivities only in areas where the earth consists of homogeneous, isotropic layers, e.g. where ρ_{ℓ} and ρ_n are equal within each layer (Keller and Frischknecht, 1966; Vanyan, 1967).

The discrepancies between inductive and direct current results on Hawaii Island might be explained by an anisotropic earth model. That volcanic areas can exhibit gross anisotropy to a large degree is shown by an analysis of well logs from the Columbia basalt plateau (Keller and Rapolla, 1974). The coefficient of anisotropy ($\sqrt{\rho_n/\rho_\ell}$) for this Columbia basalt section has been calculated to be in excess of 2.

The Hawaii strata is composed mainly of thin, basaltic lava flows (average thicknesses of 3 to 8 m, Macdonald, 1956) with broken and weathered zones between flows. To a first approximation this can be modeled as a repetitious alternation of two layers with resistivities ρ_1 and ρ_2 having P and (1-P) fractions of the total section, respectively. If we assume that the layering is too fine to be detected as discrete structures, then the model appears homogeneous but anisotropic; ρ_ℓ and ρ_m are given by

$$\rho_\ell = \rho_2[(Pk+(1-P)]^{-1}, \quad \rho_m = \lambda\rho_\ell = \rho_2\sqrt{\frac{1}{k}\,\frac{P+k(1-P)}{Pk+(1-P)}} \qquad (3)$$

where k is the resistivity contrast ($=\rho_2/\rho_1$) and λ is the coefficient of anisotropy ($= \sqrt{\frac{\rho_n}{\rho_\ell}=\frac{\rho_m}{\rho_\ell}}$, Grant and West, 1965).

In our model we will associate ρ_1 with the resistivity in the zones between flow layers of resistivity ρ_2. We expect k to be greater than 1 because of the effects of increased porosity and weathering, which will lower the resistivity in the interflow zone.

In a region of total saturation we will assume ρ_2 to be given by eq. (1). It is more difficult, however, to assign a value to ρ_1 because we have no basis to evaluate the interflow porosities and the weathering effects. ρ_1 could have any value from ρ_2 downward to the resistivity of the pore water, ρ_w. In many instances in Hawaii the lateral interflow permeability is so high that it forms the primary channels feeding Hawaiian type "shaft wells" (Macdonald and Abbott, 1970); hence, ρ_1 may be closer to ρ_w than ρ_2. For modeling, we will assume ρ_1 equal to ρ_w; then the resistivity contrast is a simple function of the basalt flow porosity fraction, e. g. $k = 3.5\,\varphi^{-1.8}$. This assumption, if in error, will not affect the main purpose of our model - to show the effects of a layered flow structure. It will, at worst overestimate the amount of interflow material.

Taking a representative porosity fraction as 0.16, which gives a k = 100 according to the above assumptions, the effective anisotropy (λ) calculated from eq. (3) ranges from 1 to about 5 for P varying from 0.0 to 1.0. An anistropy of about 1.5, which would account for the discrepancy in our data compared with data from Allison well samples, requires less than 1% (P= .01) of the section as interflow material.

Although we do not have much confidence in inductively determined resistivities for the high resistivity overburden (see the discussion in the previous section) the results reported by Keller (1971, 1973) suggest that anisotropies of over 5 may exist in the surface layer. Our data agree with this if we take our minimum inductive resistivity for the overburden (>500 ohm-m) as representative of the inductive resistivity. These anisotropies can be accounted for if k is greater than about 1000 and if P equals .01. Such a large k might be realistic if the interflow zones act as lateral channels to the horizontal movement of groundwater in the partially saturated zones above the water table.

One interesting result of the model studies is that coplanar two-loop inductive systems may underestimate the true longitudinal resistivity. This means that if d.c. data (giving $\hat{\rho}_m$ as an estimate of ρ_m) and inductive data (giving $\hat{\rho}_\ell$ as an estimate of ρ_ℓ) are used to estimate the coefficient of anisotropy as $\hat{\rho}_m/\hat{\rho}_\ell$, then this estimate may be larger than the true coefficient of anisotropy.

In a particular case (Fig. 6) where the whole section was a repetitious layering of 60 ohm-m material (10%) and 6000 ohm-m material (90%), the inductive response was, for practical purposes, indistinguishable from that of a 250 ohm-m halfspace. The Schlumberger d.c. response was essentially the same as an 1800 ohm-m half space. The response of the d.c. system was as predicted by eq. (3) (i.e., $\hat{\rho}_m \approx \rho_m$), but the inductive system response theoretically determined a resistivity $\hat{\rho}_\ell$ less than half of that predicted. The estimated anisotropy ($\hat{\lambda}$) from the theoretical data was slightly over 7 compared to the "true" model anisotropy (from eq. 3) of about 3.

We propose anisotropy as a plausible explanation for some of the apparent discrepancies between the present data and sampled water properties as well as the more general discrepancies between inductive and direct current sounding measurements. Detailed well logging in Puna would help to evaluate this hypothesis.

CONCLUSIONS

The inductive and direct current sounding results lead to the following geoelectric model for the upper strata in Puna: There is a thin surface layer of up to 8 m thickness having highly variable resistivity (3150 to 34,000 ohm-m). We suspect that this variability is related to local microstructural differences and various stages of weathering among the different lava flows. This layer is underlain by a more voluminous zone extending to the surface of the water table and having a mean direct current resistivity of about 6000 ohm-m. From comparison

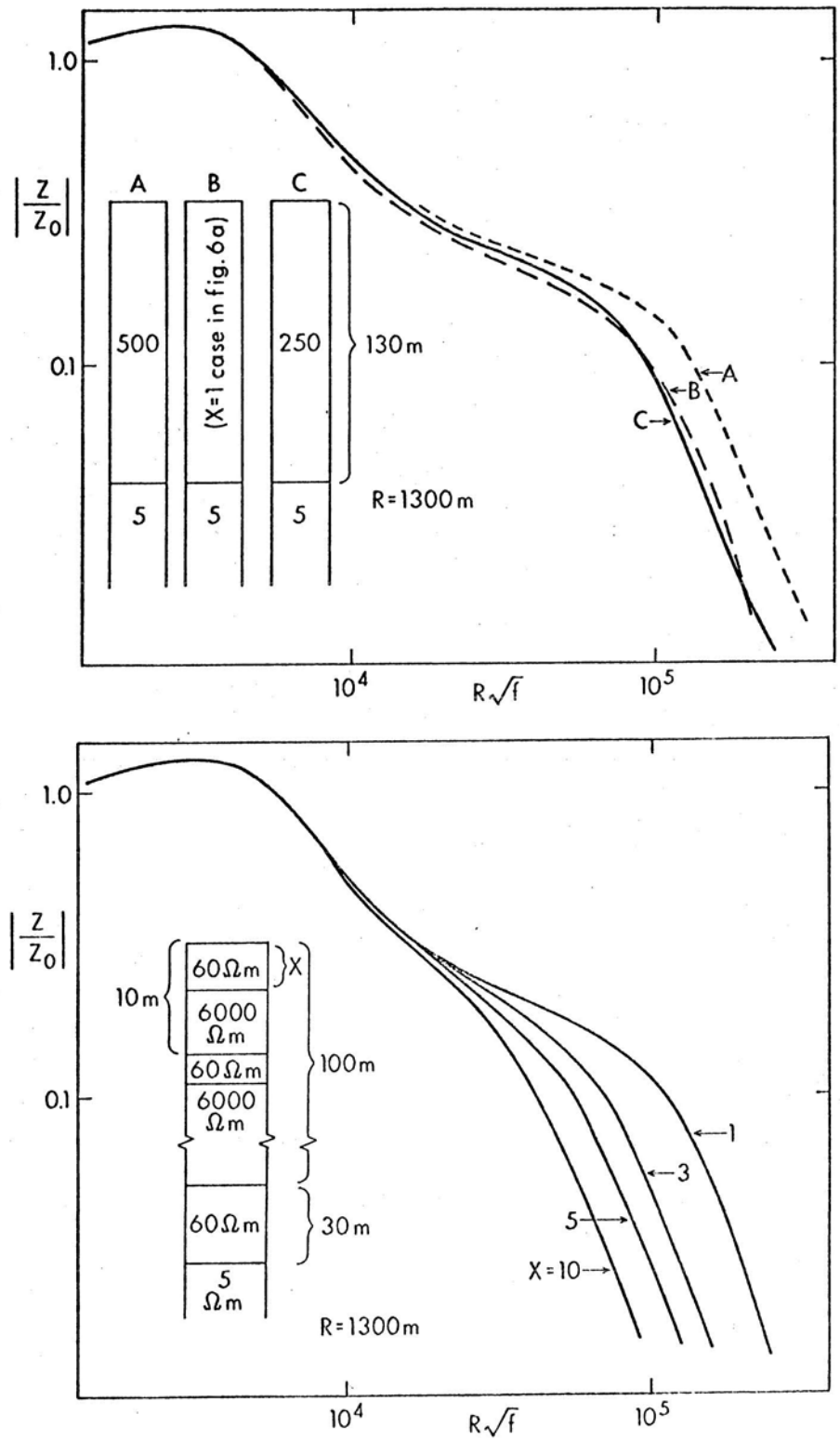

Figure 6. An example of a thinly layered section giving rise to large scale effective anisotropy. Theoretical responses to this section are for coplanar two-loop inductive systems. Possible interpretations of the theoretical data are presented that are based on the non-anisotropic modeling methods.

of direct current data with inductive data we suggest that this layer may be electrically anisotropic. The ratio of direct current to inductively determined resistivities for this layer indicates a possible coefficient of anisotropy of about 5. On the basis of our modeling studies, we suggest however, that a coefficient of about 2.5 is more likely. Such anisotropy is probably related to the effects of weathering and increased void space between the lava flows.

In the areas near Opihikao and Allison well (Fig. 2) the resistive overburden is underlain by 1 to 5 ohm-m material, as determined by inductive sounding. For other areas a layer of intermediate resistivity of about 100 to 600 ohm-m is underlain by about 6 ohm-m material. The strata of intermediate resistivity is interpreted to be saturated with fresh water. The lower resistivity material is saturated by sea water at normal temperatures for the resistivities of about 6 ohm-m, or at elevated temperatures for resistivities of less than 5 ohm. It is likely that coefficients of anisotropy of about 1.3 or less are associated with the saturated zone. The basic features of this interpretation are illustrated in Figure 7 for a section southeast of the rift zone and parallel to the coast.

The survey results indicate that potable water in the Kapoho area is restricted to a relatively small area near the present well (number 1, Fig. 2). We suggest that this occurrence of fresh water is controlled at least in part by dike structures in the rift zone. Our data also indicate the possibility of potable water in the area of inductive stations 15-2 and 11-1. There are presently no wells in this vicinity, although a well (9-7) at higher elevation about 2 or 3 km west produces potable water and may, in conjunction with the present data, imply the existence of usable water resources from out site 11-1 for some distance southward and parallel to the coast.

The anomalous sites that detect warm saline waters (estimated at over 40°C and verified at Allison well to be about 40°C) are generally seaward of recent volcanic activity in the rift zone. We presume that these waters have come in contact with hot rocks in the rift and have migrated toward the sea. Our probing depth was insufficient to provide estimates of the volume of warm or hot water present in these areas; however the results are useful in indicating areas where deep surveys should be concentrated.

The inductive sounding method as employed here was found particularly reliable in detecting the fresh-salt water interface, and thus in detecting the presence or absence of a Ghyben-Herzberg fresh water lens. Because of the possibility of anisotropic effects, the absolute conductivities interpreted must be taken as upper limits on the mean bulk conductivity of the inductively sampled region. The inferred pore water temperature and salinity estimates are therefore not as valid as the depth estimates to the salt water interface. However, distinction was possible between rock saturated with fresh

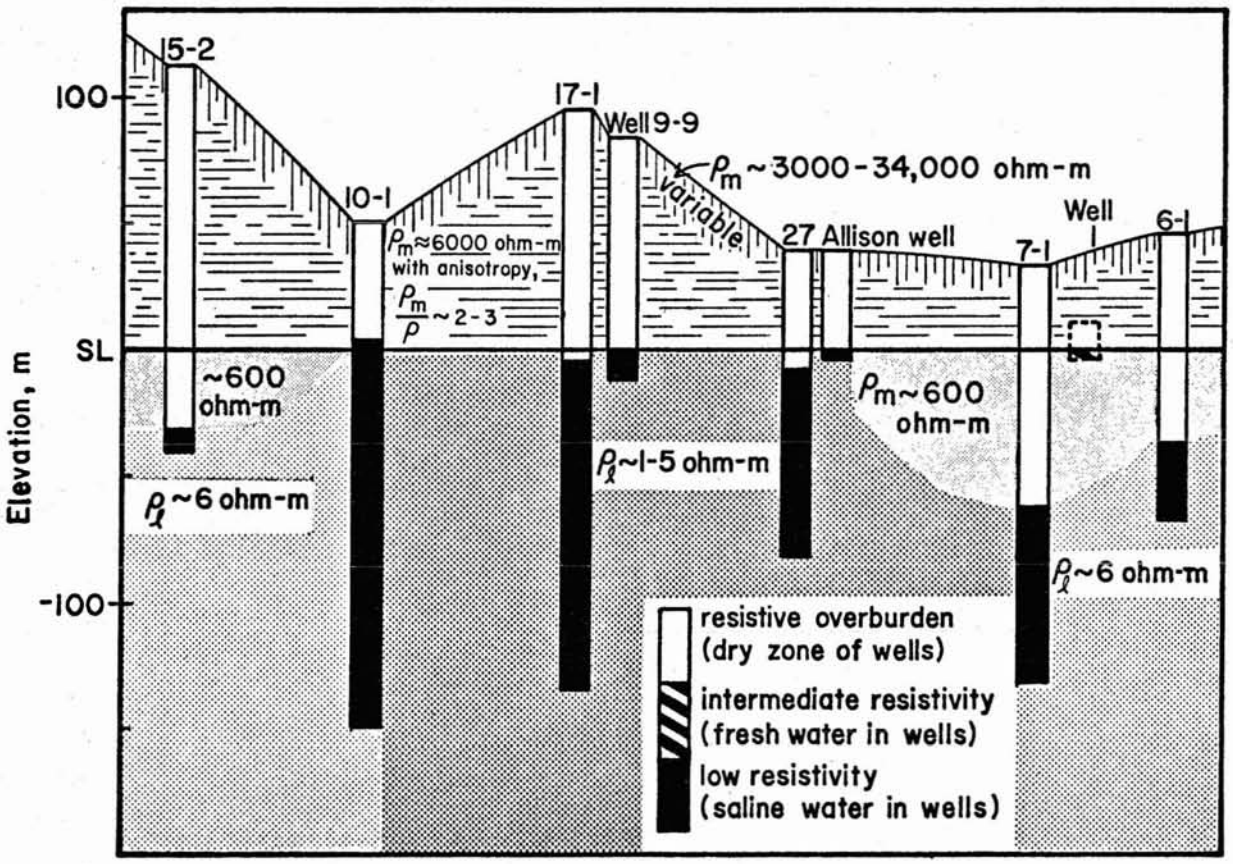

Figure 7. A geoelectric section parallel to the coast from Kapoho to the southwest of Opihikao (see Fig. 2). ρ_m is the estimated resistivity from direct current soundings, ρ_l is the estimated resistivity from the inductive soundings. See the discussion in the text regarding the anisotropy postulated here, and the inferred geological conditions associated with this diagram.

water, sea water, or warm sea water.

In contrast, the Schlumberger direct current method was able to directly estimate the depth to the water table, but with spreads of about 1000m, it provided less reliable estimates than did the inductive soundings on the resistivity of the more saline part of the water-saturated column.

ACKNOWLEDGMENTS

The authors gratefully acknowledge the encouragement and advice of Charlie Zablocki, USGS, Denver, Colorado, and the assistance and technical support of Gary McMurtry, Mike Broyles, Carrol Dodd, and Ted Murphy of the Hawaii Institute of Geophysics. Field assistants in this work were Steve Thede, Jozef Shoemaker, and Brent Miyamoto. Dr. C. M. Fullerton, Director of the Cloud Physics Observatory in Hilo, kindly allowed us the use of his facilities, and Dr. George Keller, Colorado School of Mines, provided pieces of equipment.

Brace, W.F., and A.S. Orange, 1968. Furthur studies of the effect of pressure on electrical resistivity of rocks. J. Geophys. Res., v. 73, p. 5407-5420.

Brace, W.F., A.S. Orange, and T.M. Madden, 1965. The effect of pressure on the electrical resistivity of water saturated crystalline rocks. J. Geophys. Res., v. 70, p. 5669-5678.

Dakhnov, V.N., 1962. Geophysical Well Logging, Quart. Colo. Sch. Mines, v. 57, no. 2.

Dieterich, J.H., and R.W. Decker, 1975. Finite element modeling of surface deformation associated with volcanism. J. Geophys. Res., v. 80, p. 4094-4102.

Division of Water and Land Development (DOWALD), 1970, An Inventory of Basic Water Resources Data: Island of Hawaii. Hawaii Div. Water and Land Dev. Rept. R34, Honolulu, Hawaii, 188 pp.

Fiske, R.S., and W.T. Kinoshita, 1969. Inflation of Kilauea prior to its 1967-1968 eruption. Science, v. 165, p. 341-349.

Fischer, W.A., D.A. Davis, and T. Souza, 1966. Fresh water springs of Hawaii from infrared images. USGS Hydrologic Atlas, HA-218.

Frischknecht, F.C., 1967. Fields about an oscillating magnetic dipole over a two-layer earth, and application to ground and airborne electromagnetic surveys. Quart. Colo. Sch. Mines, v. 62, 326 pp.

Grant, F.S., and G.F. West, 1965. Interpretation Theory in Applied Geophysics. McGraw-Hill Book Co., New York.

Jackson, D.B., and G.V. Keller, 1972. An electromagnetic sounding survey of the summit of Kilauea volcano. J. Geophys. Res., v. 77, p. 4957-4965.

Johansen, H.K., 1975. An interactive computer/graphic-display-terminal system for interpretation of resistivity soundings. Geophys. Prospect., v. 23, p. 449-458.

Keller, G.V., 1970. Inductive methods in prospecting for hot water. Geothermics, Spec. Iss. 2, p. 318-332.

Keller, G.V., 1971. Natural field and controlled source methods in electromagnetic exploration. Geoexploration, v. 9, p. 99-197.

Keller, G.V., and A. Rapolla, 1974. Electrical prospecting methods in volcanic and geothermal environments. In L. Civetta, P. Gasparini, L. Luongo, and A. Rapolla (eds.), Physical Volcanology, p. 133-166, Elsevier, Amsterdam.

Koefoed, O., D.P. Gosh, and G.J. Polman, 1972. Computation of type curves for electromagnetic depth sounding with a horizontal transmitting coil by means of a digital linear filter. Geophys. Prosp., v. 20, p. 406-420.

Macdonald, G.A., 1956. The Structure of Hawaiian Volcanoes. Verh. K. Ned. Geol. Mijnbouwkd. Genoot., v. 16, p. 274-295.

Macdonald, G.A., and A.T. Abbott, 1970. Volcanoes in the Sea. Univ. Hawaii Press, Honolulu, 441 pp.

Manghnani, M.H., C.S. Rai, and T. Hanada, 1976. Physical properties of rocks. In Phase II progress report, Hawaii Geothermal Project, Univ. Hawaii, Honolulu, Hawaii.

Meidav, T., 1970. Application of electrical resistivity and gravimetry in deep geothermal exploration. Geothermics, Spec. Iss. 2, p. 303-310.

Moore, J.G., and Harold L. Krivoy, 1964. The 1962 flank eruption of Kilauea volcano and structure of the east rift zone. J. Geophys. Res., v. 69, p. 2031-2045.

Quist, A.S., and W.L. Marshall, 1968. Electrical conductances of aqueous sodium chloride solutions from 0° to 800°C and pressures to 400 bars. J. Phys. Chem., v. 72, p. 684-703.

Schlichter, L.B., and M. Telkes, 1942. Electrical Properties of rocks and minerals. In F. Birch (ed.), Handbook of Physical Constants, GSA Spec. Pap. 36, p. 299-319.

Schwartz, J.H., 1937. Resistivity studies of some salt-water boundaries in the Hawaiian Islands. Nat. Res. Council, Trans. AGU, 18th Ann. Mtg., part 2, p. 387-393.

Stearns, H.T, 1966. Geology of the State of Hawaii. Pacific Books, Palo Alto, California.

Takasaki, K.J., and S. Valenciano, 1969. Water in the Kahuku Area, Oahu, Hawaii. USGS WSP 1874.

Vanyan, L.L., 1967. Electromagnetic Depth Soundings. Consultants Bureau, New York.

Verma, R.K., and O. Koefoed, 1973. A note on the linear filter method of computing electromagnetic sounding curves. Geophys. Prosp., v. 21, p. 70-76.

Wright, T.L., and R.S. Fiske, 1971. Origin of differentiated and hybrid lavas of Kilauea volcano, Hawaii. J. Petrol., v. 12, p. 1-65.

Zablocki, C.J., R.K. Tilling, D.W. Peterson, R.I. Christiansen, G.V. Keller, and J.C. Murray, 1974. A deep research drill hole at the summit of an active volcano, Kilauea, Hawaii. Geophys. Res. Lett., v. 1, p. 323-326.

Zohdy, A.D.R., and D.B. Jackson, 1969. Application of deep electrical soundings for groundwater exploration in Hawaii. Geophysics, v. 34, p. 584-600.

INTERPRETATION OF ELECTROMAGNETIC TRANSIENT SOUNDINGS MADE ON THE EAST RIFT OF KILAUEA VOLCANO, HAWAII

James P. Kauahikaua*
Douglas P. Klein

Hawaii Institute of Geophysics
University of Hawaii
Honolulu, Hawaii 96822

*now with the U. S. Geological Survey

ABSTRACT

Electromagnetic transient soundings were made on the lower east rift of Kilauea volcano, in the Puna area, Hawaii. These soundings employ the magnetic response of the earth to a step function of current in a horizontal linear source. Interpretation of these data is based on a general inversion technique that uses linear comparisons between the data and model values. A comparative study of various interpretational techniques leads to the conclusion that certain of the more commonly used methods, which employ the reduction of transient voltage data to the logarithmic domain, tend to emphasize those data with lower amplitudes and signal-to-noise ratios that can produce unjustified complexity in the interpretations. The results show that the conductivity structure in Puna is vertically uniform to a depth of about 1000 m below sea level. There is a broad, but distinct, lateral variation in the conductivity ranging from 0.10 to 0.16 S/m in most of the survey area to anomalous values of 0.30 to 0.50 S/m in a zone south of the rift at Puu Honuaula. Groundwater temperatures in the anomalous zone are expected to approach 150°C.

INTRODUCTION

Electromagnetic transient sounding data were obtained on the east flank of Kilauea volcano, Hawaii (Fig. 1) in 1974 as part of a geothermal exploration program conducted by the Hawaii Institute of Geophysics. The data were interpreted using several different techniques to provide a basis for evaluating the transient sounding method.

Transient sounding refers to measurements of the time-variations of electromagnetic fields that are generated by an electric source whose current is varied in a controlled manner with time. The source used here was a finite-length, horizontal line whose current was varied in the form of a step function (see Fig. 2). The magnetic field associated with such a source induces secondary electrical currents in the earth's conducting regions whose amplitude and rate of decay is controlled by the subsurface conductivity structure. Surface measurements of either the electric field or the associated magnetic fields, in conjunction with knowledge of the source fields, provide response data that can be used to determine the conductivity structure. In this study, time-variations of the vertical magnetic field were measured as voltages induced in a horizontal sensing coil. A typical setup, along with idealized diagrams of the source current and the corresponding sensor voltage functions, are shown in Figure 2.

Inductive methods, such as transient sounding, are especially sensitive to high conductivity anomalies such as those associated with geothermal resources, while being relatively unaffected by the low overburden conductivities (Keller, 1970). Inductive soundings should be able to detect a conductivity discontinuity at a depth between 1 and 1/16 skin depth units of the overburden with sufficient resolution to determine the conductivities both above and below the discontinuity (Mundry, 1966). If the discontinuity is shallower than these limits then the response will be that of a halfspace with the conductivity of the material below, whereas if the discontinuity is deeper then the response will be that of a halfspace with the conductivity of the material above.

Transient sounding surveys on Kilauea volcano's summit (Jackson and Keller, 1972) and lower east rift zone (Skokan, 1974) and California's Long Valley (Stanley et al., 1976) have demonstrated that the method can obtain large amounts of data

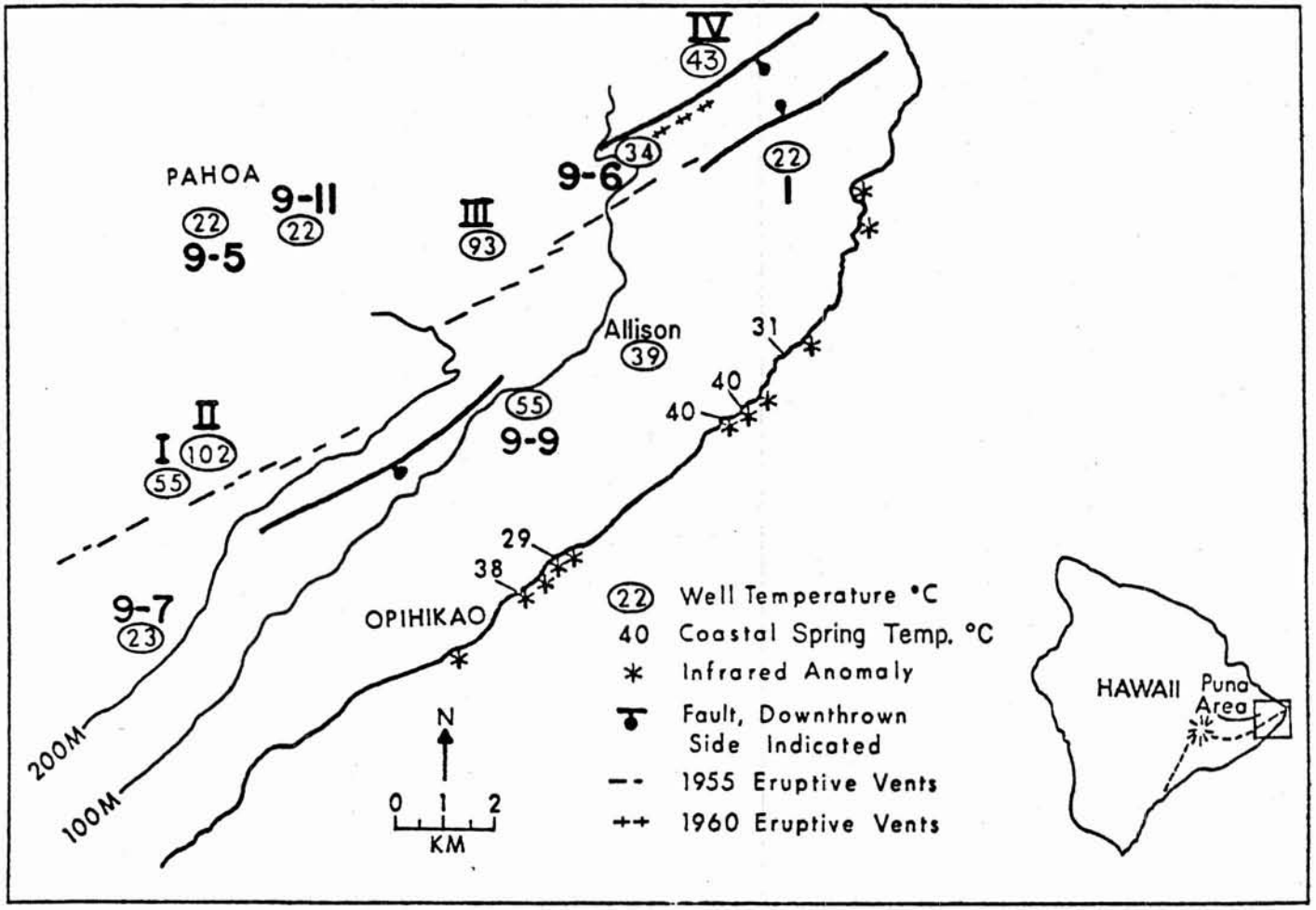

Figure 1. Major structural features and water temperatures in Puna. The numbers above the well temperature symbols are the well referenced by Roman numerals are geothermal test borings (Stearns, 1965).

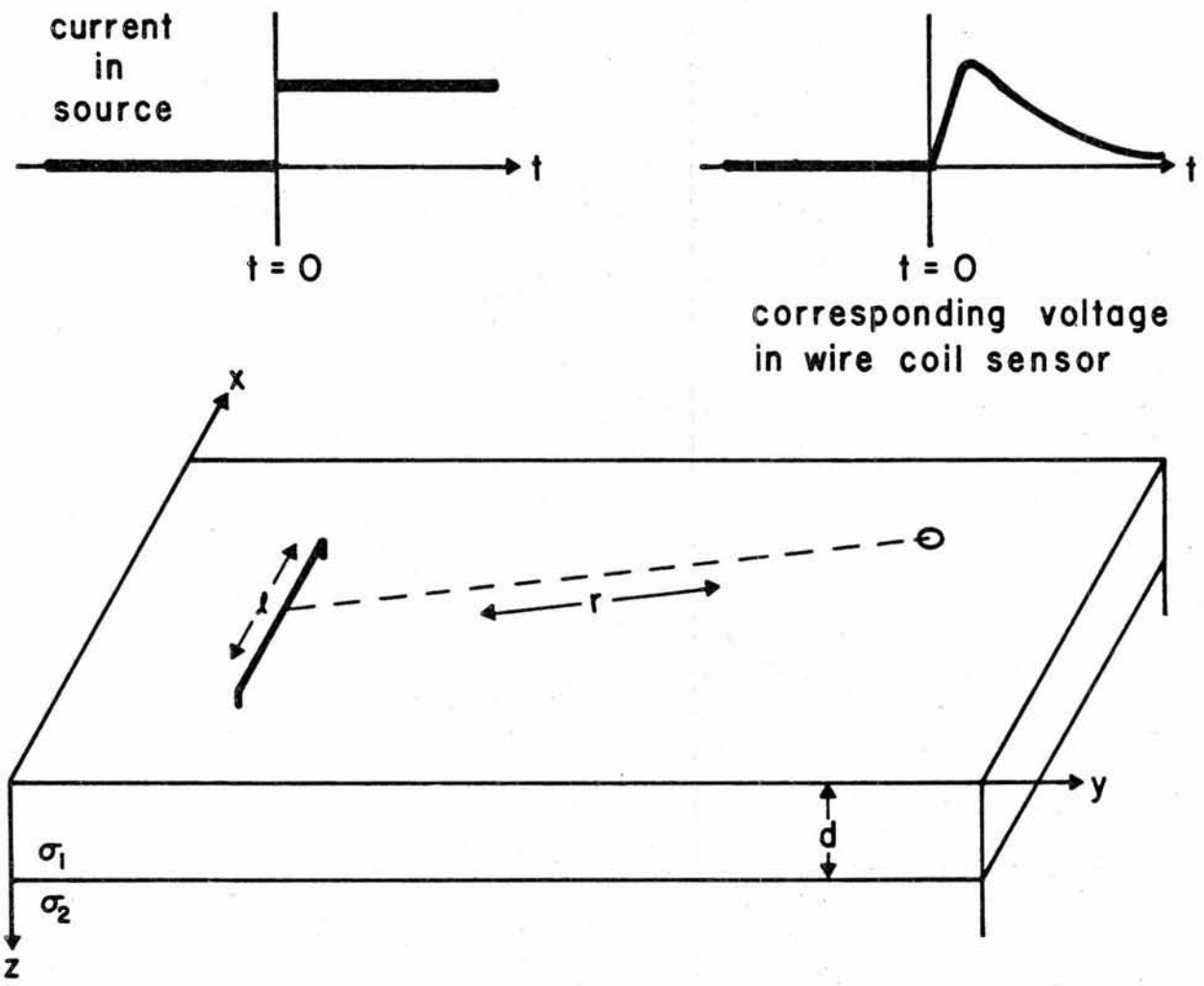

Figure 2. Transient sounding setup showing a typical set of source current and sensor coil voltage functions. The setup is over an idealized two-layer earth.

for geothermal exploration purposes both quickly and economically. However, the interpretations on the summit and east rift zone of Kilauea were not a good description of subsurface conditions when compared with the results of deep research drill holes in each area (Zablocki et al., 1974; G. A. Macdonald, personal communication, 1976). The reason for this discrepancy may be found in the interpretational techniques, which worked with the logarithms of the data values instead of the actual values. This procedure emphasizes small voltages over large ones, and may therefore in the presence of noise suggest more complicated models than would be necessary to fit the data. This possibility prompted the introduction and use of a restricted generalized inversion for time-domain data, called partial inversion. For comparison, more conventional interpretations were also employed and are described here.

GOVERNING EQUATIONS

We are concerned with the time response of a vertical magnetic field of a horizontal electric dipole source on the surface of a horizontally layered earth. The theory is initially stated in the frequency domain where the field has time dependence $e^{i\omega t}$ where $\omega = 2\pi f$, f is in Hz. The final expression is the transient (time) response to a step function of current through the electric dipole source. The equations here summarize the main results given by Vanyan (1967, p. 125) and Wait (1951, 1966). SI (rationalized MKS) units are used within a cartesian coordinate system throughout.

We assume that the electric dipole is situated at the origin and oriented along the x-axis. The surface of an N-layered earth is at z=0 and the layer boundaries are planar and perpendicular to the z-axis. The upper halfspace has the electromagnetic properties of free space and its parameters are denoted by the subscript zero. At z=0, and in the frequency domain, the vertical magnetic field (units of tesla = webers/m^2 is given by:

$$B_z = \frac{I\mu_o}{2\pi}\left\{\frac{y}{k_1^2 r^5}\left[3-(3+3k_1 r+k_1^2 r^2)e^{-k_1 r}\right]+\frac{y}{r}\int_0^\infty m^2 R(m) J_1(mr)\,dm\right\} \qquad (1)$$

where ε_i = electric permittivity ($\varepsilon_o = 8.854 \times 10^{-12}$ farad/m)

μ_i = magnetic permeability ($\mu_o = 4\times10^{-7}$ henry/m)

σ_i = conductivity (siemens/m = S/m)

$r^2 = x^2 + y^2$

$k_i^2 = \omega^2 \mu_i \epsilon_i + \omega \mu_i \sigma_i$ $(k_o^2 = 0)$

J_1 is a Bessel function of the first kind and order one

m is a variable of integration

$$R(m) = R_{0,N}(m) - V_{0,1}$$

$$R_{i-1,N}(m) = \frac{V_{(i-1),i} + R_{i,N}(m)\, e^{-2d_i V_i}}{1 + V_{(i-1),i} R_{i,N}(m) e^{-2d_i V_i}}$$

$$R_{N,N}(m) = 0$$

$$V_{i,k} = (V_i - V_k)/(V_i + V_k)$$

$$V_i = m^2 + k_i^2$$

The subscript "i" denotes layer i. We assume that σ_i will be much larger than $\epsilon_i \omega$ (the quasi-static assumption) and that $\mu_i = \mu_0$ for all layers; therefore, we approximate $k_i^2 \approx i\omega\mu_o\sigma_i$. The first half in brackets of eq. (1) is the response of a halfspace of conductivity σ_1. The second half is the perturbation response due to layering.

For the setup of Figure 2, the vertical magnetic response of the earth to a step function of current in the source dipole is measured as a voltage induced in a wire coil. Thus the coil responds to $\frac{\partial}{\partial t} b_z(t)$ rather than simply $b_z(t)$. The time function, $b_z(t)$, is related to $B_z(f)$ of eq. 1, by an inverse Fourier transform. The step function of current at the source is zero for negative times and a positive constant for times greater than or equal to zero. The source function in the frequency domain is then $1/i\omega$, so

$$\frac{\partial}{\partial t} b_z(t) = \frac{1}{2\pi} \int_{-\infty}^{\infty} B_z(\omega) e^{i\omega t} d\omega = L[B_z(\omega)] \,. \qquad (2)$$

Substituting eq. (1) into (2) results in (Wait, 1951),

$$\frac{\partial}{\partial t} b_z(t) = \frac{I\mu_o}{2\pi}\left\{\frac{3y}{\mu_o\sigma_1 r^5}\left[\operatorname{erf}(u) - \frac{2}{\sqrt{\pi}}\left(u + \frac{2}{3}u^3\right)e^{-u^2}\right]\right.$$

$$\left. + \frac{y}{r} \cdot L\left[\int_o^\infty m^2 R(m) J_1(mr)\, dm\right]\right\} \qquad (3)$$

where

$$u = \frac{r}{2}\sqrt{\frac{\mu_o\sigma_1}{t}}, \quad (t \text{ in seconds})$$

$$\operatorname{erf}(u) = \frac{2}{\sqrt{\pi}}\int_o^u e^{-x^2} dx.$$

Again, the first half of eq. (3) is the halfspace response of conductivity σ_1 and is denoted below by $\frac{\partial}{\partial t} b_z^0(t)$. The second half is the perturbation of the transient response due to layering and is denoted by $\frac{\partial}{\partial t} b_z^P(t)$. Their separate expressions are

$$\frac{\partial}{\partial t} b_z^0(t) = \frac{3Iy}{2\pi\sigma_1 r^5}\left[\operatorname{erf}(u) - \frac{2}{\sqrt{\pi}}\left(u + \frac{2}{3}u^3\right)e^{-u^2}\right] \qquad (4)$$

and

$$\frac{\partial}{\partial t} b_z^P(t) = \frac{I\mu_o y}{2\pi r} L\left[\int_o^\infty m^2 R(m)\, J_1(mr)\, dm\right] \qquad (5)$$

so we may write

$$\frac{\partial}{\partial t} b_z(t) = \frac{\partial}{\partial t} b_z^0(t) + \frac{\partial}{\partial t} b_z^P(t). \qquad (3a)$$

Equations (4) and (5) have properties we must note at this stage as they are critical to the justification of the inversion scheme discussed later. For the halfspace response, eq. (4), if one starts at some finite, positive time,

$$\lim_{t\to 0} \frac{\partial}{\partial t} b_z^0(t) = \lim_{u\to\infty} \frac{\partial}{\partial t} b_z^0(t) = \frac{3Iy}{2\pi\sigma_1 r^5} \tag{6}$$

$$\lim_{t\to\infty} \frac{\partial}{\partial t} b_z^0(t) = \lim_{u\to 0} \frac{\partial}{\partial t} b_z^0(t) = 0. \tag{7}$$

The halfspace transient response rises from zero to $3Iy/2\pi\sigma_1 r^5$ at zero time and subsequently decays back to zero with increasing time. For the perturbation response, eq. (5), if one again starts at some finite, positive time,

$$\lim_{t\to 0} \frac{\partial}{\partial t} b_z^P(t) = \lim_{\omega\to\infty} B_z^P(\omega) = 0 \tag{8}$$

$$\lim_{t\to\infty} \frac{\partial}{\partial t} b_z^P(t) = \lim_{\omega\to 0} B_z^P(\omega) = 0 \tag{9}$$

$$\lim_{t\to\infty} \int_0^t \frac{\partial}{\partial t} b^P(t)\,dt = \lim_{\omega\to 0} \frac{B_z^P(\omega)}{i\omega} = 0 \tag{10}$$

where we note that

$$B_z^P(\omega) = \frac{I\mu_o y}{2\pi r} \int_0^\infty m^2 R(m) J_1(mr)\,dm \tag{11}$$

is equivalent to the first half of eq. (1) (Wait, 1951). The perturbation response is zero at time zero. For two or more layers, it departs from zero after time zero, but its integral with respect to time (the sum of the deviations from zero) and the perturbation response itself approaches zero as time increases.

DATA ACQUISITION AND ANALYSIS

The magnetic transient sounding technique used here employed as a current source a single wire from 400 m to 1.4 km long, which was grounded at each end with 20 to 40 steel stake electrodes (about 0.5 m long) connected in parallel. Electrical ground contacts were improved by soaking the soil around the stakes with a mixture of salted water and highly-conductive drilling mud. Power was supplied by a three-phase, 15-KVA diesel generator through a rectifier and automatic solid-state switcher connected in series with the grounded line. During operations, the line voltage was kept constant at nearly 1000 v so the current is inversely proportional to the resistance measured between the electrodes. Due to the high resistivity of surface rocks in Puna, currents of only 2 to 6 A were realizable, although the equipment is capable of producing up to 15 A. The switcher automatically turned the current on and off at a half-period of about 8.5 sec, producing a continuous square wave signal. This period is longer than the time required for the transient response to decay to negligible voltage levels, so the step function idealization is valid.

Variations of the vertical magnetic field generated by this source were recorded as voltages induced in a square coil of wire laid horizontally on the ground. The voltage induced in the coil, v(t), is related to the average magnetic field within the coil by

$$v(t) = NA \frac{\partial}{\partial t} b_z(t) \qquad (12)$$

where N is the number of turns of wire in the coil, A is the area enclosed by the coil, and $b_z(t)$ is the mean transient vertical magnetic field in the coil. The coil had 42 turns enclosing about 5800m^2. The transient coil voltages were passed through a one-pole, low-pass filter (corner frequency of 4 Hz) and two band-rejected filters (to reject 60 to 120 Hz) to reduce natural ambient and 60-Hz cultural noise. The filtered signal was recorded by a Hewlett-Packard oscillographic chart recorder capable of detecting one microvolt and recording at speeds up to 125 mm/sec.

From the chart records for each sounding, between 7 and 12 transients (defined as the voltage response to a single current step at the source) were manually digitized at 4-msec intervals for up to one second. Since each transient was a repeat measurement of the same response, they were stacked to reduce noise and obtain an average response, $\bar{v}(t)$. The stacking allowed an estimation of the data variance,

$$s^2 = \sum_{u=1}^{k} \sum_{i=1}^{n_u} [v_u(t_i) - \bar{v}(t_i)]^2 \qquad (13)$$

where k is the number of transients being stacked, n_u is the number of voltage samples for transient u, $v_u(t_i)$ is the voltage at time t_i, (i=1, 2, ...n_u) for transient u, $\bar{v}(t_i)$ is the average voltage at time t_i, and ν is the number of degrees of freedom for s^2 given by:

$$\nu = \sum_{u=1}^{k} (n_u - 1) \qquad (14)$$

(Draper and Smith, 1966). The signal-to-noise ratio, defined as the largest observed voltage divided by the data standard deviation, s, ranged from 4.2 to 74.6 and averaged about 12.

The averaged transient, v(t), is not the desired earth response because the signal is distorted by the measuring equipment. The transient signal must be compensated for the effect of this distortion before further analysis. The distortion was estimated in the laboratory as the impulse response of the filters and the chart recorder, denoted I(ω). After stacking, each transient was transformed to the frequency domain, compensated using the relation

$$E(\omega) = \frac{V(\omega)}{I(\omega)} \qquad (15)$$

where E(ω) is the earth response and V(ω) is the Fourier transform of v(t), and transformed back to the time-domain.

The result of the stacking and compensation procedure described above should be the true earth response. The resultant transients, however, were "noisier" than when originally measured, due to aliasing of the original transient data. The highest frequency resolvable for a transient sampled at 4-msec intervals is 125 Hz. The filters used in recording produced 37-db attenuation at 125 Hz, while the dynamic range of the recorder was nearly 60 db. The recorded transients can thus contain significant amounts of information at frequencies higher than the digital Nyquist limit of 125 Hz which are folded back onto the transformed digitized transient (Jenkins and Watts, 1968). The frequency region most affected was between 35 and 125 Hz (this range was empirically determined). This problem was not realized until after the data had been collected. The remedy was to delete the most aliased data; thus, in the final

compensation procedure, all components for frequencies higher than 35 Hz were set to zero before transformation back to the time domain. This procedure is equivalent to low-pass boxcar filtering in the frequency domain.

The earth response, now sampled at 4-msec intervals (e.g., at 4, 8, 12, 16, 20, 24 msec), was resampled at geometric intervals (e.g., at 4, 8, 16, 32, 64 msec), which shortened the digital series from between 125 and 250 points, to between 20 and 30 points, and thus was more economical. First, the portion of each transient in which initial build-up occurred (usually within the first 20 msec) was discarded, leaving only the transient's long decay. The build-up was removed because it is primarily the result of the low-pass boxcar filtering and is thus not representative of the earth response. Second, the remaining decay was averaged arithmetically over a band two intervals wide extending from the time

$$(4 \text{ msec}) \times 10^{.07(i-1)}, \quad i=10, 11, 12, \ldots$$

to the time $(4 \text{ msec}) \times 10^{.07(i+1)}$, $i=10, 11, 12, \ldots,$

resulting in a shortened digital transient resampled at the times

$$(4 \text{ msec}) \times 10^{.07i}, \quad i=10, 11, 12, \ldots$$

The logarithmic interval of 0.07 was used so that none of the sampled intervals is ever shorter than 4 msec between 20 msec and 1 sec.

Jackson and Keller (1972) used a filter similar to this one to transform their arithmetically sampled transients to geometrically sampled ones, with the important exception that the transient was averaged logarithmically, as:

$$\bar{a} = \left(\prod_{i=1}^{m} a_i\right)^{1/m}, \tag{16}$$

rather than arithmetically,

$$\bar{a} = \frac{1}{m} \sum_{i=1}^{m} a_i \tag{17}$$

as was done here. Their use of the logarithmic average appears justified because the logarithmic average is equivalent to averaging the transient as it appears on a bilogarithmic plot. However, particular properties on the logarithmic average can render its estimates very inaccurate. The most obvious difficulty is with negative numbers, which commonly occur in noisy data. In this case, the root of the logarithmic average expression above may not be real numbers.

INTERPRETATIONS

Several interpretation methods have been used for transient sounding data. Many of these techniques, as well as two new ones, were utilized for the 17 soundings considered here (see Fig. 3 and Table 1). The conventional techniques used were logarithmic curve-matching and early time and late-time asymptote evaluation. The new techniques were partial inversion, which can be used to determine the best-fit halfspace response, and a half-amplitude decay-time method, which can be used in the field for quick determinations of apparent conductivity.

Both the logarithmic curve-matching and partial inversion methods use the sounding data to determine subsurface layering by minimizing the differences between the data and models. The difference between the two approaches is in their minimization criteria. With curve-matching, one minimizes the sum of squares of the logarithmic residuals:

$$\sum_{i=1}^{n} [\log \bar{v}(t_i) - \log f(t_i, \vec{\theta})]^2 = \sum_{i=1}^{n} [\log \frac{\bar{v}(t_i)}{f(t_i, \vec{\theta})}]^2 \qquad (18)$$

where $\bar{v}(t_i)$ is the transient voltage data at times t_i, and $f(t_i, \vec{\theta})$ is the transient voltage model for the parameters in the vector $\vec{\theta}$. With the partial inversion method, one minimizes the weighted sum of squares of the observed residuals:

$$S(\vec{\theta}) = \sum_{i=1}^{n} \frac{1}{s(s_i)^2} [\bar{v}(t_i) - f(t_i, \vec{\theta})]^2 \qquad (19)$$

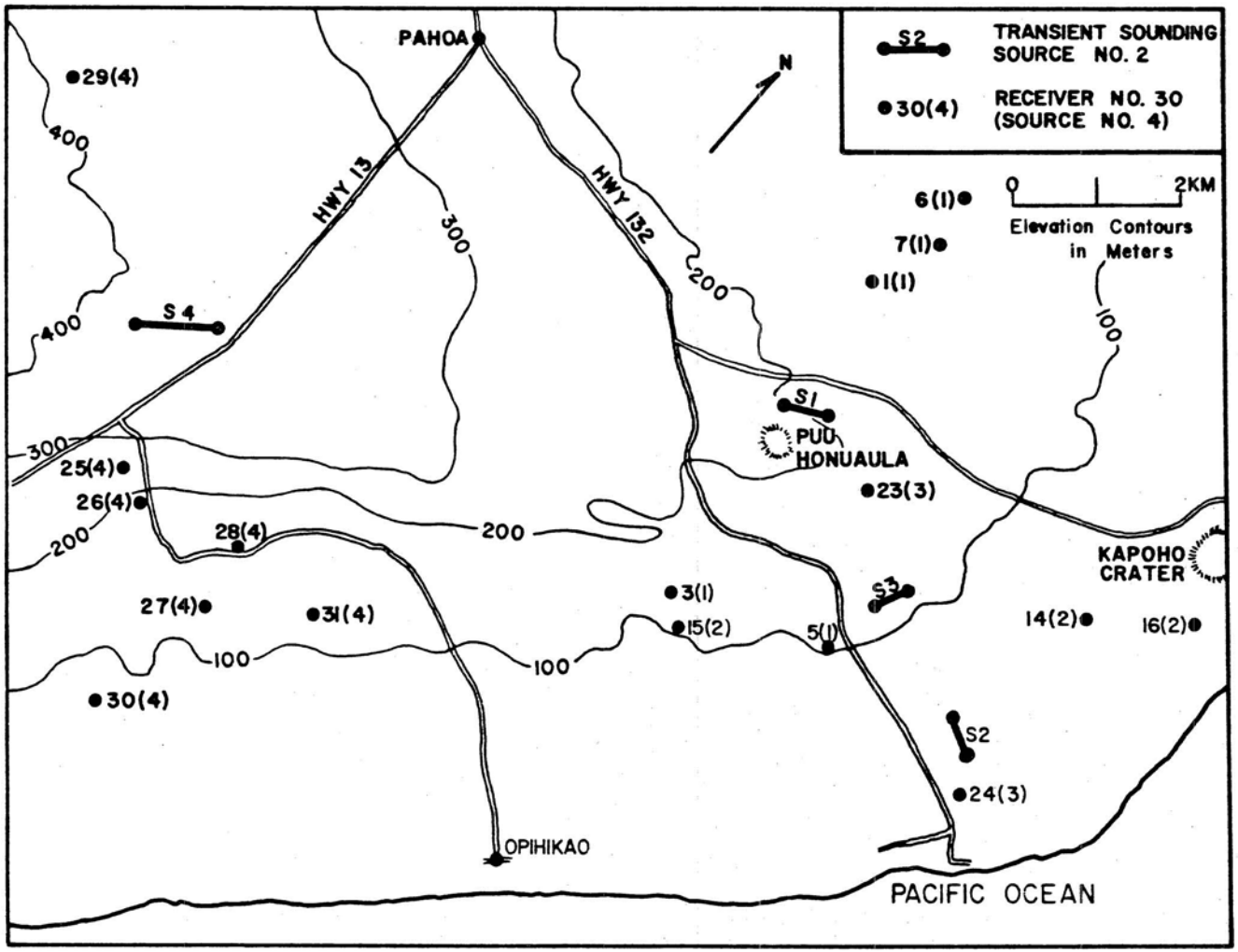

Figure 3. Current source and sensor coil locations for the soundings interpreted in this report.

Table 1. Principal facts: Puna transient data

Sounding	Source	r(m)	r/ℓ	$\cos^{-1}(y/r)$	$s^2(\times 10^{-8})$	υ	n
1	1	1678	2.4	75	84.40	1301	17
3	1	2620	3.8	66	1.36	1203	19
5	1	2750	4.0	71	33.90	1318	20
6	1	3140	4.6	65	2.05	1272	21
7	1	2500	3.6	60	9.27	906	15
14	2	2040	3.3	64	2.16	794	20
15	2	3500	5.6	54	.45	1899	21
16	2	3100	5.0	82	1.89	2350	19
23	3	1290	2.3	78	15.00	1188	19
24	3	2450	4.3	90	5.37	2591	25
25	4	1780	1.8	72	8.90	879	18
26	4	2080	2.1	80	10.60	990	20
27	4	3290	3.3	82	8.00	1589	17
28	4	2650	2.7	72	10.70	1224	19
29	4	3190	3.2	62	19.70	1101	16
30	4	4460	4.5	80	.69	2098	24
31	4	3700	3.7	63	1.07	1702	23

Definition of the parameters. The equations refer to the main text.

- r : Source: receiver separation (meters).
- ℓ : Source length (meters).
- $\cos^{-1}(y/r)$: angle between the source direction and the line between source and receiver.
- s^2 : data variance, eq. (13).
- υ : degree of freedom in s^2.
- n : number of data points in the logarithmically resampled data.

where s_i^2 is the variance of $\bar{v}(t_i)$. Equation (19) is the general least-squares minimization criterion (Draper and Smith, 1966). Equation (18) is similar to a special case of eq. (19) where the data standard deviation, s_i, is always proportional to $\bar{v}(t_i)$. This situation is approximately correct in resistivity work where the data are generally measured with a constant relative precision, say 5%. For this example, eq. (19) yields

$$\frac{1}{(0.05)^2} \sum_{i=1}^{n} \left[1 - \frac{f(t_i, \vec{\theta})}{\bar{v}(t_i)}\right]^2 \qquad (20)$$

The above expression and eq. (18) are both minimized by having the ratios of data and model values approach unity, rather than having their differences approach zero as in eq. (19). Transient sounding data, however, are usually measured with a constant absolute precision of perhaps 5 μv and should use eq. (19), as such conditions do not fit into the special case outlined above.

The logarithmic curve-matching and partial inversion used here differs from that of curve-matching methods in most resistivity interpretation studies in that the shape and amplitude of the transient data were interpreted independently and evaluated on their separate merits. Studies of the effects of various kinds of errors on resistivity determination from transient data (Vanyan, 1967, p. 201) show that these errors affect transient amplitudes and shapes differently. For example, the equations of transient sounding generally assume infinitestimal, horizontal current source and wire coil receiver. This applies to practical cases for which the maximum dimension of either source or receiver is less than one-fifth the distance between them (Keller and Frischknecht, 1966, p. 288). Halfspace model studies on the effect of finite source length (Kauahikaua, 1976, Appendix A) show that when the separation-length conditions are not fulfilled, the transients will still have the shape as predicted by the infinitesimal current-source theory but they will not have the same amplitudes. Separate resistivity interpretations by the use of amplitude and shape with noisy data will differ from each other. If resistivity determination from shape and amplitude were constrained to yield the same surface layer resistivity, as Skokan (1974) has suggested, then the data might be interpreted to suggest two layers, when in reality the response would best be interpreted as a halfspace. Errors in the measurement of source length, current, receiver coil area, or orientation can also have large effects upon the amplitude of a transient, but relatively small effects upon its shape.

Partial Inversion

The most promising interpretation technique for determining layered conductivity structure from electromagnetic sounding data is nonlinear regression or inversion. The value of the method is its ability to determine not only the layer parameters, but also their variances and covariances (Glenn et al., 1973; Inman, 1975). This approach has not previously been applied to transient data.

For full transient data inversion, one seeks the set of parameters (layer conductivities and thicknesses) for which the sum-of-squares function (eq. 19) is minimized. The model function $f(t_i, \vec{\theta})$ is given in general by:

$$f(t_i,\vec{\theta}) = n_t A \left\{\frac{\partial}{\partial t} b_z^0 (t_i) + \frac{\partial}{\partial t} b_z^P (t_i)\right\} \qquad (21)$$

which follows from eqs. (4), (5), and (12).

Many algorithms have been developed for automatically minimizing expressions like eq. (19) but they all require iterative evaluations of the model functions, $f(t_i, \vec{\theta})$, and its derivatives with respect to the parameters for each inversion. For full inversion, each model and derivative evaluation would require the numerical computation of a double integral. The method of partial inversion, on the other hand, separates the halfspace and perturbation components (see eq. 3a) of the data for separate analysis (Yost, 1952). The method allows full quantitive treatment of the upper layer problem and semiquantitative treatment (equivalent to curve matching) for interpretation of deeper layering, and does not require expensive numerical evaluation of complicated model functions.

The transient data are inverted to determine the best-fit halfspace response with the following model (see eq. 4):

$$f(t_i,\theta) = \theta_1 + \theta_2 \left[\mathrm{erf}(u) - \frac{2}{\sqrt{\pi}} \left(u + \frac{2}{3} u^3\right) e^{-u^2}\right] \qquad (22)$$

where

$$\theta_2 = \frac{3 I y}{2\pi\sigma_1 r^5} n_t A ,$$

$$\theta_3 = r\sqrt{\mu_o \sigma_1} ,$$

$$u = \theta_3 / 2\sqrt{t_i} \quad ,$$

and θ_1 is included to determine the base voltage datum (the ambient voltage upon which the transient voltage is superimposed). This parameter, θ_1, allows the following condition to be satisfied

$$\sum_{i=1}^{n} \frac{1}{(s_i)^2} \left[\bar{v}(t_i) - f(t_i, \vec{\theta})\right] = 0 = \frac{\partial}{\partial \theta_1} S(\theta)\Big|_{\vec{\theta}} = \hat{\vec{\theta}} \; . \qquad (23)$$

The derivatives are

$$\frac{\partial}{\partial \vec{\theta}} S(\vec{\theta}) = -2 \sum_{i=1}^{n} \left(\frac{1}{s_i}\right)^2 \left[v(t_i) - f(t_i, \vec{\theta})\right] \frac{\partial}{\partial \vec{\theta}} f(t_i \vec{\theta}) \qquad (24)$$

where

$$\frac{\partial}{\partial \theta_1} f(t_i, \vec{\theta}) = 1$$

$$\frac{\partial}{\partial \theta_2} f(t_i, \vec{\theta}) = \operatorname{erf}(u) - \frac{2}{\sqrt{\pi}} \left(u + \frac{2}{3} u^3\right) e^{-u^2}$$

$$\frac{\partial}{\partial \theta_3} f(t_i, \vec{\theta}) = \theta_2 \frac{4}{3\sqrt{\pi t_i}} u^4 e^{-u^2}$$

Equation (23) along with eq. (10) are sufficient reasons to believe that the inversion can correctly estimate the

parameters of the first layer, and that the resultant residuals, defined by

$$r(t_i) = \bar{v}(t_i) - f(t_i, \vec{\theta}), \qquad (25)$$

will contain the perturbation of any deeper layers along with noise. This conclusion follows only if the transient is sampled over a time span sufficient to include the beginning and end of the perturbation. The residuals can thus be used to estimate the deeper layer parameters.

Davidon's method (Fletcher and Powell, 1963) was chosen as the inversion algorithm because it has quick and stable convergence properties and it estimates the second derivatives of $S(\vec{\theta})$ at $\vec{\theta}$ for the proper computation of non-linear parameter covariances (Beal, 1960). Before inversion, the data were scaled so that θ_1, θ_2 and θ_3 would all be of equivalent magnitude, as suggested by Bard (1963) for improved covergence.

To characterize the perturbation response, several two-layer model perturbation responses were calculated using a computer program modified from Skokan (1974). The model responses all showed an initial peak followed by a smaller peak of opposite polarity (a sample is plotted in Fig. 4). The polarity of the initial peak indicates whether the ratio σ_2/σ_1 is greater than or less than unity (positive for $\sigma_2/\sigma_1 < 1$). The peak amplitude increases as σ_2/σ_1 departs from unity. For a constant σ_2/σ_1, the peak amplitude decreases approximately exponentially and its arrival time increases linearly with increasing surface layer thickness. Since surface layer thickness and σ_2/σ_1 are uniquely defined by the polarity, amplitude, and arrival time of the initial peak, this information is plotted in Figure 4, which can be utilized to interpret residuals if the data quality allows (two data tests are described below).

If the residuals are more than noise and a perturbation model response shape is discernible, the normalized time of the initial peak maximum, defined by

$$\tau = \frac{2t}{\mu_o \sigma_1 r^2} \qquad (26)$$

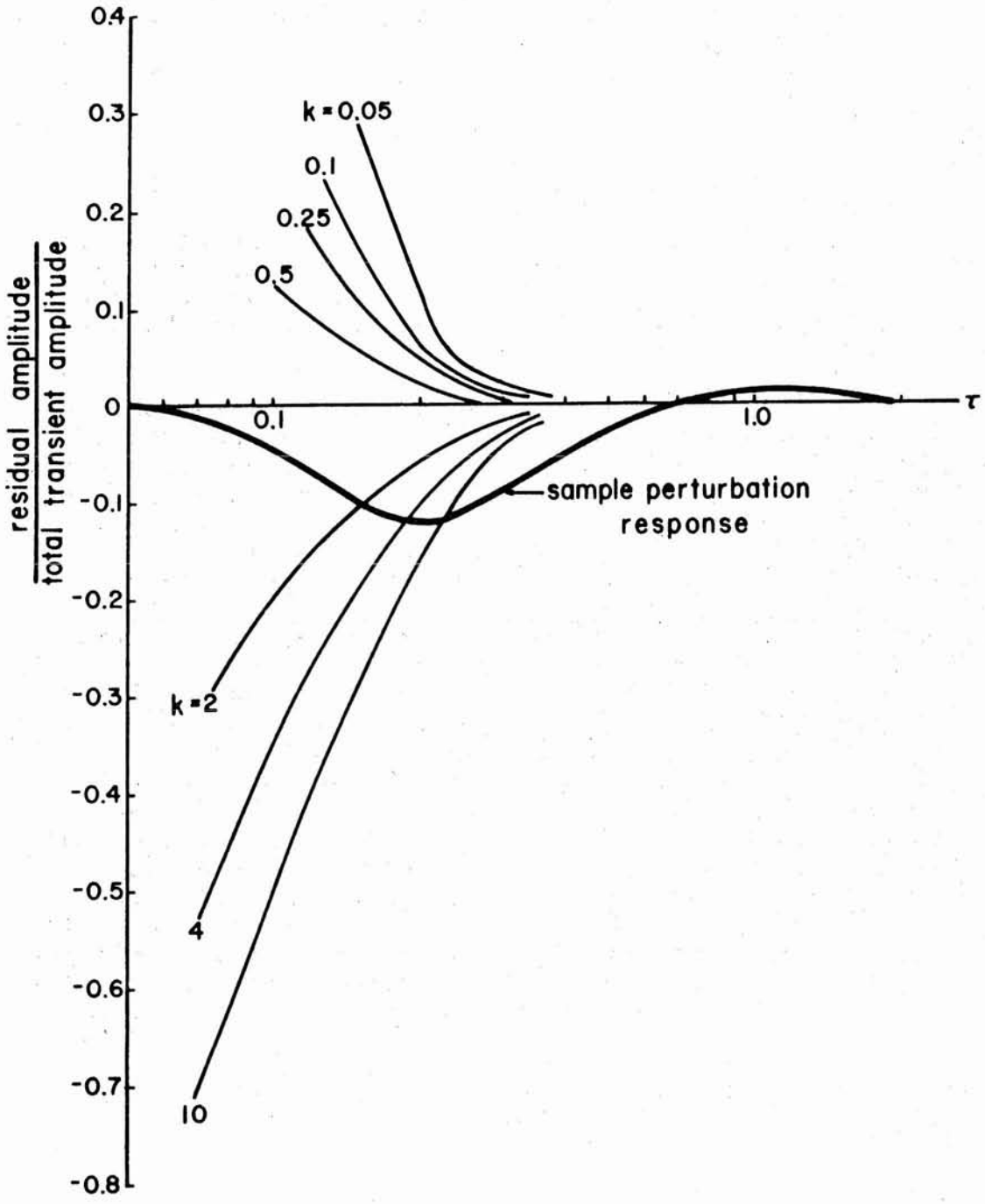

Figure 4. Polarity and magnitude of the first peak maximum of two-layer perturbation responses (eq. 37) plotted versus arrival time. The sample perturbation response is for the case of $k = \sigma_2/\sigma_1 = 4$ and $d/r = 0.375$. The abscissa is scaled to normalized time, $\tau = 2t/\mu_o\sigma_1 r^2$. For comparison with noise amplitudes, the ordinate would be equivalent to the reciprocal of the noise ratio.

where t is the actual time, defines the surface layer thickness as $2r\tau$ (Kauahikaua, 1976). The peak maximum's amplitude divided by θ_2 and plotted on Figure 4 versus τ will allow an estimate σ_2/σ_1.

Figure 4 can also be used to quantitatively determine the limits of resolution of the transient sounding method. For example, with data having a noise ratio of 10 to 15 (like most of the data in this study), it can be anticipated that it would be very difficult to distinguish a perturbation response from noise if σ_2/σ_1 is between 0.05 and 10 and if the surface layer thickness is greater than half the source-sensor separation, r.

For the present interpretation, in the inversion step, each resampled data point was weighted by the number of original data points used for its estimation in the resampling procedure (e.g. if the fifth data point was the average of four original data points, then its weight in eq (19) is $4/s_5^2$). When weighted in this way, the resampled data produce best-fit parameters within one percent of those produced by the original data. Iteration was stopped when each of the derivatives became less than 10^{-6} (usually within ten iterations). The two estimates of σ_1 were calculated from (see eq. 22):

$$\sigma_{\theta_2} = \frac{3Iyn_t A}{2\pi r^5 \hat{\theta}_2} \qquad \sigma_{\theta_3} = \frac{(\hat{\theta}_3/r)^2}{\mu_o} \tag{27}$$

These are listed in Table 2 under "σ_{θ_2}" and "σ_{θ_3}". Standard deviations for each of the parameters were calculated as the square root of the covariance, cov $\hat{\bar{\theta}}$, given by

$$\text{cov}(\hat{\bar{\theta}}) = 2S^{-1} \tag{28}$$

where S^{-1} is the inverse of a 3 x 3 matrix whose elements are $S_{ij} = \frac{\partial^2 S(\theta)}{\partial\theta_i \, \partial\theta_j}$, i, j= 1, 2, 3 (Beale, 1960), and which is provided by Davidon's minimization algorithm. The standard deviations are listed beside σ_{θ_2} and σ_{θ_3} in Table 2. Each of the

Table 2. Summary of transient sounding interpretations. All numbers refer to estimates of σ_1 unless noted otherwise.

Sounding	PARTIAL INVERSION σ_{θ_2}	PARTIAL INVERSION σ_{θ_3}	$F(\bar{\theta})$	σ_a	CURVE-MATCH		ASYMPTOTE EVALUATION Early		Late	
1	.142 ± .3200	.161 ± .020000	1.091	.25	.15		.15	.17	$\sigma_2 \leq .10$	$d \approx 4300$
3	.119 ± .0066	.111 ± .000028	1.089	.12	.09		.11	.09	$\sigma_2 \leq .05$	$d \approx 5000$
5	.089 ± .0075	.113 ± .000036	1.100	.14	.10		.10	.12		
6	.156 ± .0650	.142 ± .002900	1.092	.08	.15		.14	.15		
7	.116 ± .0270	.121 ± .000470	1.140	.13	.08		.09	.20		
14	.266 ± .0230	.327 ± .000170	1.086	.27	.38	$\sigma_2 \leq .32$ $d \leq 60$	.22	.30		
15	.016 ± .0250	.473 ± .000670	2.150	.20	.50	$\sigma_2 = .43$ $d \leq 50$	.10	.50		
16	.147 ± .2800	.308 ± .000330	1.100	.21	.46	$\sigma_2 = .14$ $d = 390$	.14	.40		
23	.306 ± .0450	.301 ± .000120	1.070	.36	.26		.71	.33	$\sigma_2 \leq .10$	$d \approx 3300$
24	.145 ± .2300	.335 ± .009900	1.094	.29	.34		.23	.40		
25	.127 ± .0160	.054 ± .000013	2.570	.17	.04		.08	.10	$\sigma_2 \leq .03$	$d \approx 4300$
26	.068 ± .0160	.116 ± .000072	.810	.16	.07		.09	.10		
27	.075 ± .0110	.159 ± .000100	1.074	.15	.16		.07	.17		
28	.063 ± .0150	.105 ± .000061	.970	.11	.08		.07	.16	$\sigma_2 \leq .01$	$d \approx 4500$
29	.009 ± .0420	.016 ± .000022	1.040	.06	.02		.02	.03	$\sigma_2 \leq .02$	$d \approx 4500$
30	.091 ± .0370	.101 ± .003000	.360	.10	.00	$\sigma_2 = .08$ $d \leq 450$	.06	.09	$\sigma_2 \leq .02$	$d \approx 4500$
31	.103 ± .2700	.118 ± .057000	.988	.18	.00	$\sigma_2 = .12$ $d \leq 185$	.08	.14	$\sigma_2 \leq .02$	$d \approx 4500$

Definition of the parameters.

σ_{θ_2}, σ_{θ_3}: estimates by amplitude and shape, respectively, from partial inversion.

$F(\bar{\theta})$: F-statistic of inversion by which σ_{θ_2} and σ_{θ_3} were estimated.

σ_2, d: parameters of two-layer interpretation. σ_2 is conductivity of deepest layer; d is its depth.

shortened transient data sets are included in the Addendum along with the best-fit halfspace model and the parameter correlation coefficients given by

$$[\mathrm{cor}(\vec{\theta})]_{ij} = \frac{[\mathrm{cov}(\hat{\vec{\theta}})]_{ij}}{[\mathrm{cov}(\hat{\vec{\theta}})]_{ii}^{\frac{1}{2}}[\mathrm{cov}(\hat{\vec{\theta}})]_{jj}^{\frac{1}{2}}} \qquad (29)$$

(Draper and Smith, 1966). A sample interpretation is presented in Figure 5.

The agreement (within one standard deviation of σ_{θ_2}) between σ_{θ_2} and σ_{θ_3} for soundings 1, 3, 5, 6, 7, 16, 23, 24, 29, 30, and 31(see Table 2) suggests that the halfspace model fits the data well for these soundings. The fit may be tested by a comparison of the sum-of-squares function minimum value, $S(\hat{\vec{\theta}})$, and the data variance, s^2, for each sounding. A comparison of variances as an F-test at the $(1-\alpha)$ confidence level is done by calculating $F(\hat{\vec{\theta}})$ for each fit by

$$F(\hat{\vec{\theta}}) = \frac{[(S(\hat{\vec{\theta}}) - s^2)/(n-p-\nu)]}{s^2/\nu} \qquad (30)$$

where n is the number of data points used in the fit, p=3 is the number of parameters used in the model, and ν is the number of degrees of freedom in the data variance estimate, and then comparing $F(\hat{\vec{\theta}})$ to the corresponding value in an F-table, denoted by $F_\alpha(n-p-\nu;\nu)$ (Draper and Smith, 1966, p. 306). The model explains the non-random elements of the data if $F(\hat{\vec{\theta}})$ is less than or equal to $F_\alpha(n-p-\nu;\nu)$. For the eleven soundings listed above, $F(\hat{\vec{\theta}})$ never exceeds 1.14, and the fit of the halfspace model appears to be adequate at the 95% confidence level.

For soundings 14, 26, 27, 28, $F(\hat{\vec{\theta}})$ is also less than 1.14; however, σ_{θ_2} is significantly less than σ_{θ_3}. The consistent values for σ_{θ_2} for soundings 26, 27, 28, 30, and 31 (between 0.10 and 0.16 S/m), which are located in the same area, and the good fit of the halfspace model suggests that the discrepancy between σ_{θ_2} and σ_{θ_3} for soundings 26, 27, and 28 is probably the result of measurement errors. σ_{θ_3} is assumed to be the best estimate of σ_1 in this case.

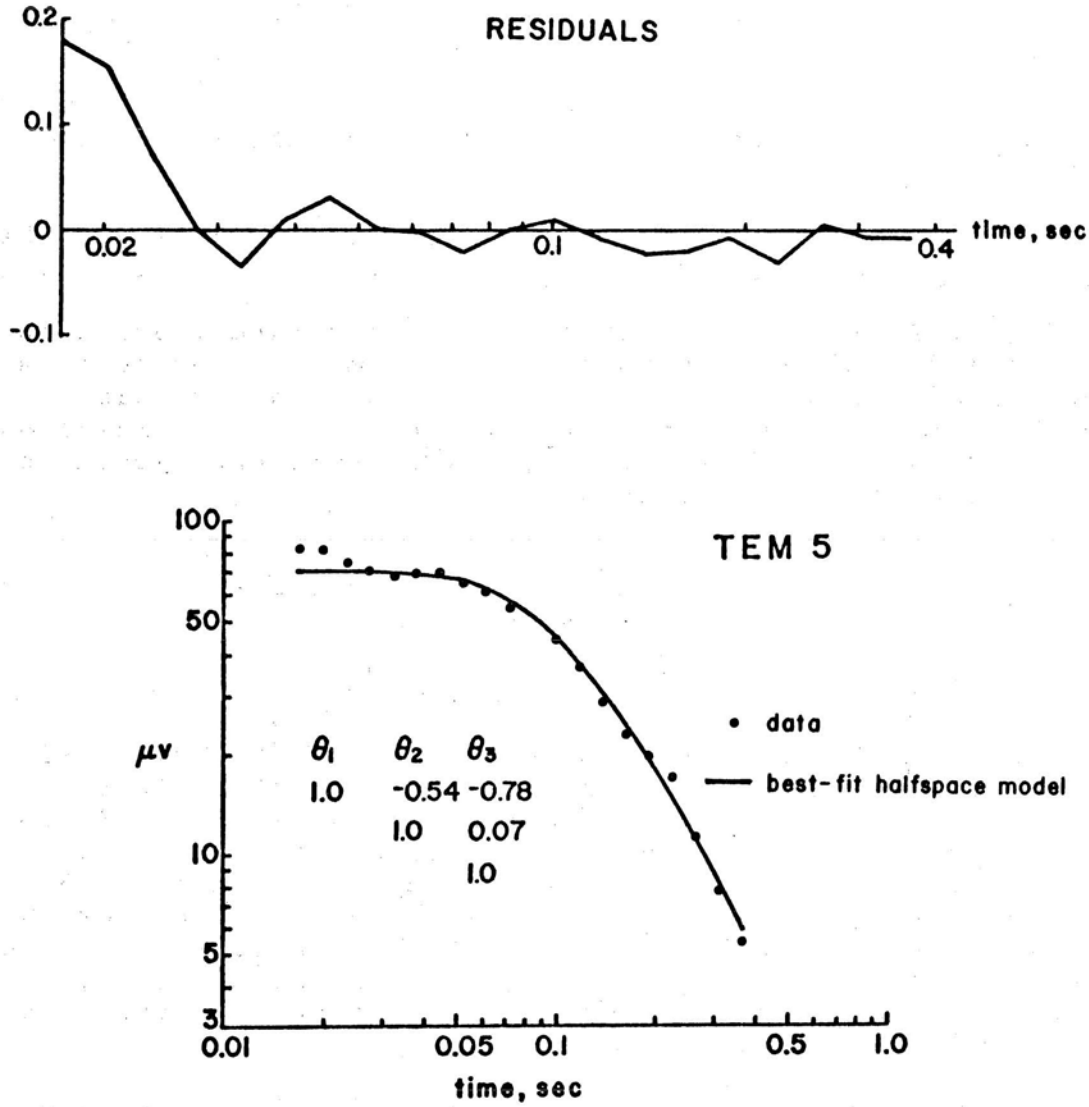

Figure 5. Data and the best-fit halfspace model with residuals for sounding 5. The ordinate for the residual plot is the voltage divided by $\hat{\theta}_2$.

The $F(\vec{\theta})$ value exceeds 1.14 for soundings 15 and 25 and indicates that the halfspace model is inadequate. We also note that σ_{θ_2} differs from σ_{θ_3} by a factor of at least two for soundings 15 and 25.

Although the statistics of the invers on indicated that the halfspace model is adequate for most of the data sets, further tests were performed to see if the residuals contained anything more than random noise. The test for randomness were done on the residuals at the 95% confidence level. First a "run" test was performed to locate consistencies in sign. Soundings 15, 16, 24, 26, 27, 30, 31 contain too few runs (common sign groups in the sequence) to accept randomness.

For the soundings that showed "runs" consistency, the data were next tested by a comparison of the residual amplitudes with the data standard deviation, s. Soundings 3, 6, 16, 25, 26, 27, 28, 30, and 31 contain residual values in excess of 1.96s, the 95% confidence level limit. The largest residual values, however, were always the earliest two or three points, which is typical of distortions due to coil misorientation or to thin, low-conductivity surface layers (Vanyan, 1967, p. 201), and not of perturbations due to deep layering. Because of the generally small amplitude of the residuals and the lack of resemblance to perturbation model shapes, the residuals were not analyzed further. A sample residual is plotted in Figure 5 for sounding 5. Residuals for all the soundings are included in the Addendum.

The results of partial inversion show that 15 of the 17 transient data sets can be most simply and adequately interpreted as halfspace responses. An interpretation with more layers may be possible; however, the quality of the present data could not support the added complexity.

Curve-Matching

The transient data are first converted from voltages to apparent resistivities defined by

$$\rho_a = \frac{2\pi r^5}{3Iyn_t A}\,\overline{v}(t) \qquad (31)$$

and plotted bilogarithmically versus time. The data curves are then matched to standard model curves, which are plotted as ρ_a/ρ_1 versus normalized time, τ, defined by

$$\tau = \frac{2\rho_1}{\mu_o r}^2 \qquad (32)$$

where $\rho_1 = 1/\sigma_1$ and τ is the time in seconds. Two-layer model sets have been published by Silva (1969), three-layer model sets by Skokan (1974), and four-layer model sets by Vanyan (1967). Computer programs for the numerical calculation of multi-layered models have been published by Skokan (1974) and Anderson (1973). A match of the data curves to a model curve by shape alone yields the number of layers and their thicknesses and the ratio of the layer resistivities to ρ_1. The match of both abscissas and ordinates (ρ_a/ρ_1 and τ axes) allows two separate estimates of ρ_1, which completes the interpretation. Only the ρ_1 estimate from the τ-axis match is used here, since the other is discussed below with the asymptotic interpretation.

Out of 17 soundings, only 5 deviated noticeably from the halfspace model shape. Soundings, 14, 15, and 16 suggested a shallow layer slightly more conductive than the halfspace below, and 30 and 31 suggested a resistive surface layer with a more conductive halfspace below. Noting that $\rho = 1/\sigma$, the curve-match interpretations for layer thicknesses and conductivities are listed in Table 2.

Asymptotic Interpretations

The halfspace transient voltage response (see eq. 4) can be approximated asymptotically in two different time ranges. For early times, $0 \le t \le 0.05 \frac{\mu_o r^2}{\rho}$, the response is given approximately by

$$\bar{v}(t) \cong \frac{3Iyn_t A}{2\pi r^5} \rho \qquad (33)$$

(from eqs. 6 and 12). For late times, $1.1 \frac{\mu_o r^2}{\rho} \le t \le 50 \frac{\mu_o r^2}{\rho}$, the voltage response is approximately given by

$$\bar{v}(t) \cong \frac{n_t AIr\mu_o}{40\pi^{3/2}\rho^{3/2}}^{5/2} t^{-5/2} \qquad (34)$$

(Silva, 1969, p. 37). By solving these two asymptotic expressions for ρ and observing how the resulting functions behave for an N-layered earth model (Jackson and Keller, 1972), we find that

$$\rho_1 \approx \frac{2\pi r^5}{3\overline{I}yn_t A}\,\overline{v}(t) \quad , \quad \text{if } 0 \le t \le 0.05\,\frac{\mu_o r^2}{\rho_1} \tag{35}$$

and

$$\rho_n \approx \left(\frac{4n_1 AIr}{5v(t)\,t^{5/2}}\,\pi \times 10^{-17.5}\right)^{2/3} \tag{36}$$

if

$$1.1\,\frac{\mu_o r^2}{\rho_n} \le t \le 50\,\frac{\mu_o r^2}{\rho_n} \tag{37}$$

Generally, these values, ρ_1, ρ_n, are calculated for all times for each sounding and plotted versus time. The resulting functions will approach constant-resistivity asymptotes when the respective time criterions are met.

Examples of these two functions are plotted in Figure 6. Other plots of the early time data reduced by eq. (35) are deleted because the curves are identical to those in the Addendum with the ordinate converted to resistivities by eq. (31). Early-time interpretations are listed in Table 2 as conductivities. The late-time curves (data reduced by eq. 37) are given in the Addend Strictly, late-time asymptotic interpretations were not valid for most of the data because only soundings 25, 26, and 29 were sampled at large enough times to satisfy the criterion in eq. (37). Nevertheless, the data were extraplolated and the attempted interpretations are listed in Table 2 as conductivities.

Some of the late-time curves showed deflections suggestive of two layers. In such cases extrapolations were made to determine the resistivities. The depths were approximated from models in Vanyan (1967). These interpretations suggest a resistive basement 3 to 5 km deep, which exceeds the source-sensor separation for most of the sounding. The deflection in the late-

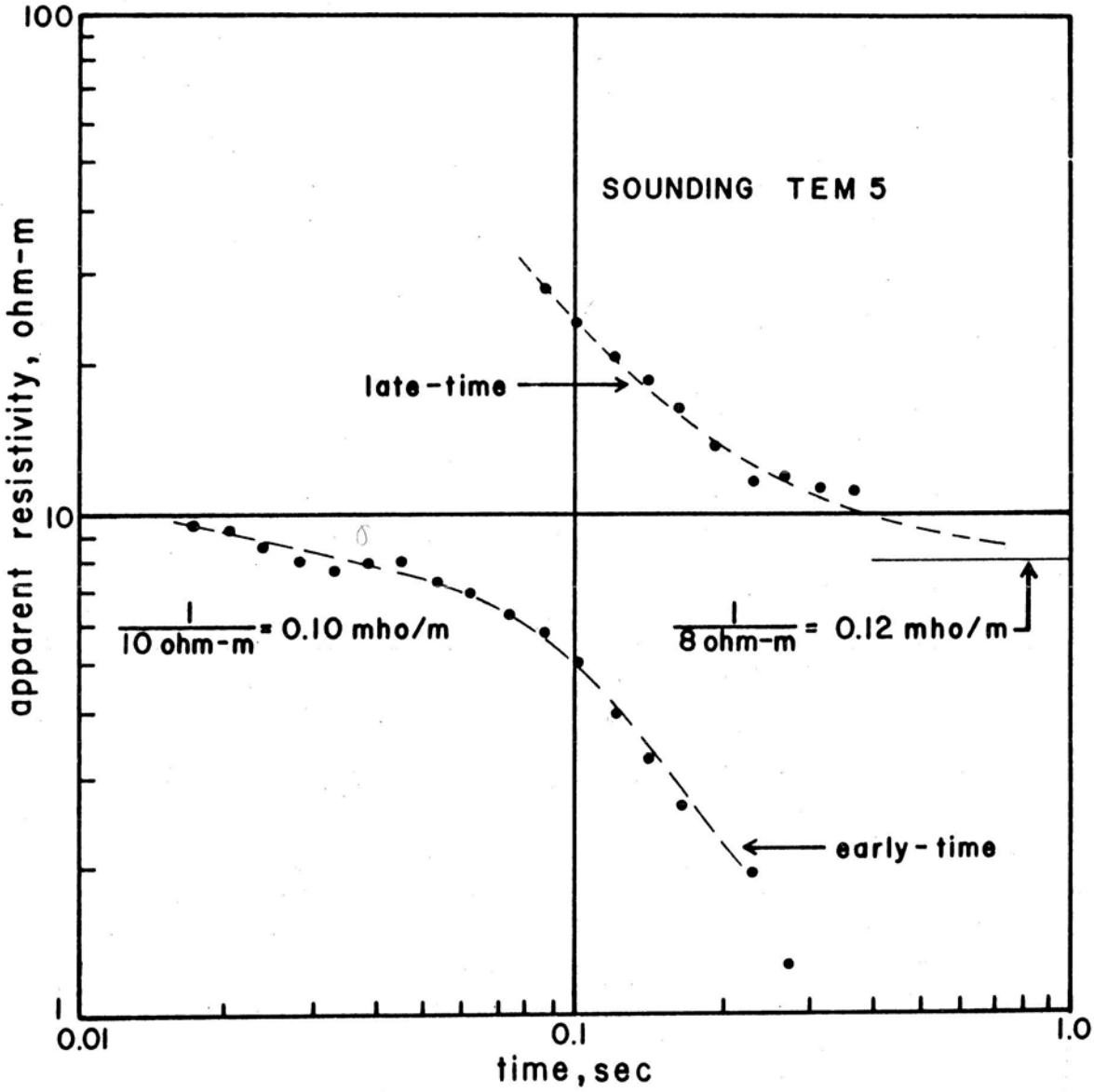

Figure 6. Early and late time asymptotic expressions and their interpretations for sounding 5. Constant conductivity asymptotes of 0.10 S/m for the early-time curve and 0.12 for the late-time curve have been picked.

time curves that indicate the existence of the basement corresponds to the smallest voltages in the data set and could be the result of insignificant voltage variations. Therefore, the interpretations listed in Table 2 for the resistive basement indications should be taken with some suspicion.

Interpretations of Half-Amplitude Decay Times

This method (suggested by C. Zablocki, personal communications, 1974) is simple and can provide rapid but approximate results in the field. The principle of this method is that an "apparent conductivity" can be calculated from the time it takes the transient to decay to some arbitrary fraction of its initial amplitude. We used the half-initial-amplitude criterion. The half-amplitude decay time, $t_{1/2}$, for a theoretical halfspace transient response (eq. 4) is given by

$$t_{1/2} = \frac{\mu_o r^2 \sigma}{2} \quad 0.23. \tag{38}$$

Solving for σ, we define the apparent conductivity as:

$$\sigma_a = 6.92 \times 10^6 \quad \frac{t_{1/2}}{r^2} \tag{39}$$

The apparent conductivity values as determined in the field for each sounding (Klein and Kauahikaua, 1975) are listed in Table 2.

DISCUSSION OF RESULTS

The interpretational methods used above represent the common techniques by which transient data can be interpreted. They differ from each other on several basic points, but most of the results generally agree in assigning "normal" conductivities of about 0.10 to 0.16 S/m to soundings 1, 3, 5, 6, 7, 26, 28, 30, and 31 and "anomalous" conductivites of 0.30 to 0.50 S/m to soundings 14, 15, 16, 23 and 24. Sounding 29 showed the lowest conductivity value of 0.016 S/m. The conductivity estimates based on shape are considered more reliable because of

the greater consistency of results. This is expected from the consideration of the possible experimental errors.

The superiority of the partial inversion method is the capacity to test the goodness-of-fit of the model to the data by standard statistical means. Fifteen of the seventeen sets of sounding data were fitted adequately by a homogeneous earth response. Furthermore, the two homogeneous earth conductivity estimates for each sounding (by shape as a function of time and by amplitude) were nearly identical for eleven of those fifteen soundings. The soundings for which the two homogeneous earth conductivity estimates did not match and those soundings that were fit inadequately by the halfspace response are most likely because of errors in measuring experimental parameters (current amplitudes or distances), becuase of high noise levels in the received voltage signals, or possibly because the layered earth model does not fit the true earth. A look at the residuals from the two inadequately fit soundings did not suggest that a more complicated layered model would improve the fit.

The data were interpreted by logarithmic curve-matching primarily for comparative purposes. Twelve of the seventeen transient responses appear to fit the halfspace model quite well, while the other five fit models having thin surface layers of varying resistivity over halfspaces. The data points most indicative of the contrasting surface layer for the five soundings were always the earliest 2 to 5 points. Vanyan (1967, p. 201) points out that the earliest portion of the transient signal can be greatly distorted by experimental conditions such as laying the measuring coil on a sloping surface or at a different elevation from the current source. The early transient can also be distorted by excessive filtering (Skokan, 1974). Since the suggestion of contrasting surface layers by these five soundings is not based on the most reliable data points, it should probably be dismissed.

Another disadvantage of logarithmic curve-matching is that it involves some manipulation of the smaller transient data values. The data and model values are visually compared so as to minimize the logarithms of their ratios (eq. 18). This comparison does not discriminate between small or large amplitude values. In this case of constant absolute precision in the measurements this consideration is critical for those parts of the records where the signal becomes small.

The asymptotic evaluation techniques are valid if the conditions of eqs. (35) and (37) are fulfilled. In Puna, only a few of the early-time asymptotes and none of the late-time asymptotes were sufficiently developed because, for the conditions encountered, the transients could not be sampled over a wide enough range of times. This is largely a function of the

dynamic range of the instrumentation and the signal-to-noise ratio. The method was, therefore, of little use in Puna.

The early-time asymptote method has the theoretical advantage that conductivity values are estimated by the larger, and supposedly better defined amplitudes of the early portion of the transient data curve. The problems in the early-time signal, however, were pointed out earlier. On the other hand, the late-time asymptote method (eq. 17) utilizes both the time dependent shape and the amplitude in the later portion of the data curve, where the transient amplitudes can be quite small. The deflections in the Puna late-time curves that suggested a 3- to 5-km-deep resistive basement were the result of very small amplitude variations in the data (usually less than 1% of the transient's maximum amplitude) amplified through the use of eq. (37). Although the late-time asymptote method is very promising for well-conditioned or low-noise transient signals, its results can be misleading if based on insignificant voltage variations. We generally discount the late-time interpretations here.

Estimation by half-amplitude decay time was intended for obtaining approximate results in the field. The apparent conductivities calculated in the field, however, rarely differed from other halfspace conductivity estimates by more than a factor of 1.5. The accuracy of this method is rather surprising, since the decay time was estimated from the transient data before it was compensated for the instrumentation effects. The distortion by the recording equipment seems to have had little effect on these decay times, which suggests that estimation by half-amplitude decay time can be used as a field technique for the detection of conductivities at least in the range of 0.05 to 0.40 S/m. The accuracy of the apparent conductivity estimates may stem from the fact that the observed transient responses did not differ markedly from the response shape of a highly conductive halfspace. For lower conductivities, which have a faster decay response, the instrumental distortion would be more significant. The presence of large contrasts in layered conductivity structure would also lower the accuracy of estimates by this method..

GEOELECTRIC STRUCTURE AND GEOLOGICAL IMPLICATIONS

The results of this study show that the subsurface in east Puna responds electromagnetically as a homogeneous halfspace with "normal" conductivities of 0.10 to 0.16 S/m for soundings 1, 3, 5, 6, 7, 26, 28, 30, and 31 and "anomalous" conductivities of 0.30 to 0.50 S/m for soundings 14, 15, 16, 23, and 24. Sounding 29, the only one northwest of the rift

zone, responded as a halfspace with a low conductivity of 0.16 S/m. The results are plotted on Figure 7 with conductivities next to each station. In this figure the values in parentheses are soundings interpreted by the half-decay method in the field (Klein and Kauahikaua, 1975) but deleted in the detailed interpretation here due to excessive noise levels.

In totally saturated rocks, the bulk rock conductivity can be described in terms of the average porosity fraction, ϕ, and the pore water conductivity, σ_ω, by the empirical relationship

$$\sigma = G\sigma_\omega \phi^m \qquad (40)$$

where σ is the bulk rock conductivity and G and m are empirically determined constants (Keller and Frischknecht, 1966). For Hawaiian basalts, Keller (1973) and Manghnani et al. (1976) have calculated (G,m) to be about 0.29, 1.8), respectively. Using this relationship for a porosity of about 25% (a reasonable average for surface lavas, from Zablocki et al., 1974) and the normal bulk conductivities 0.10 to 0.16 S/m, we find that the pore water conductivity is about 4 to 6 S/m. For the anomalous bulk conductivities of 0.30 to 0.50 S/m, we determine the pore water conductivity to be about 13 to 21 S/m.

The normal values of 4 to 6 S/m are much too high for fresh water but correspond closely to those for normal seawater at 20°C (5 to 6 S/m, from Schlichter and Telkes, 1942). This correspondence is not surprising because seawater should underlie the bulk of the region at depths greater than a few hundred meters. Fresh water, if present, should form a thin layer floating upon the seawater. Dry lavas as well as lavas saturated with fresh water would be several times more resistive than the lavas saturated with seawater below, and are not detected by these transient soundings.

The higher pore water conductivity values of 13 to 21 S/m may indicate seawater at temperatures higher than 20°C. According to Dakhov (1962), the conductivity of a fluid at temperature T, $\sigma_\omega(T)$, is related to its conductivity at 18°C, $\sigma_\omega(18°C)$, by

$$\sigma_\omega(T) = \sigma_\omega(18°C)\ [1 + \alpha(T - 18°C)] \qquad (41)$$

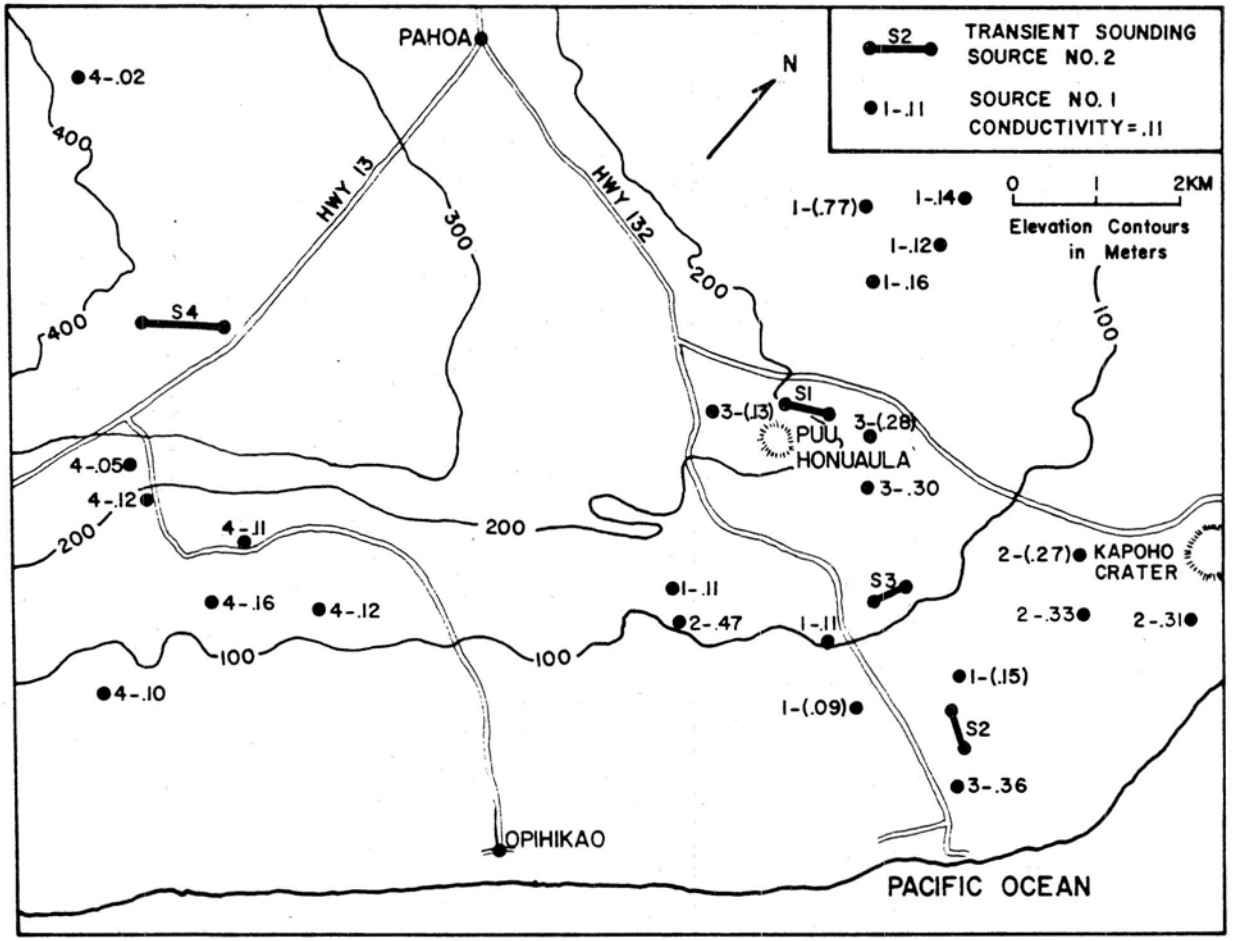

Figure 7. Sounding data plotted at the receiver station. The data in parentheses are field estimates of conductivity from stations not interpreted in this report (see Klein and Kauahikaua, 1975).

where α is the temperature coefficient of conductivity (generally taken as 0.025/°C). Comparison with the data of Quist and Marshall (1968) confirms that the relationship is valid for temperatures from 18°C to 250°C. If σ_ω(18°C) is taken to be 5 S/m, then 13 to 21 S/m corresponds to temperatures of about 82° to 146°C.

The anomalously low bulk conductivity of 0.016 S/m for sounding 29 northwest of the rift corresponds (by eq. 40) to pore water with a conductivity of 0.67 S/m. This is too low for seawater except at near-freezing temperatures, so the pore waters must be less saline than seawater and are probably at normal temperatures. Pore water conductivity increases nearly linearly with salinity and is approximated by

$$\sigma_\omega \propto S^{0.916} \tag{42}$$

where S is the pore water salinity in ppt (parts per thousand) (Logan, 1961). Using the fact that seawater has a salinity of 35 ppt, water of conductivity 0.67 S/m must have a salinity of about 3.9 ppt.

The anomalous conductivity estimates are confined to a 30- or 40-km^2 area south of the rift between Puu Honuaula and Kapoho Crater. For an area of lateral variation in earth conductivity, it is important to know the region of greatest influence on the observed signal at each sounding location. Vanyan (1967), p. 70) plots his interpretations at the point midway between source and sensor. Model studies over a conducting cylinder (Wait and Hill, 1973) show that the effect of the lateral conductivity variation is a maximum when the cylinder is between the sensor coil and the midpoint. We consider it reasonable to place the conductivity estimates at each sounding configuration midpoint rather than at the source or sensor location. The resulting map (Fig. 8, deleting the parenthesized values of Fig. 7) shows the anomalous area as the group of conductivity estimates exceeding 0.3 S/m.

The depth range represented by the (halfspace) interpreted conductivities is also an important consideration. It can be estimated qualitatively from model studies. Frequency response models (Frischknecht, 1967) and current source over a two-layer earth show conclusively that the response is not appreciably different from a halfspace response with a conductivity of the first layer if the second layer is generally at depths greater than r/3. A perfectly resistive second layer can be detected if it is shallower than r/2, and a perfectly conductive second layer can be detected shallower than

3r/4. The maximum depth of resolution for a halfspace is independent of the source-sensor separation, r, and is equal to the skin depth δ ($= \sqrt{\omega\mu\sigma}/2$) (Mundry, 1966). For Puna, the maximum skin depths of 0.1 to 0.5 S/m material using the frequencies from 1 to 35 Hz, as was done in this survey, are 4500 and 2000 m, respectively. The actual depths of resolution achieved by transient soundings would not be this large and probably did not exceed 1500 m, owing to the source-sensor separations. Mundry (1966) points out that if the surface layer of a two-layer model is thinner than $\delta/16$, then the response will not be appreciably different from that of a halfspace with the conductivity of the second layer. This explains why the resistive material above sea level (conductivities less than 0.0015 S/m) in Puna was far less apparent from the transient sounding results than it was from the results of direct-current soundings (Klein and Kauahikaua, 1975; Keller, 1973).

We conclude that the transient soundings from east Puna show sub-sea level conductivities corresponding to water-saturated basaltic lavas, which vary laterally, reaching a maximum south of Puu Honuaula. Vertical changes in conductivity by a factor of 10 or more are inconsistent with the data, at least to depths approaching 1 km below sea level. The lateral conductivity variation is interpreted to indicate temperature variation of the order of 150°C. The area of anomalous temperature is generally outlined in Figures 8 by the 0.3-S/m contour. This is the same area where coastal springs and well waters off the rift are the warmest (see Fig. 1). The groundwater has apparently been disturbed by these thermal effects because no Ghyben-Herzberg lens exists there. Coverage of the rift trace and adjacent areas by transient soundings was insufficient to fully outline the thermally disturbed zone, but it appears to be distinct from the rift structure at depths above 1 km below sea level. The transient sounding results are inconclusive regarding the location of the heat source.

Comparison of these results with the dipole mapping results of Keller (1973) and the transient sounding results of Skokan (1974) in east Puna allows some generalizations to be made about the basic structure in Puna. The transient sounding results in this study and those in Skokan's study cover mutually exclusive areas (this study covers the areas south and east of the Skokan area). Skokan interpreted her data by the logarithmic curve-matching technique, which yielded as many as three layers with the last layer deeper than the r/3-limit discussed above. We consider this complexity difficult to justify. If we omit from her interpretations any structure deeper than 1500 m (maximum r/3) and view the surface-layer conductivity interpretations only as possible maximums, her results are similar to those normal values from the present study. The rift trace appears as a less conductive zone bordered by broad areas with conductivities of about 0.1 to 0.2 S/m in both the transient

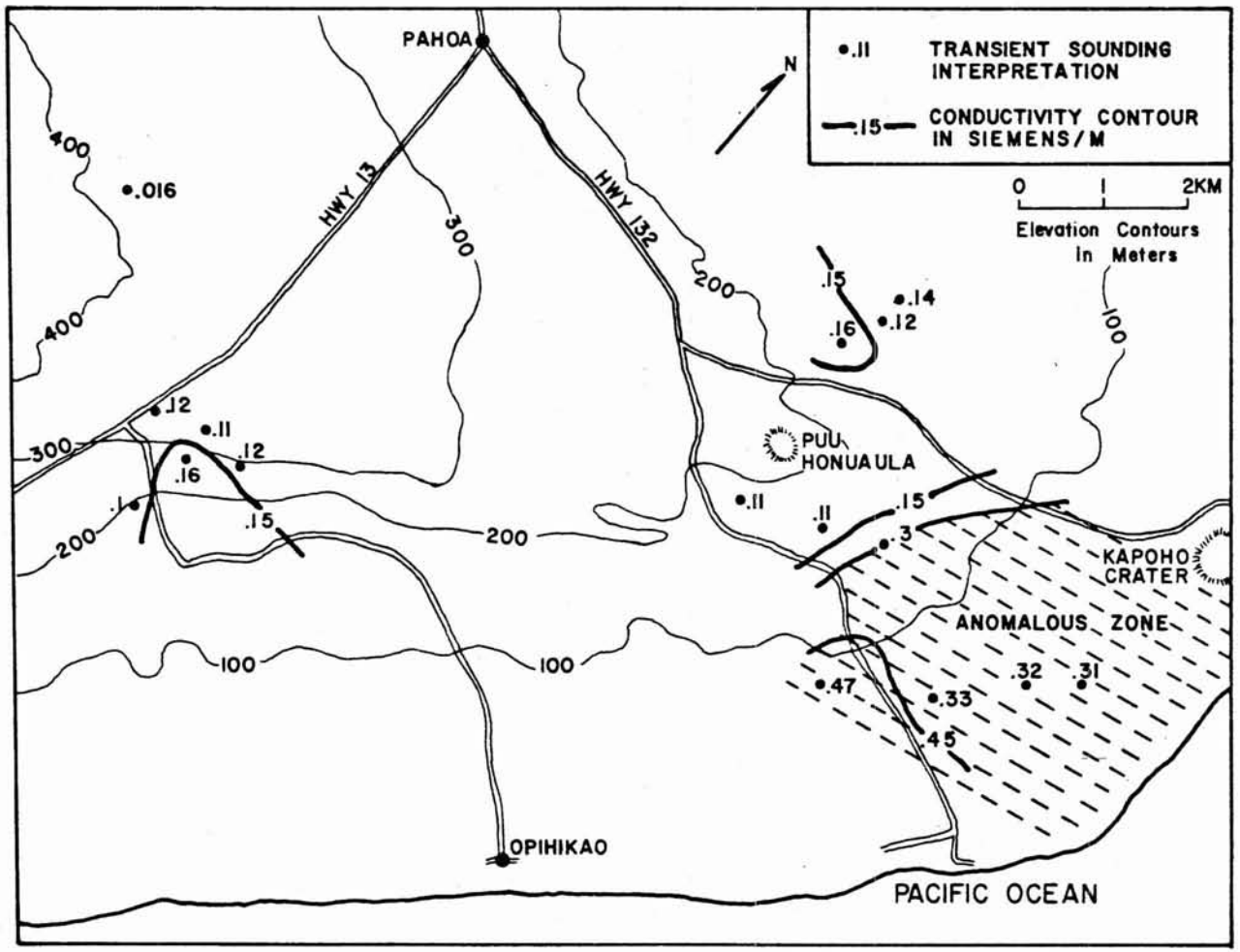

Figure 8. Sounding results plotted at the midpoint between source and sensor. The values are in S/m and the contour interval is 0.15 S/m.

sounding and bipole mapping studies. The poorly conducting rift zone could be attributed to dike-trapped water of low salinity, or to low porosity material, or to a combination of both.

ACKNOWLEDGMENTS

The authors thank Drs. Robert Harvey and Mark Odegard for their assistance in various aspects of this research. The investigation is also indebted to: Carroll Dodd for designing, building, and testing the special electronics equipment required for transient sounding; Steve Thede, Darrel Kohara, and Steve Minoha for assisting with the field work; and Edwin Sakoda for doing the meticulous drafting. This work was accomplished as partial fulfillment of the requirements for the degree of M.Sc. for J. Kauahikaua.

Research funds were provided by Grant GI38319, NSF, and continued on ERDA E(04-3)-1093 Hawaii Geothermal Project, Geophysics.

REFERENCES

Anderson, W.L., 1973. FORTRAN IV Programs for the determination of the transient tangential electric field about a vertical magnetic dipole for an M-layer earth by numerical integration and digital linear filtering, NTIS report PB-221 240, 24 pp.

Bard, Y., 1968, On a numerical instability of Davidon-like methods, Math. of Computation, v. 22, p. 665-666.

Beale, E.M.L., 1960, Confidence regions in non-linear estimation, J. R. Statis. Soc., v. B-22, p. 41-76.

Dakhnov, V.N., 1962. Geophysical Well Logging. Colo. Sch. Mines Quart.v v. 57, no. 2.

Draper, N.R. and H. Smith, 1966. Applied Regression Analysis, John Wiley and Sons, Inc., New York, 407 p.

Fletcher, R. and M.J.D. Powell, 1963. A rapidly convergent descent method for minimization. Computer J., v. 6, p. 163-168.

Frischknecht, F.C., 1967. Fields about an oscillating magnetic dipole over a two-layer earth, and application to ground and airborne electromagnetic surveys. Colo. Sch. Mines Quart., v. 62, no. 1.

Glenn, W.E., J. Ryu, S.H. Ward, W.J. Peeples and R.J. Phillips, 1973. The inversion of vertical magnetic dipole sounding data. Geophysics, v. 38, p. 1109-1129.

Inman, J.R., 1975. Resistivity inversion with ridge regession. Geophysics, v. 40, p. 798-817.

Jackson, D.B. and G.V. Keller, 1972. An electromagnetic sounding survey of the summit of Kilauea volcano, Hawaii. J. Geophys. Res., v. 77, p. 4957-4965.

Jenkins, G.M. and D.G. Watts, 1968. Spectral Analysis and its Applications. Holden-Day, San Francisco, 525 p.

Kauahikaua, J.P., 1976. Electromagnetic Transient Soundings on the East Rift Geothermal Area of Kilauea Volcano, Hawaii: A Study of Interpretational Techniques. M.Sc. Thesis, University of Hawaii, 88 pp.

Keller, G.V., 1970. Inductive methods in prospecting for hot water. Geothermics, Spec. Iss., 2, 318-332.

Keller, G. V., 1973. An electrical resistivity survey of the Puna and Kau districts, Hawaii county, Hawaii. Unpub. report prepared for the Research Corporation, Univ. Hawaii.

Keller, G. V., and F. C. Frischknecht, 1966. Electrical Methods in Geophysical Prospecting, Pergamon Press, New York, 517 p.

Klein, D. P., and J. P. Kauahikaua, 1975. Geoelectric-Geothermal Exploration on Hawaii Island: Preliminary Results. Hawaii Inst. Geophys. Rep. HIG-75-6, 23 p.

Logan, J., 1961. Estimation of electrical conductivity from chemical analyses of natural waters. J. Geophys. Res., v. 66, p. 2479-2483.

Manghnani, M. H., C. S. Rai and R. Hanada, 1976. Physical properties of rocks. In Phase II Progress Report, Hawaii Geothermal Project, p. 50-62.

Mundry, E., 1966. The vertical magnetic field of an alternating current dipole for horizontally stratified media. Geophys. Prospect., v. 14, p. 468-479.

Quist, A. S. and W. L. Marshall, 1968. Electrical conductances of aqueous sodium chloride solutions from 0 to 800° C and pressures to 400 bars. J. Phys. Chem., v. 72, p. 684-703.

Schlichter, L. B. and M. Telkes, 1942, Electrical properties of rocks and minerals. In Handbook of Physical Constants, F. Birch (ed.), Geol. Soc. Am. Spec. Pap. 36, p. 299-319.

Silva, L. R., 1969, Two-layer master curves for electromagnetic sounding. Thesis 1250, Colo. Sch. Mines, 79 pp.

Skokan, C. K., 1974, A time-domain electromagnetic survey of the east rift zone, Kilauea volcano, Hawaii. Thesis 1700, Colo. Sch. Mines, 150 pp.

Stanley, W. D., D. B. Jackson and A. R. Zohdy, 1976. Deep electrical investigations in the Long Valley Geothermal Area, Calif. J. Geophys. Res., v. 81, p. 810-820.

Stearns, H. T., 1966, Geology of the State of Hawaii. Pacific Books, Palo Alto, California, 266 p.

Vanyan, L. L., 1967. Electromagnetic Depth Soundings (G. V. Keller, trans.). Consultants Bureau, New York, 312 pp.

Wait, J. R., 1951. The magnetic dipole over the horizontally stratified earth. Can. J. Physics, v. 29, p. 577-592.

Wait, J.R., 1966. Electromagnetic fields over an anisotropic half-space. Can. J. Phys., v. 44, p. 2387-2401.

Wait, J.R., and D.A. Hill, 1973. Excitation of a homogeneous conductive cylinder of finite length by a prescribed axial current distribution. Radio Sci. v. 8, p. 1169-1176.

Yost, W.J., 1952. The interpretation of electromagnetic reflection data in geophysical exploration-part I, general theory. Geophysics, v. 17, p. 89-105.

Zablocki, C.J., R.I. Tilling, D.W. Peterson, R.I. Christiansen, G.V. Keller, and J.C. Murray, 1974. A deep research drill hole at the summit of an active volcano, Kilauea, Hawaii Geophys. Res. Lett. v. 1, p. 323-326.

ADDENDUM:
TRANSIENT DATA PLOTS

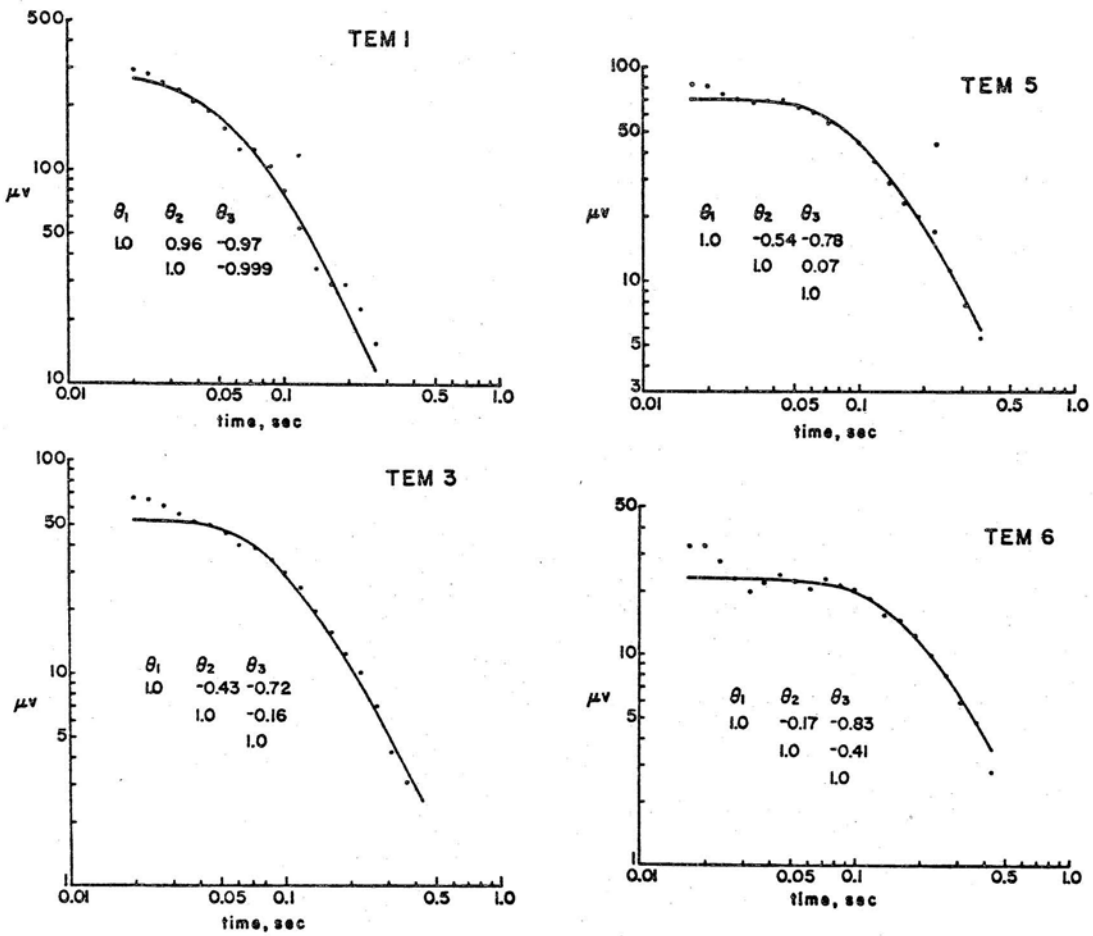

Figure 9. Transient sounding interpretations. The actual voltages are plotted versus time along with the best-fit halfspace transient response. The parameter correlation matrices are included.

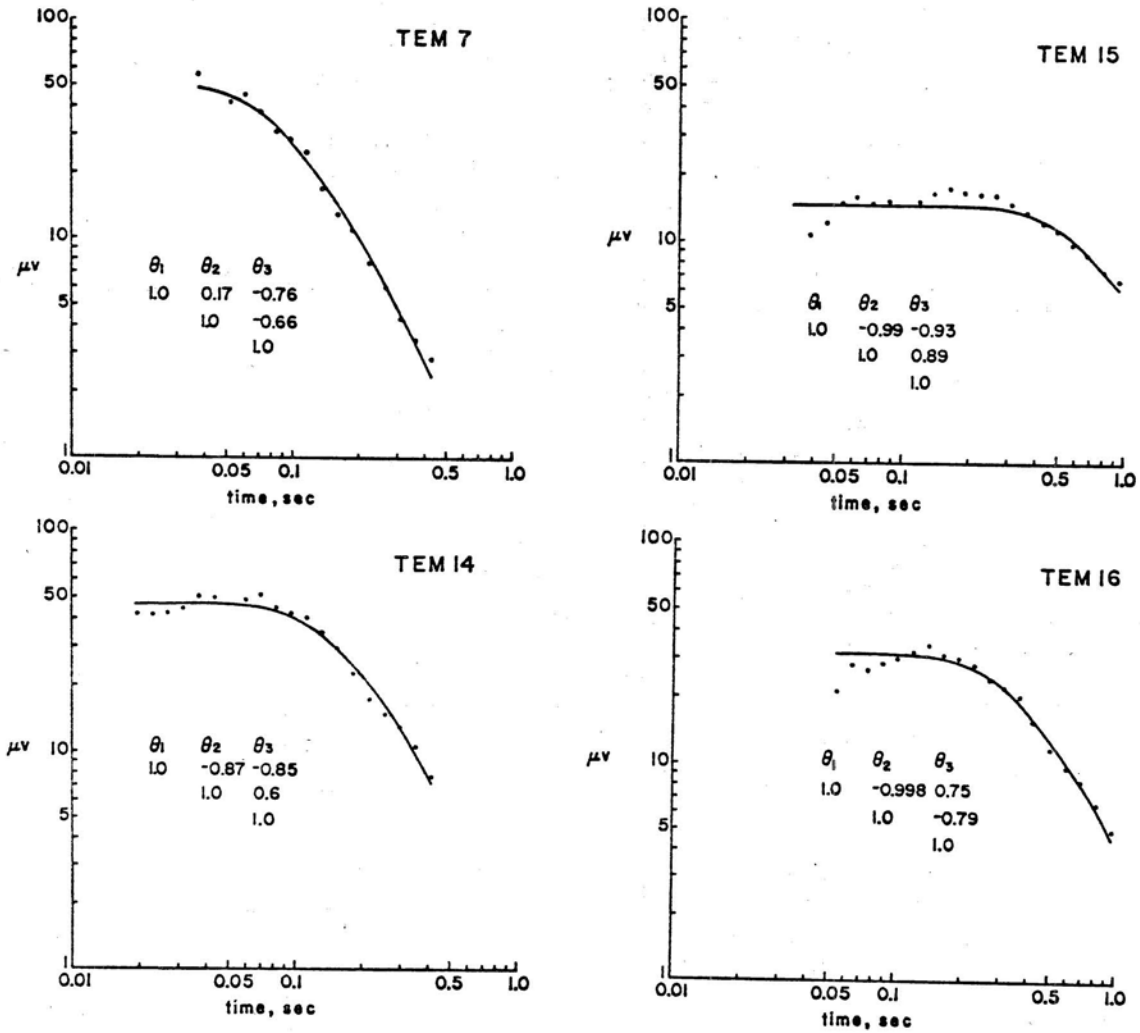

Figure 9. (continued)

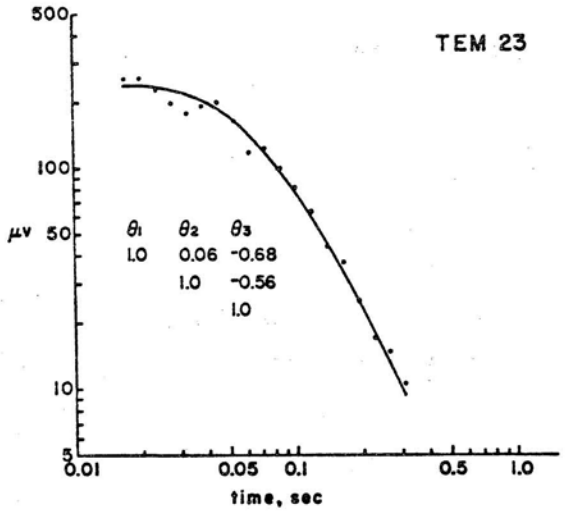

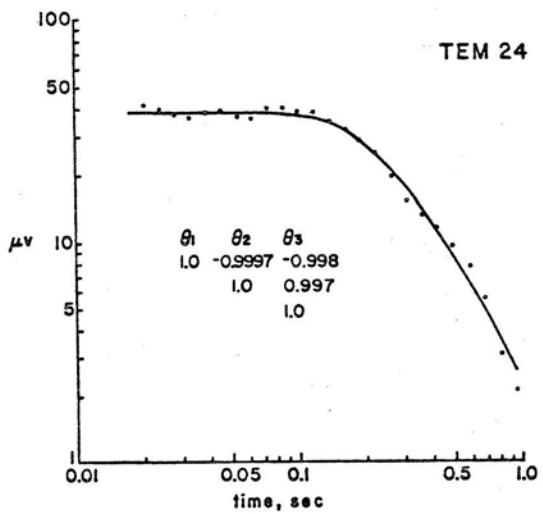

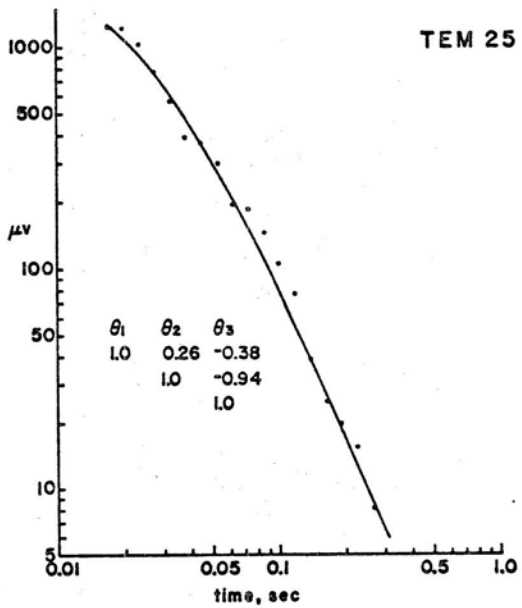

Figure 9. (continued)

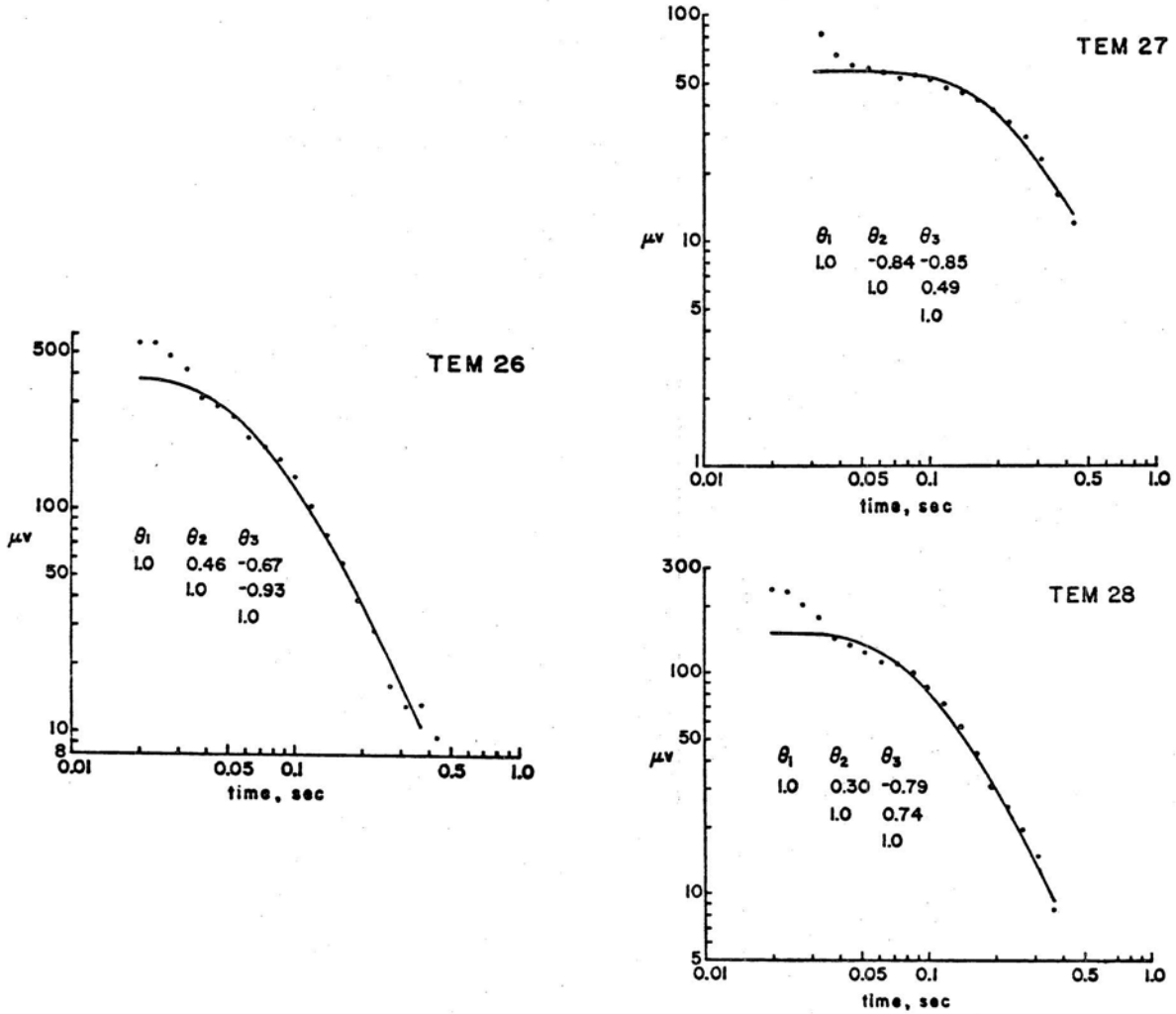

Figure 9. (continued)

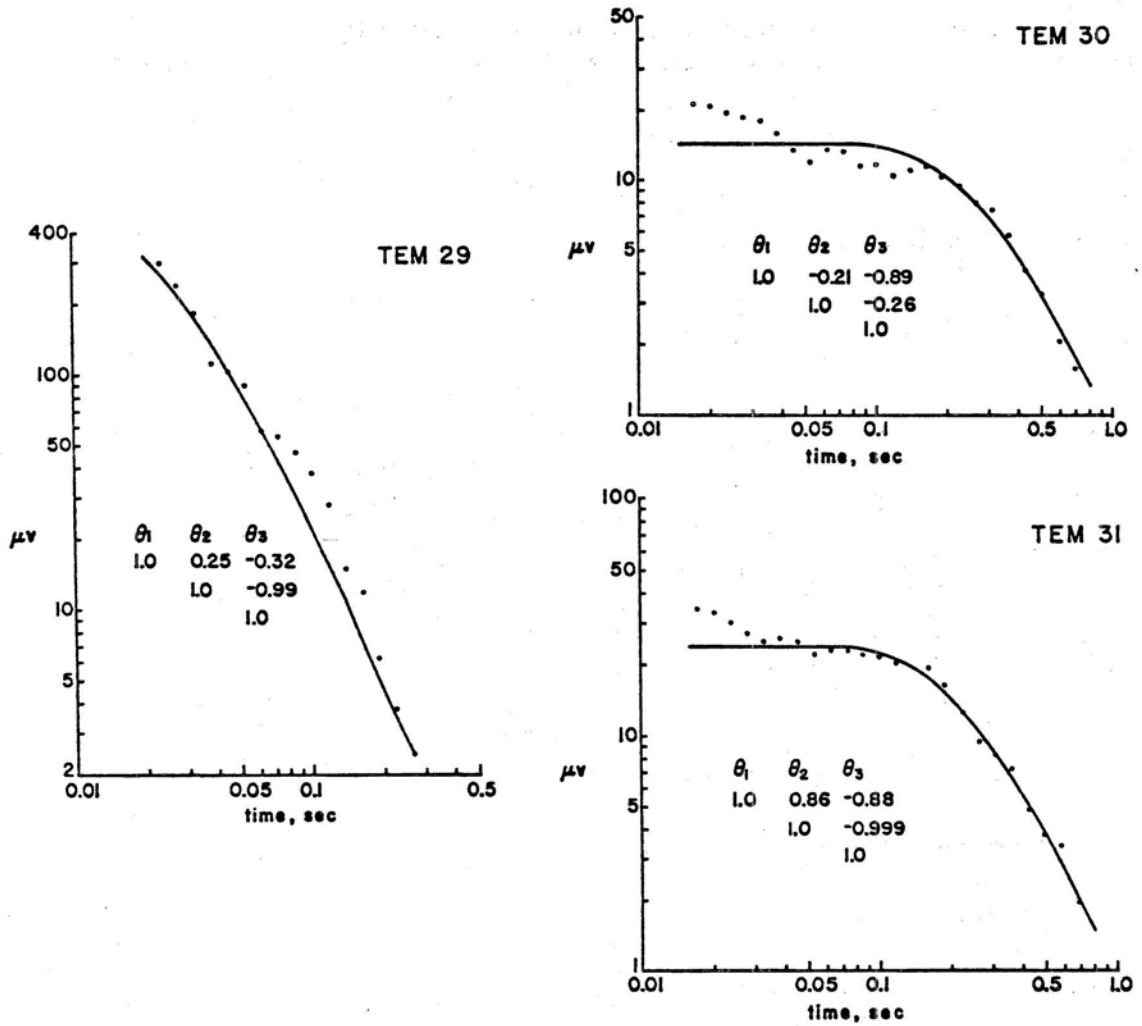

Figure 9. (continued)

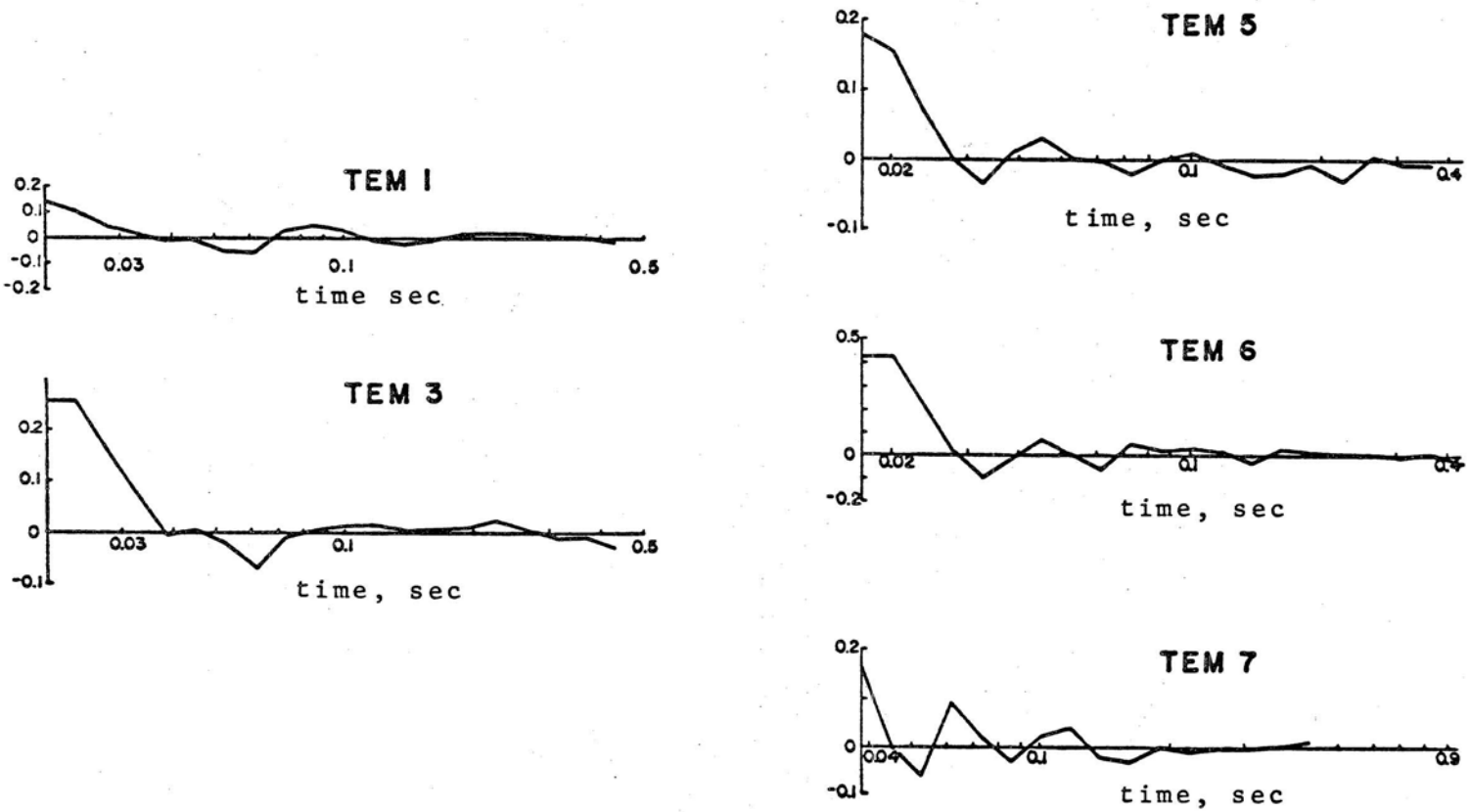

Figure 10. Data residuals. The ordinate in all plots is the residual amplitude divided by $\hat{\theta}_2$.

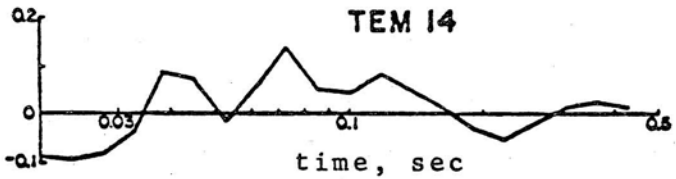

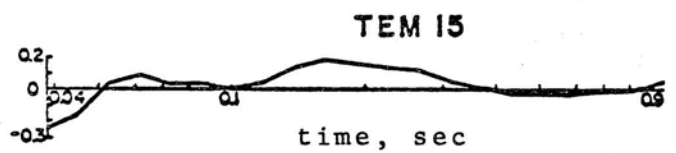

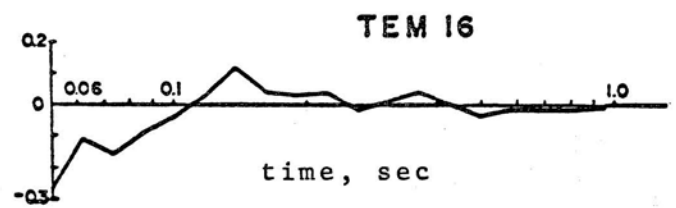

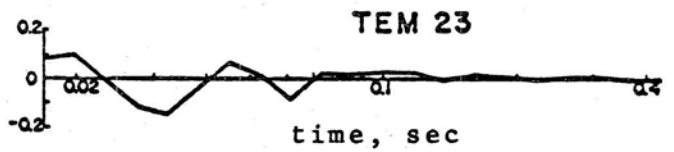

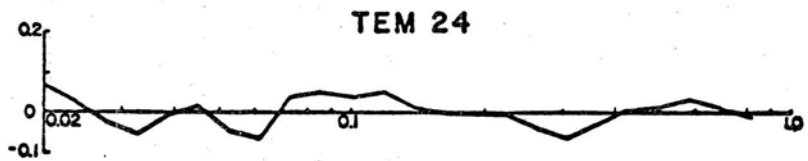

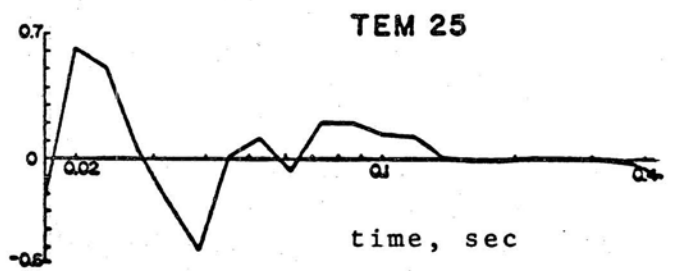

Figure 10. (continued)

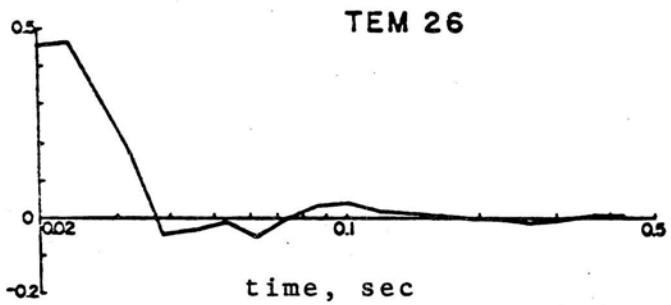

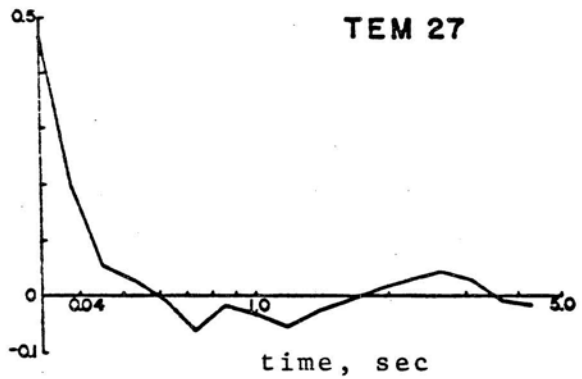

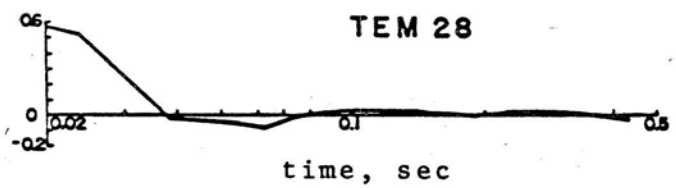

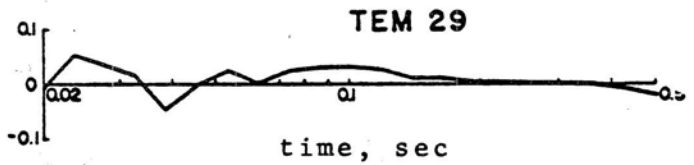

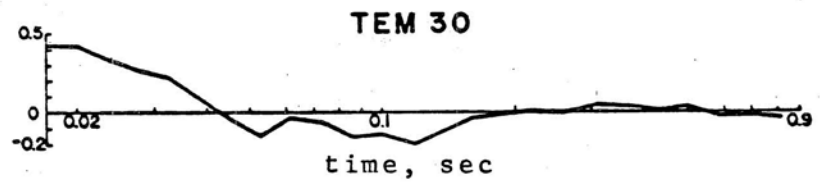

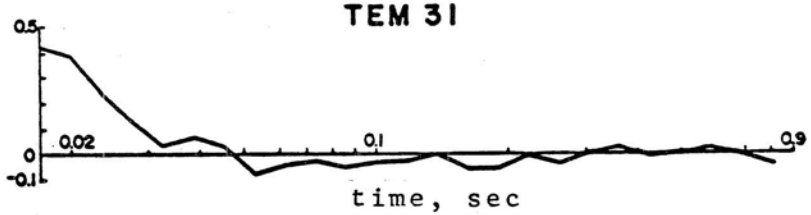

Figure 10. (continued)

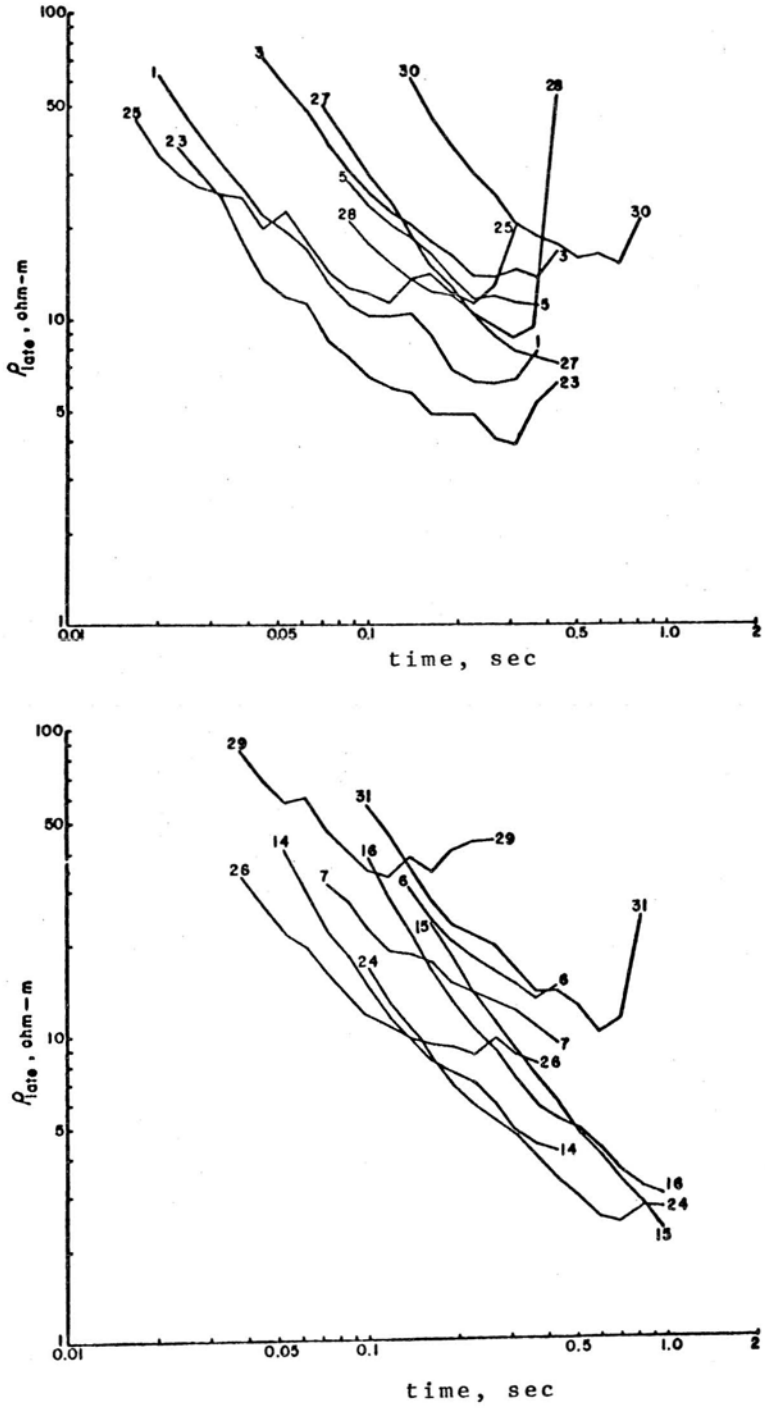

Figure 11. Late-time resistivity function, from eq. (37) for the data plotted in Fig. 9. The numbers at the end of each trace identify the transient soundings.

SELF-POTENTIAL STUDIES IN EAST PUNA, HAWAII

Charles J. Zablocki

U. S. Geological Survey, Denver Federal Center, Box 25046
Denver, Colorado, 80225

ERRATA

Please make corrections as follows:

1. *p. 179:*
   GENERALIZED GEOLOGIC SETTING
   East Puna is located.....155° W Longitude

2. *p. 185, line 5:*
   ...diffusion-rate ions such as hydrogen or hydroxyl.

3. *Insert missing pages:*
   p. 182a *follows* p. 182
   p. 188a *follows* p. 188

SELF-POTENTIAL STUDIES IN EAST PUNA, HAWAII

Charles J. Zablocki

U. S. Geological Survey, Denver Federal Center, Box 25046
Denver, Colorado, 80225

ABSTRACT

Self-potential (SP) studies made in the area of Kilauea volcano's lower east rift zone (East Puna) delineated four positive-potential anomalies that are most likely related to magma or hot intrusions at depth. Previous and concurrent SP studies in Kilauea's summit area showed that similar types of anomalies can be related unambiguously to such localizations of heat. The sources of these potentials are thought to arise from selective ion displacement in the pore fluid by temperature and/or pressure gradients.

Three of the anomalies mapped in East Puna are elongate parallel to the rift zone. One of these, just north of Puulena crater, is associated with a small-amplitude linear anomaly whose axis is transverse (N47°W) to the trend of the rift zone. The transverse feature is located where there appears to be an areal offset (left lateral) in the rift zone and is coincident with the epicentral area of recurrent, shallow (~4 km) earthquake swarms in recent years. These factors, together with some hydrologic and geologic inferences, collectively suggest that the SP features in this area reflect permeable, vertical fractures that have hot-water continuity with a relatively broad heat source at depth. The results and conclusions derived from this study were instrumental in siting a test hole that was subsequently drilled as part of the University of Hawaii's geothermal program.

INTRODUCTION

A detailed self-potential (SP) survey of the lower east rift zone of Kilauea volcano (East Puna) (Fig. 1) was undertaken in mid-1974 to help locate a site for the University of Hawaii's exploratory geothermal drilling project. The rationale for making this survey was that extensive studies by the author in many other areas of Kilauea have shown that SP measurements appear to be the single most useful method for identifying anomalous thermal areas in Kilauea (Zablocki, 1976). In these studies, positive-potential anomalies, of as much as 1600 mV across lateral distances of a kilometer or less, were found to be related unambiguously and exclusively to subsurface localizations of heat. Further impetus for the detailed SP survey in East Puna was provided by an earlier SP reconnaissance survey there in which two prominent anomalies were detected. One anomaly was associated with some steaming fissures formed by the 1955 eruption that crossed the Pahoa-Kaimu highway (Macdonald and Eaton, 1964, their Fig. 4); the other was located just north of Puulena crater (Fig. 1) in an area where no surface thermal manifestations are evident. This report summarizes the results and conclusions derived from this study that led to the siting of the University of Hawaii's drill hole.

GENERALIZED GEOLOGIC SETTING

East Puna is located on the east flank of Kilauea volcano from about 155°N Longitude to the easternmost tip of the island of Hawaii (Fig. 1). The east flank is a broad, gently plunging, constructional arch that has been built by the extrusion of numerous tholeiitic basalt lava flows from vents along the east rift zone. The rift zone extends along the crest of the arch in an east-northeast direction from near the summit to about 65 km offshore. In East Puna, the rift zone is about 3 km wide and is marked by linear fissures, spatter and cinder cones, and a few pit craters (Fig. 1). Late prehistoric and historic eruptions in this area occurred in about 1750, 1790, and in 1840, 1955, 1960, and 1961. Historic eruptions have been more numerous uprift (west-southwest) and at the summit. Ground deformation and seismic evidence have strongly suggested that the magma that feeds most of these eruptions is supplied from a shallow (3- to 5-km) reservoir

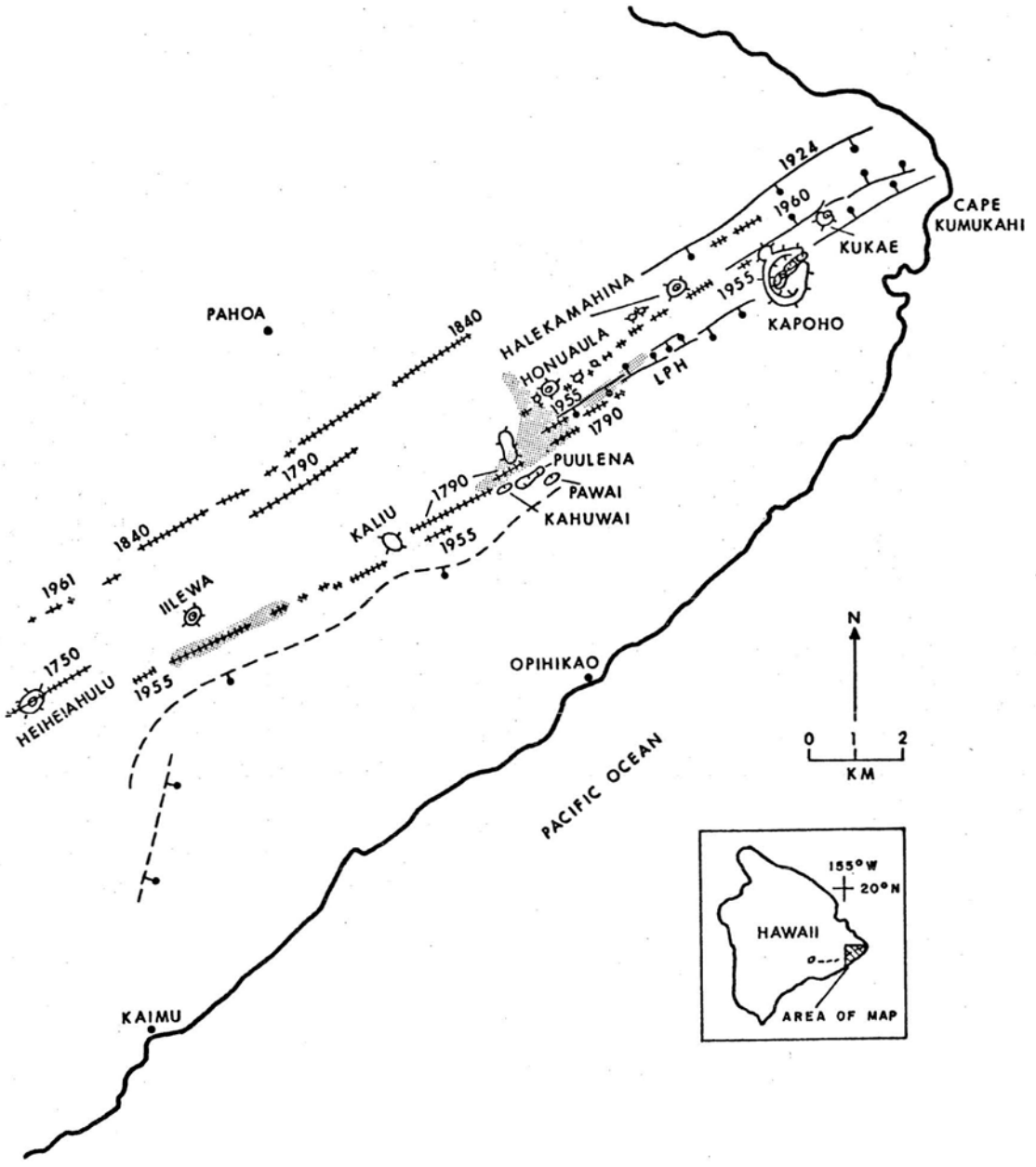

Figure 1 Preliminary geologic map of East Puna in the vicinity of Kilauea's lower east rift zone (compilation via aerial photographs by R.T. Holcomb, U.S. Geological Survey, written communication, 1977). Eruptive fissures (cross-hatched) and faults (solid lines with ball on downthrown side), dated where historic; otherwise late prehistoric (LPH). Dashed faults are inferred. Outside-hachured features are cinder cones; inside-hachured features, labeled Kuhuwai, Puulena, and Pawai, are pit craters. Hachured feature and dashed line on index map show location of Kilauea's summit caldera and axis of east rift zone, respectively. Shaded areas approximately delimit the extent of the four most significant anomalies shown in Figure 2 and discussed in the text.

complex beneath Kilauea Caldera (Eaton, 1962; Fiske and Kinoshita, 1969) and is injected toward the surface as thin, steeply dipping, bladelike dikes (Fiske and Jackson, 1972; Jackson et al., 1975; Swanson et al., 1976a,b). Similar evidence, with petrochemical support, has implied the presence of some summit-supplied, shallow reservoirs within the east rift zone that feed magma to the surface rather than directly from the summit reservoir (Wright and Fiske, 1971; Swanson et al., 1976b).

MEASUREMENT EQUIPMENT AND TECHNIQUES

The basic equipment used for SP measurements consisted of a pair of nonpolarizing electrodes (conventional copper-copper sulphate porous pots), a connecting, insulated, single-conductor cable, and a high-input impedance (10^{14} ohms) electrometer amplifier whose output was connected to a 3-1/2 digit panel meter. Electrical contact with the ground was adequate, since sufficient moisture usually was found within a few centimeters of the surface. In a few areas covered by recent lava flows, contact resistance was reduced by placing a moist sponge between the electrode and the ground surface.

Potential differences were measured between a fixed electrode and a moving electrode advanced in 100-m or smaller increments that were marked on a calibrated, 800-m-long connecting cable. When the cable was fully extended along a traverse, the advanced electrode became the stationary electrode for the subsequent extension of the traverse. The potential differences between electrode positions, 800 m apart, were progressively added algebraically to obtain the potential distribution relative to a starting point. As the survey progressed, tie-ins to formerly occupied electrode sites on subsequent days may have resulted in some small, but undetermined, errors caused by electrochemical changes of the electrodes or temporal changes in near-surface potentials. Such errors could distort the derived potential distribution obtained from these gradient measurements over distances greater than several kilometers. In the immediate areas of the two prominent anomalies, tie-in errors were minimized by laying out some traverses in a closed polygon and linearly distributing the closure errors (typically < 30 mV/km).

RESULTS

The contour map (Fig. 2) shows the surface self-potential distribution derived from these gradient measurements. The potential values used to contour the map were referenced to a common measurement location that was arbitrarily established as zero. The traverse network was largely limited to existing roads and trails, except in a few wooded areas where more detail was desired (see Fig. 3 for traverse locations). Virtually none of the original data were smoothed in constructing this map. Therefore, except for some isolated single-contour closures shown, a generally low background noise level (< 50 mV) can be inferred.

The most prominent features of the contour map are four distinct, localized, positive-potential anomalies (identified in Fig. 2 and referred to in following discussions as A, B, C, and D) and a large amplitude regional potential gradient whose direction generally trends downslope to the ocean. The previously detected anomalies A and B, together with anomaly D, are elongate parallel to the rift zone and are arranged en echelon, each one slightly offset to the left. In contrast, anomaly C is oriented transverse to the trend of the rift zone.

SOURCE MECHANISMS

The origin of the large potentials shown in Figure 2, and even larger ones measured near the summit of Kilauea, is not yet well understood. Various types of evidence, however, favor an electronkinetic phenomenon as the primary source. The potentials are thought to result from the differential displacement of certain ion species in the thermal waters that overlie deeper-seated hot zones. Other potential-generating processes such as isothermal diffusion-adsorption or oxidation/reduction are discounted as probable primary sources on the basis of their limited electric potential capacity or the many restrictive conditions required to produce them. Thermoelectric processes, involving a direct interaction between liquid and subsolidus lava, also are discounted because of the unrealistically shallow depths of magma inferred from analyzing some SP anomalies. Further, a clearly defined magnetic field intensity anomaly was outlined over a mapped shallow SP feature at the summit (Zablocki, 1976). The interpreted source depths were about the same, and hence, implied that the rocks in the anomalous region were below their Curie temperature ($< 580°C$).

Two plausible mechanisms capable of producing large potentials by thermally-induced, ion-displacement processes are electrofiltration and thermal diffusion. Electrofiltration (streaming) potentials can arise when a differential fluid pressure exists in the pore-water system of a rock (Dakhnov, 1959). Ions of the same polarity in the pore water are absorbed preferentially along the pore walls, leaving an excess of opposite-charged ions in the pore water. Charge separation occurs when the water flows because of the differential pressure. Simultaneously, a counter-electromotive force is established to impede the water flow. Most rocks absorb anions, so that the free water will contain excessive cations. Accordingly, the resulting potential gradient will be positive in the direction toward the low-pressure side of the system. The magnitude of the potentials is directly proportional to the differential pressure, the ion-adsorption efficiency of the rock (zeta potential), and the resistivity of the pore water. Laboratory studies on sedimentary rocks and on quartz capillary tubes, using moderately conducting electrolytes, have yielded values of streaming potential coefficients of a few to tens of millivolts per atmosphere (Nourbehecht, 1963; Bogoslovsky and Ogilvy, 1972). Remarkably high values of 21 V/atm have been measured by Raza and Marsden (1967) across Pyrex tubes containing nonionic, aqueous foams. The possibility of electrofiltration processes to account for the large-magnitude, positive-potential anomalies measured in Kilauea would depend largely on the dynamic pressures developed in a hydrothermal convection cell that might be formed above a magma body or high-temperature lavas and the nature of the convecting interstitial fluids. For example, it is generally assumed that the pore waters overlying a heat source have low resistivities because of their high temperatures, and possibly, because of increased concentrations of dissolved minerals. Such a condition would presumably decrease the efficiency of the enclosing wallrock's absorption ability and, hence, would result in the development of low-amplitude streaming potentials. If, however, the pore fluid at some depth existed partially or wholly in a vapor phase, the electrical conductivity of the fluid might be markedly reduced. It is conceivable that under this condition, large-magnitude potentials could develop in a crudely analogous way to the foams used by Raza and Marsden. It is interesting to note that Dorfman (written communication, 1976) recently measured dynamic changes in self potentials in the vicinity of an oil well in Texas during a steam injection experiment. Again, it is possible that these potentials resulted from the movement of steam through the rock pores.

In general, the presence of a temperature gradient in an electrolyte gives rise to a potential gradient, the thermal diffusion potential. The potential gradient arises from the tendency of the ions to diffuse at different speeds, the polarity and magnitude being such as to equalize these diffusion rates. For most electrolytes composed of neutral salts, the

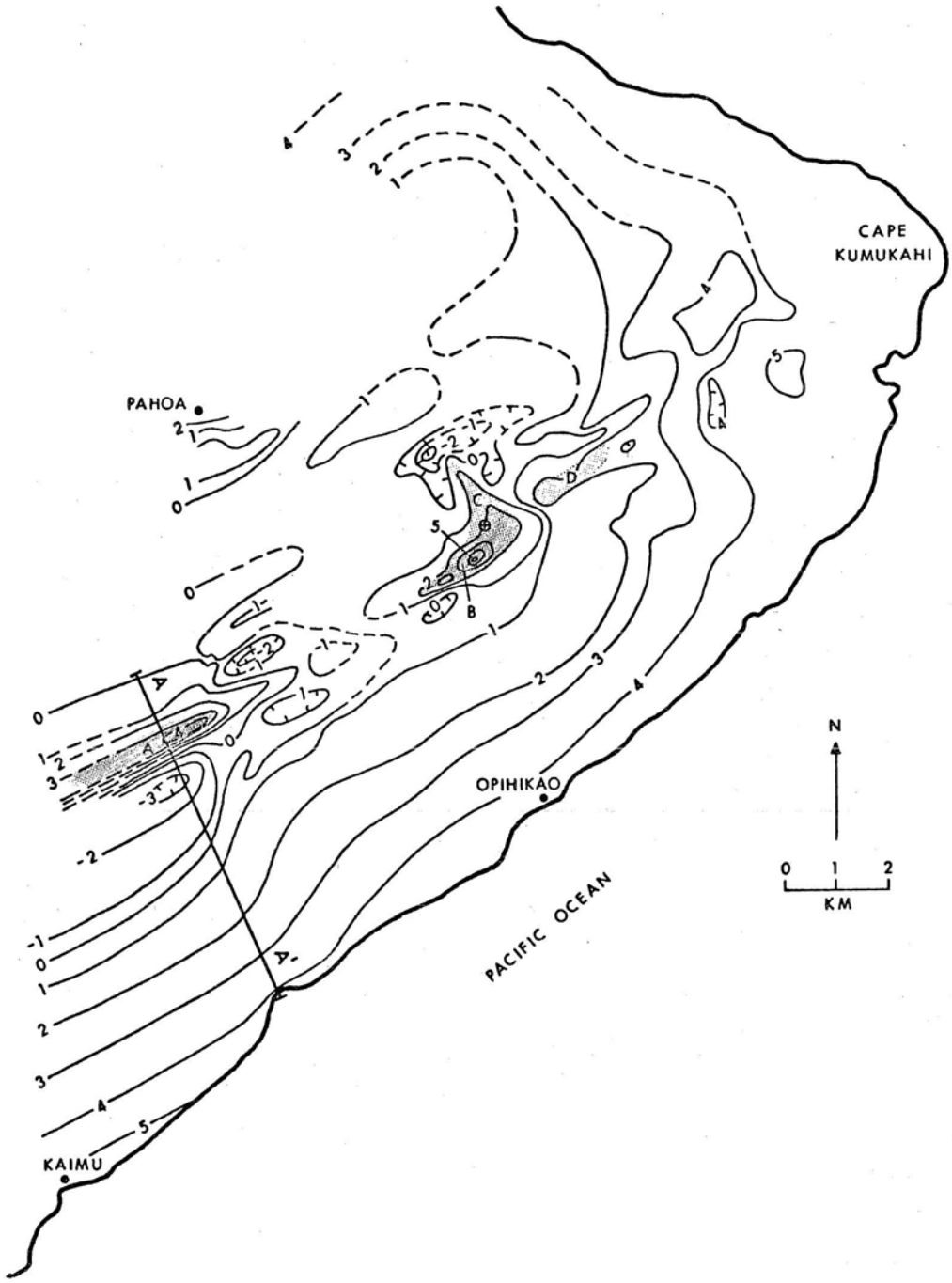

Figure 2 Contour map of the self-potential distribution in the area of Kilauea's lower east rift zone (dashed where inferred). Hachures indicate negative potentials. Each unit contour interval represents 0.1 V. A-A' traverse (barred line) indicates location of profile shown in Figure 4. Crossed circle shows location of the University of Hawaii's geothermal drill hole. Shaded areas, labeled A, B, C, and D, are the same as in Figure 1.

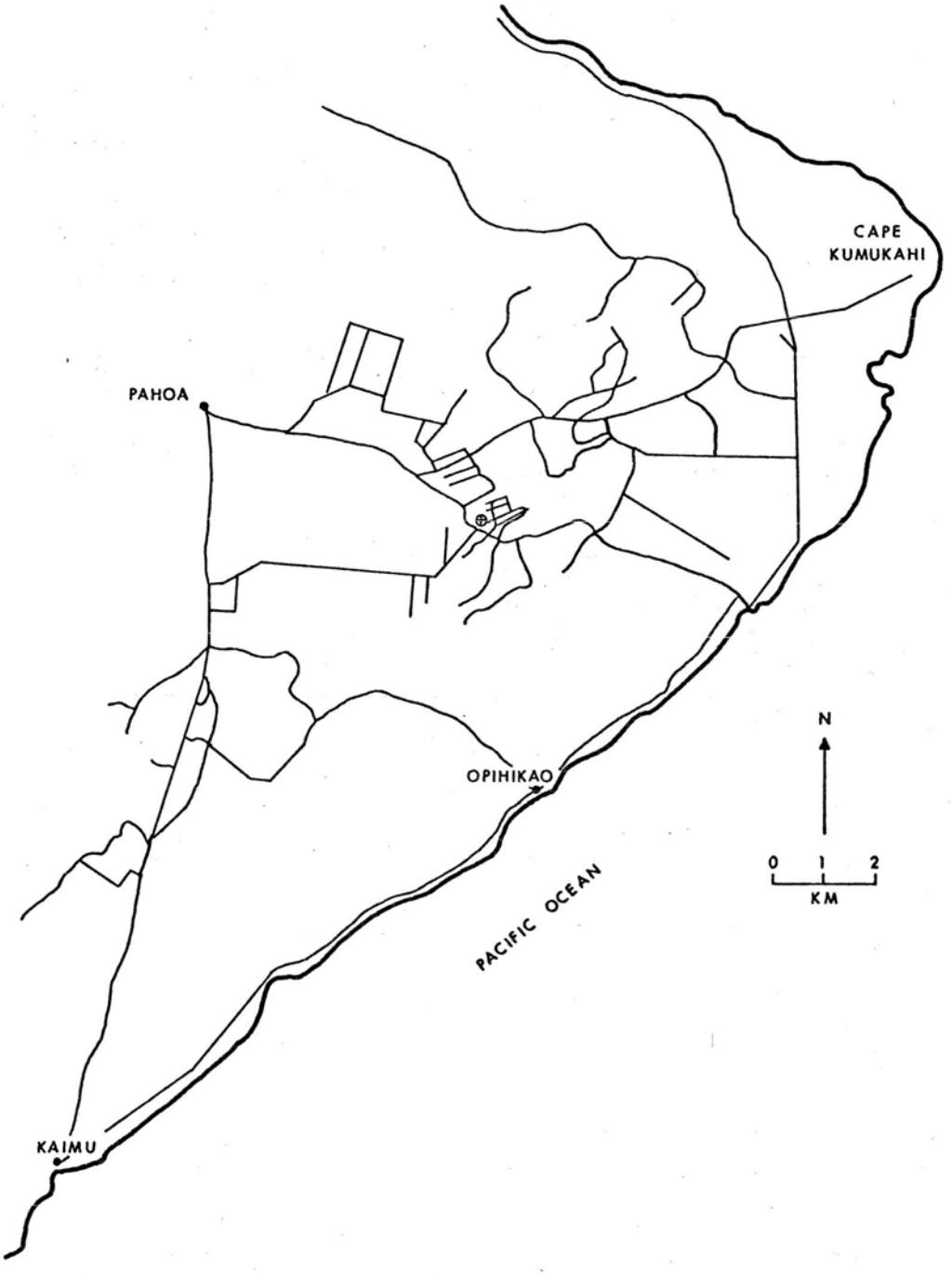

Figure 3 Map showing location of traverses along which self-potentials were measured. Crossed circle shows location of the geothermal drill hole.

hotter side of the system is positive. Reported values of thermal potential coefficients of common electrolytes are of the order of 0.2 to 0.5 mV/deg (Tyrrell and Colledge, 1954), but were shown to be much larger by the presence of high diffusion-rate ions such as hydrogen of hydroxyl. It is possible that these potentials could be several times larger under a dynamic state, as might occur in situ, than in the static condition as measured in the laboratory (M. Sato, U.S. Geological Survey, written communication, 1976).

Clearly, these proposed source mechanisms are speculative, and a systematic study of these and other processes is required for a complete utilization of SP data in quantifying the configuration of subsurface heat sources as well as the mode of distribution of the associated hydrothermal fluids.

DISCUSSION OF RESULTS

Anomaly A has the largest amplitude mapped in this study and is the only one that is related to a surficial thermal feature. A profile of the potential distribution transverse to the axis of this anomaly and extending southeast to the ocean (traverse A-A', Fig. 4) serves as a basis for the following discussion. The positive peak of the anomaly occurs directly over some steaming eruptive vents formed by the 1955 eruption (Fig. 1). Unlike the other delineated anomalies (B, C, and D), or those mapped previously at and near the summit, a relatively large-amplitude low, or negative, potential feature is developed on its southeast side. The peak-to-peak amplitude of the composite dipolar anomaly is about 800 mV over a lateral distance of about 800 m.

The large, smooth, potential gradient continuing southeast to the ocean cannot result from the establishment of a concentration gradient between fresh meteoric ground water and sea water (diffusion potential). Notwithstanding a four-decade difference in salinity, the maximum potential difference generated would be only about 30 mV (Corwin, 1976). It is likely, however, that this regional gradient could result from streaming potentials developed by the descent of meteoric water through the undersaturated lavas to the local water table near sea level. The difference in potential with respect to surface elevation in this area is -1.8 mV/m and would correspond to about -18 mV/atm, assuming some hydraulic continuity of the meteoric water in the vadose zone. With this assumption, an "elevation" correction was subtracted from the profile along traverse A-A'. It is seen that the elevation-corrected profile does not alter significantly the shape of the dipolar anomaly. The pronounced low is still preserved, although diminished in amplitude and gradient on its southeast side.

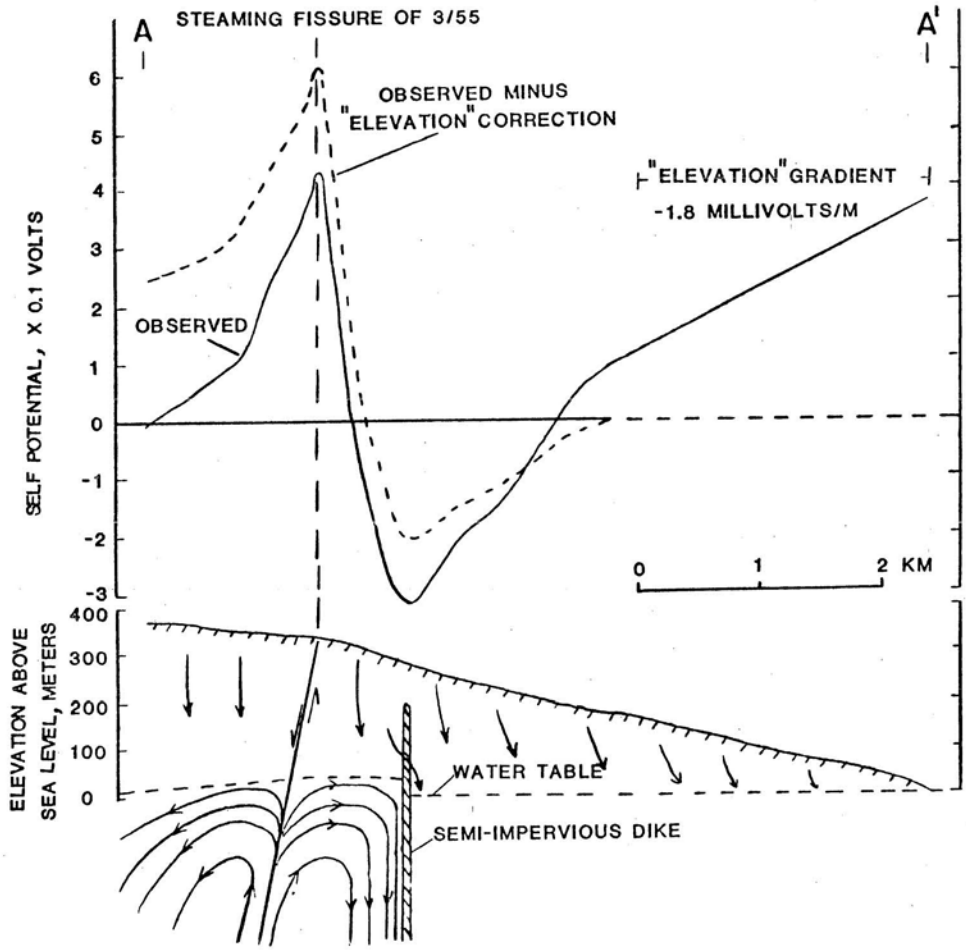

Figure 4 Self-potential profile (solid) along traverse A-A' (Fig. 2) and modified profile (dashed) after removal of an "elevation" gradient. The cross section shown below the profile is a conceptual model of the hydrology and substructure that may account for the potential distribution as discussed in the text. Arrowed-lines below water table are idealized streamlines of fluid (liquid and vapor) flow, and above water table, are downward migration of meteoric water.

A long, thin, and vertical heat source implaced in a laterally homogeneous medium would result in a symmetric distribution of the potentials over the source. The pronounced asymmetry in anomaly A suggests either a non-vertical inclination of the causative hot dike and the resultant fissure to the surface, or some marked difference in the gross distribution of fluid permeability of the rocks that flank the fissure. These two possibilities are illustrated together in the conceptual model shown in Figure 4. If the mass transfer of heat from depth is guided along a northwest-dipping fissure, the streamlines of fluid flow on the footwall side will turn down with less horizontal extension than on the hangingwall side. This laterally asymmetric pattern of fluid flow also could result, or become enhanced, if a steeply dipping, moderately impervious dike was located several hundred meters parallel to and south of the fissure. There, the convecting fluid would be constrained in its horizontal extension and forced to descend in a tighter pattern than in an unbounded region on the northwest side. Both concepts are geologically reasonable. A northwest dip for the fissure could correspond to a southeast-bounding fault of a graben formed during, or prior to, this eruption. The formation of grabens is common along rift zones in Hawaii as a result of the stretching of the rift-zone arch and subsequent settling of a keystone block along its axis (Wentworth and Macdonald, 1953). During the eruption of 1955, Macdonald and Eaton (1964) observed the formation of northwest-facing fault scarps, with offsets up to 0.5 m, that marked the south edge of narrow graben in the vicinity of the eruptive fissures bounded by anomaly A. The north edge of the graben, just north of the fissures, was a zone of flexure marked by a series of open cracks but without any true faulting.

The concept of an impervious dike constraining the fluid flow on the southeast side of these eruptive fissures is a permissible hypothesis based on known steeply dipping dikes in many of the rift zones in Hawaii that impound ground water to high levels (Stearns and Macdonald, 1946). Also, it is noteworthy that although 102°C steam was measured at 169-m depth in an exploratory hole drilled in 1961 directly on the axis of the eruptive fissures (surface elevation of 315 m), a water well drilled only 2.3 km to the south encountered fresh basal water of good quality and normal temperatures (Macdonald, 1973). Additional evidence tending to support the existence of a thermal-water barrier in this area is that warm basal springs issue from some beaches between Cape Kumukahi and Opihikao village (Fig. 1), but no anomalous warm water is known to occur at the shoreline directly downslope from the steaming fissures.

Anomaly B has a positive peak value similar to A (~ 450 mV), but is essentially monopolar. The axis of anomaly B lies partly

on a 1790 eruptive fissure rather than along the axis of one of the more recent 1955 fissures (Fig. 1). Curiously, except for A, only weak to negligible anomalies are associated with the other eruptive vents of 1955 or those formed farther northeast in 1960 (Fig. 1). The potential distributions of anomaly B extend horizontally slightly more on the northwest side than on the southeast side (see detailed contour map in Fig. 5). This asymmetry might imply a northwest dip of the causative fissure similar to the alternative explanation offered for anomaly A. The lack of a negative component to anomaly B suggests that no impervious dike exists on its southeast side as was considered for anomaly A. The numerous warm basal springs along the downslope beaches and the occurrence of hot (55°C) brackish water in a well located about 2 km southeast of the anomaly (Macdonald, 1973) support this inference.

The axis of anomaly C strikes approximately N47°W (transverse to the direction of the rift zone) and has a strike length of about 2 km (Fig. 5). Such an orientation has not been observed for any of the linear SP anomalies mapped in Puna or in parts of the east and southwest rift zones near Kilauea's summit. All other linear anomalies either coincide with or are parallel to the strike of eruptive and noneruptive fissures. Although there are no indications of fractures along the axis of anomaly C, its location suggests the presence of a transform fault at depth. Some reasons and observations that tend to support this hypothesis are summarized here. First, it is thought that the SP feature reflects a permeable fracture that maintains fluid continuity with a heat source at depth (see discussion in Conclusions section). The formation of such a deep, transverse fracture could have resulted from net-differential horizontal tensional stresses developed on opposite sides of the feature (similar to those across transform faults along mid-oceanic ridges). Uprift (southwest) of the anomaly, ground-deformation studies, frequent stress-release earthquakes, and the influence of Mauna Loa's gravitational stress system all support the concept of seaward movement of Kilauea's south flank from intrusion of magma into the rift zone (Swanson et al., 1976a). Northeast of the anomaly, however, the region is markedly aseismic (Koyanagi et al., 1972, Fig. 2; R.Y. Koyanagi, personal communication, 1977) and is largely beyond any buttressing or gravitational-stress effects from Mauna Loa (Swanson et al., 1976a, p. 25). These facts suggest that horizontal intrusion-induced dilation in this part of the rift zone is more or less symmetric, and no appreciable stresses can accumulate. The change in the topographic expression of the east-rift arch from asymmetric (steeper slopes on south side) uprift of the anomaly to symmetric downrift, and even slightly asymmetric in the opposite sense (steeper slopes on north side) along its submarine extension to 70 km beyond Cape Kumukahi (Malahoff and McCoy, 1967; Moore, 1971), would seem to corroborate this suggestion.

Finally, the mode of ground displacements of the major graben near Kapoho (Fig. 1) in 1924 (asymmetric subsidence) led Swanson et al. (1976a, p. 12) to suggest that the north side of the graben may possibly have moved more northward than the south side moved southward. A similar asymmetric subsidence of this graben took place during the 1960 eruption (Richter et al., 1970, p. E38). In contrast, the ground displacements related to the graben formed in 1955 near anomaly A (discussed in a previous section) would imply that larger horizontal displacements took place on its south side.

Anomaly D is fairly broad and is located over a prehistoric fissure (Fig. 1), but its relatively small amplitude suggests that the pore-fluid temperatures and pressures at shallow depths are not very large.

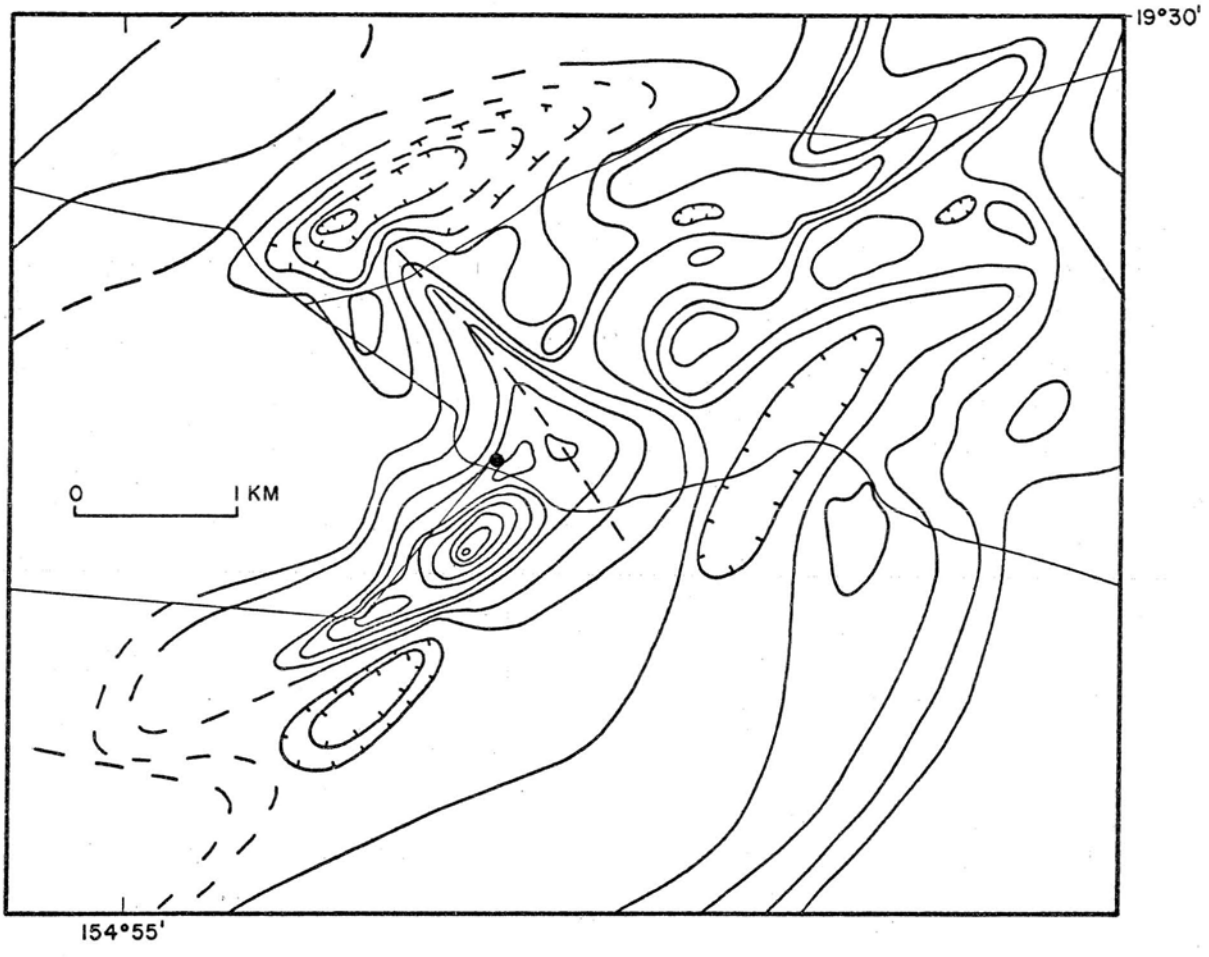

Figure 5 Detailed contour map of the self-potential distribution in the vicinity of the geothermal drill hole (solid circle). Contour interval is 50 mV (see Fig. 2 for absolute values); contours are dashed where inferred. Hachures indicate closed lows (negative potentials); thin lines indicate location of major roads in the area; dashed line through anomaly C (Fig. 2) is projection of inferred transform fault.

CONCLUSIONS

Based on the results from this study, a site for the University of Hawaii's exploratory geothermal drill hole was recommended in the immediate area of anomalies B and C. The reasons this area was favored are:

1. The wavelengths of these linear anomalies suggest that top-of-source depths are shallow, corresponding to the local basal water table (~ 200 m). It seems unlikely that the SP features result directly from shallow,bladelike intrusions. Repeated surveys over recent eruptive fissures near the summit showed that the amplitudes of the associated SP anomalies diminish with time (Zablocki, 1976), suggesting rapid cooling of the thin dikes. Further, many characteristically short-wave-length SP anomalies detected in the summit area coincide with earthquakes at depths of 2 to 3 km and can be explained by collimation of the hydrothermal fluids by vertical gravitational forces (Zablocki, 1976). Considering the length of time since the most recent eruptive activity in East Puna (1955 and 1960), the weak to negligible anomalies measured over many of these vents and the lack of steam or other thermal manifestations at the surface of B and C, it was concluded that these anomalies reflect permeable, steeply dipping fractures containing water in the liquid and vapor phase that is heated by high-temperature lavas or magma at depth. This model requires the wallrocks bounding the fractures, at least to shallow depths, to be relatively impervious. It is generally recognized that such a subsurface condition would be necessary for the existence of any viable hydrothermal resource in Hawaii.

2. Anomalies B and C probably are interrelated because of their proximity (Figs. 2 and 5), and if so, they may have resulted from a common, broad heat source at depth.

3. The possibility that a local, shallow (~ 4-km) heat source, or magma reservoir, may underlie the area of anomalies B and C was reinforced by the following observations:

a. The mode of eruption in 1955 (Macdonald and Eaton, 1964) suggests a common source location for the eruptive lavas. The initial outbreak occurred in the vicinity of anomaly C, southwest of Honuaula, and the eruption proceeded to the northeast in a series of en echelon fissures (Fig. 1). After a five-day pause, activity resumed in a southwest direction from near Kaliu producing similar, but opposite-sense, en echelon eruptive fissures. The southwest eruptive segment was offset significantly from the northeast segment. The trace of these fissures follows an apparent areal offset in the rift zone, and anomaly C lies along this offset (Fig. 1).

b. Inflation of the lower east rift occurred just prior to the initial 1955 outbreak, but there was a delay of nearly two weeks in subsidence of the summit of Kilauea (Macdonald and Eaton, 1964, Fig. 33). Subsidence of the summit usually precedes, or is concurrent with, flank eruptions or intrusions as magma drains from the summit reservoir complex (Kinoshita et al., 1974). This fact, together with detailed petrochemical analysis of the 1955 lavas, led Wright and Fiske (1971) to suggest that a local reservoir was present within the east rift near the site of eruption before the initial outbreak.

c. Anomaly C is coincident with the epicentral distribution of three separate episodes of shallow earthquake swarms (~ 4 km deep) that were monitored in early 1970 by the U.S. Geological Survey (Hawaiian Volcano Observatory, unpub. data, 1970). Earthquake swarms in Kilauea are generally thought to be related directly to magmatic activity (Koyanagi et al., 1972). Hill (1977) recently has proposed a model to account for these types of earthquake swarms in which magmatic pressures are required to produce cascading shear failures along a system of conjugate fault planes (strike-slip motion). If anomaly C is related to a transform fault, it could have developed by such stress-release processes.

d. The onset of seismic activity that preceded the 1960 eruption near Kapoho was located in the area of the initial outbreak of the 1955 eruption (Richter et al., 1970, p. E36-37).

4. High temperatures exist in some shallow wells a few kilometers downslope from this area (see Furumoto, 1976, Figs. 9 and 10). The temperature profiles show that higher temperatures are confined to a narrow zone at the surface of the basal water table; below several meters, the temperatures decrease. The temperature inversion in these wells implies that the hot water must be flowing laterally (downslope) from a hotter source in the vicinity of anomalies B and C.

Collectively, these factors outweighed the favorable evidence for drilling in other areas in Puna (for example, over anomaly A) despite the lack of corrobative support from some other geophysical data available at that time (Skokan, 1974; Furumoto, 1976). Accordingly, a drill-hole site was initially recommended over anomaly B (Fig. 2). Because of land ownership problems, however, the site was relocated about 400 m to the north between anomalies B and C (Figs. 2 and 5). This new site was considered to be almost as favorable as the original recommendation because a potentially commercial hydrothermal resource would require a target that was more pervasive and deeper than that expressed by these shallow, linear SP anomalies. Moreover, the steeper potential gradient of anomaly C on its northeast side (Fig. 5) would imply that the

related fracture zone dips steeply, if not vertically, to the southwest. If so, then a hole placed on the downslope side would more likely intersect, or come closer to, a favorable target. Finally, if these mapped SP features reflect leaks in a broader hydrothermal system at depth (~ 2 km), as suggested herein, then the exact location of an anticipated 2 km-deep drill hole would not be too critical.

In April 1976 a hole was drilled to a depth of 1962 m and temperatures of about 350°C were encountered toward the hole bottom. Various hydrothermal reservoir tests are currently underway to assess its potential as a viable source for electric power generation.

ACKNOWLEDGMENTS

I express my thanks to Maurice K. Sako (U.S. Geological Survey, Hawaii Volcano Observatory) who contributed much toward gathering and reducing the SP data. Also my thanks go to the Hawaii Institute of Geophysics (University of Hawaii) for furnishing field assistants to help in mapping this large area in a relatively short time.

REFERENCES

Bogolovsky, V.V., and A.A. Ogilvy, 1972. The study of streaming potentials on fissured media models. Geophys. Prospect. v. 20, p. 109-117.

Corwin, R.F., 1976. Self-potential exploration for geothermal reservoirs. In Proceedings of the Second U.N. Symposium on the Development and Use of Geothermal Resources, San Francisco, Calif., May 1975, v. 2, p. 937-945.

Dakhov, U.N., 1959, Geophysical well logging (English translation). In Colorado School Mines Quart., v. 57, no. 2, April 1962.

Eaton, J.P., 1962. Crustal structure and volcanism in Hawaii. In E.T. Endo (ed.), Crust of the Pacific Basin, Geophys. Mongogr. Ser., v. 6, p. 13-29, AGU, Washington, D.C.

Fiske, R.S. and W.T. Kinoshita, 1969. Inflation of Kilauea Volcano prior to the 1967-68 eruption. Science, v. 165, p. 341-349.

Fiske, R.S., and E.D. Jackson, 1972. Orientation and growth of Hawaiian volcanic rifts: The effect of regional structure and gravitational stress. Proc. R. Soc. London, Ser. A, no. 329, p. 299-326.

Furumoto, A.S., 1976. A coordinated exploration program for geothermal sources on the island of Hawaii. In Proceedings of the Second U.N. Symposium on the Development and Use of Geothermal Resources, San Francisco, Calif., May 1975, v. 2, p. 993-1001.

Hill, D.P., 1977. A model for earthquake swarms. Submitted to J. Geophys. Res.

Jackson, D.B., D.A. Swanson, R.Y. Koyanagi, and T.L. Wright, 1975. The August and October 1968 flank eruption of Kilauea Volcano, Hawaii: U.S. Geol. Surv. Prof. Pap. 890, 33 pp.

Kinoshita, W.T., D.A. Swanson, and D.B. Jackson, 1974. The measurement of crustal deformation related to volcanic activity at Kilauea Volcano, Hawaii, In L. Civetta, P. Gasparini, G. Luongo, and A. Rapolla (eds.), Physical Volcanology. Elsevier, Amsterdam, p. 87-115.

Koyanagi, R.Y., D.A. Swanson, and E.T. Endo, 1972. Distribution of earthquakes related to mobility of the south flank of Kilauea Volcano, Hawaii. In Geological Survey Research 1972 U.S. Geol. Surv. Prof. Pap. 800-D, p. D89-D97.

Macdonald, G.A., 1973. Geological prospects for development of geothermal energy in Hawaii. Pac. Sci. v. 29, no. 9, p. 209-219.

Macdonald, G.A., and J. P. Eaton, 1964. Hawaiian volcanoes during 1955: U.S. Geol. Surv. Bull. 1171, 170 pp.

Malahoff, A. and F. McCoy, 1967. The geologic structure of the Puna Submarine Ridge, Hawaii. J. Geophys. Res., v. 72, no. 2, p. 541-548.

Moore, J.G., 1971. Bathymetry and geology-East cape of the Island of Hawaii. U.S. Geol. Surv. Misc. Geol. Inv. Map I-677, scale 1:62,500.

Nourbehecht, B., 1963. Irreversible thermodynamic effects in honogeneous media and their applications in certain geoelectric problems: Ph.D. thesis, Mass. Inst.Tech., Cambridge, Mass., 121 pp.

Raza, S.H., and S.S. Marsden, 1967. The streaming potential and the rheology of foam. Soc. Pet. Eng. J., December, p. 359-368.

Richter, D.H., J.P. Eaton, K.J. Murata, W.U. Ault, and H. L. Krivoy 1970. Chronological narrative of the 1959-60 eruption of Kilauea Volcano, Hawaii: U.S. Geol. Surv. Prof. Pap. 537-E, 73 pp.

Skokan, C.K., 1974. A time-domain electromagnetic survey of the east rift zone, Kilauea Volcano, Hawaii. Ph.D. thesis no. T-1700, Colo. Sch. Mines, Golden, Colo., 152 pp.

Stearns, H.T., and G.A. Macdonald, 1946. Geology and groundwater resources of the island of Hawaii. Hawaii Div. Hydrog. Bull. 9, 363 pp.

Swanson, D.A., W.A. Duffield, and R. S. Fiske, 1976a. Displacement of the south flank of Kilauea volcano: The result of forceful intrusion of magma into the rift zones. U.S. Geol. Surv. Prof. Pap. 963, 39 pp.

Swanson, D.A., D.B. Jackson, R.Y. Koyanagi, and T.L. Wright, 1976b. The February 1969 east rift eruption of Kilauea volcano, Hawaii. U.S. Geol. Surv. Prof. Pap. 891, 30 pp.

Tyrrell, H.J.V., and R. Colledge, 1954. Thermal diffusion potentials in non-isothermal electrolytic systems-part 3. Trans. Faraday Soc., v. 50, part 10, no. 382, p. 1056-1066.

Wentworth, C.K., and G. A. Macdonald, 1953. Structures and forms of basaltic rocks in Hawaii. U.S. Geol. Surv. Bull. 994, 98 pp.

Wright, T.L., and R.S. Fiske, 1971. Origins of the differentiated and hybrid lavas of Kilauea Volcano, Hawaii. J. Petrol, v. 12, no. 1, p. 1-65.

Zablocki, C.J., 1976. Mapping thermal anomalies on an active volcano by the self-potential method, Kilauea, Hawaii. In Proceedings of the Second U.N. Symposium on the Development and Use of Geothermal Resources, San Francisco, California, May 1975, v. 2, p. 1299-1309.